Mesozoic Strike-slip faults in the Northern Dutch offshore;

New insights from Seismic- and Physical Modeling Data

A Msc. Thesis by

Stefan Peeters[1]

Supervisors

Dr. Jeroen Smit[1]

Dr. Renaud Bouroullec[2]

Prof. dr. Dimitrios Sokoutis[1]

Date

July 2016

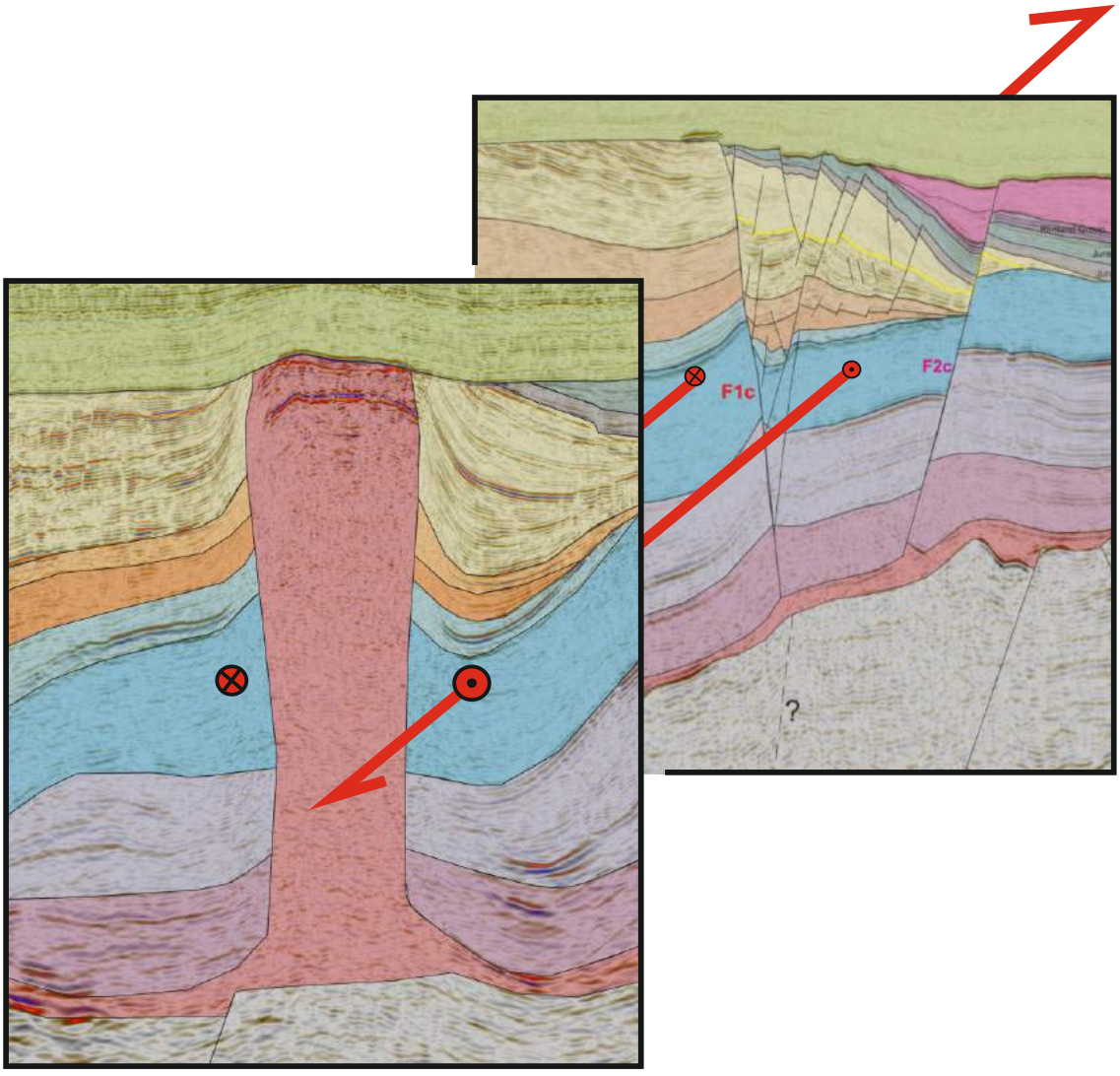

[1] Utrecht University; Heidelberglaan 8, 3584 CS Utrecht, the Netherlands

[2] TNO; Princetonlaan 6, 3584 CB Utrecht, The Netherlands

TNO innovation for life

Universiteit Utrecht

Abstract

Mesozoic Strike-slip features in the northern Dutch offshore that occurred under regional extensional and compressional tectonics are often not recognised as such and even when they are, they often remain poorly understood. This study provides new insights into various strike-slip faults in the Northern Dutch Offshore in terms of location, timing, sense- and amount of displacement and fault salt interaction. These insights are gained by combining several detailed seismic analyses with an analogue modelling study.

On the Elbow Spit High and Elbow Spit Platform, a group of SW-NE to WSW-ENE strike-slip faults is present that have accommodated approximately 500m to 900m of dextral displacement on individual faults during the Upper Cretaceous and Early Paleogene. Because of the absence of Zechstein salt in this area, these faults display the clear characteristics of strike-slip faults; i.e. vertical fault planes, an upward widening of the fault pattern, local zones of transtension and transpression and (reactivated) Riedel faults.

Dextral movements along two identified strike-slip faults in the Dutch Central Graben, which are estimated to lie in the range of 900m to 2500m, occurred during the Upper Jurassic and possibly Early Cretaceous. In the Dutch Central Graben, the presence of Zechstein salt causes decoupling of the subsalt basement from the supra salt overburden, which changes the structural style of deformation. The identified supra salt strike-slip faults in the Dutch Central are characterised by a more curved strike. Additionally, the strike-slip faults link salt structures, which suggest that strike-slip motions were also accommodated by Zechstein salt structures. This is supported by analogue models, which show that strike-slip motions are preferentially accommodated by salt structures, as they are the mechanically weakest part of the rock column. The two observed strike-slip faults in the Dutch Central Graben are likely caused by differential motions on sub salt normal faults, enhanced by a component of gravitational gliding. No evidence is found for strike-slip movements along N-S trending basement faults that bound the Dutch Central Graben.

Dextral basement strike-slip movements did occur during the Middle to Late Triassic on the Variscan inherited NW-SE to WNW-ESE trending Rifgronden Fault Zone (RFZ) and Hantum Fault Zone (HFZ) that bound the Terschelling Basin. Evidence for these motions includes the right stepping of N-S to NNE-SSW trending Late Early Triassic to Late Triassic low angle detachment faults across the RFZ and HFZ, as well as the overall geometry of features in the Terschelling Basin with respect to features on the adjacent platforms. Displacements along the HFZ are estimated to be in the order of 5 à 6km. Displacements along the RFZ are estimated to be in the order of 2 à 3km. Additionally, thin skinned strike-slip motions occurred in the Terschelling basin due to differential motions between adjacent supra salt Triassic compartments. These Triassic compartments are largely enclosed by salt walls, which accommodated the strike-slip movements.

Table of Contents

1. Introduction

The geology of the Dutch subsurface is characterized by a wide-array of different structures formed during various tectonic phases. By making use of a dense network of seismic lines and wells, a lot of these structures have been extensively studied, both on a regional and local scale. As a consequence, features corresponding to extensional- and compressional tectonics have been widely recognized in the Dutch subsurface (i.a. Ziegler, 1990a; Ziegler1990b; Baldschun et al., 1991; Nalpas et al., 1995; De Jager, 2003; Geluk, 2005). Also the influence of Zechstein salt on the structural style of deformation and on stratigraphic depositional patterns has been widely recognized and intensively studied (i.a. Nalpas et al., 1995; Geluk et al., 2007; Ten Veen et al., 2012; Harding and Muts, 2015; Msc. Thesis van Winden, 2015).

A relatively underexposed research area in the Dutch subsurface are strike-slip tectonics. A likely reason for this is that strike-slip features are not easily recognized on seismic images, as they are characterized by complex vertical and horizontal geometries that change rapidly along strike and with depth (Sylvester, 1988; Mann, 2007; Dooley and Schreurs, 2012). Often, strike-slip movements are recognized when observed geometries, both structural and stratigraphic, can't be solely explained with extensional and compressional tectonics. For instance, Late Permian dextral strike-slip movements were recognized in the southern North Sea area due to systematic lateral displacements of alluvial fan systems along NW-SE striking faults (George and Berry, 1997). These observations fit within a regional framework of wrench tectonics that is widely accepted for the Permian and Late Carboniferous interval (Ziegler, 1990a; Mattern, 1996; Lamarche et al., 2002; Ziegler, 2004). Strike-slip movements have also been recognized in the Dutch subsurface when older fault trends are systematically being offset, when profound flower structures are present or when local zones of transpression and transtension are present. The latter observations have led to a number of strike-slip features that are related to Late Cretaceous/Early Paleogene inversion.

However, during the majority of the Mesozoic period; i.e. Triassic, Jurassic and Early Cretaceous periods, strike-slip movements have been barely recognized. During this time, the southern North Sea region underwent several active rifting pulses in an overall extensional setting. Normal movements are indeed dominant during this time period in the southern North Sea area. However, the formation of dominant structural trends such as the WNW-ESE to NW-SE alignments and possibly also the N-S alignment preceded the Mesozoic rifting phases as they originate from the Paleozoic Variscan or even Caledonian orogenies. This means that these trends were reactivated during the Mesozoic; initially by roughly E-W oriented extension in the Triassic and later by roughly NE-SW extension during the Upper Jurassic and Early Cretaceous (Munsterman et al., 2012). Hence, some of the older fault systems were oriented almost parallel to the direction of extension, making it highly plausible that they have accommodated strike-slip movements, thereby linking the normal movements in the active rifting basins and functioning as transform faults (Kley et al., 2008b). Some direct evidence of strike-slip motions along these preformed basement faults is present in the Dutch offshore; for example, the en enchelon pattern of the Rifgrunden fault zone bounding the Terschelling basin which indicates that it has accommodated dextral strike-slip movements (De Jager, 2007). Usually though, direct evidence of Mesozoic strike-slip movements on preformed basement faults is absent, likely because of the complex reactivation history of the faults and because of the presence of a thick layer of remobilized Zechstein salt. Also the timing and amount of displacement on these preformed basement faults is poorly constraint. Additionally, supra salt Mesozoic strike-slip motions in the northern Dutch offshore are often neglected or poorly understood in terms of timing, sense and amount of displacement and fault salt interaction.

Hence, the main aim of this study is to gain better insight into several strike-slip features in the northern Dutch offshore during the Mesozoic (see fig. 4 for the outline of the wider study area). To achieve this, the following research questions are addressed in this study;

- Where are Mesozoic strike-slip faults located in the northern Dutch offshore?
- What is the timing, sense of displacement and amount of displacement of the identified strike-slip faults in the Northern Dutch offshore?
- How are strike-slip motions on subsalt preformed basement faults distributed into the supra salt interval in a salt-dominated basin?
- Are the identified strike-slip faults linked to deeper rooted basement faults?

To answer these research questions, this study consists of the following parts;

1) Regional identification of strike-slip faults at various Mesozoic stratigraphic levels in the northern Dutch offshore, based on literature and regional seismic interpretation.
2) Four in depth case studies of strike-slip faults in the Northern part of the Dutch offshore via detailed 3D seismic interpretation by making use of stratigraphic thickness maps and seismic attribute maps
3) Analogue Modelling performed at the Tectonics lab of Utrecht University on strike-slip faults and their interaction with salt. The aim of this part is to learn more about the distribution of strike-slip faults along preformed basement faults in a salt dominated basin.
4) The integration and interpretation of the results of part 1,2 and 3.

2. Background

In this section, some research background will be given regarding the geological history of the Northern Dutch offshore (section 2.1), the main stratigraphic groups (section 2.2), as well as the main structural elements encountered in the research area (section 2.3). Additionally, previous work on strike-slip tectonics in the Dutch subsurface will be discussed in section 2.4. Finally, some relevant findings from extensional and strike-slip analogue models including a weak layer to represent salt, will be discussed in section 2.5. These sections will allow the reader to better understand and appreciate the present research, which methods will be described in section 3.

2.1 Geological history of the Northern Dutch Offshore

In the following sections, a general geological history of the Northern Dutch offshore is given in the wider context of the southern North Sea area that developed as part of the Central European Basin (CEB) system. The main tectonics events that have affected the geological evolution of the Terschelling Basin are (Ziegler, 1990; Geluk, 2005):

- The Paleozoic Caledonian and Variscan orogenies
- An Early to Middle Permian phase of wrench tectonics
- Mesozoic rifting phases
- Alpine inversion phases

2.1.1 Paleozoic

Several compressional tectonic phases occurred in the present Southern North Sea Area during the Paleozoic. These compressional tectonic phases were caused by the convergence of a number of tectonic plates including; Baltica, Laurentia, Gondwana and the microcontinent of Avalonia.

At first, during Ordovician to Silurian times, Baltica and Laurentia collided, subsequently forming the continent of Laurussian. A few million years later, the Gondwana-derived Avalonia microcontinent, which included the stable London Brabant Massif, collided with the southern edge of Baltica. Due to this collision, Avalonia was incorporated into the Laurussian continent. Both events are generally known as the Caledonian orogeny (Ziegler, 1990b). A recent study suggests that the suture zone between Baltica and Avalonia is located in the subsurface of the Netherlands; trending NW-SE (Smit *et al*., in press). This implies that the basement crust in the southern part of the Netherlands is derived from the Avalonia continent, wile the basement rocks in the northern part of the Netherlands is derived from the Laurussian continent. After the formation of the Laurussian continent, which was now composed of Avalonia-, Laurentia- and Baltica derived continental fragments, the Iapetus Ocean between Gondwana and Laurussia gradually closed. During the Early Carboniferous, the Iapetus Ocean had fully closed due to ongoing subduction underneath the Laurussian continent. The subsequent full-scale collision resulted in the Himalaya type Variscan orogeny, towards the south of the current North Sea area (Geluk, 2005; De Jager, 2007). The most northern position of this Variscan fold and thrust belt runs approximately W-E through Belgium, and central Germany, just south of the Netherlands (De Jager, 2007). No evidence of Variscan compressional tectonics is found in the southern North Sea Area. Instead, the Southern North Sea area, including the Northern Dutch offshore, developed as a foreland basin during the Late Carboniferous. Thick Carboniferous sequences of the Limburg Group were deposited in this foreland basin, locally exceeding 5500m in the northern Dutch offshore area (Ziegler, 1990a). These deposits are often characterized by large amounts of organic material, as the Southern North Sea area was located just south of the equator during this time.

Towards the very end of the Carboniferous, the tectonic regime in the Carboniferous foreland basin changed, as the area was affected by post-orogenic collapse of the Variscan orogeny and associated wrench tectonics caused by ongoing crustal shortening in the Uralian and Appalachian domains (Ziegler, 1990a; Geluk, 2005; De Jager, 2007) These wrench tectonics led to transtensional faulting,

which was accompanied by intrusive and extrusive magmatic events and subsequent thermal uplift during the Early and Middle Permian. Faults that were active during this period, particularly show a NW-SE to WNW-ESE lineament in the Southern North Sea area (Ziegler 1990a; Schek-Wenderoth and Lamarche, 2004; Schroot and De Haan, 2003; Van Duin *et al*., 2006). However, the NW-SE strike of the Avalonia-Baltica suture zone might indicate that this approximate NW-SE alignment was already established during the Caledonian orogeny. The thermal uplift caused by the Early to Middle Permian heating event caused widespread and deep erosion in the southern North Sea area, leading to significant hiatus of 60 to 70Ma. This hiatus is commonly known as the Saalian erosional phase in its broader sense (Ziegler, 1990a; Geluk, 2005; de Jager, 2007). Towards the end of the Permian, the lithosphere of the Southern North Sea area had cooled down again and consequently began to subside. This subsidence due to thermal sag led to the formation of a large E_W trending basin that stretched from current Great Britain to Poland, commonly known as the Southern Permian Basin (Fig. 1)(Bachman and Kozur, 2003 Geluk, 2005; van Wees *et al*., 2000; de Jager; 2007). Towards the end of the Permian, the southern North Sea area had moved out of the equatorial zone and was now located around 20degrees north, where arid conditions prevailed (Geluk, 2005). Sediments of the Rotliegend Group were deposited in this arid environment. Because subsidence rates exceeded sedimentation rates, the area became landlocked (Ziegler, 1990a). During the Late Permian, seawaters invaded the landlocked basin episodically, leading to the cyclic deposition of the evaporites of the Zechstein Group (Geluk *et al.,*2007).

2.1.2 Mesozoic and Cenozoic

During the end of the Early Triassic, continental break-up of the Pangea super continent initiated in the North Atlantic (Ziegler, 1990b). A branch of this rift system extended southward into the current southern North Sea area and caused E-W rifting during the Middle and Late Triassic (Ziegler, 1990a; Ziegler, 1990b; Kockel, 1995; Geluk, 2005). Several rifting pulses occurred in the southern North Sea area during this time period. Each rifting phase was preceded by a thermal heating event and initial uplift, leading to several regional unconformities such as Hardegsen unconformity and the Early Kimmerian unconformity. After each rifting phase, a period of tectonic quiescence followed due to regional thermal subsidence. The biggest tectonic pulse though occurred during the Middle Jurassic (158-154Ma) (Ziegler, 1990a; van Duin *et al*., 2006). During this time, thermal doming related to mantle plume activity caused widespread uplift and subsequent erosion in the southern North Sea area, leading to the formation of the Mid-Kimmerian unconformity. This heating event was followed by a period of NE-SW extension during the Upper Jurassic and Lower

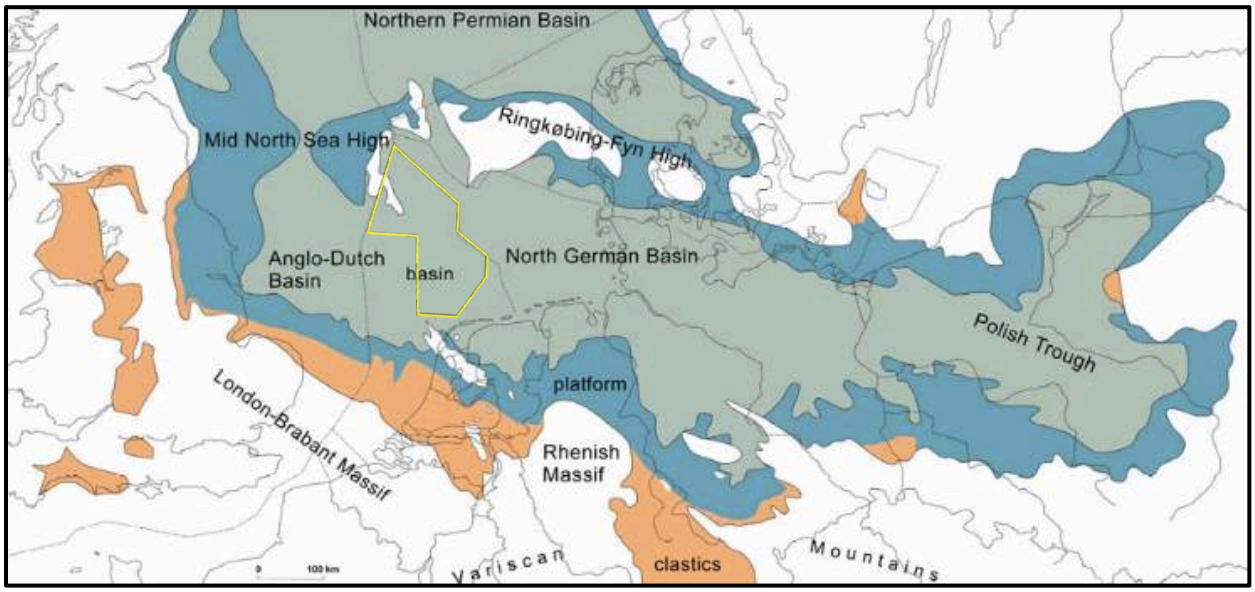

Fig.1. Map showing the Southern Permian Basin during the end of the Permian. White areas indicate crystalline Massifs, proximal areas are indicated in orange, green and blue indicate the outline of the distal part of the Southern Permian Basin. The research area of this study is indicated in yellow. Figure from Geluk, 2005.

Cretaceous in the southern North Sea area, forming new NW-SE faults but also reactivating older fault trends. Crustal extension was accommodated over a broad area, but most extension was created in the structural lows such as the Terschelling Basin and West Netherlands Basins, which subsided significantly due to their preformed basement structures that were favorable for reactivation by NE-SW extension. Additionally, significant subsidence occurred in the Dutch Central Graben during this time period. The basins were filled during the Upper Jurassic with detritic material that was derived from the rift shoulders. Towards the Middle Cretaceous, the North Atlantic had opened and active Mid-Oceanic spreading took place in this area. As a consequence, crustal extension focused in the North Atlantic and active rifting waned in the southern North Sea area (Ziegler 1988,; 1990a; van Duin, 1996; De Jager, 2007). Because of thermal subsidence, though, the southern North Sea area continued to subside during the Middle and Late Cretaceous. As subsidence proceeded, depositional conditions gradually changed and over time the North Sea area evolved into a large open shallow marine basin (Ziegler, 1988; 1990a). During the early part of the Late Cretaceous, continental fragments of the African and Arabian lithosphere began to collide with Eurasia. This convergence led to the formation of the Alpine orogenic belt (de Jager, 2007). As convergence proceeded into the Late Cretaceous and Early Paleogene, compressional stresses from the Alpine convergence were increasingly transmitted into the Alpine foreland, including the Southern North Sea area, thereby reactivating older Variscan and Mesozoic faults and causing inversion tectonics (van Duin, 2006; De Jager, 2007). Inversion during this time is believed to have occurred during distinct pulses, of which the Laramide, Pyrenean and Savian inversion pulses were the most important (De Jager, 2007). Generally though, the Southern North Sea area continued to subside throughout the Cenozoic due to thermal subsidence. During the Neogene sedimentation rates increased, as large westward prograding deltaic systems deposited large amounts of sediments, derived from the Fennoscandian and Baltic shields, in the Southern North Sea area (Verweij, 2003; De Jager, 2007).

2.2 Stratigraphy

In this section, the most important stratigraphic groups in the northern Dutch offshore will be described. The stratigraphy in this section and in this report is based on the classification from Adrichem Booger and Kouwe (Fig. 2) (1993-1997). Where later revision has been applied on the stratigraphy, the concerning study is mentioned.

Limburg Group (DC)

The sediments of the Limburg Group comprise the Upper part of the Carboniferous. Sediments in the Limburg group are predominantly of siliciclastic and organic origin. The strata were deposited in the Variscan foreland basin (Kombrink, 2008). The Limburg Group is particularly known for its vast and good quality coal bearing formations, which also function as gas source rock in the northern onshore and offshore Netherlands.

Upper Rotliegend Group (RO)

Sediments of the Upper Rotliegend Group unconformably overlie sediments of the Limburg Group, separated by the Saalian Unconformity. Sediments in this stratigraphic group are mainly composed of siliclastic sediments. Towards the basin margins, thick sandstone sequences were deposited, while argillaceous material was deposited in the basin center.

Zechstein Group (ZE)

The Zechstein Group mainly comprises evaporitic deposits, of which halite is predominant. The evaporites precipitated in several cycles during the time that the Southern Permian Basin became landlocked. Estimates of its original depositional thickness vary from 650m (Verweij and Witmans, 2009) to 1500m (MSc. Thesis van Winden, 2015).

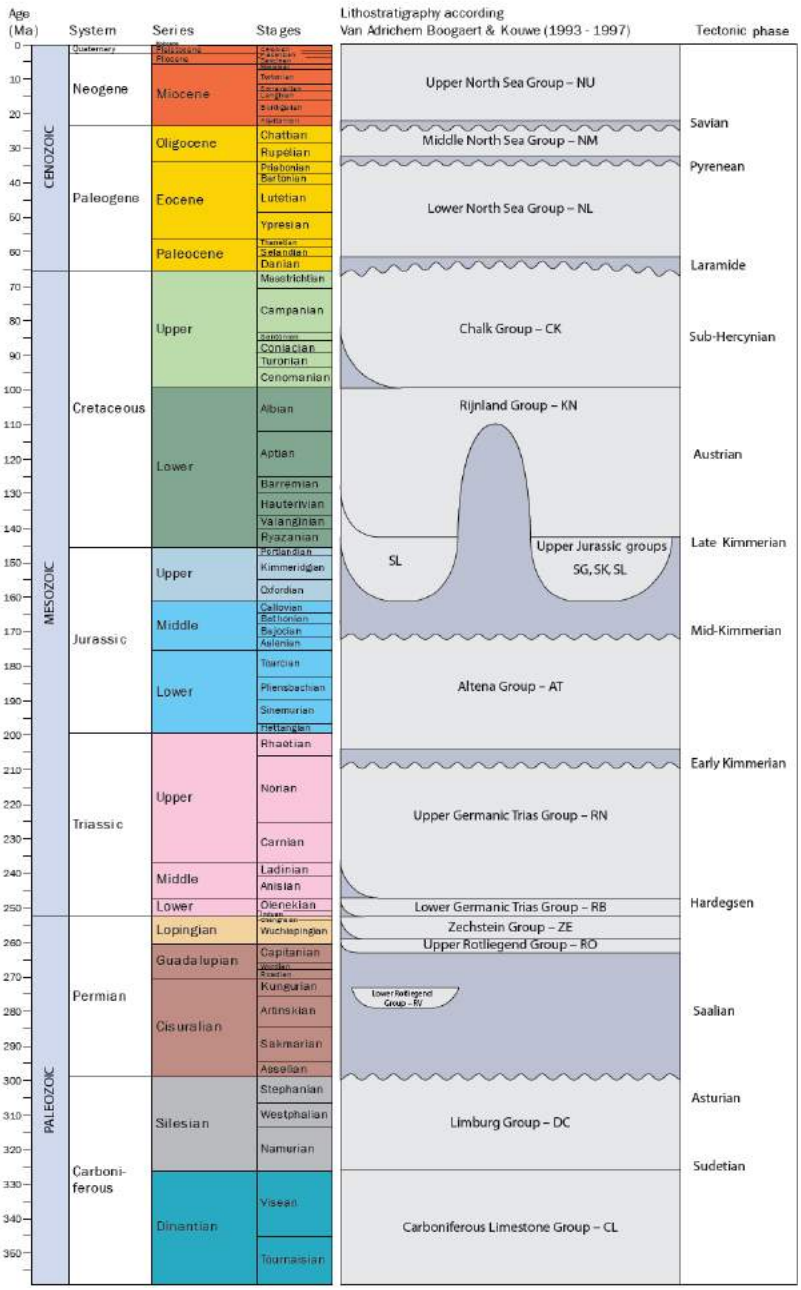

Fig.2. Schematic stratigraphic diagram of the Dutch subsurface, indicating the main stratigraphic groups according to van Aadrichem Boogaart and Kouwe (1993-1997)

Lower Germanic Trias Group (RB)

The Lower Germanic Trias Group is comprised of sandstone and shale alternations. The sandstones of the Lower Germanic Trias Group are known for their good reservoir qualities and contain sufficient amounts of gas in the Dutch offshore, especially in the relatively thick and widespread Lower Volpriehausen sandstone formation. The sediments of the Lower Germanic Trias Group were deposited in a dry and hot environment that was characterized by endless flat plains where ephemeral braided streams and temporal lakes formed after occasional rains (Van der Zwan an Spaak, 1992)

Upper Germanic Trias Group (RN)

The Upper Germanic Trias Group comprises sediments of the Solling, Rot, Muschelkalk and Keuper formations. These formations are mainly comprised of evaporites and argillaceous sediments. In contrast to the sediments from the Lower Germanic Trias Group, these sediments were deposited in a marine environment that became landlocked several times.

Lower Jurassic Altena Group (AT)

The Altena Group comprises marine argillaceous sediments that were deposited during a period of Lower Jurassic quiescence during which the area of the northern Dutch offshore was gradually subsiding. During the latest part of the Lower Jurassic, closed and anoxic marine conditions due to Mid-Kimmerian uplift led to the deposition of the bituminous rich Posidonia shale formation in the Dutch Central Graben. This Mid-Kimmerian uplift and subsequent erosion are also the reason that the Altena Group has only been preserved in the Dutch Central Graben, the West-Netherlands basins and the Lower Saxony Basin.

Upper Jurassic Schieland (SL) and Scruff Group (SC)

The Upper Jurassic is characterized by a complex stratigraphic sequence comprising open marine, continental and various types of near shore deposits. The first characterization of Upper Jurassic sediments was made by Van Adrichem Boogaert and Kouwe (1997). The last few years, more data

has led to a better understanding of this complex stratigraphic interval. The Stratigraphic definitions adhered in this report are based on the new insights and definition as described by Abbink *et al*., 2006 and Munsterman *et al*., 2012 who classified the Upper Jurassic into 3 sequences (Fig. 3);

- Sequence 1 is the stratigraphic equivalent of the Schieland Group and is divided into 6 formations (fig. 4), which are generally characterized by Fluvio deltaic, near shore and marginal marine conditions. The following formations were recognized in case study B;
    - Lower Graben Formation, comprises fluvio-deltaic and coastal plain deposits
    - Middle Graben Formation, comprises lacustrine to marginal marine deposits
    - Upper Graben Formation, comprises marginal marine and barrier island deposits
    - Puzzle Hole Formation, comprises lower deltaic plain deposits as well as lagoonal, estuary and various types of near shore deposits. Due to this wide variety of deposits and continental signature with various channels providing the system with clastic input, the puzzle hole formation is characterized by a distinct slightly chaotic seismic response of high amplitude reflectors.
- Sequence 2 is the stratigraphic equivalent of the Scruff Group. In the northern part of the Dutch Central Graben, this sequence comprises the relatively deep marine sediments of the Kimmeridge Clay Formation. Further towards the south, coarser material was deposited in more lagoonal and near shore conditions, including the sands of the Terschelling Sandstone Member and the Noorvaarder Member.
- Sequence 3 mainly comprises marine deposits that are predominantly composed of shales. Altough some sandstone intervals due occur.

Where possible, individual formations are indicated in this report(fig. 3), otherwise the Jurassic sequences 1, 2 and 3 are used for the interpretation of the seismic sections in this report.

Rijnland Group

Sediments of the Rijnland Group were deposited during the very end of the Late Jurassic (fig. 3) as well as during the Early Cretaceous. Sediments were deposited in open marine conditions. Sediment types include shales and marls. Especially at the base of the Rijnland Group, some sandstone intervals occur as well.

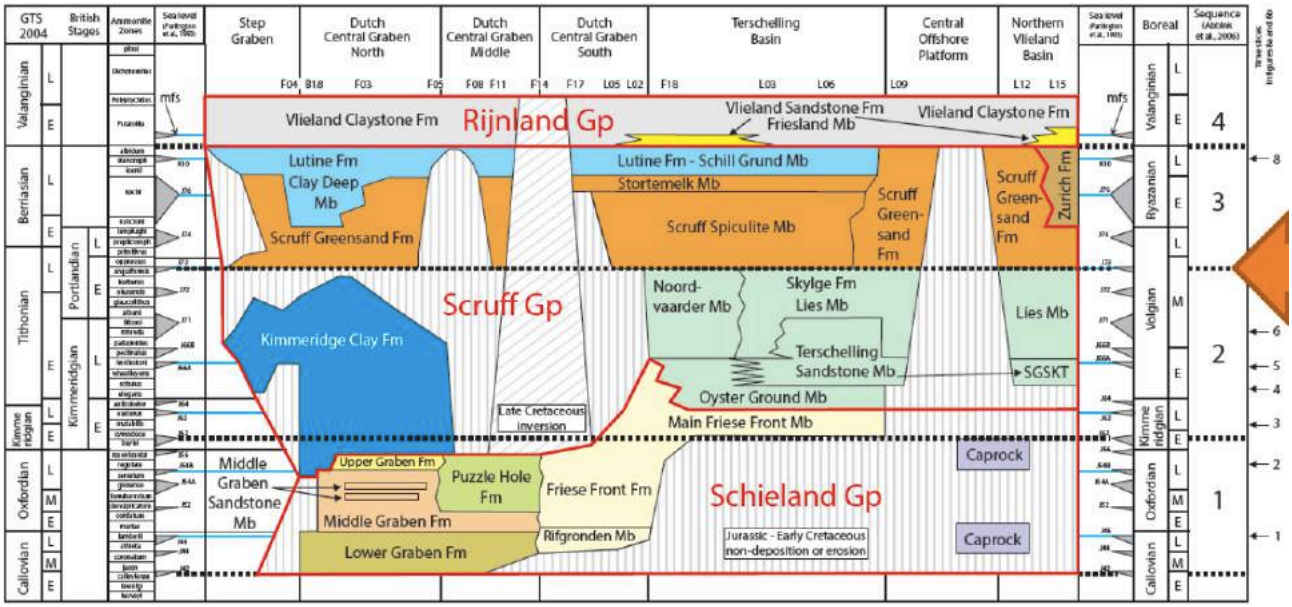

Fig.3. Stratigraphic diagram of the Upper Jurassic interval for the Northern Dutch offshore. Indicating the main stratigraphic groups, as well as the formations in which they are subdivided. Figure from Munsterman et al., 2012.

Chalk Group

The Chalk Group comprises sediments of the Late Cretaceous and is mainly composed of carbonate successions that were deposited in a clear shallow marine environment. Deposition was of this stratigraphic group was often controlled by inversion tectonics.

Cenozoic sediments of the Lower-, Middle-, and Upper- North Sea Groups

Sediments in these groups were mostly deposited during shallow marine conditions and are characterized by prograding deltaic sequences that transported material from the Baltic and Fennoscandian shields towards the southern North Sea area. Sediment types include clays, silts and sands.

2.3 Structural elements in the Northern Dutch Offshore

The Dutch subsurface is divided in a number of regions based on stratigraphic similarities (fig. 4) (Heybroek, 1974; van Wijhe, 1987; van Duin *et al*., 2006; Kombrink *et al*., 2012). Three types of these structural elements exist; basins, platforms and highs. The term basin is applied for areas that are bounded by large normal/reverse faults and where at least Upper Jurassic strata have been deposited and preserved (van Duin *et al*., 2006; Kombrink *et al*., 2012). The term platform is used for areas where Late Kimmerian uplift and subsequent erosion has removed all of the Jurassic strata and parts of the Triassic strata. Permian strata have been preserved entirely on the platforms (van Duin *et al*., 2006; Kombrink *et al*., 2012). The term highs is used to describe areas where Late Jurassic uplift was strongest and where erosion has taken place down into Permian and Carboniferous strata (van Duin *et al*., 2006; Kombrink *et al*., 2012). Based on this classification scheme, which was first proposed by Heybroek (1974) and revised by Kombrink *et al*. (2012), the structural elements appear to be of Mesozoic origin. However, the major fault trends that are present in the subsurface of the Netherlands are of Variscan and possibly Caledonian origin. Hence, it is likely that the outline of the structural elements already formed before the Mesozoic. Nevertheless, the classification of the structural elements as redefined by Kombrink *et al*., (2012) is adhered in this study because it immediately tells something about the deformation history of a region in terms of subsidence, faulting, uplift and erosion. In the following subsections, the main structural elements of the Northern Dutch offshore are briefly described.

Dutch Central Graben

The Dutch Central Graben is bounded in the east and in the west by roughly N-S trending faults. The base of the Zechstein Group increases gradually towards the north, where it lies deeper than anywhere else in the Dutch subsurface. The major opening of the Dutch Central Graben occurred in the Middle and Upper Triassic due to E-W extension. However, thickness maps of the Rotliegend interval indicate that it was already a low before this major E-W rifting phase, probably even in the Carboniferous (Ziegler, 1990a; Geluk, 2005). In the Dutch Central Graben, the entire Upper Triassic, as well as Lower Jurassic interval is present. However, Late Cretaceous inversion and subsequent erosion affected especially the southern part of the Dutch Central Graben. Due to this inversion, Cenozoic deposits directly overlie deposits of the Upper Jurassic sequence 1 in the center of the inverted Graben (Fig. 3).

Terschelling Basin

The Terschelling Basin is bounded in the north by the ENE-WSW trending Rifgronden Fault Zone and in the south by the ENE-WSW trending Hantum Fault Zone (Fig. 4). These fault zones are of Variscan and possibly Caledonian origin and have been repeatedly reactivated during Mesozoic times. The base of the Zechstein gradually increases towards the west, in the direction of the Dutch Central Graben. The area was affected by E-W extension, as is indicated by the presence of Upper Triassic low angle detachment and growth faults. However, the lack of major movements on N-S basement trends suggest that most of the E-W extension was accommodated in the Dutch Central Graben. During the Upper Jurassic, the Terschelling basin accommodated more extension as the HFZ

and RFZ were reactivated by the now NE-SW oriented stress regime. In the Terschelling Basin, Mid Kimmerian uplift and subsequent erosion has removed the Lower Jurassic strata as well as part of the Upper Triassic strata. Upper Jurassic strata of sequences 2 and 3 are deposited and preserved in the Terschelling Basin.

The Cleaverbank Platform, Elbow Spit platform and Elbow Spit High

This structurally high region is located west of the Dutch Central Graben and Step Graben and is part of the larger Mid North Sea High that stretches towards the northwest, into UK territorial waters (Fig. 4). On the Elbow Spit platform and Cleaverbank platform, Upper Cretaceous strata directly overlie Upper Triassic or Permian strata. On the Elbow Spit High, Upper Cretaceous strata directly overlie Carboniferous or locally even Devonian rocks. This area has likely been a high throughout the geological history, which has been attributed to the existence of a lower Devonian magmatic body, causing the crust to be relatively buoyant here (Donato *et a*l., 1983)

The Schill Grund platform and Central Offshore Platform

The Schill Grund Platform and Central Offshore platform bound the Terschelling Basin towards the north and the south (Fig. 4). On these platforms, Lower Cretaceous rocks overlie Lower Triassic rocks or locally Upper Triassic rocks. These areas have been affected by thin skinned extension during the Upper Triassic as is indicated by a zone of roughly N-S trending low angle detachment faults that developed above salt rollers and have accumulated thick sequences of Upper Triassic strata.

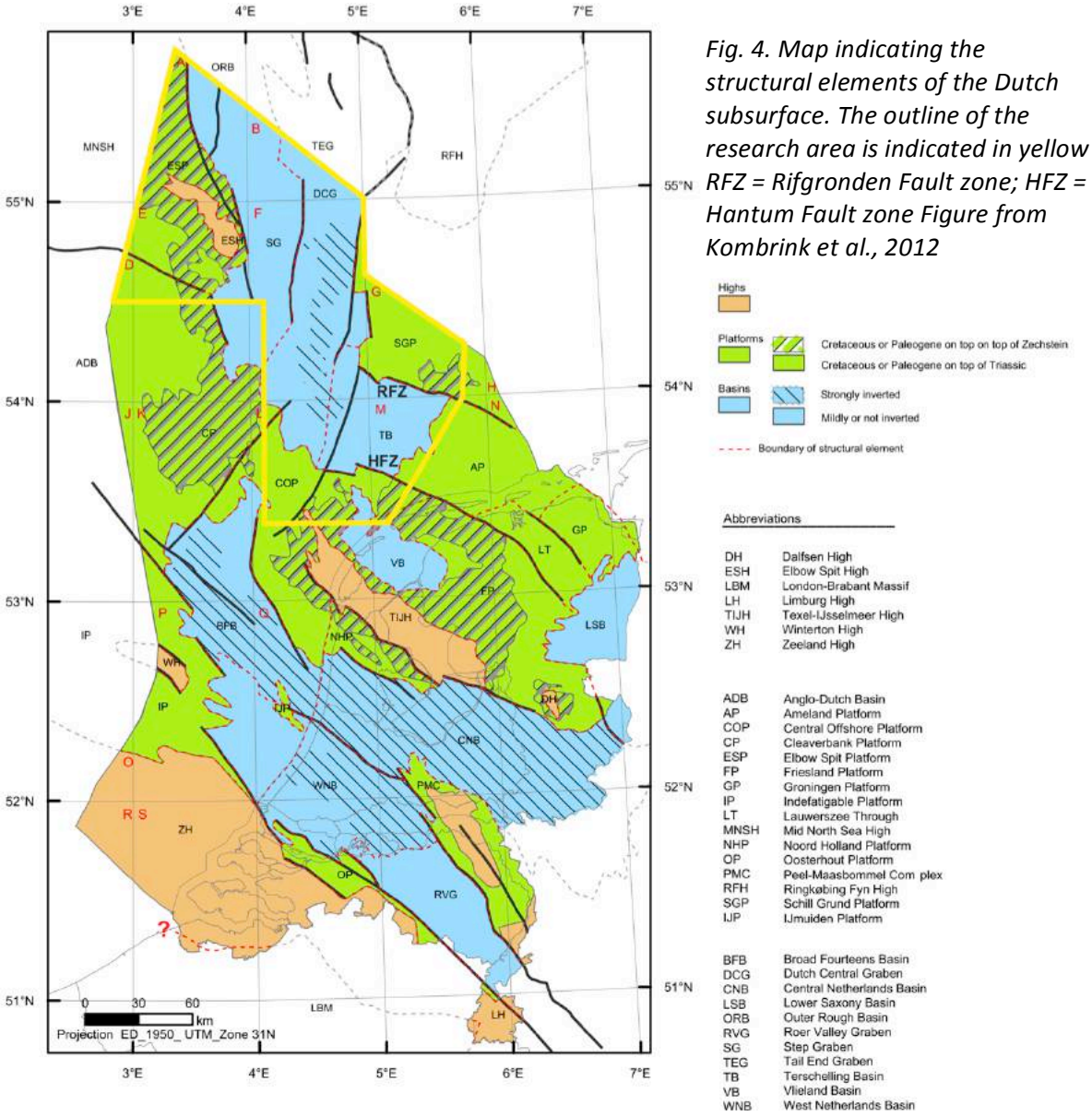

Fig. 4. Map indicating the structural elements of the Dutch subsurface. The outline of the research area is indicated in yellow RFZ = Rifgronden Fault zone; HFZ = Hantum Fault zone Figure from Kombrink et al., 2012

2.4 Strike-slip tectonics in the Dutch offshore; *What is known?*

Although often overlooked or disregarded, some strike-slip motions have been recognized in the Dutch subsurface. This section summarizes some of the previous work that has been done on strike-slip tectonics in the Dutch subsurface.

2.4.1 Late Paleozoic wrench tectonics

The first episode of strike-slip faulting that is recognized in the Dutch subsurface are the Late Carboniferous to Early Permian wrench tectonics (Ziegler, 1990a; Geluk, 2005; Gast and Gundlach 2006). With the term wrench is meant that deformation occurred in a zone of overall strike-slip and extension (transtensional) movements. These wrench tectonics are believed to have been caused by ongoing crustal shortening in the Urals and the Appalachians, creating a dextral mega-shear system that accommodated these motions in the present Southern North Sea area (Arthaud and Matte, 1977; Ziegler, 1990a). This wrench model for the early Permian is supported by the presence of small pull-apart basins were early Permian sediments were deposited in the Elbe fault system as well as close to the Teisseyre-Tornquist zone (Kiersnowski and Buniak, 2006). Additionally, the en echelon pattern of sub-basins that developed in the Southern Permian Basin area during the Early and Permian favors this tectonic model. In the Dutch and in the UK sectors of the southern north sea, strike slip-motions as part of the regional wrench tectonic system are indicated by the presence of early Upper Rotliegend fans that display a systematic lateral displacement along synsedimentary faults (George and Berry, 1997). George and Berry (1997) concluded that the systematical rejuvenation trend of these fans indicates that dextral faults were active during deposition of these fans along NW-SE trends in the Southern North Sea area (Fig. 5). More recently, an internal TNO project has revealed a SE-NW trending fault in the northern Dutch offshore as well (de Bruin et al, 2015). The vertical geometry of this fault, its upward widening fault pattern and the concave upward bending of strata on either side of the fault plane indicate that this fault accommodated strike-slip motions. The thickening of Upper Rotliegend strata in the downthrown side of the fault, has led to the conclusion that this fault was active during deposition of the Upper Rotliegend.

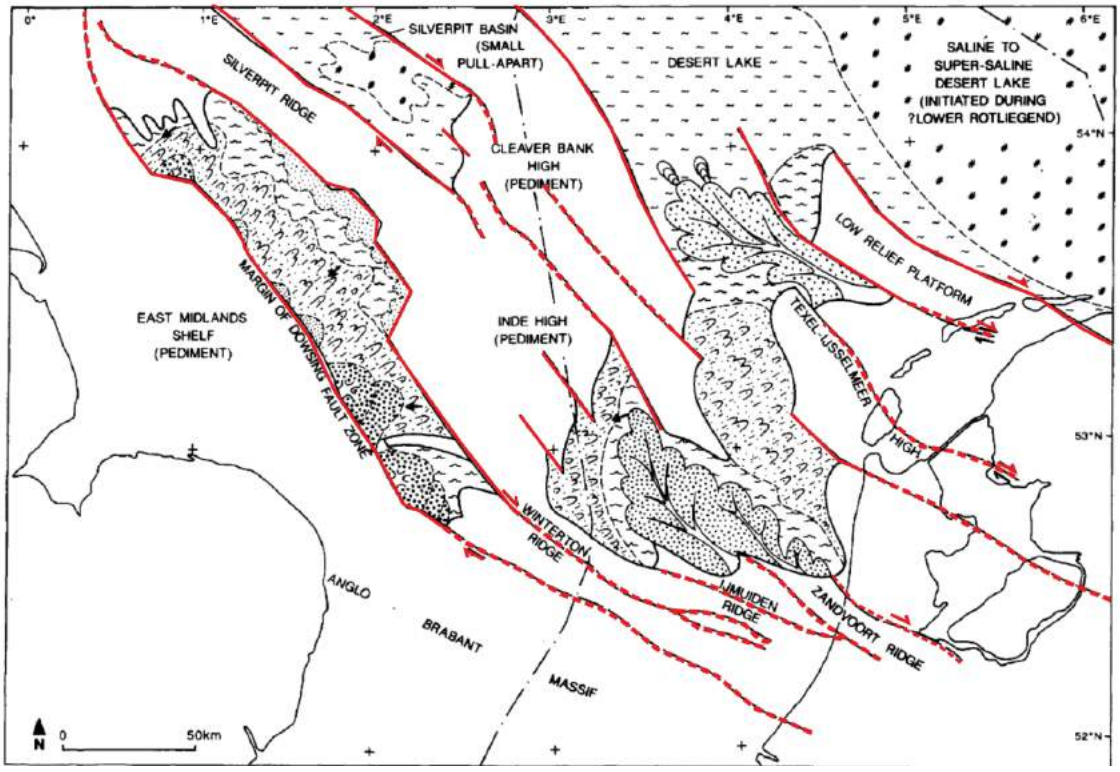

Fig. 5. Interpretation of the Upper Rotliegend depositional environment by George and Berry (1997) According tot his model deposition of alluvial and detaic fan deposits were influenced by dextral strike-slip faults during the Early part of the Upper Rotliegend. Figure from George and Berry (1997)

2.4.2 Mesozoic strike-slip movements in an extensional regime

While the transtensional tectonic model is widely accepted for the Upper Carboniferous and Rotliegend interval, strike-slip movements in the Mesozoic have not been recognized extensively in the Southern North Sea Area as it is commonly accepted that regional pulses of extension prevailed during this time period. However, according to the regional tectonic model for the Central European Basin system from Kley et al., 2008, strike-slip faults also occur in an overall extensional setting to accommodate differential motions on preformed basement faults. Kley et al., (2008) state that the opening of a set of parallel grabens (including the Central Graben, Horn Graben and Glückstadt Graben in Fig. 6) during the Triassic must have led to strike-slip faults at the northern and southern edges of these grabens to accommodate the motions that resulted from the active rifting of these grabens. This tectonic model is supported by the presence of a series of en echelon faults towards the north of these four parallel grabens (indicated in red in Fig. 6). Additionally, strike-slip motions towards the south of these grabens could have been accommodated by Variscan inherited NW-SE trending faults (Kley et al., 2008), although direct evidence on these complex fault systems is not observed.

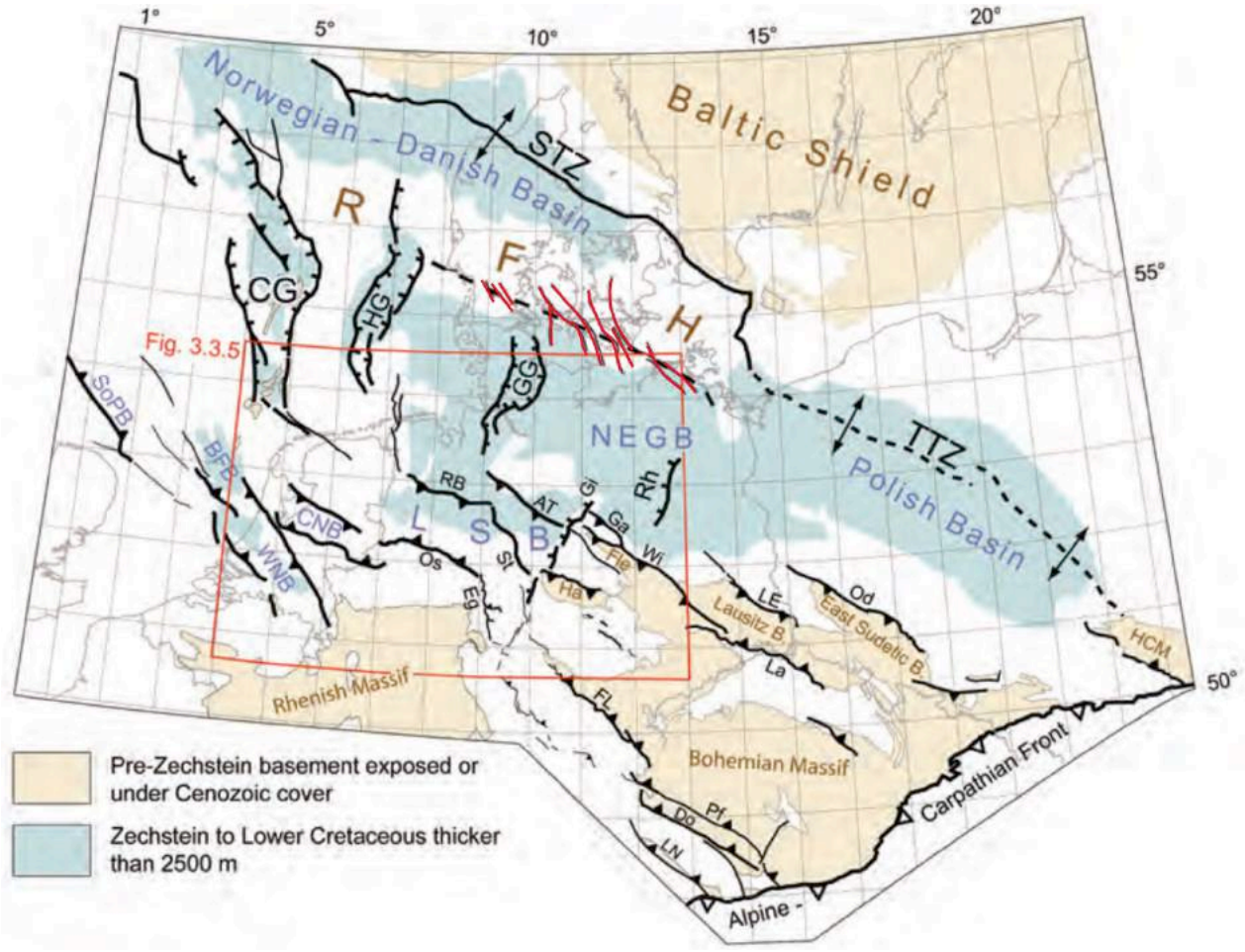

Fig. 6. Map showing the structural framework of the Central European Basin or Southern Permian Basin. Abbreviations are: Fault zones/structures (black): STZ Sorgenfrey-Tornquist Zone, TTZ Teisseyre-Tornquist Zone; CG, HG, GG Central, Horn and Glückstadt grabens, Rh Rheinsberg Trough; RB Rheder Moor-Blenhorst, AT Allertal, Gi Gifhorn, Ga Gardelegen, Wi Wittenberg, LE Lausitz Escarpment, La Lausitz Thrust, Od Odra, Os Osning, St Steinhuder Meer, Eg Egge, FL Franconian Line, LN Landshut-Neuötting, Do Donau, Pf Pfahl. Subbasins (blue): SoPB Sole Pit, BFB Broad Fourteens, WNB West Netherlands, CNB Central Netherlands, LSB Lower Saxony, NEGB Northeast German. Basement highs (brown): RFH Ringkøbing-Fyn High; Ha Harz, Fle Flechtingen High, B. "Block", HCM Holy Cross Mountains. Figure from Kley 2008b.

2.4.3 Late Mesozoic/Early Paleogene strike-slip movements in a compressional regime

During the Late Cretaceous and Early Paleogene Alpine inversion pulses , dextral reactivation along NW-SE fault trends in the Broad fourteens basin and in the West Netherlands Basin occurred due to N-S compression (Brun and Nalpas, 1996; Racero-Baene and Drake, 1996; De Jager, 2007). These strike-slip movements have been widely recognized, i.a. via flower structures that offset strata up to and including the Cretaceous interval. A well known example of a strike-slip formed hydrocarbon trap is the Pijnacker oil Field (Racero-Baene and Drake, 1996). In the Lower Saxony Basin, also the Schoonebeek Graben was inverted with a dextral component during this time period (MSc. Thesis Smoor, 2016).

2.5 Analogue modeling background on extension and strike-slip in the presence of a weak layer

Basins that contain a thick sequence of ductile substrates (e.g. evaporates or shales), tend to deform in a different way than basins that lack the presence of such a sequence (Hudec and Jackson, 2007). This can be attributed to the mechanical properties of salt, which are inherently different from siliciclastic and carbonate rocks. For instance, salt is incompressible which causes it to be less dense than its overburden. Additionally, salt has the tendency to flow under geological conditions, as it deforms visco-elastically (Spiers *et al*., 1990; Hudec and Jackson, 2007). This material behavior can be attributed to its mechanical weakness, which causes salt to decouple, or isolate the rock units above and below the salt in such a way that the deformation pattern of the two units differs (Vendeville and Jackson, 1992). The degree of similarity in the structural deformation style of the two units depends both on the thickness of the ductile layer, the rheology of the ductile layer and the rate of deformation (Vendeville and Jackson, 1992; van Keken *et al.*, 1993). Much of what we know today on the structural style of deformation in salt controlled basins comes from analogue modeling. Hence, some main findings from analogue models on the behavior of a weak layer in both an extensional and strike slip regime are described in this section.

2.5.1 Salt tectonics under extensional conditions

The ascent of salt and the subsequent formation of various kinds of salt structures had long been solely ascribed to density differences between the salt layer and the overburden that were assumed to be inherently unstable (i.a. Trusheim, 1960). According to this model, first described by Trusheim (1960), diapiric rise is a spontaneous process, triggered by Rayleigh-Taylor instabilities (similar to the ascent of a relatively dense fluid in a less dense fluid) and hence independent of regional tectonics. Supra salt extensional faulting was by these authors ascribed to be caused by the intrusion, withdrawal or dissolution of salt. In contrast to this, Vendeville and Jackson (1992) showed that salt diapirsm is in general triggered by regional tectonics. Under extension, salt diapirism occurs in response to regional thin skinned extension of the brittle overburden rather than vice versa. This thin-skinned extension can either be caused by regional crustal scaled extension or by gravitational gliding. Based on analogue modelling, Vendeville and Jackson (1992) extensively describe three stages of salt ascent in an extensional setting;

1) The Reactive stage; During this stage, salt ascents in response to normal faulting and associated graben formation in the overburden (fig. 7). Salt is able to do so because faulting decreases the thickness of the overburden, thereby making it mechanically weaker. Additionally, the thinning of the overburden creates differences in supra salt loading. Since the pressure at the top of the salt layer, caused by the overlying rock column is lowest at the point were the roof is thinnest. Salt will preferentially ascent at this place.
2) The Active Stage; when the graben above the salt becomes deeper than a certain threshold and the roof is sufficiently thinned; the diapir pierces through the remaining part of the overburden, thereby shouldering aside the remaining material. During this stage, the diapir will emerge at the surface. And may start to extrude when sedimentation rates are to low in order to keep pace with the ascent of salt.
3) The Passive Stage; When the accumulation of sediments around the diapir balances the net ascent of salt, the diapir is able to grow vertically due to the down building of sediments around the diapir. If regional extension continues, the diapir will also widen.

Regional sedimentation has a profound influence on salt ascent and the evolution of diapirism (Vendeville and Jackson, 1992; Scheffer, 2016). High rates of sedimentation during extension tends to fill the grabens created during thin skinned extension, thereby maintaining the strength of the overburden. Consequently, high rates of sedimentation keep diapirs longer in the reactive stage because the thin-skinned graben is filled with sediments. Vendeville and Jackson (1992) found in their analogue models that the ascent of diapirs could be stopped if sedimentation is fast enough to counteract the thinning of the overburden caused by extension.

Sedimentation doesn't only influence the ascent of salt, locally it is also controlled by the ascent of salt itself. (Trusheim, 1960; Vendeville, 2002). According to a reinterpretation of Trusheims model (1960) by Vendeville (2002), the initial thinning of strata towards a dipair, which is often observed in salt dominated basins, can be explained by a so called pillowing stage of the diapir. This pillowing stage (or reactive stage in the model from Vendeville and Jackson, 1992) leads to initial uplift of the area above the salt structure, causing the strata to thin towards the salt structure (Fig. 7.). When active piercement of the salt structure has occurred and the salt structure ascents passively, salt is withdrawn from the basal layer in the proximity of the salt structure, leading to subsidence around the ascending salt structure. This is a very effective way of increasing accommodation space around the salt structure and leads to the formation of a thick rim syncline around the salt structure (Vendeville, 2009; Harding, 2015). Overall, it can be concluded that the interplay between regional tectonics, rheological properties and sedimentation controls the exact structural style of deformation in salt dominated basins.

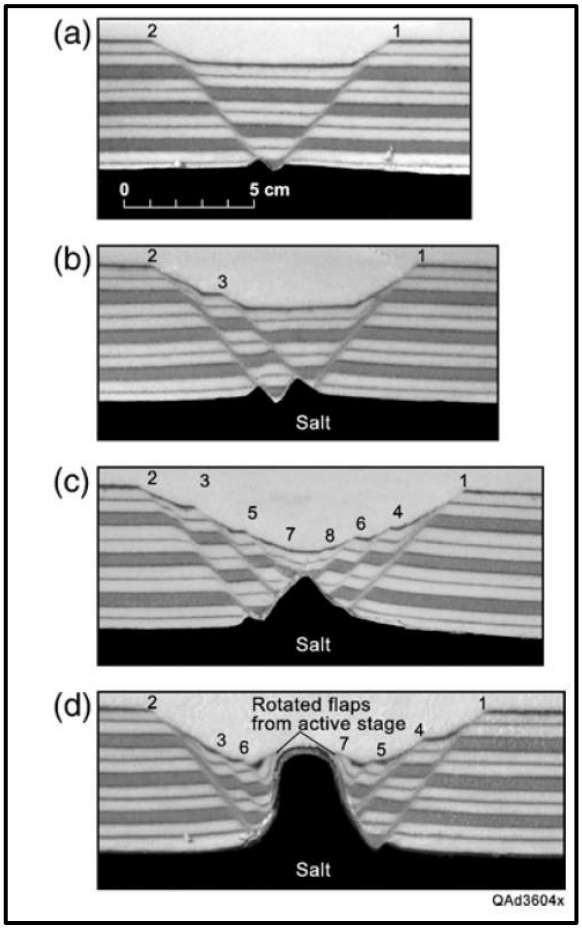

Fig. 7. Cross section through an analogue model indicating reactive- (A,B and C) and active (D) stage of salt ascent under regional extension. A) the first ascent of putty is triggered due to the thinning of its roof. This process continues in image B. C) The diapir is about to shoulder aside the overburden. D) the active stage of diapirism is reached. Figure from Hudec and Jackson, 2007.

Salt Rollers

If one supra salt graben fault during the reactive stage, accommodates more subsidence than the other one, an asymmetric salt structure, generally known as a salt roller, is formed (Fig. 8) (Bally *et al*., 1981; Brun and Mauduit, 2009). Such a structure is inherently asymmetric and when sufficient amounts of sediments are deposited, the salt will not reach the active diapir stage, but a listric growth fault will develop that detaches on the salt. When extension continues and sedimentation rates remain relatively high, a thick package of growth strata can develop in the hanging wall of the listric fault, thereby causing the pre-kinematic layer to drift away from its original position.

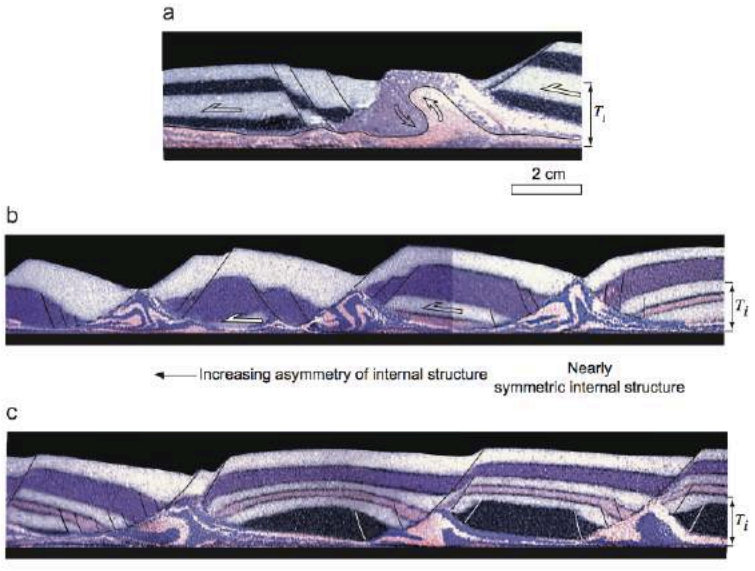

Fig. 8. Three images from salt rollers in analogue models. A) active diapir, not enough sedimentation and overburden relatively thin. B) Almost piercing salt structures underneath symmetrical (right) and asymmetrical (left) faulting. C) Asymmetric salt rollers with listric faults. Note the downlapping of strata in the hanging wall of the listric fault. Figure from Brun and Mauduit, 2009.

2.5.2 Salt tectonics under strike-slip conditions

Pure brittle strike-slip experiments

Strike-slip motions are characterised by complex 3D geometries, which rapidly change along strike, with depth and with continuous deformation. Due to their complex nature, and the difficulty of recognising strike-slip movements in seismic data, analogue modelling is a powerful tool that can help to better understand the structural evolution of strike-slip faults. The first strike-slip models investigated pure-strike-slip motions of a single brittle layer, underlain by a moving base plate. These experiments are generally known as the classic Riedel experiment (Riedel, 1929; Tchalenko, 1970; Richard *et al*., 1995). These Riedel experiments describe the subsequent formation of R-shears, splay faults and P shears into an anastomosing main displacement fault zone that accommodates strike-slip motions after significant amounts of base plate displacement (Fig. 9, 10). Various amounts of classic riedel experiments have been published using different brittle materials such as (wet) clay, sand and glass beds (Tchalenko, 1970; Atmaoui *et al.*, 2006) The formation of local zones of transtension and transpression has also been studied, this is generally done by adding a step in the base plate (i.a. Dooley, 1994; Smit, 2008a; Smit, 2008b). All of these experiments have been particularly useful to better understand the geometries and evolution of large strike-slip zones that form in the absence of an upper crustal weak layer.

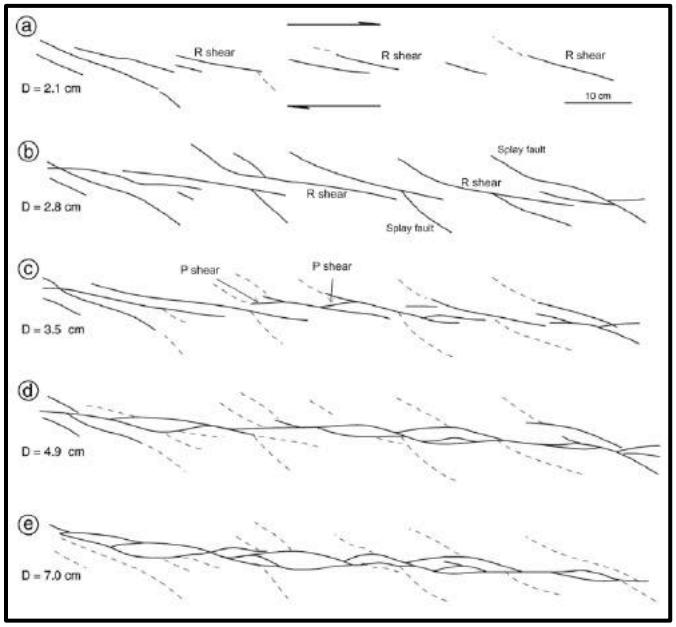

Fig. 9. Evolution of faults during a dry sand classic Riedel experiment. First R shears and splay faults form which are then subsequently linked by P shears to form anastomosing fault zone. Figure modified from Naylor et al., 1986

Multilayer strike-slip experiments

However, like in an extensional setting, the presence of an upper weak layer, such as an evaporite layer, has a profound influence on the style of deformation during strike-slip motions. Analogue models performed by Smit (2005) and by Dooley and Schreurs (2012) show that the presence of a weak body in the experiment causes either left or right stepping of the main displacement fault zone. Whether right or left stepping of the main displacement fault zone occurs, depends primarily on the initial geometry of the weak body with respect to the main displacement zone (Fig. 11). From Fig. 11 can also be inferred that the strike-slip faults deviate from their original strike as they approach the weak body, thereby showing a curved geometry towards the weak body. The right or left stepping of the main strike-slip fault at the weak body causes either transtension (right stepping on a dextral strike-slip fault or left stepping on a sinistral strike-slip fault) or transpression (left stepping on a dextral strike-slip fault or right stepping on a sinistral strike-slip fault) (Dooley and Schreurs, 2012). These zones of transpression or transtension, also trigger movements of the weak body. The strongest movements occur in zones of transtension, when the weak body is actively forced upwards. The weak body also ascents in zones of transtension, but here it ascents in a reactive way due to the thinning of its roof.

The weak layer used in the above described experiment from Dooley and Schreurs (2012) was placed in the experiment with a controlled and preformed outline and geometry. However, when a uniform weak layer is deformed by a pure strike-slip basement fault, no profound diapirs form. In this case, more subtle, appendix-like salt structures form in the weak layer (Appendix A; Smit,

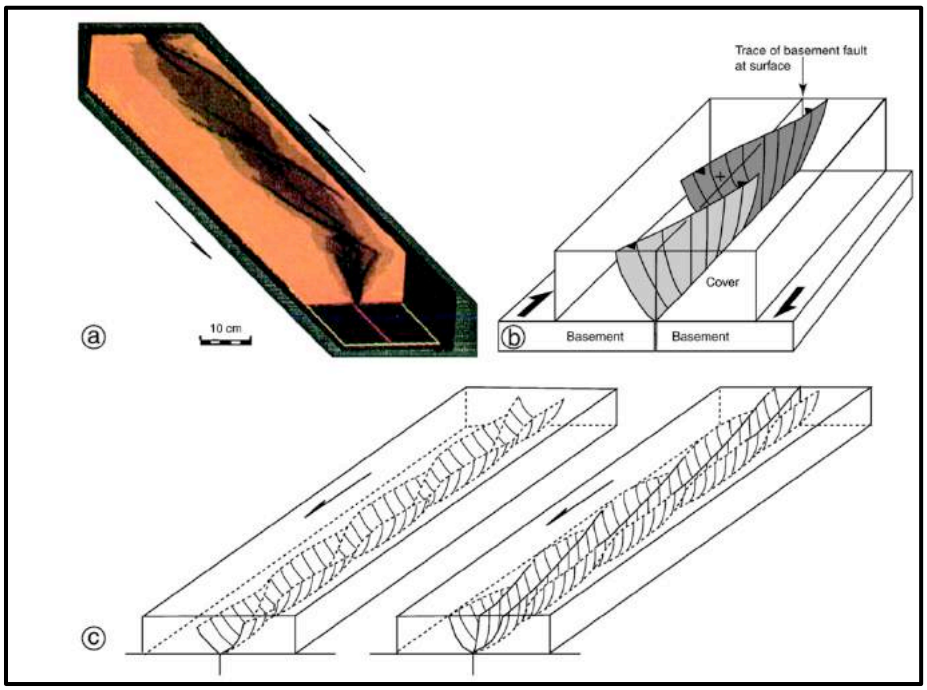

Fig. 10. Illustrating the curved concave upward geometry of R shears in a classic riedel experiment. The R shears are en echelon arranged at the surface but with depth they root into the basement strike-slip fault. Figure from Dooley and Schreurs, 2012.

2016). The geometry of these structures is much narrower and more arcuate than salt walls and diapirs that form under extensional settings as described in section 2.5.1 (Smit, 2016. Salt ascent of an initial homogenous layer does occur in a pull-apart basin, but this is caused by local extension within the basin and the salt structures that evolve therefore show similarities with the salt structures formed under pure extension (Smit, 2008b).

Multilayer experiments with multiple deformation phases

To study the role of pre-existing normal faults above a basal ductile layer, Dooley and Schreurs (2012) applied two deformation phases. First a graben was created during extension. During the second phase, strike-slip deformation was applied via distributed strike-slip at the base of the ductile layer. They authors found that the strike-slip faults during the second phase of distributed strike-slip preferentially followed the outline of the preformed normal faults during the extension phase (Dooley and Schreurs, 2012). In their experiments, the ductile layer was positioned at the base of the experiment to simulate the presence of a ductile lower crust. Due to the relatively high viscosity of the weak layer, no significant uplift of this weak layer occurred during the extension phase. Hence, the base layer of silicon putty largely remained its original thickness during the extension phase. Because the strength of ductile and brittle materials depends on the thickness of the material, the model performed by Dooley and Schreurs (2012) was not characterised by large internal strength contrasts.

In the current study, analogue models are presented that were deformed by the same deformation as the models from Dooley and Schreurs (2012). However, the models in the current study, are composed of an initially uniform high layer of ductile material (silicon putty), underlain by a brittle basement to simulate the presence of an upper crustal evaporite layer.

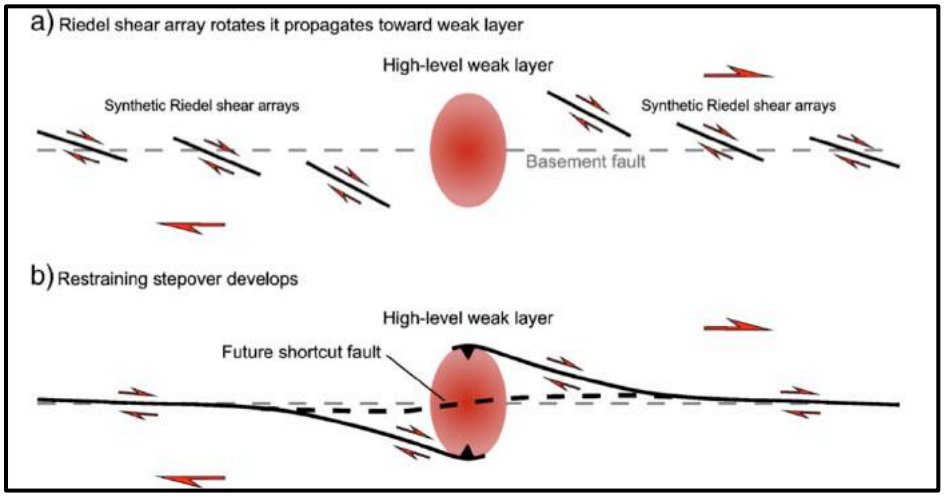

Fig. 11. Sketch illustrating the formation of a restraining step-over, over a high level weak layer. Note the rotation of the main strike-slip fault as it approaches the weak layer. Figure from Dooley and Schreurs, 2012.

3.1 Seismic interpretation methods

The seismic interpretation part of the study consists of two sections;

1) Identification of strike-slip faults in the northern Dutch offshore with the purpose of locating strike-slip features in the northern Dutch offshore.
2) 4 in to depth case studies of strike-slip faults in the Northern Dutch offshore with the purpose of gaining a better understanding of specific structures in terms of timing, sense of displacement, amount of displacement and fault-salt interaction.

3.1.1 Identification of strike-slip faults in the northern Dutch Offshore

The first section of the seismic interpretation part of this study is the identification of strike-slip faults in the northern Dutch offshore. For this purpose, multiple 3D seismic surveys and 2D

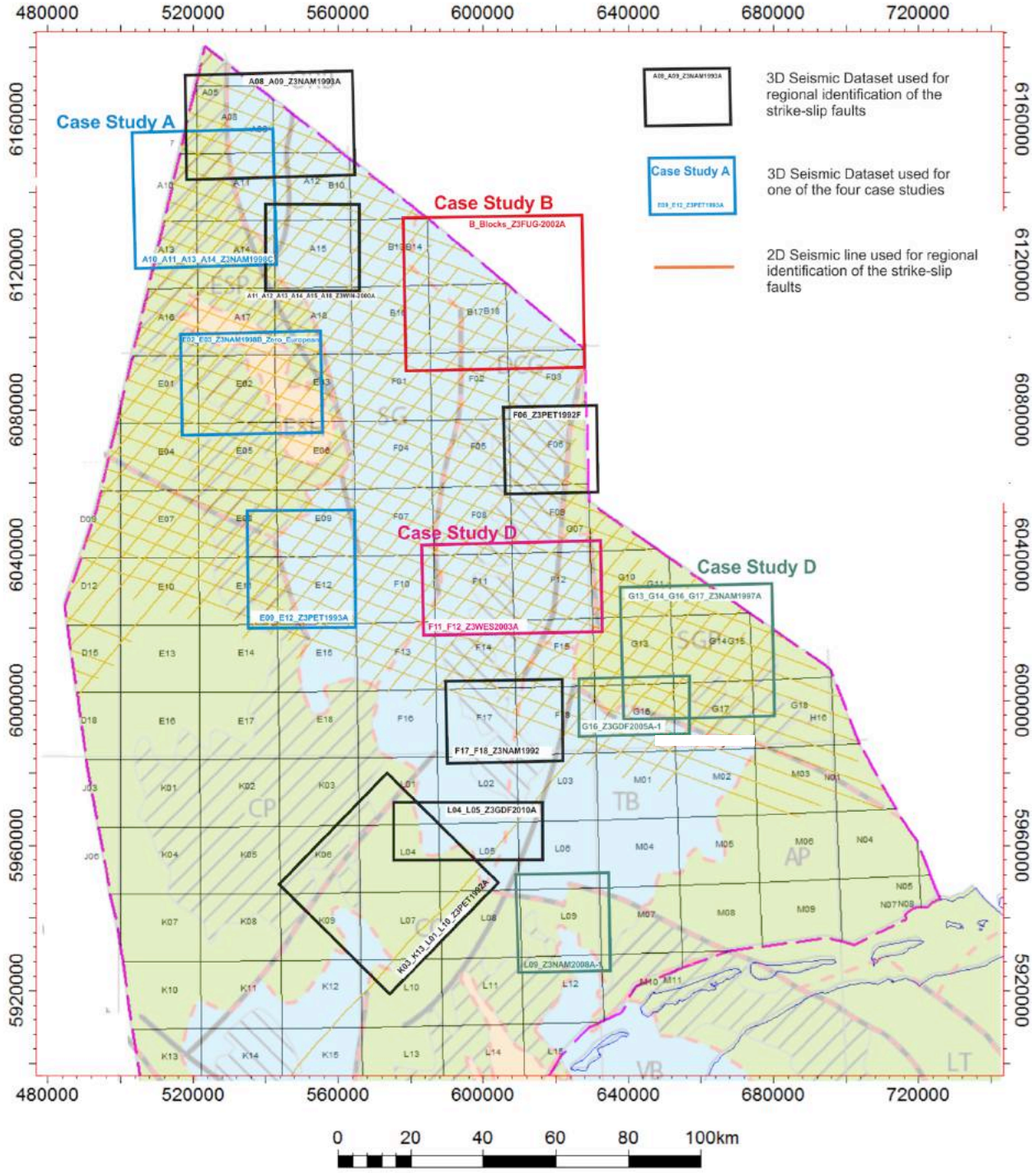

Fig. 12. Location of the seismic datasets that were used in this study. The background indicates the location of the seismic datasets with respect to the structural elements in the Dutch offshore. Modified after Kombrink et al., 2012.

seismic lines were analysed. Figure 12 shows the location and the name of the 3D seismic datasets and 2D seismic lines that were used for the regional identification of strike slip faults (indicated in black in Fig. 12), as well as the 3D seismic surveys that were used for one of the four case studies (indicated in colour in Fig. 12). All of the 3D seismic datasets adhered the non-SEG convention, which means that an increase in acoustic impedance over an interface is displayed as a through and a decrease in acoustic impedance over an interface is displayed as a peak (see Fig. 13). Parts of the 2D seismic lines, known as the NSR lines, have not been completely converted to zero-phase, meaning that a peak and through don't exactly resemble the transition in acoustic impedance.

When analysing the seismic datasets, the following criteria were used to recognise strike-slip faults:

- A steep dip angle of the fault
- An upward widening of the fault pattern (i.e. flower structures)
- Stratigraphic mismatches on either side of the fault such as differences in thickness that can't be explained by original depositional patterns or any other type of faulting
- Lateral offsets of older structures such as older faults or sedimentary features such as channels
- The bending of older structures, caused by drag on opposite sides of strike-slip faults.
- The presence of local zones of uplift (transpression) and/or subsidence (transtension).
- A concave upward rotation of strata towards the fault plane; a so called tipi shape of the strata
- En echelon fault pattern in map view

3.1.2 Detailed analysis of specific strike-slip faults

After the identification of the strike-slip faults, an analysis on specific strike-slip structures was conducted to unravel their timing, sense of displacement, the amount of displacement and their interaction of the faults with Zechstein evaporites. The analysis was conducted by creating:

- 3D surfaces
- True thickness maps (isopach maps)
- Attribute maps

In the following subsections will be briefly explained how these maps were created.

3D surfaces and isopach maps

To properly pick a seismic signal, representing the formation of interest, it is necessary to understand the seismic signal and to make a seismic to well tie. For this purpose, synthetic seismograms were generated in this project for 5 wells (For an extensive description of the formation of synthetic seismograms see Peeters, 2015). The wells, as well as the case study for which they were constructed are indicated in table 1. Once the seismic to well tie was made, 3D horizons were made with Petrel software and converted into a 3D surface. Isopach maps were constructed out of the created 3D surfaces by subtracting the top of the formation of interest from the base of the formation of interest. Isopach maps resemble the true Stratigraphic thickness of the formation of interest, which means that the dip of the strata is taken into account when the software calculates the thickness maps

Seismic Attribute maps

A seismic attribute map displays a quantity that is extracted or derived from the seismic dataset.
They are used to extract more information out of a seismic dataset and to enhance subtle trends that otherwise might remain hidden in a seismic dataset. A seismic attribute can be

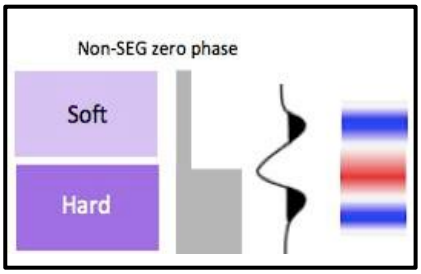

Fig. 13. The seismic convention that was used for the 3D seismic datasets in the research area.

applied either on a horizon, or on a seismic line, including a vertical time slice (Z-slice). A variety of seismic attributes exist and different software programs typically have developed their own seismic attributes. In this study, seismic attribute maps were constructed with OpendTect software. This software offers a wide variety of seismic attributes. The 3 attributes that were used the most are briefly explained below:

Similarity attribute;

A seismic dataset is composed of a 2D array of traces in the x and y direction. The traces are usually spaced in the order of 25m, depending on the resolution of the dataset. Each trace is composed of sample values in the Z direction (usually every 4mm), which contain information about the removal of the signal. The similarity attribute indicates how much a group of sample values on adjacent traces looks alike in terms of waveform and amplitude (OpendTect, manual) A similarity of 0 indicates that a group of samples on a specific trace is completely dissimilar to a group of samples on adjacent traces. The higher the similarity value, the more a group of samples on adjacent traces looks alike. A value of 1 indicates that they are completely similar. Hence, an area with a high degree of dissimilarity may indicate the presence of a fault or the presence of evaporites (which are usually characterized by a chaotic seismic signature). Stratigraphic features are slightly harder to detect with the similarity attribute (though not impossible), as stratigraphic features such as channels are often only defined in a seismic dataset by very subtle changes in amplitude.

Spectral Decomposition attribute;

The spectral decomposition attribute disentangles the seismic signal into the original frequencies of which it is composed. Therefore it applies basically a reverse Fourier Transform. This way, amplitude differences can be analyzed at a specific frequency, which might help to better detect subtle features that particularly stand out at a certain frequency. Spectral decomposition is particularly useful to detect and enhance very subtle stratigraphic features such as channels, turbidites and sedimentary fan deposits.

Case Study	Location of case study	Wells for which synthetic was created	3D surfaces created; base of stratigraphic intervals
A	Elbow High Spit High Elbow Spit Platform Step Graben	E02-01	Lower North Sea Group Zechstein Group
B	Northern part of Dutch Central Graben	B18-02, B18-03	Lower North Sea Group Chalk Group Base Rijnland Group Reflector in Kimmeridge Clay formation of the Scruff Group Scruff Group Schieland Group Altena Group
C	Central part of the dutch Central Graben	F11-02, F12-03	Puzzle Hole Formation Posidonia Shale Formation Altena Group Upper Triassic Muschelkalk formation
D	Terschelling Basin, northern part of the Central Offshore Platform and Schill Grund Platform	-	Rot evaporite Muschelkalk evaporite

Table 1. Table shows the formations that were mapped for the case studies and the wells for which synthetics were made.

3.2 Analogue modelling methods

3.2.1 Experimental set-up

The experimental set-up of the analogue models consisted of a plastic sheet (600x17x0.1cm), which lied upon a table (table2 in Fig. 14 and 15). Half of the model was built on top of the plastic sheet, the other half was build directly on top of table 2. Wooden bars (indicated in yellow in Fig. 14 and 15) were attached at the plastic sheet. One wooden bar on the long side and one wooden bar on the short side of the plastic sheet. These wooden bars were used to transfer the movement from the engine (positioned on table 1 and indicated in red in (Fig. 14 and 15) on to the plastic sheet. For the extension phase, the plastic sheet was pulled by the engine via the wooden bar on the long side of the plastic sheet (Fig. 14). For the strike-slip phase, the plastic sheet was pulled by the engine via the wooden bar on the short side of the plastic sheet (Fig. 15). To switch from extension to strike-slip or vice-versa, the engine was decoupled from the plastic sheet and the table on which the model was built, was rotated 90 degrees.

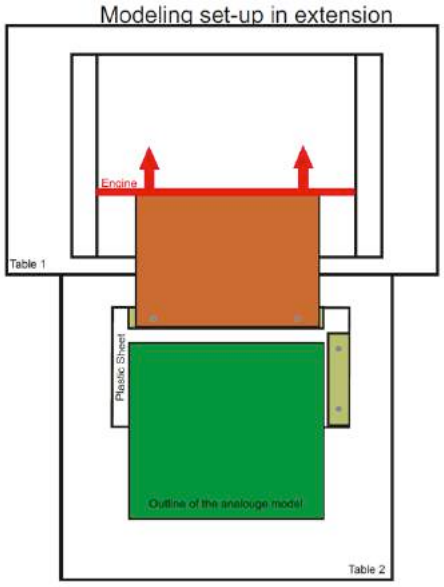

Fig.14. Schematic illustration of the experimental set-up during the extension phase

To record deformation during the course of the experiment, photographs were taken at regular time intervals (generally every 2 minutes), with a camera that was positioned above the model. When the experiment was finished, the experiment was covered with sand and subsequently poured with water to preserve the structures that had formed during deformation. To analyse the structures at the end of deformation, vertical cross-sections were cut with a knife at regular intervals.

In total, four analogue models are described and discussed in this report. In section 3.2.6 the experimental procedure of the four models, as well as their stratigraphic sequence is described. The following sections first describe the properties of the materials that were used to build the models and explain why these materials where used.

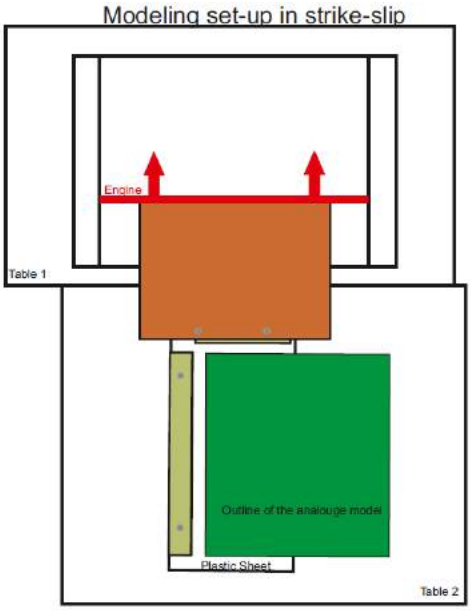

Fig. 15. Schematic illustration of the experimental set-up during the strike-slip phase

3.2.2 Material properties

Quartz sand was used to simulate the brittle behaviour of natural rocks in the upper crust. The quartz sand that was used had a density (ρ) of 1500kgm^3, a grainsize between 100µm-300µm, a negligible cohesion (C) and a coefficient of internal (φ) of 0.58. Silicon putti was used to represent the ductile behaviour of salt under geological conditions. The silicon putti that was used in the experiments had a density of 970kg/m3 and a dynamic viscosity of 2.4*10^{4}Pa.s.
In the following sections will be explained why these model materials were chosen and why the analogue models are a valid first order approximation of reality.

3.2.3 Scaling of the models

An analogue model that simulates a natural occurring process, can only be a good approximation of reality if it is geometrically, dynamically, kinematically and rheologically similar to the natural process. (Hubbert, 1937, Ramberg, 1981, Davy and Cobbold, 1991). If this is the case, the model will resemble a similar evolution as the process occurring in reality, even though the dimension (i.e. length width and height) scale is much smaller and the time-scale is much faster.

Scaling of dimensions

The scaling conditions that must be satisfied in order for analogue models to represent a natural process can be derived from the equation of dynamics (as performed i.a. by Davy and Cobbold, 1991; Brun, 2002; Smit, 2005) and are as follows;

$$\sigma^* = \rho^* g^* L^* \quad (1)$$
$$\varepsilon^* = g^* (t^*)^2 \quad (2)$$

Where σ is the vertical stress in Nm^{-2}, ρ is the material density in kgm^3, g is the gravitational acceleration in ms^{-2}, L is the dimension of the model in m. The designation * refers to the ratio between the model and the natural prototype (e.g. $\sigma^* = \frac{\sigma_{model}}{\sigma_{natural\ prototype}}$) .

Where $\rho^* = 1$ because the density of upper crustal rocks in nature (ranging from $2300kgm^{-3}$ to $3000kgm^{-3}$) and the density of quartz sand used in the laboratory ($1500kgm^{-3}$) are in the same order of magnitude. Also $g^* = 1$, as gravity is approximately equal everywhere on earth. Therefore equation 1 can be written as:

$$\sigma^* \sim L^* \quad (3)$$

This means that the stress ratio has to be approximately equal to the ratio of dimensions for the model to be a realistic representation of the natural prototype. The dimension scale ratio (L^*) between the model and prototype is $L^* = 10^{-5}$, which means that 1cm in the experiment is approximately equal to 1km in nature.

Scaling of material properties.

Brittle materials

The brittle deformation of rocks is described by the Mohr coulomb criterion (Byerlee, 1978);

$$\tau = \mu\sigma_n + C \quad (4)$$

Where τ is the shear stress on the fault plane, σ is the normal stress on the fault plane, C is the cohesion of the material and μ is internal coefficient of friction. When dividing equation 4 by σ, substituting $\rho g h$ for σ and taking into account that the models should be dynamically scaled to nature according to equations 1 and 3, The following expression is obtained according to Bonini et al., 2000;

$$\mu_{model} + \frac{C_{model}}{\rho_{model} g L_{model}} = \mu_{nature} + \frac{C_{nature}}{\rho_{nature} g L_{nature}} \quad (5)$$

Besides the density and gravity values, also the values of μ_{model} and μ_{nature} are of a similar order of magnitude. Hence equation 5 can be written as follows;

$$\frac{L_{model}}{L_{nature}} \sim \frac{C_{model}}{C_{nature}} \sim L^* \sim C^* \quad (6)$$

Rocks in nature typically have a Cohesion around 50MPa. Since the length scale ratio (L^*) of the experiments is 10^-5, it means that the brittle materials used in the models should have a negligible cohesion compared to natural rocks. Hence because of its negligible cohesion, its density, which is in the same order of magnitude as natural rocks, and its coefficient of friction, which is in the same order of magnitude as natural rocks, quartz sand is suitable to represent brittle deforming natural rocks.

Ductile Materials

The deformation of salt under geological conditions is described by multiple mechanisms, such as dislocation creep and diffusion creep. The dominant mechanism depends on the temperature conditions, grain sizes, strain rate and whether or not fluids are involved (Spiers et al., 1990; van

Keken et al., 1993). Ductile deformation can by approximation be described via a Dorn creep power law equation of the following form, (Goetze and Evans, 1979; Weijermans and Schmeling, 1986);

$$\dot{\varepsilon} = A\exp\left(\frac{-Q}{RT}\right)(\sigma_1 - \sigma_3)^n \qquad (7)$$

Where $\dot{\varepsilon}$ is the strain rate in s^{-1}, Q is the activation energy in J, R is the gas constant in $JK^{-1}mol^{-1}$, T is the Temperature in Kelvin, $\sigma_1 - \sigma_3$is the maximum differential stress Nm^2. A is a material constant and n is the stress exponent. Experiments have shown that it is a valid assumption to assume that salt behaves as a Newtonian fluid under geological conditions, which means that its resistance to flow is linearly dependent on the strain rate. (Spiers et al., 1990; van Keken et al., 1993). Hence, the silicon putti used in the experiments is a Newtonian viscous fluid, which yields that the stress exponent (n) in equation 7 is 1. Because Newtonian fluids deform (by approximation) by simple shear (Brun, 2002), the shear strain rate is used as an approximation for the strain rate; $\dot{\varepsilon} \sim \dot{\gamma}$. The shear strain rate of a Newtonian viscous fluid is described by the following equation (Spiers et al., 1990):

$$\dot{\gamma} = \frac{1}{\eta}\tau \qquad (8)$$

Where η is the viscosity in Pa.s and where τ is the shear stress, which is related to the differential stress $(\sigma_1 - \sigma_3)$as follows:

$$2\,\tau = \sigma_1 - \sigma_3 \qquad (9)$$

By substituting equation 9 into equation 8 and by assuming that the shear strain rate can be used as an approximation to describe deformation of a Newtonian viscous fluid, equation 8 can also be written as follows (according to Brun 2002; Smit, 2005):

$$\dot{\gamma} = \frac{\sigma_1 - \sigma_3}{2\eta} \; or \; \dot{\varepsilon} = \frac{\sigma_1 - \sigma_3}{2\eta} \qquad (10)$$

Like the brittle part of the model, also the use of the silicon putti has to be scaled down to values according to equation 3. This means that the following equation has to be satisfied;

$$\dot{\varepsilon} = \frac{\sigma^*}{\eta^*} \qquad (11)$$

Where η is the viscosity in Pa.s and the designation * refers again to the ratio between the model and the natural prototype. Experiments have shown that for relatively high-temperature conditions and a small grain size, the viscosity of salt in nature is around 10^{17}Pa.s (van Keken et al., 1993). The viscosity of the silicon putti used in the models, described in this report, is $2.4*10^4$Pa.s, indicating that: $\eta^* \sim 10^{-13}$. In accordance with the adopted scaling of the dimensions; $\sigma^* \sim 10^{-5}$. Additionally, orogenic strange rates ($\dot{\varepsilon}_{nature}$) are in the range from 10^{-13} to 10^{-15} (Pfiffner and Ramsay, 1982). When a natural strain rate of 10^{13} is assumed, equation.. indicates that the model should be deformed with a strain rate that is the order of $\dot{\varepsilon}_{model} \sim 10^{-5}$. This indicates that the velocity of the base plate should be in the order of centimeters per hour. Because both the viscosity of salt in nature, as well as the natural strain rates are not exactly known, the strain rate was varied in the testing phase of the models to look for the strain rate that produced the best structures. It turned out that during the extension phase, a deformation velocity of 0.5cm resulted in the formation of well-developed silicon putti walls. During the strike-slip phase, a faster velocity of 1.5cm/hour was applied.

$$\sigma_1 - \sigma_3 = 2\eta\dot{\gamma} \; or \; \sigma_1 - \sigma_3 = 2\eta\dot{\varepsilon} \qquad (12)$$

3.2.4 Calculation of the strength profiles

The deformation pattern resulting from multilayer analogue models is largely dependent on the strength of the different materials and in particular on their strength contrast, which is tested here under different tectonic stress regimes. (Hubbert, 1937; Brun and Nalpas, 1995; Brun, 2002; Smit, 2008a; Smit, 2008b). The following section explains how the strength, which is defined as the maximum differential stress ($\sigma_1 - \sigma_3$), can be calculated for the brittle part of the models.

Calculating the Brittle strength

The vertical stress in a brittle layer is determined by the weight of the overlying rock column;

$$\sigma_v = \rho g T_b \qquad (12)$$

In an extensional setting, the maximum principle stress (σ_1) is equal to the vertical stress;

$$\sigma_v = \sigma_1 \qquad (13)$$

To determine the maximum differential stress (i.e. the strength) of the sand, an expression for the minimum principle stress (σ_3) is also required. This relation follows from the Mohr Coulomb criterion and is as follows (Jaeger and Cook, 1979):

$$\sigma_3 = -\frac{sin\Phi - 1}{sin\Phi + 1}\sigma_1 \qquad (14)$$

Where Φ is the materials angle of internal friction, which is related to the friction coefficient (ϕ) by the following relation

$$\phi = tan\Phi \qquad (15)$$

the coefficient of internal friction (ϕ) of quartz sand is 0.58 and the minimum principle stress can be expressed as a part of the maximum principle stress by filling in the equations 13 and 14 . This leads to the following expression:

$$\sigma_3 = \frac{1}{3}\sigma_1 \qquad (16)$$

From this relation and from the fact that in an extensional setting, the maximum principle stress is equal to the vertical stress, it follows that the strength of a brittle layer in extension is;

$$\sigma_1 - \sigma_3 = \frac{2}{3}\rho g T_b \qquad (17)$$

In a strike-slip setting, the intermediate principe stress (σ_2) is equal to the vertical stress;

$$\sigma_v = \sigma_2 \qquad (18)$$

The Mohr Coulomb failure criterion for three dimensions can be used to express σ_2 in terms of $\sigma_1$or σ_3:

$$\frac{\sigma_1 - \sigma_2}{2} = \left[\frac{\sigma_1 + \sigma_2}{2}\right] sin\phi + ccos\phi \qquad (19)$$

Where c is the cohesion, which is negligible in the case of quartz sand. By using relation 18 and the 3D Mohr Coulomb equation, it follows that the strength of quartz sand during strike-slip deformation can be calculated as follows;

$$\sigma_1 - \sigma_3 = \rho g T_b \qquad (21)$$

Calculating the Ductile Strength.

The strength of the ductile part of the model can be obtained from equation 12. However, from this equation, the average strength of a layer of silicon putti is obtained. The true strength of a ductile layer however, also depends on its thickness (Spiers et al., 1990; van Keken et al., 1993). Hence the strength of the silicon putti layer was calculated by using the following formula (Smit, 2005):

$$\sigma_1 - \sigma_3 = \frac{2\eta V}{T_d} \qquad (22)$$

Where V is the deformation velocity in cm/hour and Td is the thickness of the silicon putti layer in m.

3.2.5 Limitations of analogue modelling

It has to be emphasized that the analogue models described in this study are just a first order approximation of reality, as the complexity of nature can't be exactly reproduced in a lab. Hence, simplifications are made in the models regarding the rheology of the materials, but also regarding the geometrical variations. First of all it has to be noted that the models presented in this study are solely composed of a brittle basement. In nature, a ductile lower crust is present, which distributes deformation at the base of the upper crust. Hence, the results of the models described here can only be considered as an analogy for the upper brittle crust. For these brittle rocks applies that they are seldom homogenous in composition. Instead their heterogeneity or anisotropy often influences the deformation pattern. Additionally, as mentioned in section 3.2.3, the exact viscosity of salt varies under different geological conditions, as it depends on grain size, temperature and the presence of fluids. All these parameters are poorly constrained for distinct areas and time intervals and are impossible to incorporate in the model. Additionally, it is not possible to include processes like isostasy or flexural behaviour and also erosional processes were not included in the model. However, it is not the intention of analogue modelling to exactly reproduce natural structures. Analogue modelling is about studying the structural evolution of features in the lab that can be regarded as analogues to natural examples. For this purpose it provides a useful tool, as analogue models allow observing the evolution of structures. While in nature, only the present state of structures can be observed.

3.2.6 Experimental procedure; Experiments 1 and 2 (table 2)

Models 1 and 2 are purely brittle models, solely composed of different colored layers of quartz sand to represent brittle behavior. The total thickness of the layers before deformation commences is 5.5cm (see Fig. 16 and 17). Both model 1 and 2 were subjected to two deformation phases, however the sequence of these deformation phases was different. Model 1 was first subjected strike-slip, after which it was subjected to extension. Model 2 was first subjected to extension, after which it was subjected strike-slip. During the extension phase, sedimentation was applied in the graben 3 times at regular time intervals (every 20 minutes). The purpose of these two models was to test, to what extent deformation during the second deformation phase would reactivate faults that were formed during the first deformation phase.

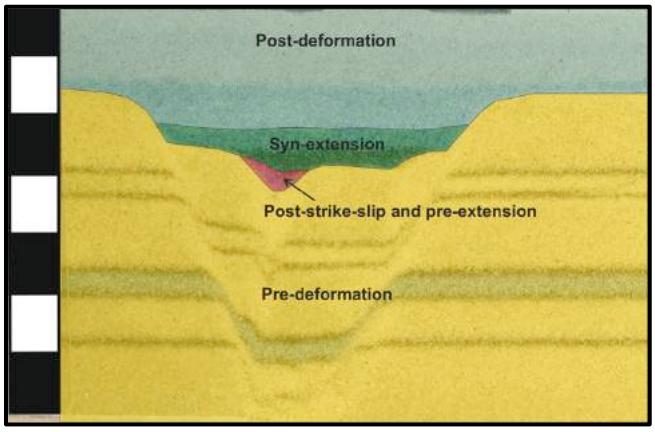

Fig. 16. Section 1.1 of model1, showing the deformation phases during or after which the sediments were deposited as well as the thicknesses of the sediments

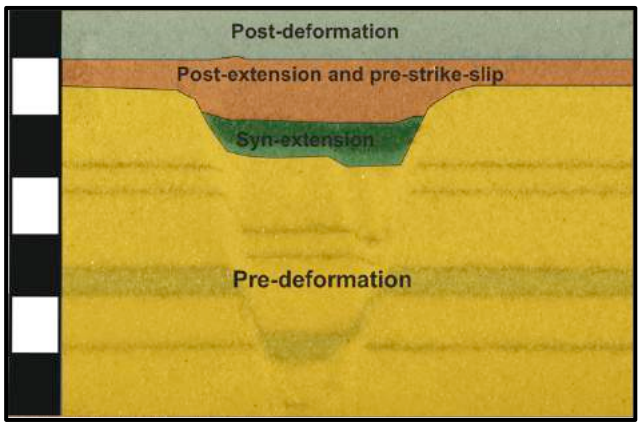

Fig. 17. Section 2.1 of model 2, showing the deformation phases during or after which the sediments were deposited as well as the thicknesses of the sediments

3.2.7. Experimental procedure; experiment 3 and 4 (table 2)

Models 3 and 4 are multilayer models, composed of both brittle and ductile materials. The two models are composed of a 5cm thick brittle basement, underlying a layer of silicon putti with an initial thickness of 1cm. On top of the silicon putti layer, a green layer of quartz sand was deposited with a thickness of 0.5cm (Fig. 18 and 19).

These pre-kinematic layers were in both models subsequently subjected to 2 deformation phases and one resting phase in the following order:

- Extension Phase; 4 hours at a deformation rate of 0.5cm/hour
- Resting Phase; 8 hours
- Strike-Slip Phase; 2 hours at a deformation rate of 1.5cm/hour

With ongoing extension and subsidence of the graben during the extension phase, sedimentation was applied at regular time intervals (every hour) to simulate syntectonic sedimentation. After the extension phase, no deformation was applied for 8 hours during the resting phase, allowing the silicon putti walls to grow passively. During this resting phase, sedimentation was applied again at regular time intervals (every two hours). The difference between experiment 3 and 4 is the following; In Experiment 3, sedimentation was applied homogeneously across the entire experiment thereby keeping the graben normally filled with respect to the platforms (i.e. no topography between the graben and platform after sedimentation). In Experiment 4, part of the graben was kept underfilled (part C in Figure 73), allowing the silicon putti to extrude laterally into the graben. The other half of the graben (Part D in Figure 73) was normally filled. During the first two hours of the resting phase, part A of the basin was kept underfilled with 6mm of difference between the graben and the platforms (indicated as extremely underfilled in Fig. 19). During the subsequent 2 hours, the basin was also kept underfilled with a 3 to 4mm difference between the graben and the platforms (indicated as underfilled in Fig. 19). During the last four hours of the resting phase, part A of the basin was kept underfilled with a difference of 1 to 2mm between the graben and the platform, thereby reducing the topography (indicated as normally filled in Fig. 19). Subsequently, the strike-slip phase of the experiment was applied parallel to the pre-formed graben, in order to test the influence of different salt geometries on the strike-slip deformation pattern.

Experiment number	First deformation phase	Sedimentation during first deformation phase	Resting Phase	Sedimentation during resting phase	Second deformation phase
Model 1	Strike-Slip; *1 hour with 3cm/ hour*	NA	NA	Every 20Minutes	Extension; *1 hours with 1cm/ hour*
Model 2	Extension; *1 hour with 1cm/ hour*	Every 20 minutes	NA	NA	Strike-Slip; *1 hour with 3cm/ hour*
Model 3	Extension; *4 hours with 0.5cm/hour*	Every Hour	8hours	Every two hours. Entire graben was kept normally filled	Strike-Slip; *2 hours with 0.5cm/ hour*
Model 4	Extension; *4 hours with 0.5cm/hour*	Every hour	8 hours	Every 2 hours. Half of the graben was kept underfilled during the first 4 hours of resting	Strike-Slip; *2 hours with 0.5cm/ hour*

Table 2. Table showing a schematic overview of experimental procedure for the 4 models.

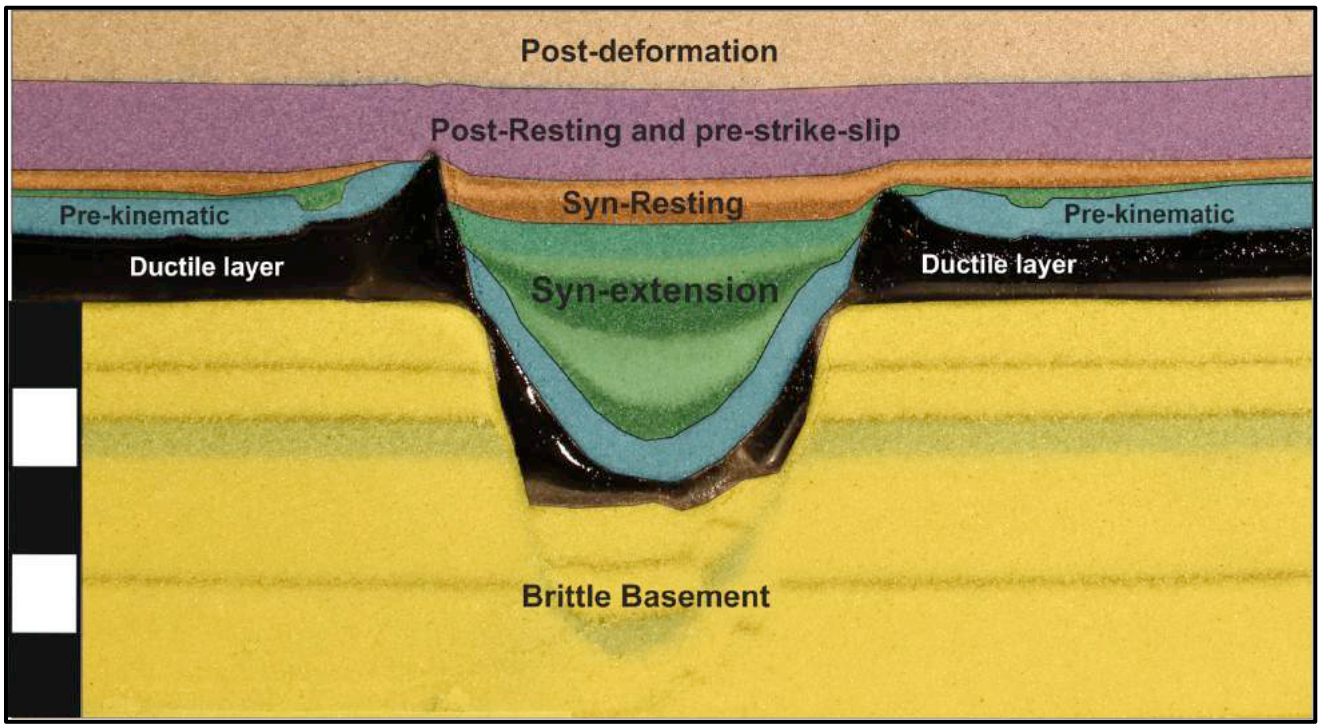

Fig. 18. Section 3.1 of model 3, showing the deformation phases during or after which the sediments were deposited as well as the thicknesses of the sediments. This figure represents model 3 as well as the normally filled part of the basin of model 4.

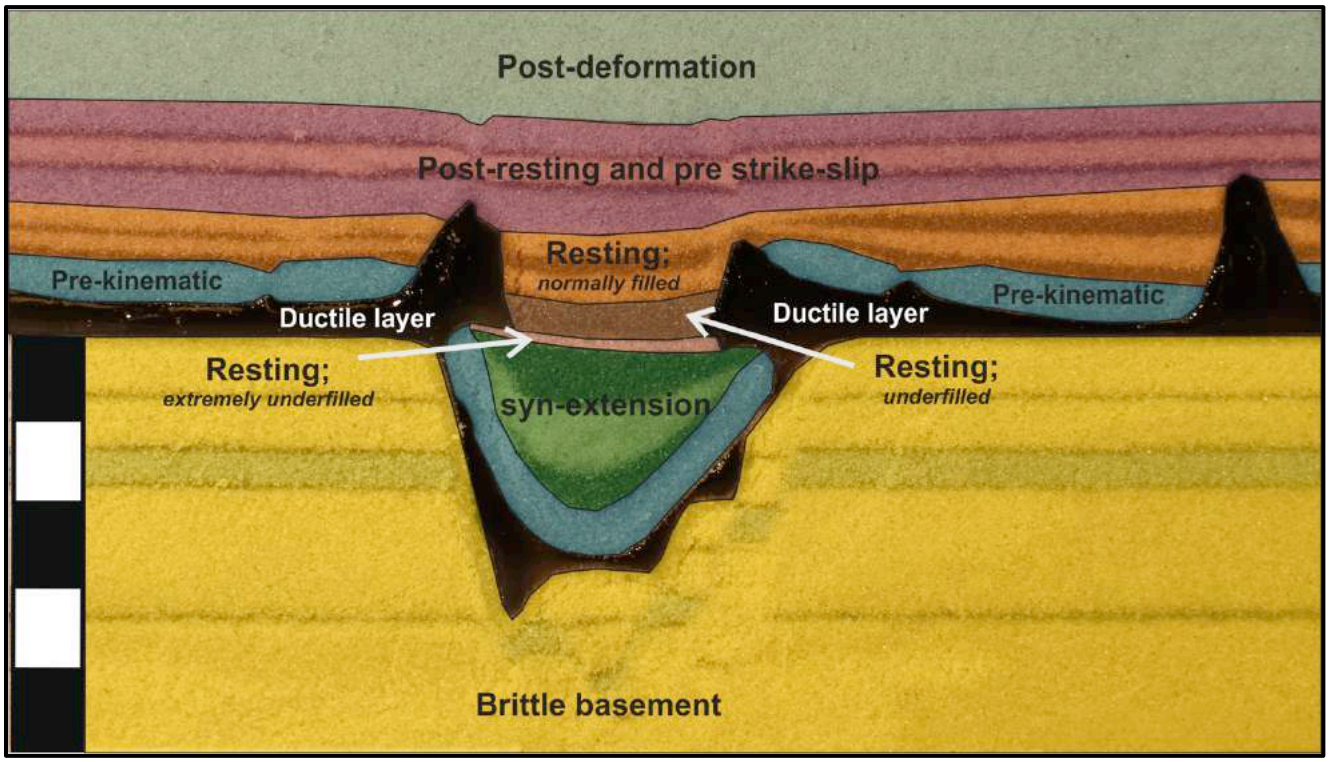

Fig. 19. Section 4.2 of model 4, showing the deformation phases during or after which the sediments were deposited as well as the thicknesses of the sediments. This figure represents the underfilled part of the basin of model 4.

4. Results obtained from seismic data

The strike-slip faults that are identified in this study are indicated in Fig. 20. The main characteristics of the identified strike-slip faults are indicated in table 3, which shows i.a. the orientation, sense- and amount of displacement and timing of the identified strike slip faults. In the next sections (4.1-4.4) will be elaborated on the fault characteristics of the four case studies (indicated by the black squares in Fig. 20), which are briefly introduced below.

From Figure 20 can be inferred that a group of roughly WSW-ENE trending strike-slip faults was identified on the Elbow Spit Platform, Elbow Spit High and Cleaverbank Platform, west of the Step Graben. These faults can only be recognised on the platform areas. As soon as they approach the Step Graben, they can't be identified anymore. This group of faults is further described in Section 4.1, as case study A. Several strike-slip faults were also identified in the Dutch Central Graben. Because of the Dutch Central Grabens complex history of multiple deformation phases, it was sometimes not exactly clear if a fault had accommodated strike-slip movements or not. Hence, a quality code is used for strike-slip motions in the Dutch Central Graben ranging from low probability strike-slip feature to a high probability strike-slip feature. Some of these strike-slip faults are indicated with a star in Figure 20. This is either because there was no available 3D seismic data to unravel the strike (as is the case for feature I, briefly described in appendix B) or because the strike of the concerning feature could not be derived (as is the case for feature II, a low probability strike-slip feature, which is described in appendix C). From the strike-slip movements that were identified in the Dutch Central Graben, two strike-slip faults are discussed in detail in case studies B

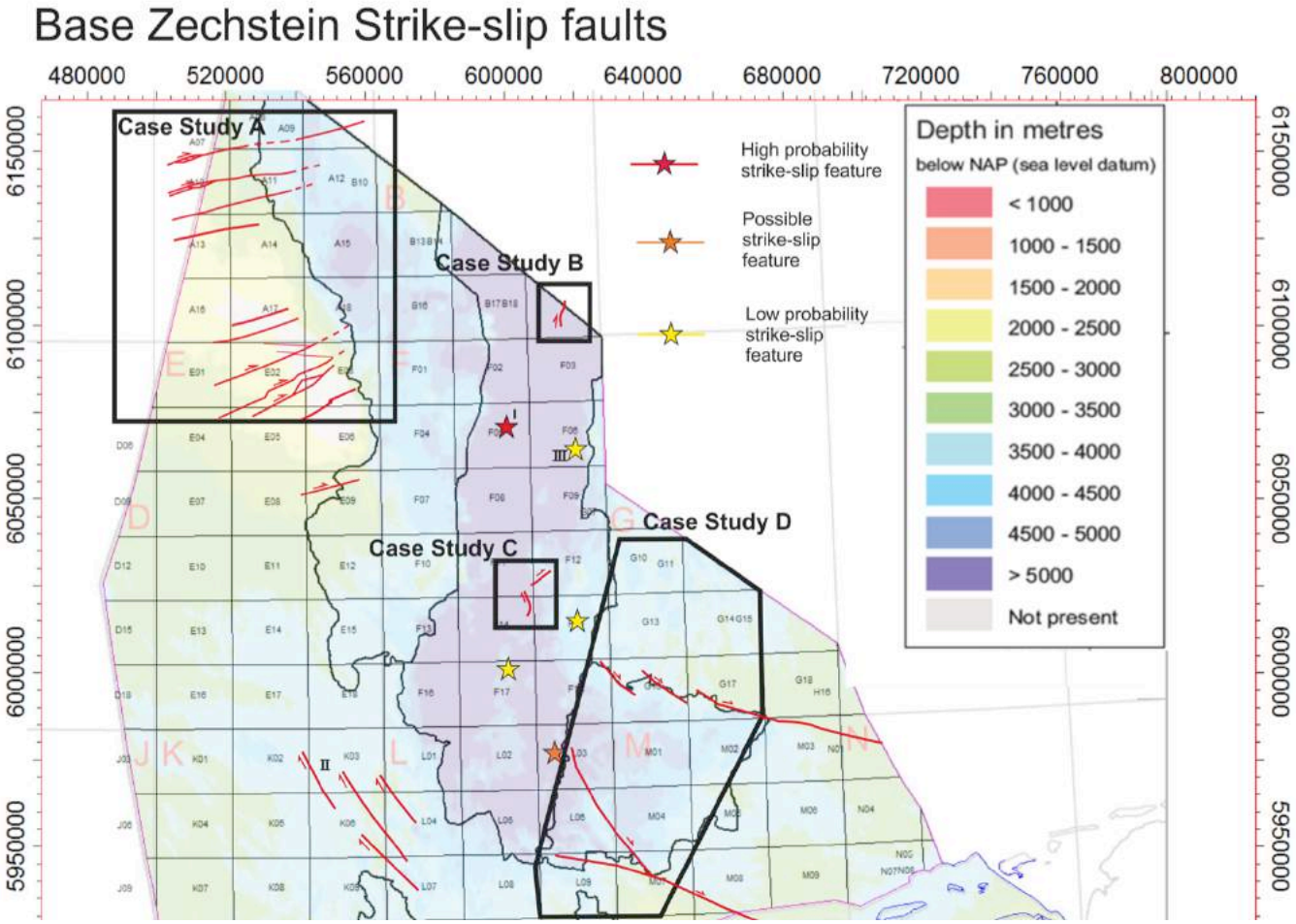

Fig. 20. Map of the base Zechstein showing the strike-slip faults that were identified in this project, as well as the outline of the case studies that are presented in the section 4.1-4.4. The fault Group that is identified in the K and L blocks was identified by Ping Chen (Ping Chen, Msc. Thesis, 2016)

(Section 4.2) and C (Section 4.3). Case study B describes a strike-slip fault in the northern part of the Dutch Central Graben. Case study C describes a strike-slip fault in the central part of the Dutch Central Graben, which has accommodated strike-slip movements in between two salt structures. Finally, case study D (Section 4.4) describes two types of strike-slip faults in the northern part of the Central Offshore Platform, Terschelling Basin and Schill Grund Platform. The first type of strike-slip faults are subtle supra salt, thin-skinned strike-sip faults. The second type are major strike-slip faults on the two faults that bound the Terschelling Basin towards the north and the south; the Rifgronden Fault Zone and the Hantum Fault Zone.

Case Study/ Reference number	Location	Fault orientation	Sense and estimation of the amount of displacement	Reactivation of older structures?	Timing	Relation with salt
Case Study A	Elbow Spit Platform and Elbow Spit High (Northern A-blocks)	N075 to N085	Dextral; 700m to 900m on single fault	Partly reactivation of older structures	Upper Cretaceous, Early Paleogene. Possibly earlier activity	No salt present; thick skinned
Case Study A	Elbow Spit Platform and Cleaverbank Platform (Northern E-blocks)	N060 to N070	Dextral; 500m to 800m on single fault	Partly reactivation of older structures	Upper Cretaceous; Possibly earlier activity	No salt present; thick skinned
Case Study B	Northern Dutch Central Graben (B18-block)	N170 to N030	Approximately 700m	No; but possibly induced by reactivation of sub-salt basement faults	Late Jurassic (post Jurassic sequence 1) to Early Cretaceous.	Supra salt strike-slip fault
Case Study C	Central Dutch Central Graben (At the gathering of the F11, F12, F14, F15-blocks)	Rapidly curving strike; varying between NE and NW	Approximately 800m-2500m	No; But possibly induced by reactivation of sub-salt basement faults	Late Jurassic (likely post Upper Jurassic sequence 1) and pre Paleogene.	Supra salt strike-slip fault. Linking strike-slip motions that are primarily accommodated by salt structures.
Case Study D; thin skinned	Terschelling Basin, Schill Grund Platform, Central Offshore Platform	N090 to N110	Up to 3000m in Terschelling Basin; up to 1500m at Schill Grund Platform	No	Late Early Triassic to Late Triassic	Thin skinned; Strike-slip features arise to accommodate for lateral differences between different raft blocks. Movements are accommodated by the salt
Case Study D; Hantum Fault Zone	Terschelling Basin	N110-N120; Curving into N-S towards DCG	2500m	Yes	Middle to Late Triassic	Strike-slip movements on pre-formed basement fault. Activity likely transmitted into overlying salt but no evidence found.
Case Study D; Rifgrunden fault zone	Terschelling Basin	N290-310	5000m à 6000m	Yes	Middle to Late Triassic	Strike-slip movements on pre-formed basement fault. Activity likely transmitted into overlying salt but no evidence found.
I; Appendix A	Northern Dutch Central Graben (F5-/block)	Exact unknown; approximately N-S	?	Uncertain but not likely	?	Strike-slip movements seem to be partly accommodated by salt structures.
II; Appendix B (Msc. Thesis Ping Chen)	Southern Cleaver Bank Platform	N320-330 or N160-170 (depending on fault dip)	Around 1000m	Yes	Late Cretaceous/Early Paleogene	?

Table 3, table summarizing the main characteristics of the identified strike-slip faults. The location of the strike-slip faults is indicated in Figure 20.

4.1 Case Study A; Strike-Slip faulting on the Elbow Spit High

Structural observations

This case study emphasizes on a family of faults that is present in the region west of the Dutch Central Graben and the Step Graben. Due to the absence of Zechstein evaporites in this area, and the relatively shallow position of Paleozoic rocks, fault patterns can be recognized in the Upper Carboniferous. This is shown in Fig. 21, which shows a similarity map of the Northern E-blocks at 2100ms TWT, roughly corresponding to the Upper Carboniferous interval of the Hanze Subgroup (DCHP) in most of this area. And in Fig.23, which shows a similarity map of the base of the Zechstein Group in the Northern A blocks.

Four fault families (FF) were recognized from Figures 21 and 23. The characteristics of these four fault families are indicated in Table 3, where the colors of the fault families correspond to the faults in the maps of Figure 21 and 23. From Fig. 21 and 23 can be inferred that FF 1 cross-cuts all the other fault families, as these other fault families display a right stepping geometry across the faults of FF1. Additionally small zones of uplift and subsidence are related to movements along faults of FF1. These small zones of uplift and subsidence can be recognized both in the A and in the E blocks. However in the E blocks they are generally larger. Fig. 22 shows a cross section through such a small zone of uplift. From this figure can be inferred that the vertical faults related to this small zone of uplift display an upward widening of the fault pattern and offset rocks up to an including the Chalk Group and locally also rocks of the Lower North Sea Group (southern part of the northern E-blocks). Additionally, rocks of the Chalk Group and Lower part of the Lower North Sea Group are thinning over this small zone of uplift. Displacements along the faults of FF1 can be measured on several points by measuring the offsets between older fault families. Displacements are in the order of 500-900m per individual fault. Noteworthy is that the faults of Family 1 can't be observed in the Step Graben, also not at deeper intervals. This is the case both in the E blocks as in the A blocks.

Fault families 2 and 3 display always offsets in the Carboniferous and Devonian interval and sometimes also in the strata up to and including the Chalk Group. Pre-Zechstein strata show signs of thickening in the hanging wall of these faults. This thickening can also be observed sometimes in the Zechstein and in the Chalk Groups. Their mutual cross-cutting relationship is a bit ambiguous, as at some places Family 2 cross-cuts Family 3 (indicated with I in Fig. 21), while at other places, Family 3 seems to cross-cut Family 2 (indicated with II in Fig.21). Additionally, some ENE-WSW trending faults can be recognized that are characterized by approximately the same orientation as FF2 but instead show a nearly vertical fault plane. These faults are oriented en echelon across faults of FF1.

Faults of fault Family 4 form the boundary between the Elbow Spit Platform and the Step Graben. In the hanging wall of these faults, a thicker sequence of Mesozoic rocks is present including Zechstein evaporates, Lower and Upper Triassic and Lower and Upper Cretaceous rocks. The Upper Cretaceous rocks of the Chalk Group are thicker in the hanging wall of these faults. They are more abundant in the A-blocks than in the E-blocks and also there orientation varies between these two blocks as they are more NNE-SSW oriented in the A-blocks and more NW-SE oriented in the Eblocks.

Fault Group	Fault orientations	Fault dip	Sense of displacement	Amount of displacement	Timing
1	060 to 070 in the Eblocks 080-085 in the Ablocks	Nearly vertical	Strike-slip; dextral	500 to 1000m	Late Cretaceous/Early Paleogene . Possibly earlier but no sedimentary record in this area.
2	90-110	Inclined	Normal faults	>800m	Carboniferous/Devonian with some later reactivation during Mesozoic times.
3	020-040	Inclined	Normal faults	?	Carboniferous/Devonian with minor reactivation during Mesozoic times
4	130 in the Eblocks 170 in the northern A blocks	inclined	Normal Faults	> 1000m	Mesozoic

Table 4; fault characteristics of the main fault families on the Elbow Spit High and Elbow Spit Platform

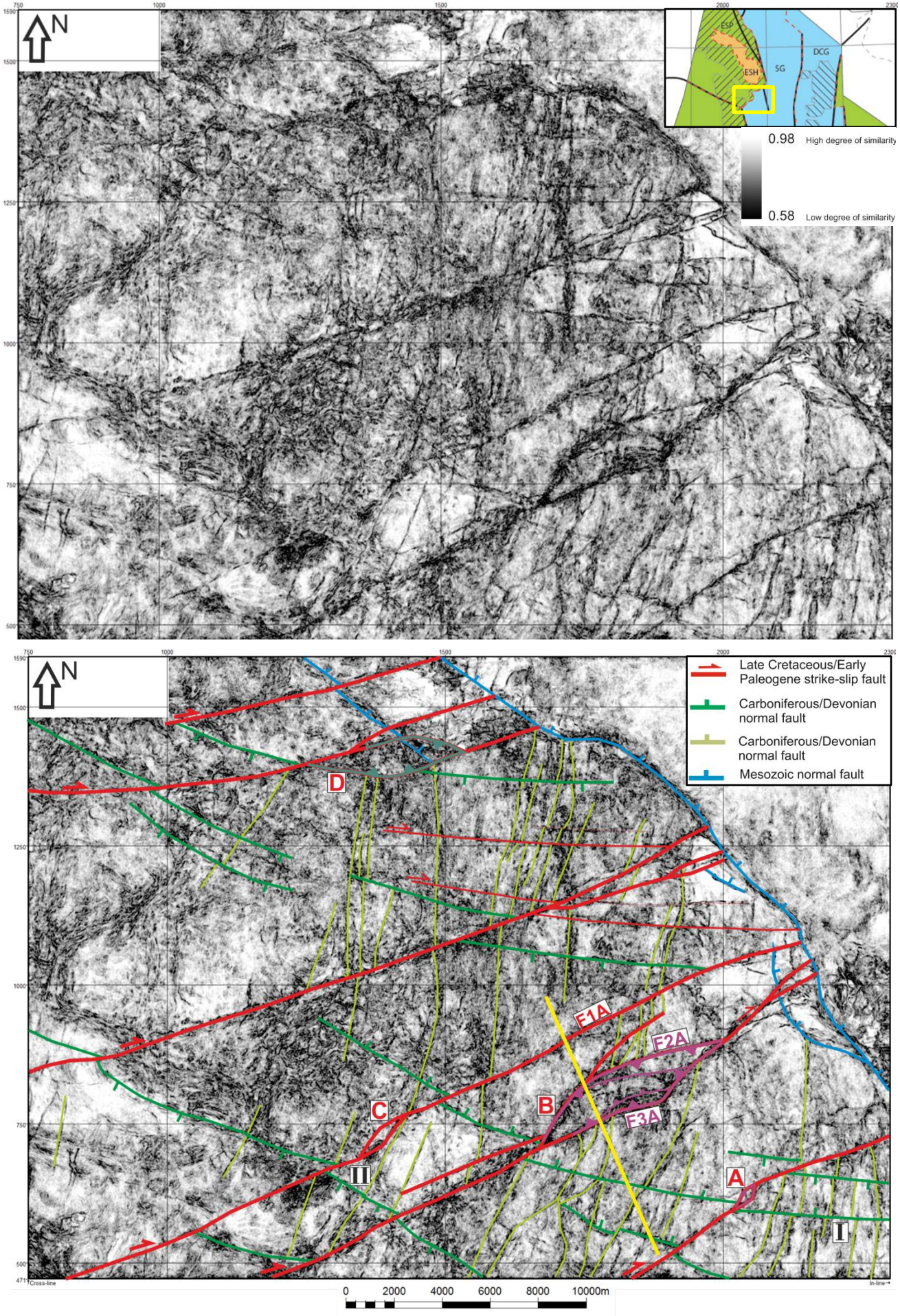

Fig.21. Similarity map at 2100ms TWT in the northern E blocks. The yellow line indicates the location of the seismic line in Fig. 22. For the classification of the different fault families see table 4.

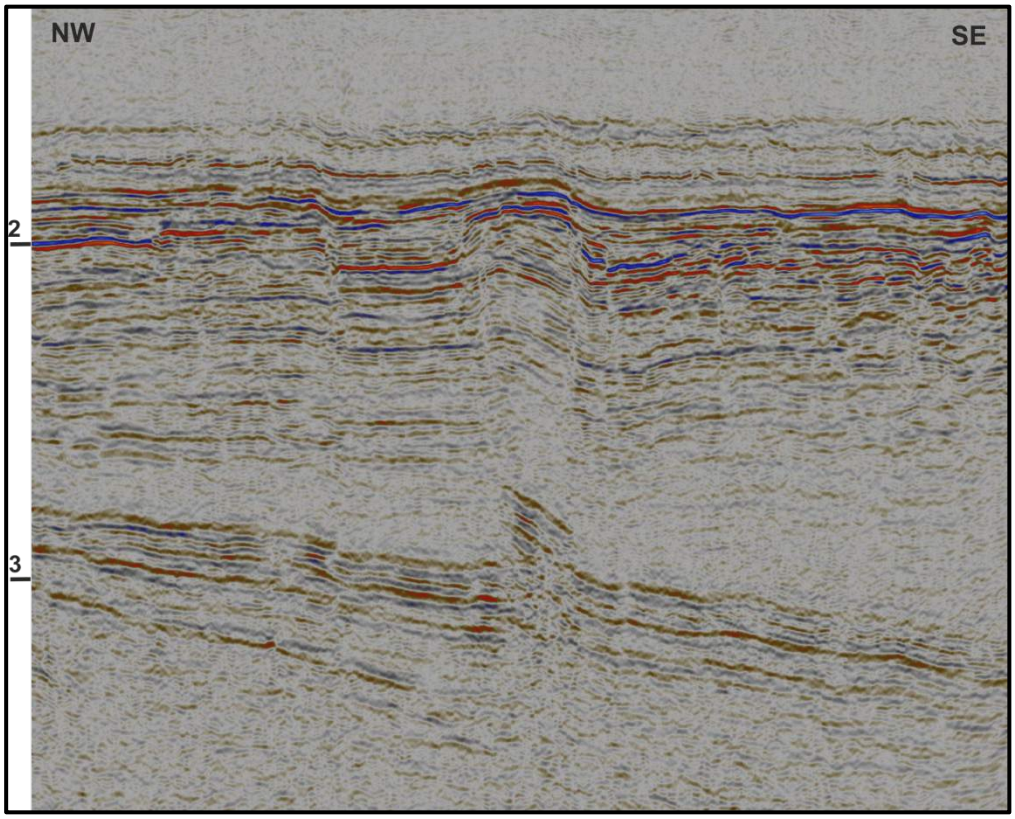

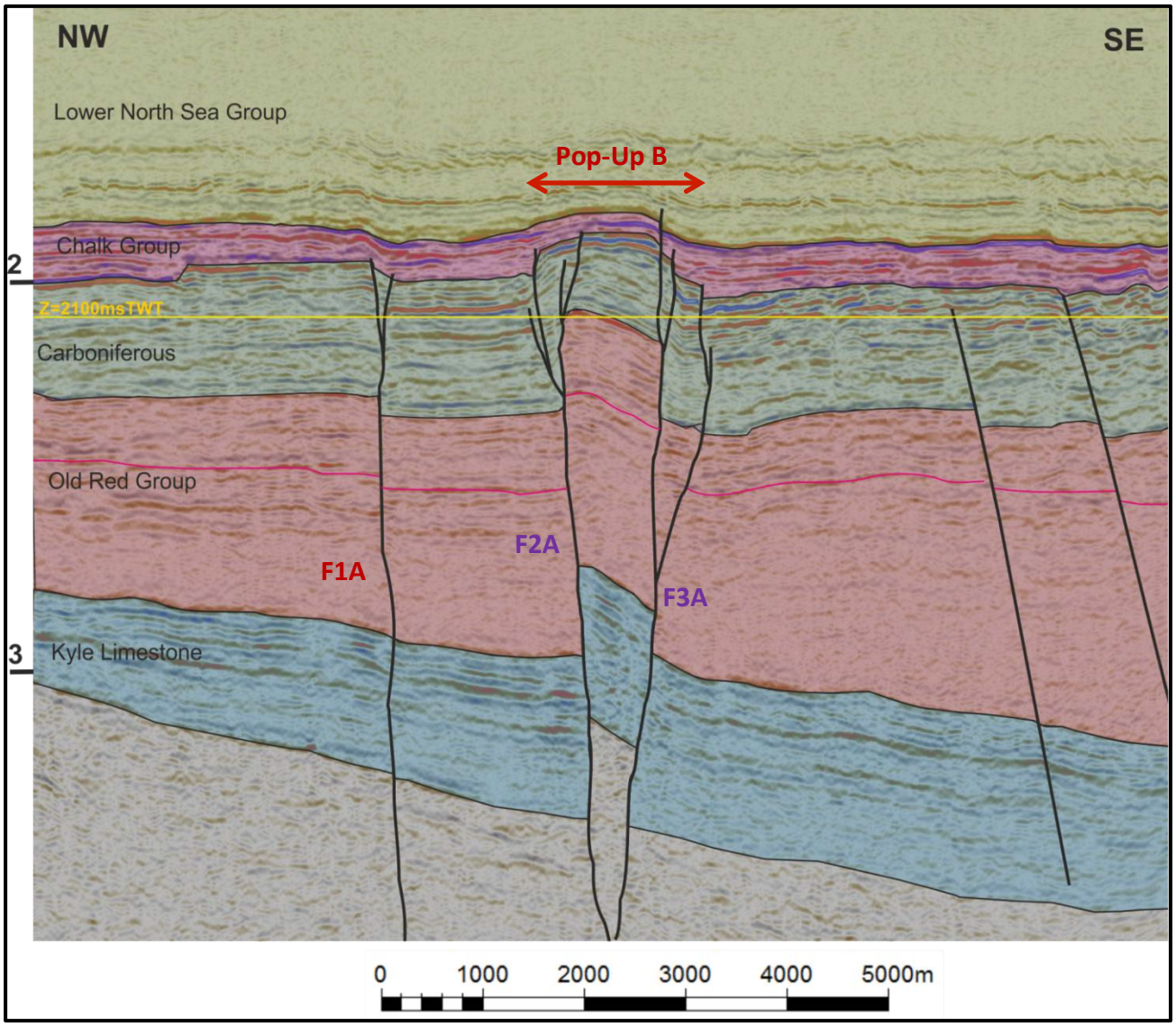

Fig. 22. Interpreted (bottom) and uninterpreted (top) seismic cross section through the southeastern E-block, showing three faults of fault family 1, including a pop-up structure, as well as two Carboniferous faults. The Carboniferous interval is composed here of the Step Graben Formation (DCHP),Yoredale Formation (CFYD), Elleboog Formation (CFEB) and Cementstone Formation (CFCS).

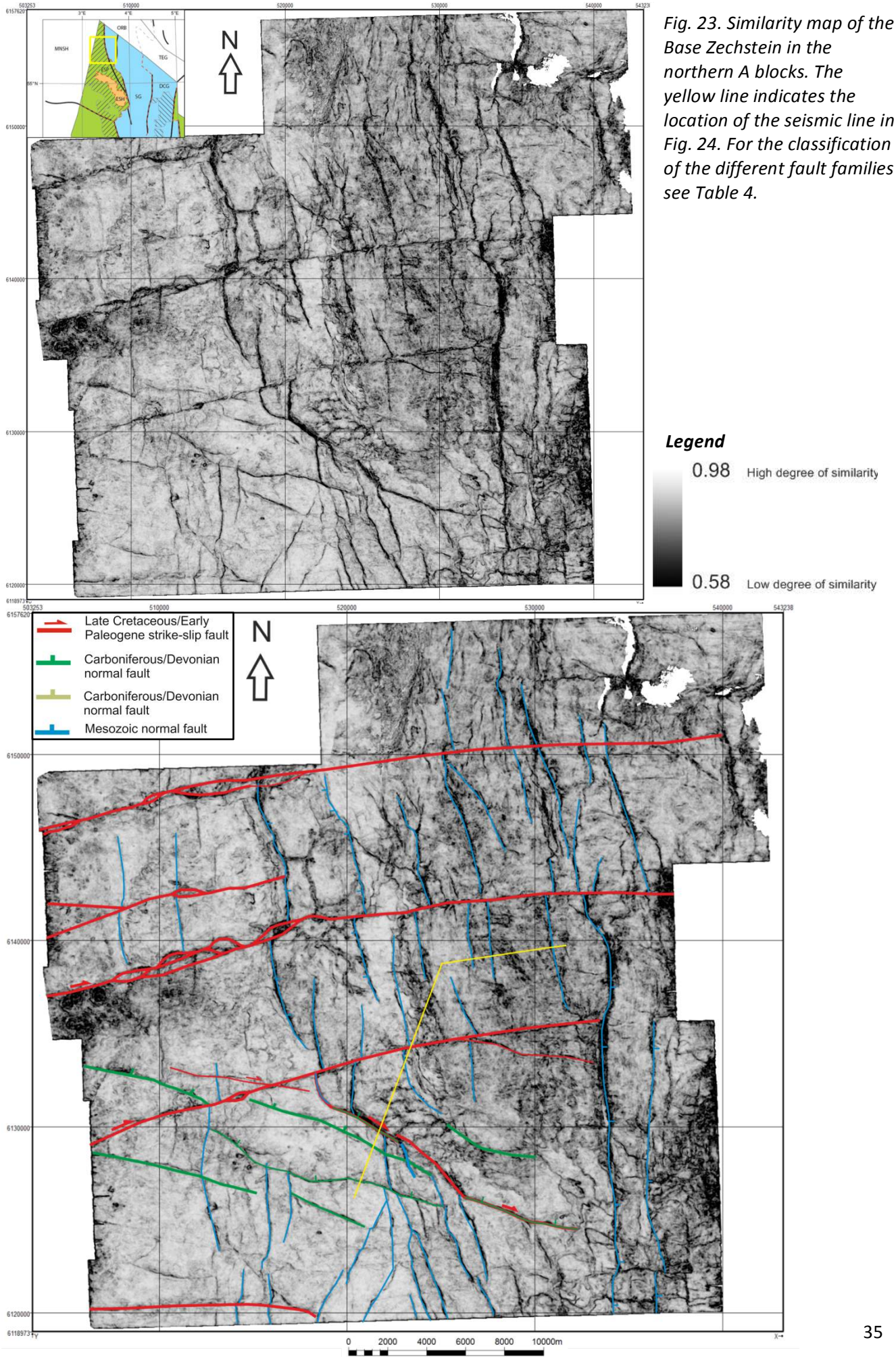

Fig. 23. Similarity map of the Base Zechstein in the northern A blocks. The yellow line indicates the location of the seismic line in Fig. 24. For the classification of the different fault families see Table 4.

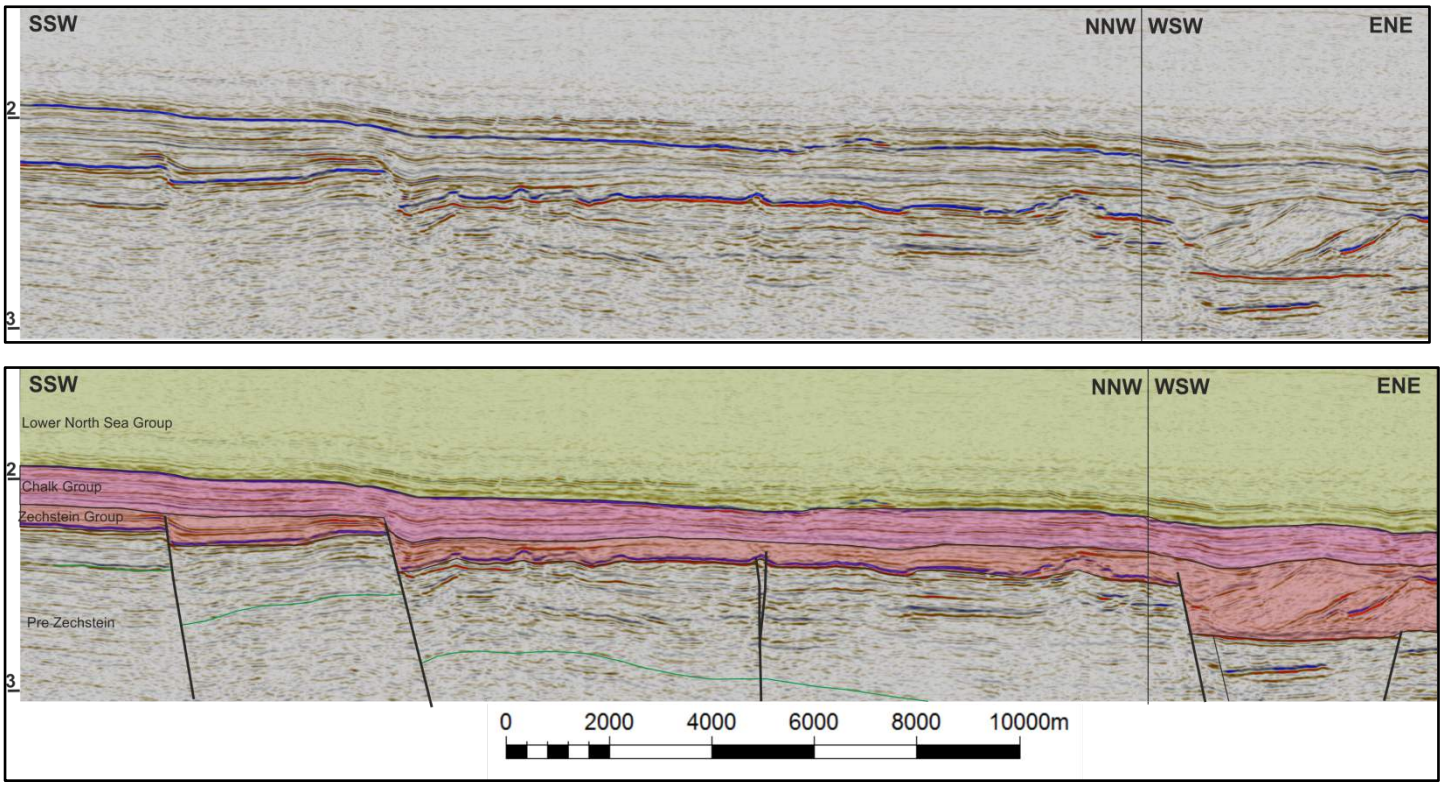

Fig. 24. Interpreted (bottom) and uninterpreted (top) seismic cross section in the northern A blocks. Showing reactivated Paleozoic faults, as well as a strike slip fault (middle fault). The Green line indicates an Upper Carboniferous reflector, showing the thickening of Upper Jurassic strata in the hanging wall of the Paleozoic faults.

Interpretations

The nearly vertical fault plane of the faults in FF, the upward widening pattern of the faults, the local zones of transpression and transtension, the en echelon pattern of (occasional) R Riedel faults and the right stepping of older faults across the fault plane of FF, indicate that these faults are strike-slip faults. The right stepping indicates that these faults are dextral faults with a displacement in the order of 500-900m on individual faults. The local zones of uplift (pop-ups) and subsidence (pull-aparts) are probably caused by interference with older fault patterns, especially in the E-blocks. In the E-blocks, it appears that interaction with faults of family 2 (orientation of around 020-040) locally causes left stepping of the dextral faults (at pop-ups A,B and C, Fig.21 and Fig. 22), leading to zones of transpression. Additionally, interaction with faults of family 2 seem to cause right stepping of the dextral faults, leading to zones of transtension (at pull-apart D in Fig.21). The pop-ups indicate that the dextral faults in the E-blocks were active during deposition of the Chalk Group, with minor and eventually waning activity during the lower Paleogene. In the A-blocks the dextral faults were active during deposition of the Chalk Group but activity had ceased before the Early Paleogene. It might very well be possible that activity initiated earlier on the dextral faults than the Upper Cretaceous. However, due to the missing stratigraphic record, this can't be ascertained.

Faults of FF2 and FF3 are formed during the Carboniferous as is indicated by a thicker Upper Carboniferous interval in the hanging wall of these faults (Fig. 24). Some of the faults of FF2 also penetrate the Zechstein and Cretaceous rocks and also show a thickening of strata in these intervals (Fig. 24). This lead to the interpretation that they were reactivated during the Mesozoic. Additionally, some parts of FF2 faults seem also to have accommodated strike-slip motions that cut structures of FF4, which were interpreted as Mesozoic faults. This might be explained by their

approximate Riedel geometry which might have been favorable for reactivation during the Upper Mesozoic strike-slip faulting in this area.

Origin of the dextral strike-slip faults

The dextral sense of displacement, combined with a NE-SW to WNW-ESE orientation of the fault plane would require a main principal stress orientation between 090 and 115 degrees (Fig. 25). The Upper Cretaceous to early Paleogene timing of dextral fault activity would correspond to the Sub-Hercynian or Laramide inversion phases related to the Alpine orogeny (Nalpas et al., 1995; van Wees and Cloetingh, 1996; De Jager, 2007)). However, the main principal stress related to these deformation phases is generally estimated to be roughly N-S to NNW-SSE (Nalpas et al., 1995; De Jager, 2007), making it unlikely that these faults have been formed by Alpine inversion. Another regional force that could be responsible for the formation of these dextral faults is the ridge push force related to the opening of the Atlantic Ocean. Sea Floor spreading initiated in the Middle Jurassic (de Jager, 2007) and the resulting gravitational positional energy, caused by the difference in topography would have been directed approximately E-W. This potential energy would increase after a few tens of Ma, when the firstly formed oceanic lithosphere had cooled down, thereby increasing the topography and hence the ridge push force.

The idea that ridge-push could be responsible for deformation has been proposed by several authors (Vagnes, et al., 1998; Clausen et al., 1999; Wessel and Müller, 2007)) and attributed at least partly to the formation of gentle anticlines and associated faulting along the western Norwegian shelf (Clausen et al., 1999). The idea that ridge-push could localize deformation at certain areas in the lithosphere is supported by numerical modelling performed by Mahatsente and Coblenz, 2015 who find that the magnitude of the ridge push force is significantly less than the strength of the oceanic lithosphere, therefore they concluded that the ridge push forces may be transmitted into the continental margin areas were deformation might occur if the ambient force exceeds the strength of the lithosphere (Mahatsente, 2015).

In any case, the orientation of the ridge push force resulting from the opening of the Central Atlantic would better correspond to the observed dextral strike-slip faults than the orientation of forces related to the Alpine inversion. However, it might very well be possible that interaction of these stresses, perhaps combined with the buoyant nature of the Mid North Sea high, have led to the formation of these strike-slip faults during the Upper Cretaceous.

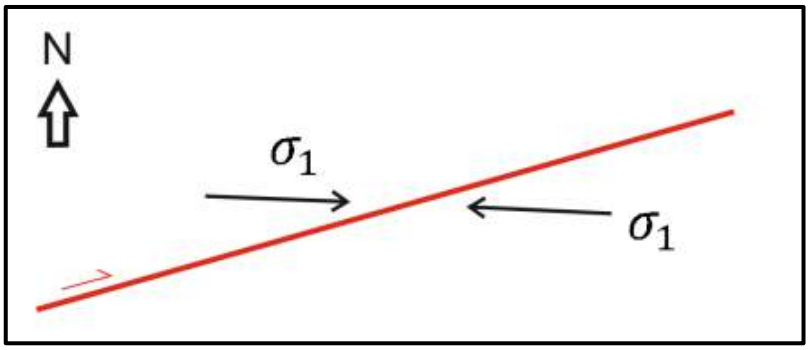

Fig. 25. Figure indicating the approximate direction of the main principle stress (σ1) direction that must have triggered activity along the faults of FF1.

4.2 Case Study B; Strike-slip fault in the northern part of the Dutch Central Graben

Observations regarding Fault F1b and related faults

Structural observations

Fault F1b is located in the B18 block, which encompasses the northern part of the Dutch Central Graben (Fig. 20). The fault is indicated as Fault F1b on the similarity map of the base Rijnland Group in Figure 26. From this Figure can be inferred that Fault F1b is characterized by a curved strike. At the faults origin in the south of the B18 block, the fault strikes almost N-S (355 degrees). Further northwards, the fault gently curves into a NNE-SSW strike. Fault F1b continues with this strike for a length of around 4km. Further towards the north, across the EEZ border with Germany, the fault bends back to its approximate N-S strike (355 degrees). Fig. 27 shows a WNW-ESE seismic cross-section through Fault F1b. From this cross-section can be inferred that Fault F1b is composed of a set of smaller faults. These smaller faults are positioned around one main sub-vertical fault (highlighted in red in Fig. 27). The faults towards the west of these two sub vertical faults dip roughly towards the east. The faults towards the east of the sub vertical faults dip roughly towards the west. Overall, these faults display an upward widening of the fault pattern in the strata of the Lower and Upper Jurassic and in the lower most part of the Rijnland Group. Strata on either side of the two main sub vertical faults are characterized by an upward concave bending, thereby forming a so called tipi-shape. This tipi shape of strata can clearly be observed in the Lower Germanic Trias Group, the Upper Germanic Trias Group, the Lower Jurassic Altena Group and the Upper Jurassic Sequences 1, 2 and 3.

Observations regarding stratigraphic thickness distribution

Noteworthy when regarding Fault F1b are the major thickness differences of the Upper Jurassic Sequence 2 on either side of Fault F1b. Although the strata of Jurassic sequence thin stratigraphically towards the ESE, as can be inferred from the western part of the fault (Fig. 27), an abrupt decrease in thickness occurs across Fault F1b. Fig. 28 shows that this thickness difference of Jurassic sequence 2 is accommodated across several reflector intervals. To a lesser extent, also the strata of Jurassic Sequence 1 and the strata of the Lower Jurassic Altena Group display this thickness difference as all these stratigraphic groups are thicker towards the west of Fault F1b than towards the east of Fault F1b. This is remarkable as Fault F1b is dipping slightly towards the east. The stratigraphic difference in thickness is visualized in Figure 29, which shows a thickness map of the Jurassic interval of the area (interval between the base of the Rijnland Group and the base of the Altena Group). From this map can be inferred that the general depocenter in this area during the Jurassic was located towards the west-southwest. It can also be inferred that Fault F1b runs parallel to the contour lines in the southern part of the fault. However, as Fault F1b gradually bends towards a more NNE-SSW orientation, Fault F1b cuts through the contour lines. The thickness pattern of the Upper Jurassic interval displayed in figure 30 seems to be affected by Fault F1b as it shows an abrupt increase in thickness towards the west of Fault F1b. On the other hand, when the thickness distribution Rijnland Group is considered (fig.31) it can be observed that the thickness pattern of this stratigraphic group doesn't change across Fault F1b.

Depositional features

Depositional features were recognized in this area by applying seismic attributes on the base of the Rijnland Group surface. These attribute maps visualized the depositional features by enhancing their slight variations in frequency and amplitude. The Channels that were recognized are indicated in yellow in fig. 26. Channels running approximately N-S can be found in the northwestern part of the area. Especially noteworthy is the channel that displays a left stepping geometry and thereby cuts the crestal faults. Additionally, by making use of a spectral decomposition attribute, two features were recognized that display a widening pattern in the direction of the main depocenter

(fig. 33). These features were interpreted as submarine depositional fans. Noteworthy is that both features don't cross Fault F1b. Instead, the eastern feature seems to follow the outline of Fault F1b.

Observations regarding Fault F2b and Fault F3b.
Fault F2b follows the same strike as Fault F1b. However, its fault plane is less steep than Fault F1b and the strata on either side of the fault don't show any sign of a concave upward dipping pattern. The fault is offsetting strata of the Upper Jurassic sequences 2 and 3, strata of the Rijnland Group, strata of the Chalk Group and strata of the Lower Paleogene North Sea Group. The strata of the Chalk Group and the Lower Paleogene North Sea Group are thicker in the hanging wall of Fault F2b than in the footwall of Fault F2b, as can be inferred from figures 27 and 32. The Upper Jurassic and Lower Cretaceous strata of the Rijnland Group don't show any differences in thickness on either side of Fault F2b. Fault F3b is dipping towards the west, into the opposite direction of Fault F2b. The fault is offsetting strata of the Upper Jurassic and Cretaceous. Strata of the Chalk Group are slightly thicker in the hanging wall of Fault F3b than in the footwall.

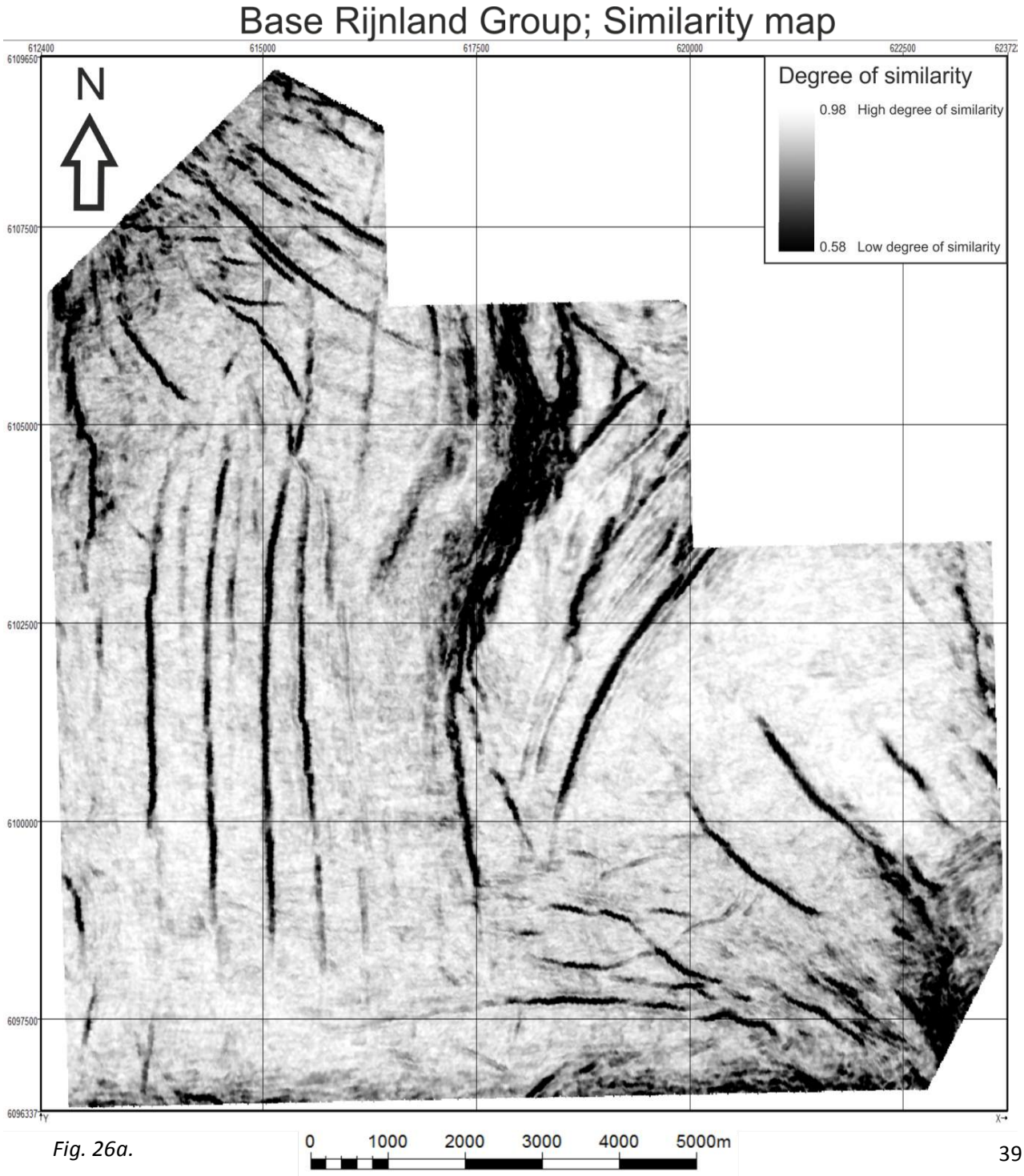

Fig. 26a.

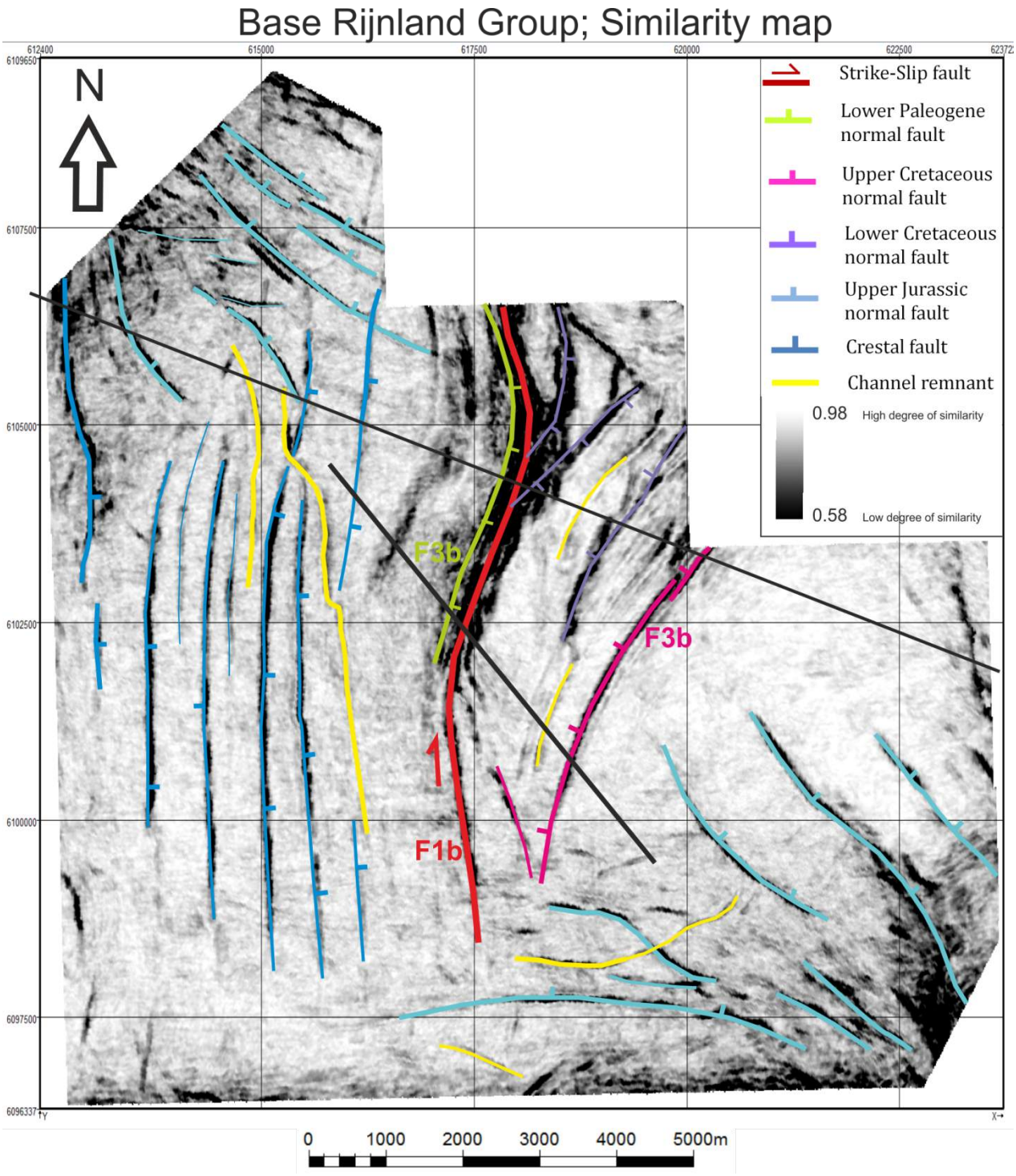

Fig. 26b. Similarity attribute map of the base of the Rijnland Group in block F11. The black areas indicate a high degree of dissimilarity, the white colors indicate a high degree of similarity (see methods). The bright green straight lines indicate the location of Figures 29,and 30. The uninterpreted Similarity map can be found in Figure 28a.

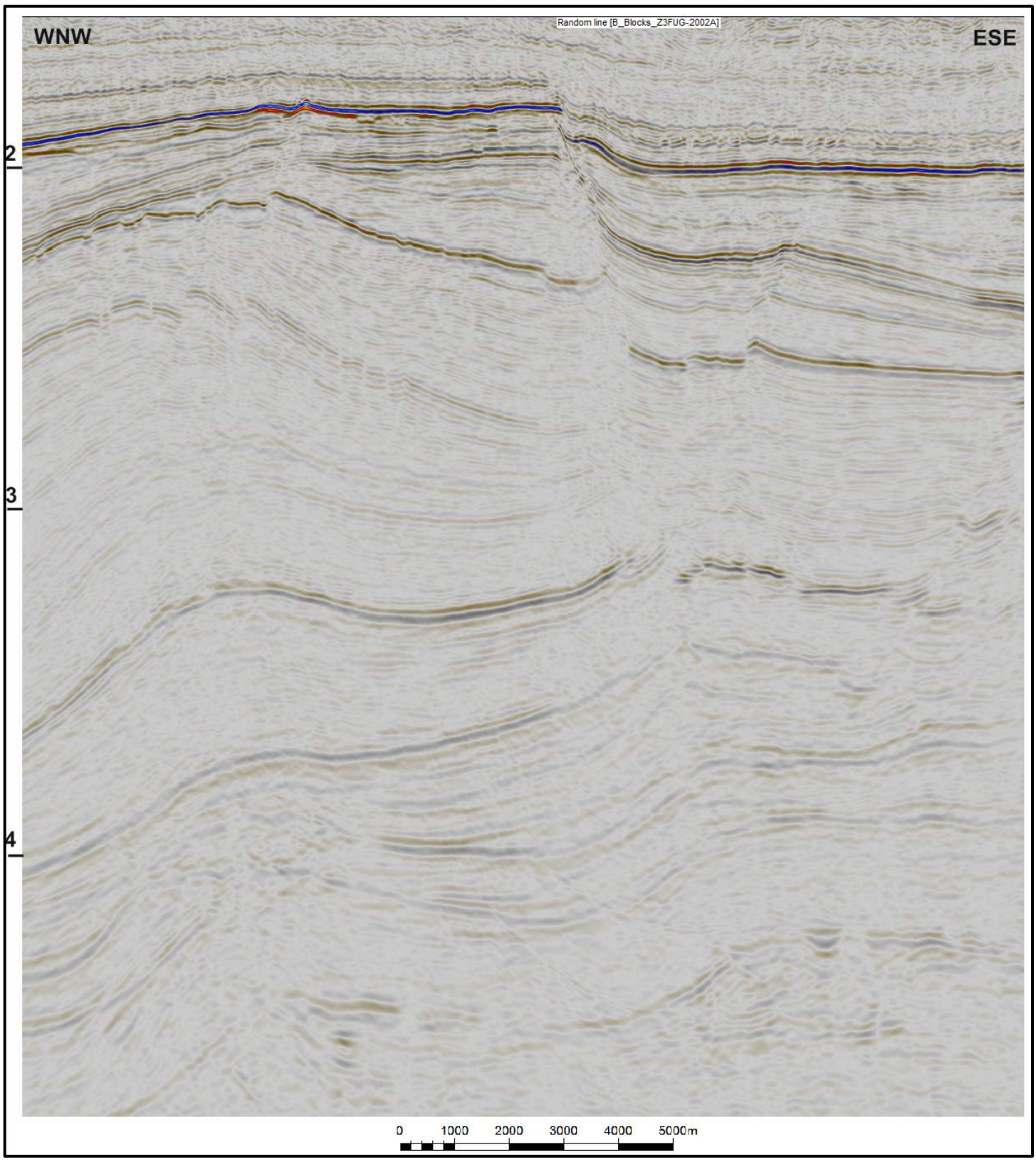

Fig. 27a. WNW-ESE seismic cross section showing the fault F1b, F2b and F3b. The location of the seismic cross-sections indicated by the straight black line in figure 26b. The Uninterpreted section can be found in figure 27a, the interpreted section can be found in figure 27b.

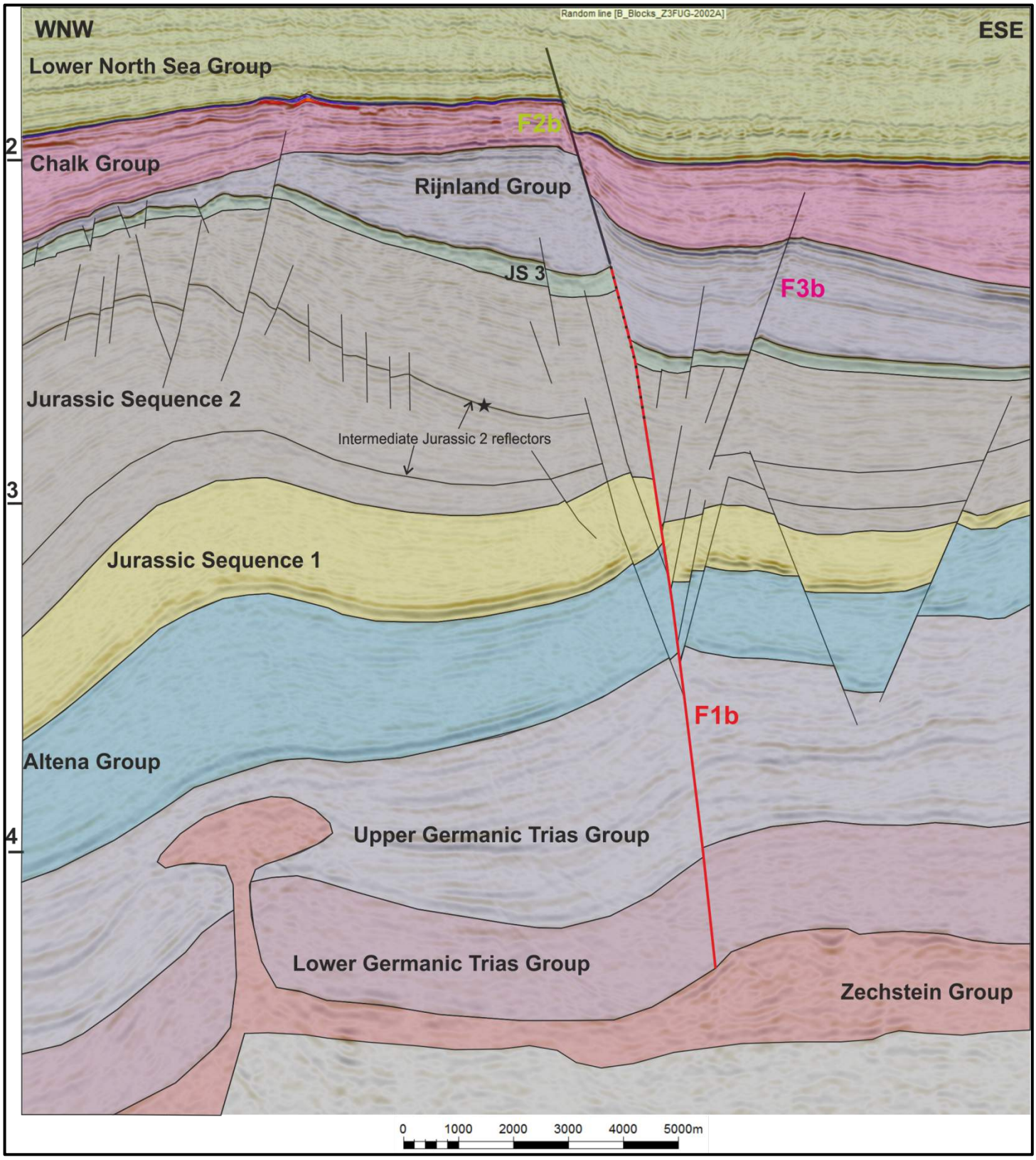
WNW
ESE
Random line [B_Blocks_Z3FUG-2002A]
Lower North Sea Group
F2b
2
Chalk Group
Rijnland Group
JS 3
F3b
Jurassic Sequence 2
Intermediate Jurassic 2 reflectors
3
Jurassic Sequence 1
F1b
Altena Group
4
Upper Germanic Trias Group
Lower Germanic Trias Group
Zechstein Group
0
1000
2000
3000
4000
5000m

Fig. 27b

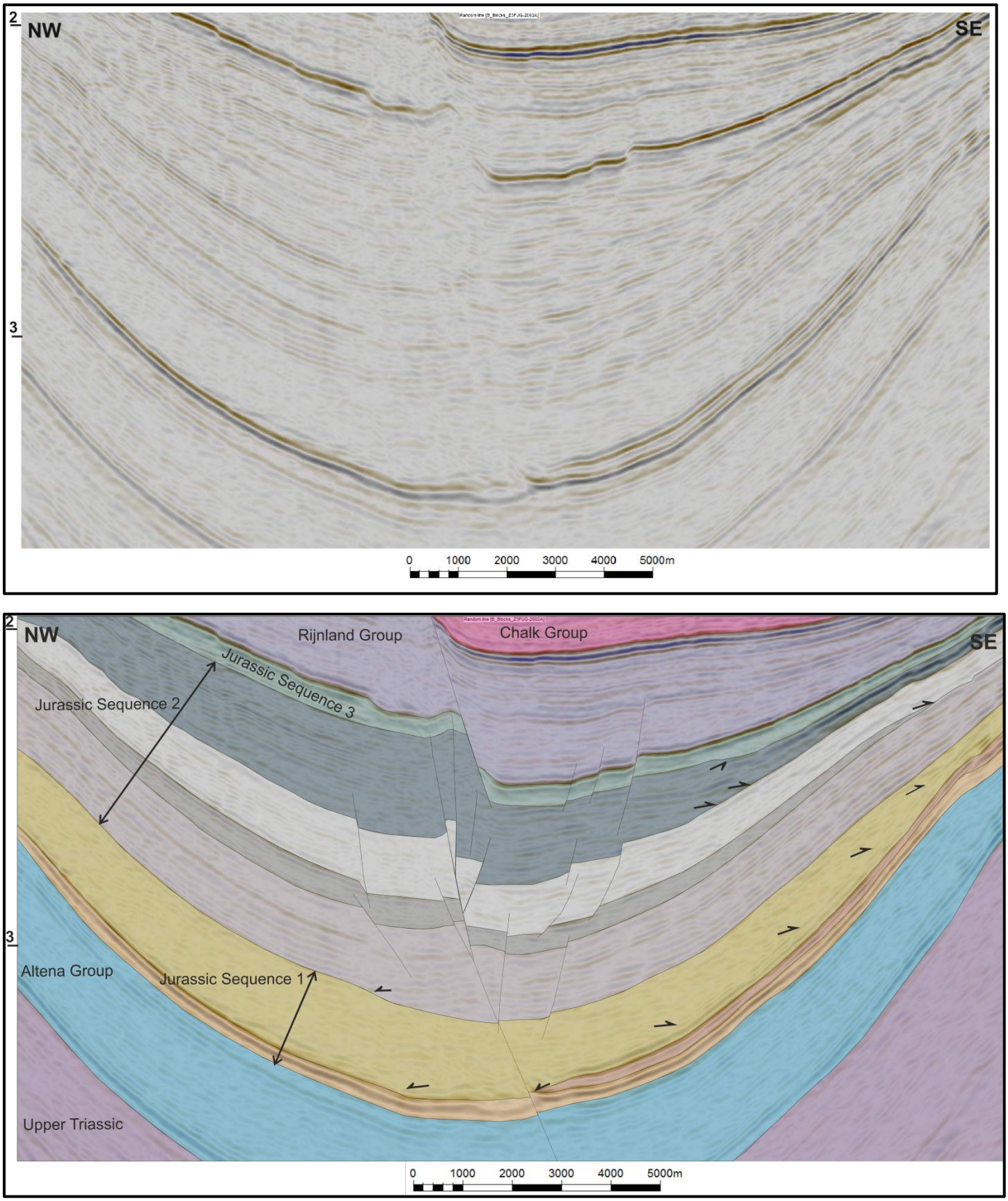

Fig. 28. NW seismic cross section showing displaying the upper Jurassic interval in more detail. Several onlaps, downlaps and toplaps can be observed, indicating a complex system of prograding and retrograding sequences with internal unconformities. Another important observation is that every interpreted interval in the Jurassic Sequence 2 is thinner towards the east of the fault system. Together this adds up to a significant thickness difference on either side of the fault.

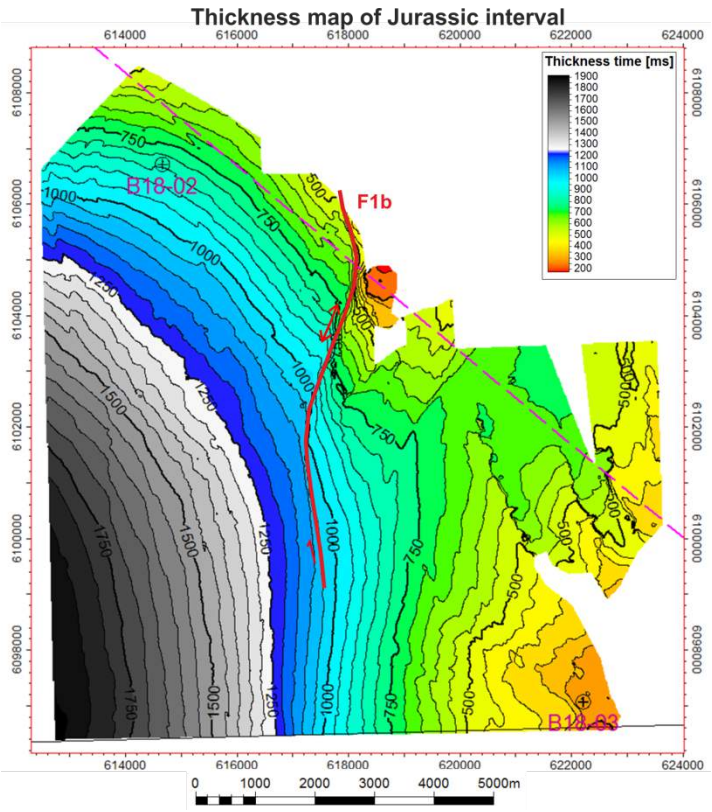

Fig. 29. Thickness map of the Jurassic, the outline of Fault F1b is indicated in red. The line along which the lateral displacement was estimated is indicated by the red arrow.

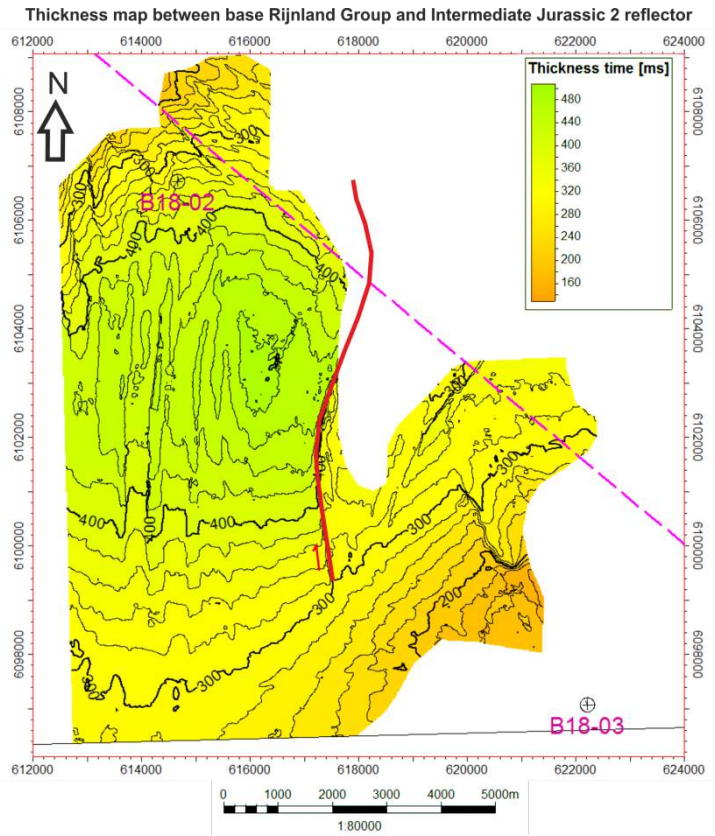

Fig. 30. Thickness map of an Upper Jurassic interval between the base of the Rijnland group and the upper black line in Jurassic Sequence 2 in Figure 27.

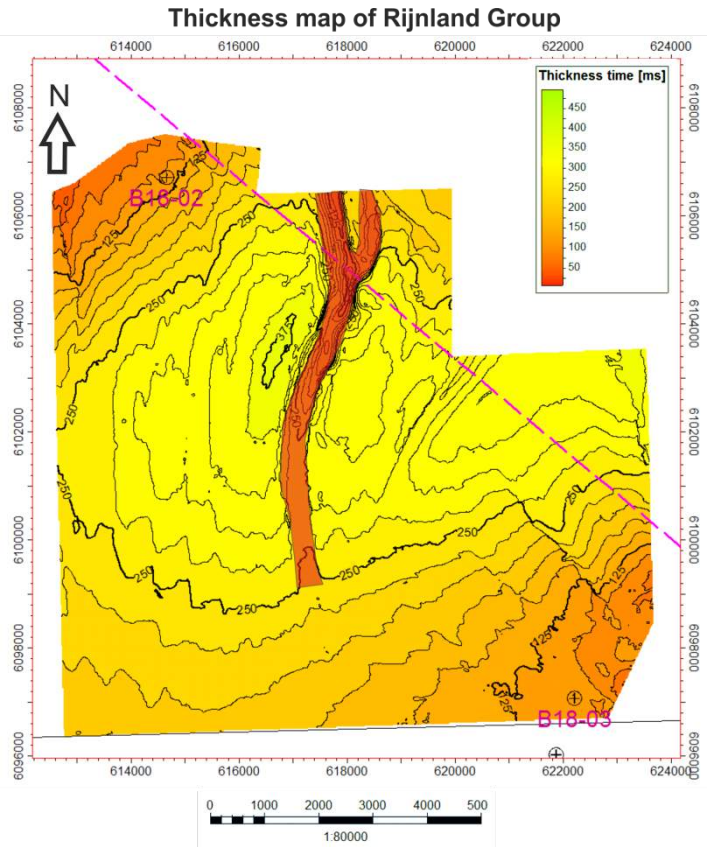

Fig. 31. Thickness map of the Rijnland Group. The fault gap of Fault F3b is indicated in red.

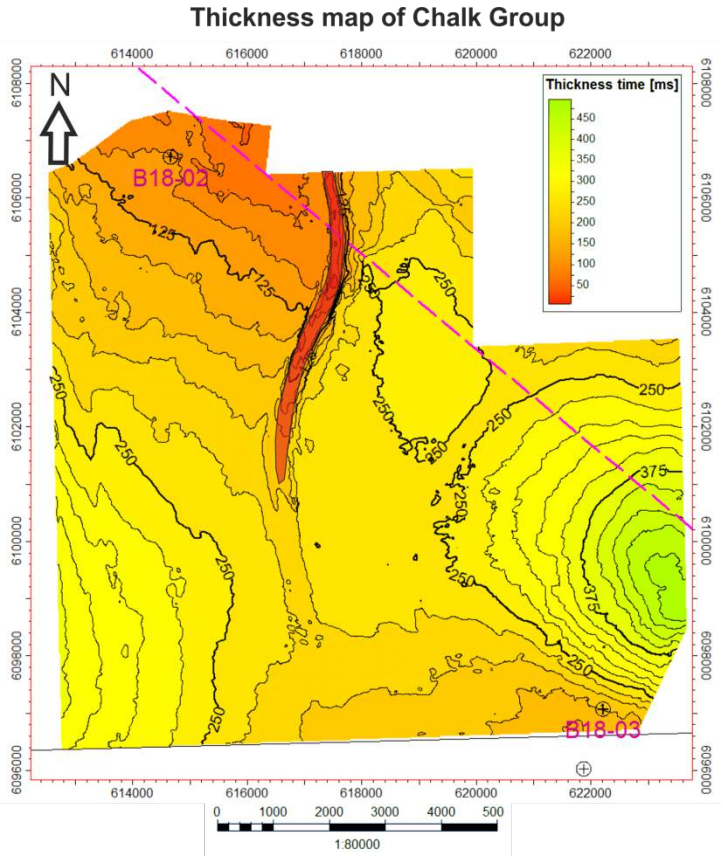

Fig. 32. Thickness map of the Chalk Group. The fault gap of Fault F3b is indicated in red.

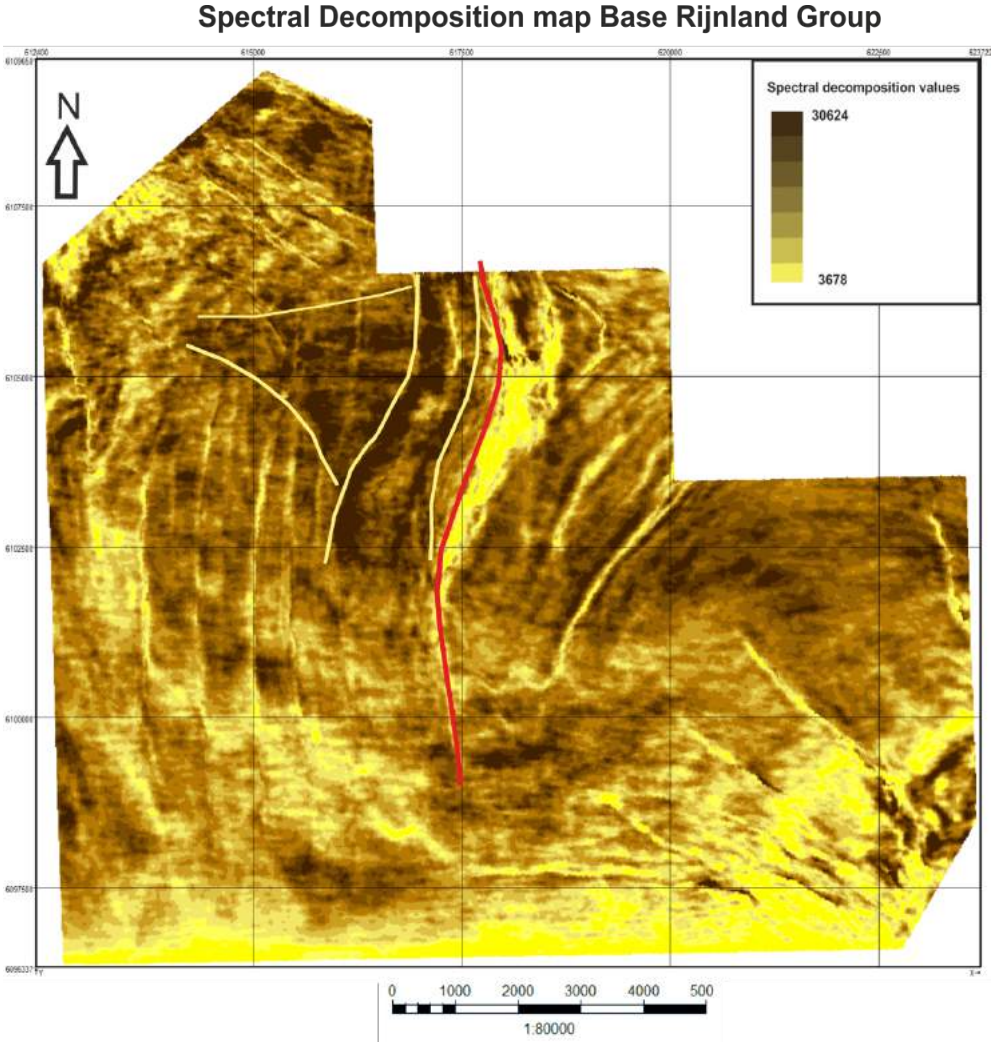

Fig. 33. Spectral decomposition of the base of the Rijnland Group. The outline of the interpreted depositional fans is indicated by the bright yellow lines. The outline of fault F1b is indicated in red.

Interpretations

Why is Fault F1b a strike-slip fault

Because of the upward widening of the fault pattern in the Jurassic interval, the unresolved stratigraphic thickness differences on either side of the fault, the nearly vertical fault plane of Fault F1b and the upward concave bending of the fault, Fault F1b has been interpreted as a strike-slip fault. This strike-slip component is hard to recognize in the southern part of the fault as Fault F1b runs parallel here to the Jurassic contour lines (Fig. 29). Along the part where Fault F1b runs more NNE-SSW though, it can be inferred that the strike-slip motion brought a deeper part of the basin where more sediments had accumulated during the Jurassic next to a more proximal part of the basin, where the Jurassic stratigraphic interval is thinner (Fig. 29) This thickness difference can't be explained by a normal fault because the fault plane of Fault F1b is too steep and is even dipping slightly towards the east, which would have caused sediments to be thicker toward the east of the fault if caused by normal faulting. And although the Jurassic strata generally tin towards the east-northeast in this area (Figs. 27, 28 and 29) it is unlikely that the abrupt thickness difference of 200ms_TWTT is of pure stratigraphic origin.

What is the sense of motion of Fault F1b and how much lateral displacement did occur along the fault plane of F1b?

The thickness of the Jurassic interval on either side of the fault, as well as the general depositional pattern during the Jurassic can be used to obtain the sense of shear of strike-slip fault F1b, as well as to make a rough estimate about the amount of displacement that occurred along fault F1b. For this purpose, the thickness map of the Jurassic in Figure 29 was used. From this map can be inferred that the general depocenter of the basin during the Jurassic was towards the west-southwest. Because movement on fault F1b positioned a deeper part of the basin on the western side against a

shallower part of the basin on the eastern side, motion along Fault F1b had to be dextral. When regarding the 750ms contour line on either side of the fault, a right stepping of this contour line can be observed across fault F1b. This step has a length of around 900 meters (measured along the arrow in Fig. 29). Consequently the amount of displacement that was accommodated by fault F1b lies in the order of 900 meters.

When was fault F1b active?

The fact that fault F1b offsets strata of the entire Upper Jurassic indicates that it was active during or after the (Upper) Jurassic. From Fig. 31can be inferred that the distribution of the Rijnland group was controlled by a larger antiform that extends across fault F1b. Hence, fault F1b already formed before the Rijnland Group was deposited. A narrower constraint on the time can be obtained from Figure 30, which shows the thickness of a Upper Jurassic sequence 2 interval. Although it was not possible to extract a detailed and complete thickness map of this stratigraphic interval on both sides of Fault F1b because of resolution difficulties, it seems that the isopach lines curve into Fault F1b on its western side, thereby suggesting that the depositional pattern was controlled by Fault F1b. This would mean that Fault F1b was active during the Later part of the Upper Jurassic. Additionally a time constraint of Fault F1b can be obtained from Figure 33, which shows a spectral decomposition map of the base of the Rijnland Group. Two depositional fan sedimentary structures can be seen in this map, as indicated by the darker, high frequency areas. The eastern structure seems to be bounded by Fault F1b as it follows the outline of the fault. This would suggest that the deposition of this fan was bounded by Fault F1b. Possibly because Fault F1b had created some topography which inhibited the fan of crossing the fault. Overall, it is concluded that Fault F1b was active during the latest part of the Upper Jurassic and perhaps during the very earliest part of the Cretaceous.

What is the relation between Fault F1b and the Faults F2b and F3b?

Fault F2b and Fault F3b are both normal faults that were active during the Upper Cretaceous and lower Paleogene (F2b). It is remarkable that both Fault F2b and Fault F3b have the same strike as Fault F1b, thereby creating a small graben above Fault F1b in the Upper Cretaceous and Lower Paleogene. This could be explained by the fact that strike-slip Fault F1b had created a weak zone, which was more easily deformed during the Late Cretaceous and Lower Paleogene in a regional setting of thermal sag, following the Jurassic rifting. An additional factor that might have played a role could be that normal faulting occurred here due to different amounts of material compaction on either side of the fault, as different parts of the basin were placed against each other

4.3 Case Study C ; Strike-slip fault with fault-salt interaction.

Observations regarding Fault F1c

Fault F1C is located in the F11 block, which encompasses the central part of the Dutch Central Graben (Fig. 20). The fault is indicated as Fault F1C on the similarity map of the base of the Altena Group in Figure 34. From Fig. 34 can be inferred that Fault F1C is characterised by a curved strike and that it connects two diapirs; Diapirs A and B. The southern part of Fault F1C strikes NNE-SSW (020) . Further towards the north, the strike of the fault slightly curves towards N-S (000) and subsequently towards NW-SE (330) upon approaching salt Diapir B. Before merging with this salt diapir at its northwestern tip, Fault 1C runs parallel to the salt Diapir B. Fig. 35 shows a ENE-WSW cross-section through Fault F1c, from this can be inferred that Fault F1c is characterised by a nearly vertical dip angle of the fault plane, which is slightly dipping towards the east. The fault also displays an upward widening of the fault pattern, as well as concave upward dipping strata on either side of the fault; a so called tipi shape of the strata. The fault is offsetting strata of the Upper Jurassic Puzzle hole formation, Middle Graben formation and Lower Graben Formation, as well as strata from the Lower Jurassic Altena Group (including the Posidonia shale formation) and strata of the Upper Germanic Trias Group. Strata of the Lower Germanic Trias Group appear also to be displaced by Fault F1c, although this can't be determined with certainty. Whether Fault F1C penetrates the salt of the Zechstein group and offsets also sub-Zechstein strata is unclear due to the reduced resolution of the seismic data at this depth. Striking, when regarding Fault F1c, are the major differences in stratigraphic thickness of the Jurassic formations on either side of the fault. Both the Lower Jurassic as well as the Upper Jurassic formations are thicker on the western side of the fault than on the eastern side of the fault. This is visualised in Fig. 36 , which shows a thickness map of the Lower Jurassic Altena Group.

Observations regarding Fault F2c

Fault F2c two forms the same curved fault pattern as Fault F1c; striking NNE-SSW (020) in the southern part and subsequently turning towards N-S (000) and NW-SE (330) towards the northern part of the fault (Fig.34). The fault terminates at salt Diapir B. The fault is dipping towards the west and the fault plane is less steep than Fault F1c (Fig. 35). Fault F2c shows clear vertical offsets of around 150ms TWT in the strata up to and including the chalk group. The strata of the Lower North Sea Group display a small vertical offset of around 20ms TWTT. Both the Triassic and the Jurassic formation don't display any thickness differences that are related to activity along Fault F2c. Strata of the Chalk Group do show a thickness increase towards Fault F2c in the form of a syn-kinematic wedge.

Observations regarding Fault F3c

Fault F3c is striking E-W to ENE-WSW. It is located between Diapir B and a salt wall towards the west (not shown in Fig. 34). Fig. 37 shows a SSW-NNE cross section of Fault F3c. From this cross section can be inferred that the dip angle of Fault F3c increases with increasing depth. It can also be inferred from Fig. 37 that Fault F3c has accommodated an offset of around 150msTWT of the Lower North Sea Group. Fault F3c has also affected the entire Jurassic interval where it has accommodated an offset of around 350ms TWT. The fault seems to detach on an Upper Triassic evaporite; either the Röt evaporate or the Muschelkalk evaporite. No signs of syn-kinematic growth strata can be observed in the hanging wall of Fault F3c

Observations regarding Fault F4c, F5c and F6c

From Fig. 34 can be inferred that the Base of the Posidonia shale northeast of salt Diapir B is affected by several faults that strike approximately NE-SW. When this fault zone is seen in cross-section (Fig. 38), it turns out that the majority of these faults detach in the evaporates of the Upper Germanic Trias Group, likely the Keuper evaporite. These faults are indicated as F5c in Fig. 38. Faults F5c are characterised by inclined fault planes and affect the strata that are present above the Triassic Keuper formation up to and including the strata of the Chalk Group. Generally, the Chalk Group is thicker in the hanging wall of these faults. Fault F6c also detaches intra Upper Triassic and affects the Lower North Sea Group, the Chalk Group, Rijnland Group, the Upper Jurassic and the

Altena Group and has accommodated a minor normal offset of around 30ms in these formations. Fault F4C on the other hand also accommodates offset in the Lower part of the Upper Germanic Trias Group, the Lower Germanic Trias Group as well as in the Altena Group. Whether or not Fault F4c offsets strata in the Upper Jurassic Group and the Rijnland Group is unclear due to the limited thickness of these Groups. The strata on either side of Fault F4c show a slight upward dip towards the fault plane. This tipi shape is profound in the Upper Germanic Trias Group and the Altena Group but is for sure absent in the Chalk Group and the Lower North Sea Group . Additionally, Fault F4c displays an upward widening of the fault pattern up to and including the strata in the Altena group.

Because of Mid-Kimmerian and/or Alpine erosion, which has affected the Jurassic strata up to and including the Altena Group west of the fault, it is hard to say something about the stratigraphic thicknesses of the Jurassic strata on either side of Fault F4c. The Upper Germanic Trias Group has been entirely preserved on either side of the fault. The Lower part of the Upper Germanic Trias Group (probably the Röt and the Muschelkalk formations) are thinning towards salt Diapir C. Strata of the upper Germanic Trias Group (likely the Keuper formation) strongly increase in thickness towards salt Diapir C. However, despite this increase in thickness towards salt Diapir C, the strata of the Upper Germanic Trias Group appear to make a sudden increase in thickness across Fault F4c.

Observations regarding the salt structures

Salt Diapir A is only partly located within the seismic dataset of case study C but it appears to have a circular geometry (confirmed with other seismic data). Strata of the Upper Germanic Trias Group display thinning towards the salt dome. Strata of the Lower Jurassic Altena Group as well as strata of the Upper Jurassic become thicker towards the salt Diapir A.

Salt Diapir B has an elongated geometry. The salt structure is at its widest in the NW-SE direction (around 7km) and at its shortest in the NE-SW direction (around 2km). Salt Diapir B furthermore also extends towards the east, outside of the seismic dataset. Strata of the Uppermost part of the upper Germanic Trias Group, as well as strata of the Lower Jurassic Altena group become thinner towards the salt dome. Strata of the upper Jurassic become thicker towards salt Diapir B.

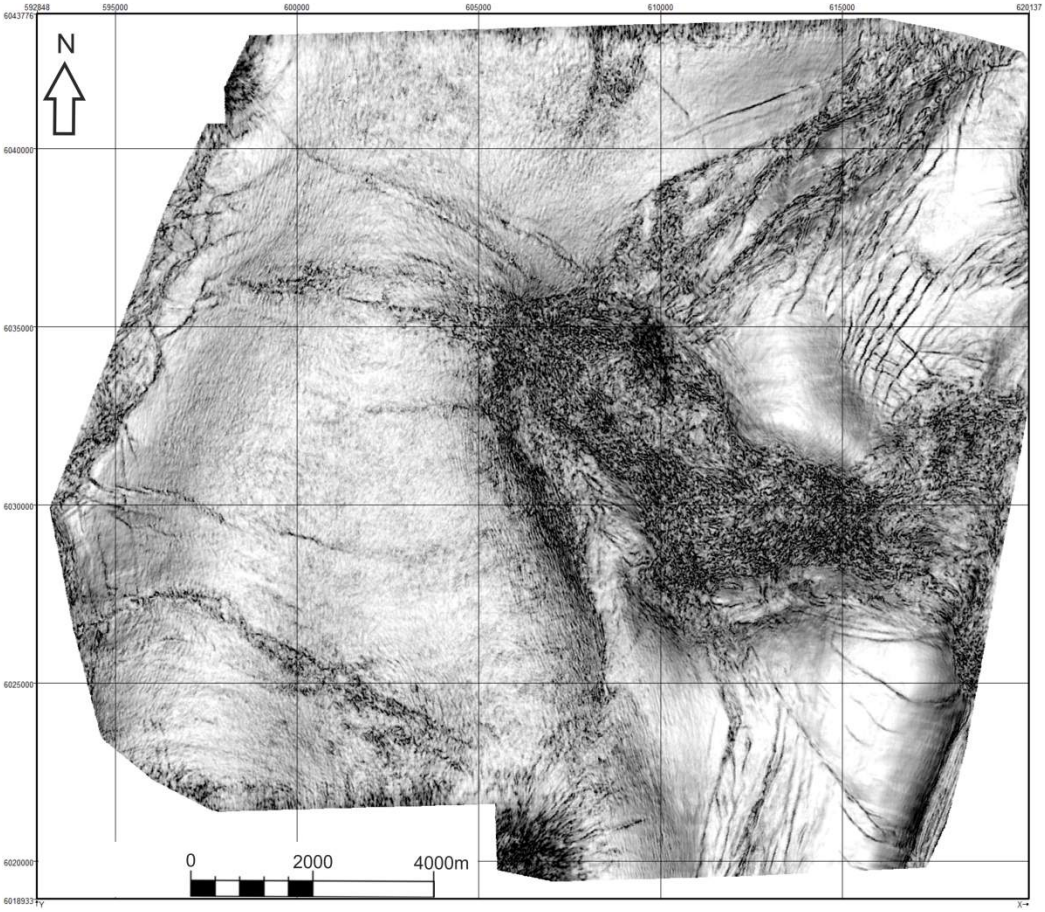

Fig. 34a. Uninterpreted similarity attribute map of the

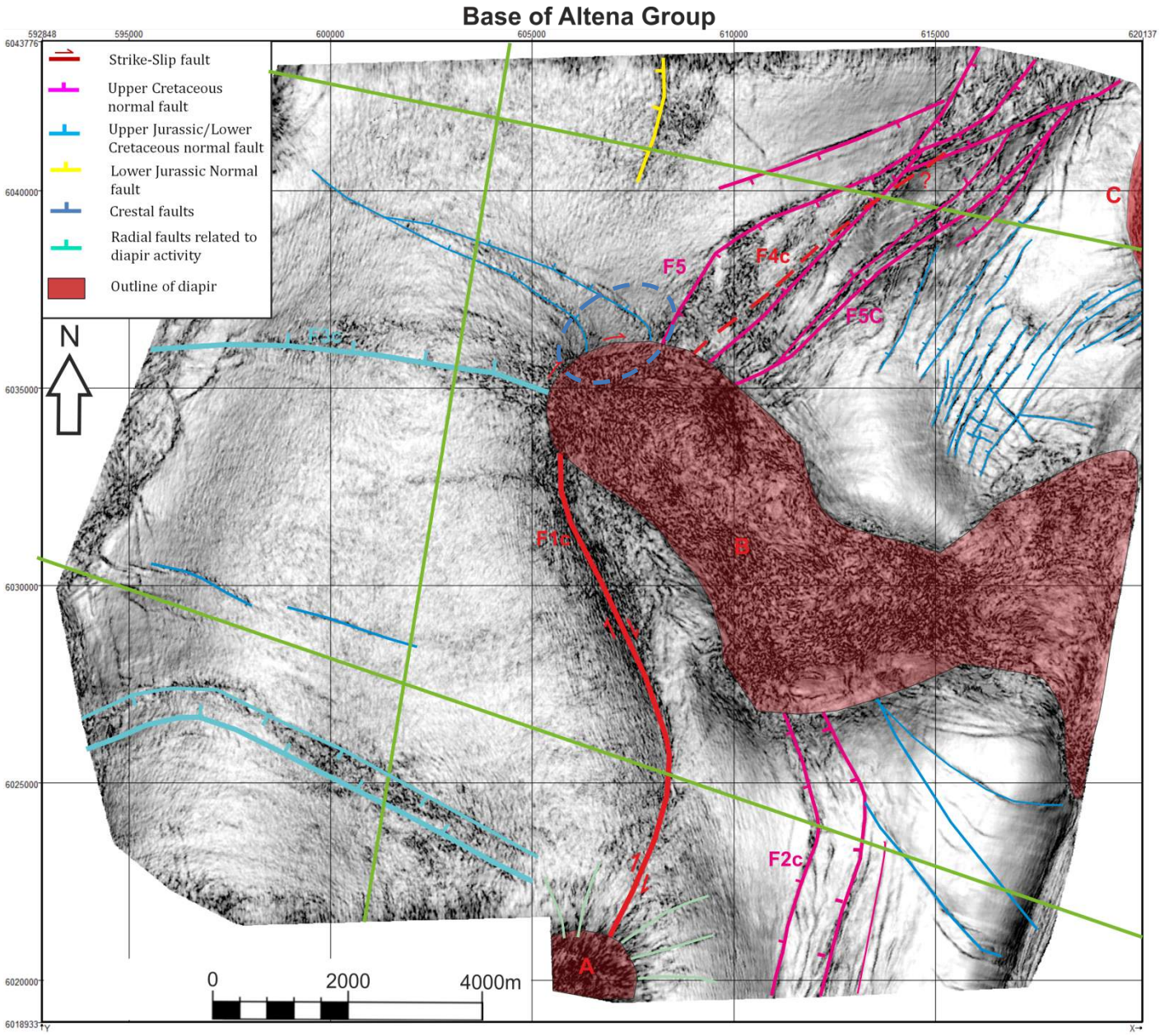

Fig. 36b. Similarity attribute map of the base of the Altena Group in block F11. The black areas indicate a high degree of dissimilarity, the white colours indicate a high degree of similarity (see methods). Fig 36a shows the interpreted similarity map of the base Altena Group. The bright green straight lines indicate the location of the seismic lines in the Figures 37, 39 and 40.

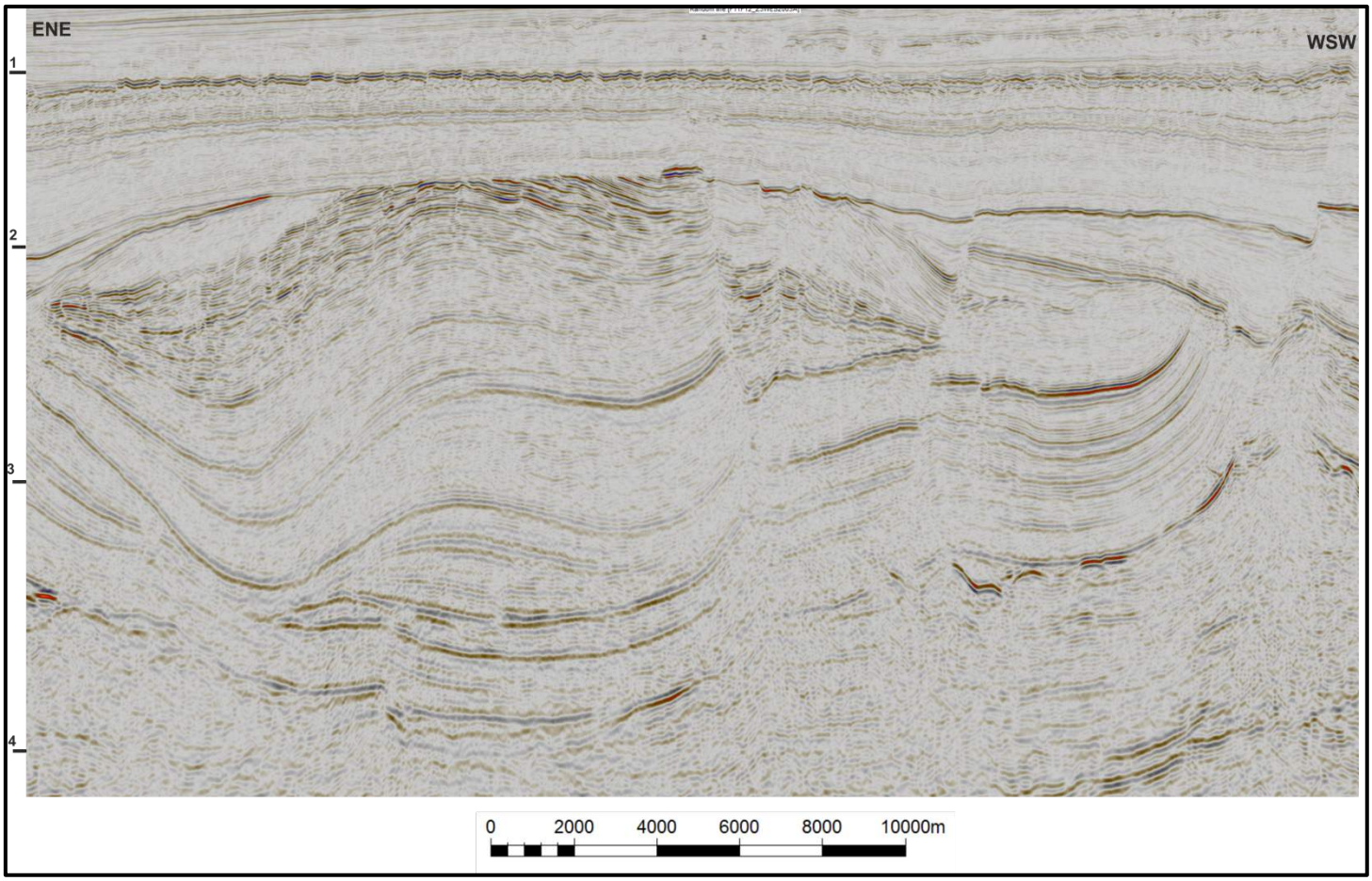

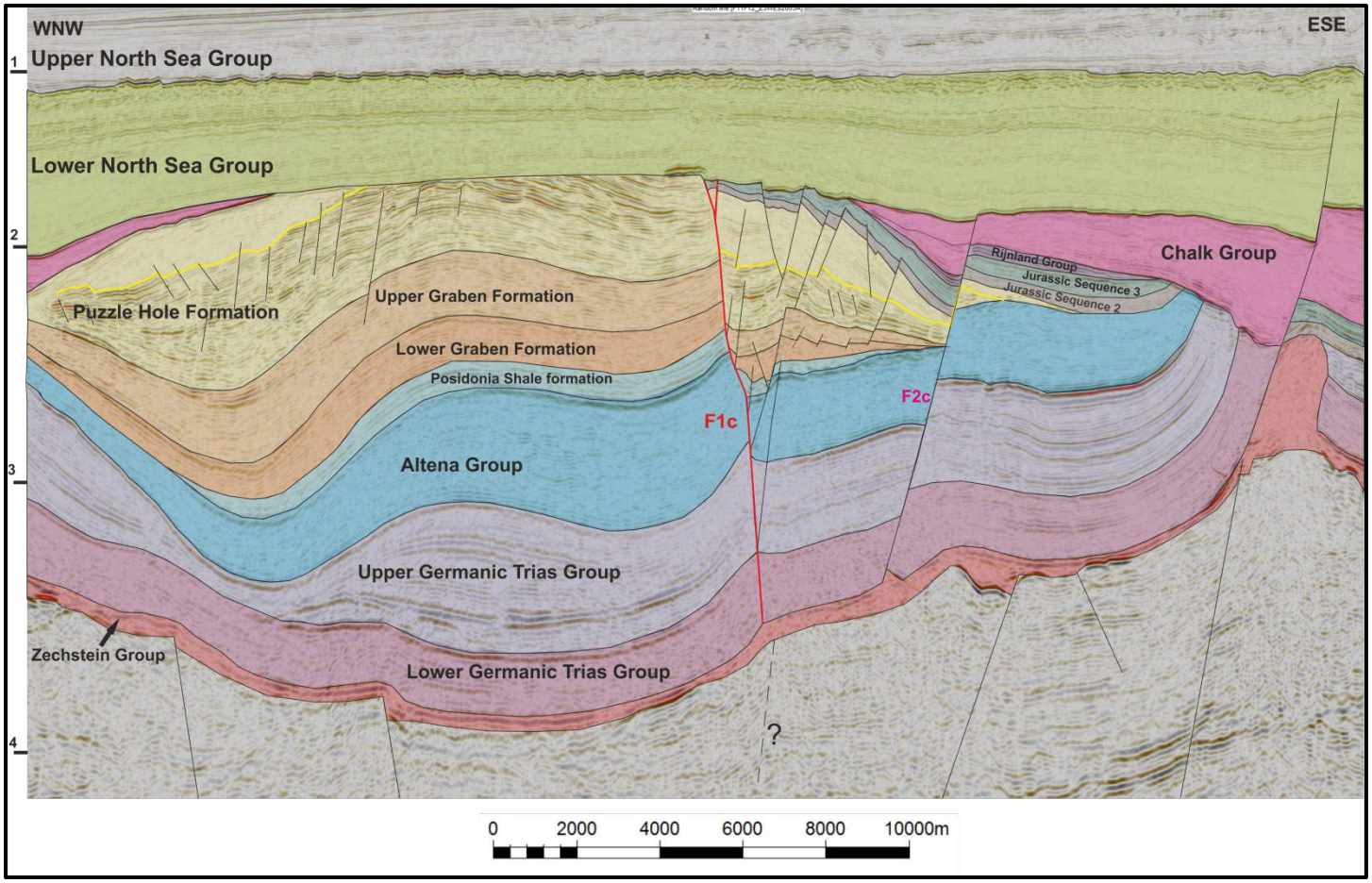

Fig. 35. ENE-WSW cross-section showing fault F1c and fault F2c. The top figure shows the uninterpreted seismic line, the bottom figure shows the interpreted seismic line. The location of the seismic line is indicated by the straight bright green line in Figure 36b.

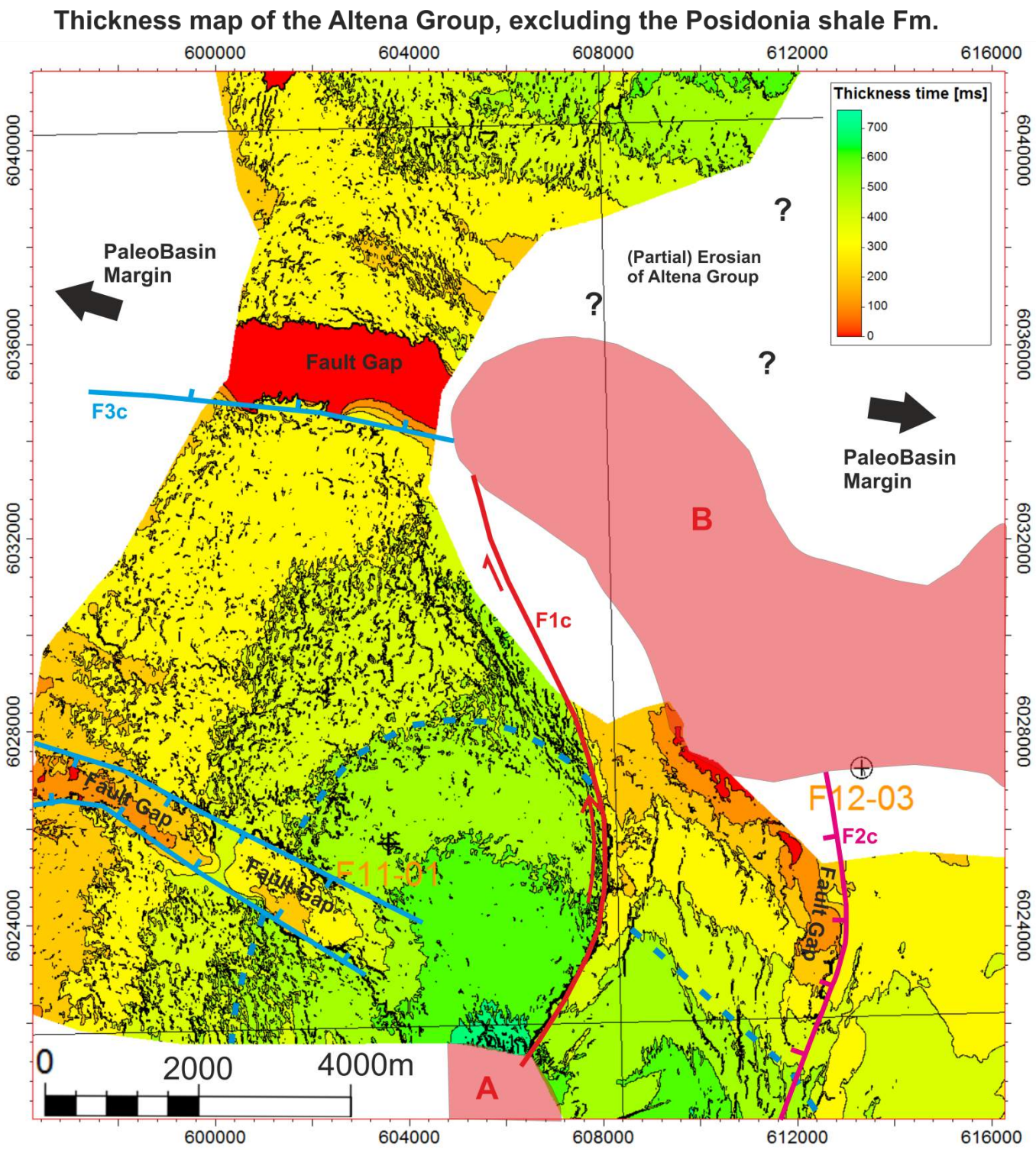

Fig. 36. Isopach (TVT) map of the Altena Group in the F11 block. The Dashed Blue line indicates the approximate position of the 500ms contour line from which an estimate of the amount of displacement along Fault F1c is made. A reliable thickness map of the area could not be made towards the north of salt Diapir B as the Altena Group is not complete there because of Mid-Kimmerian erosion.

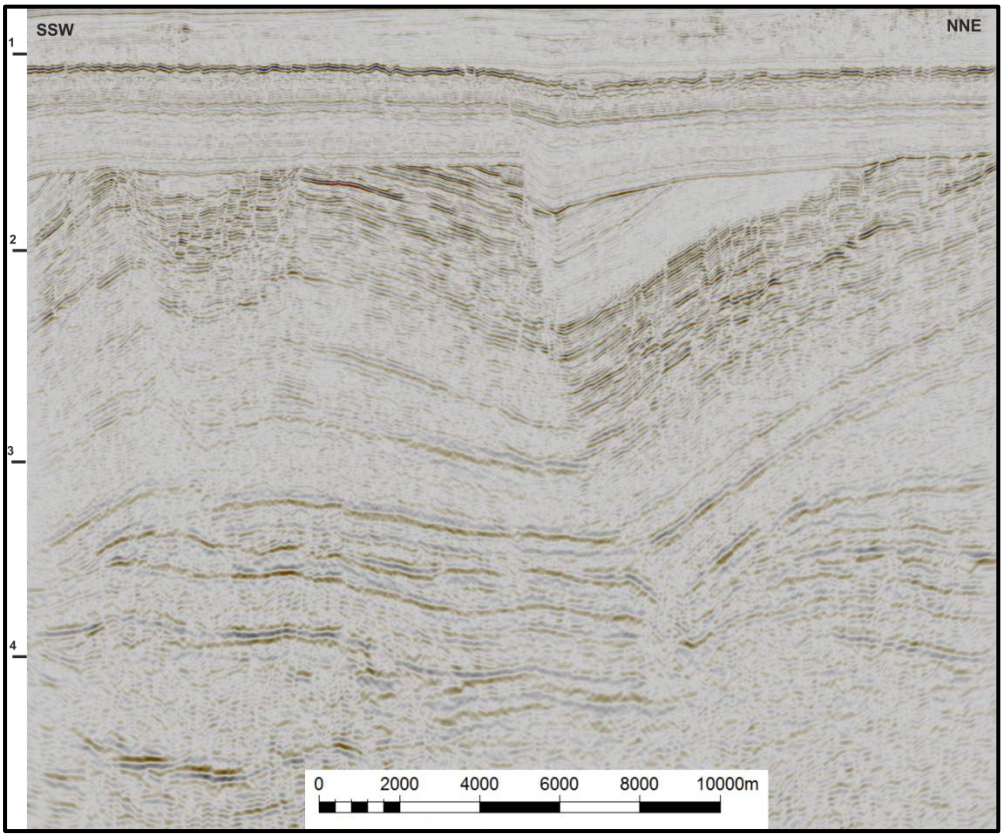

Fig. 37. NNE-SSW seismic cross-section showing fault F3c. The location of the seismic line is indicated by the straight bright green line in Figure 34b.

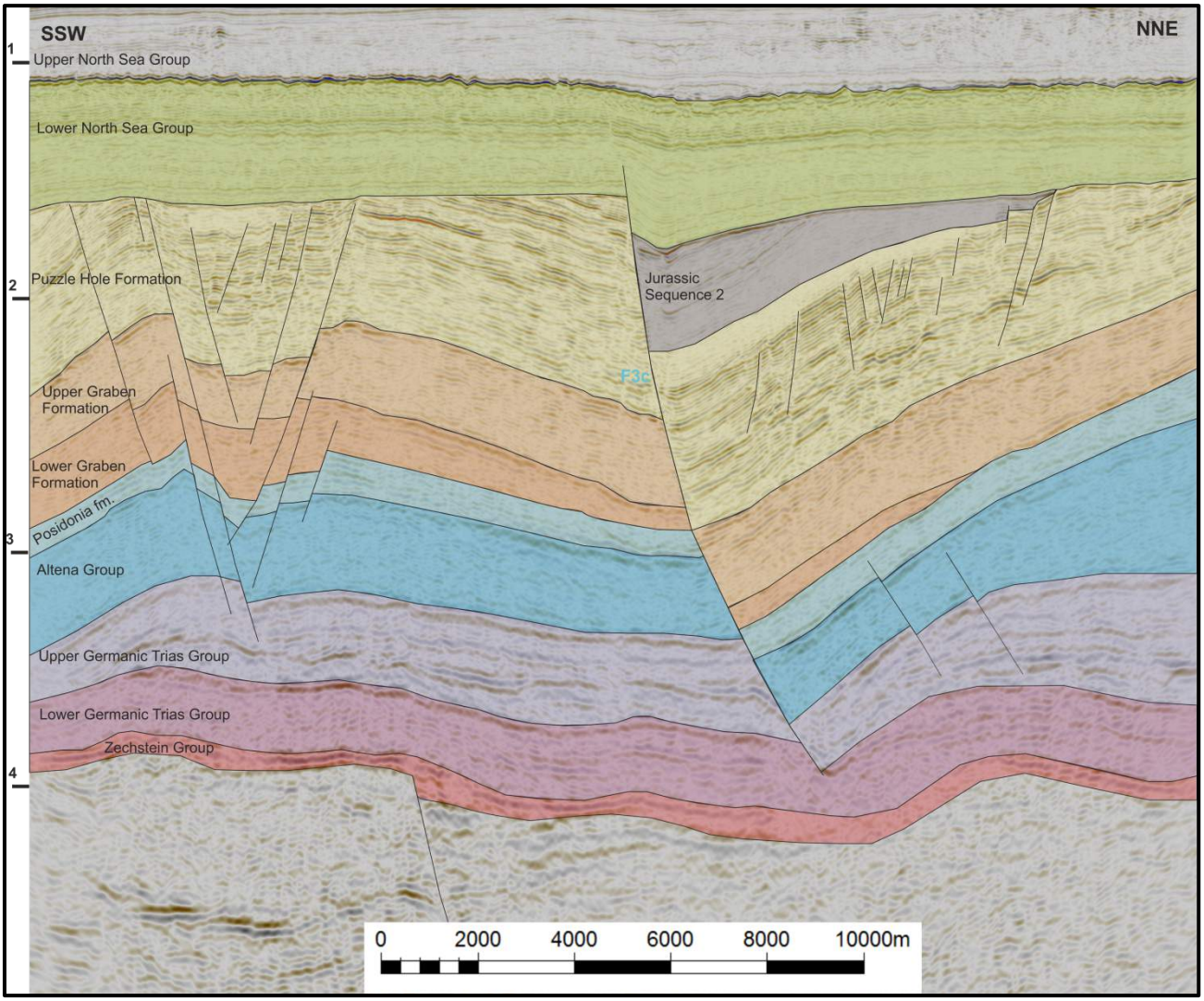

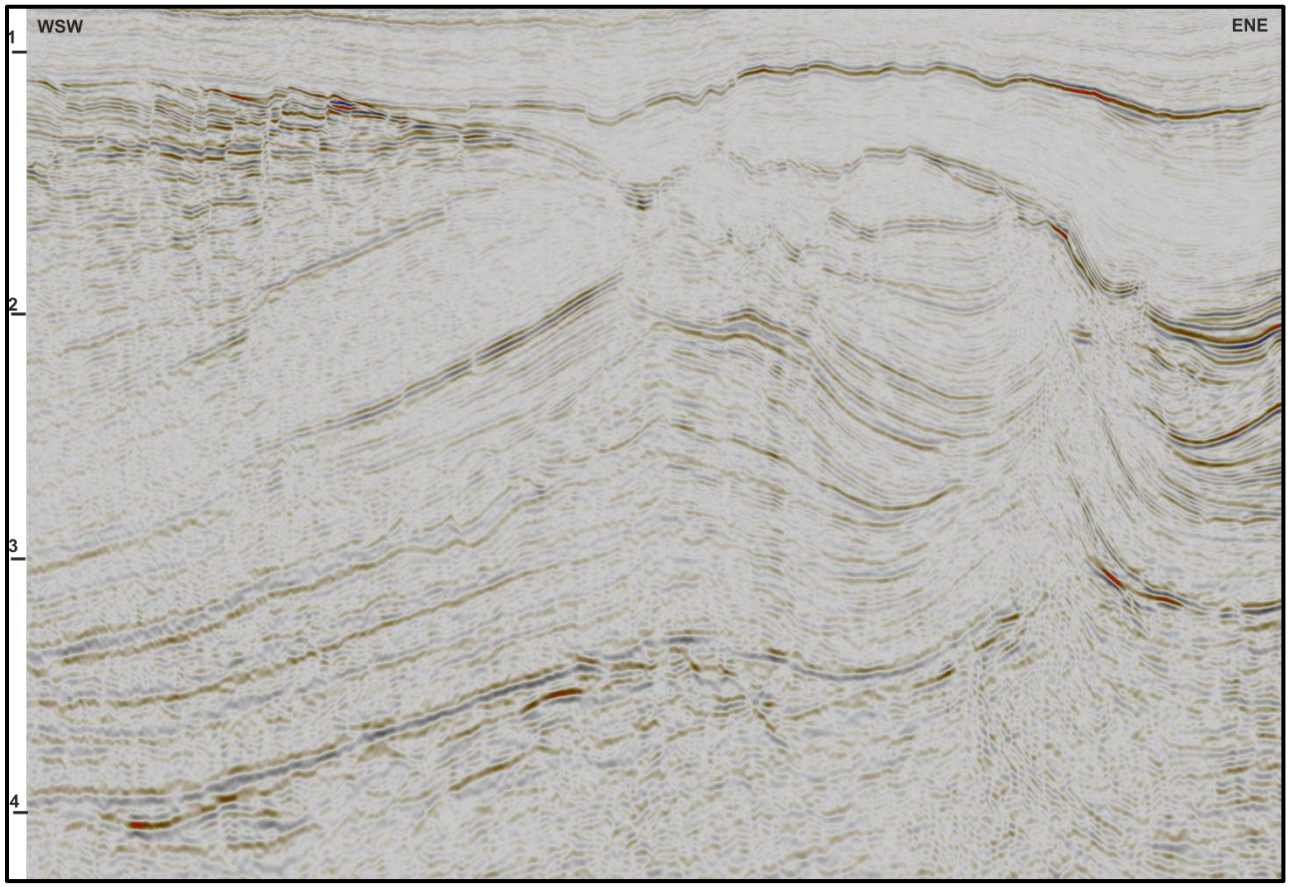

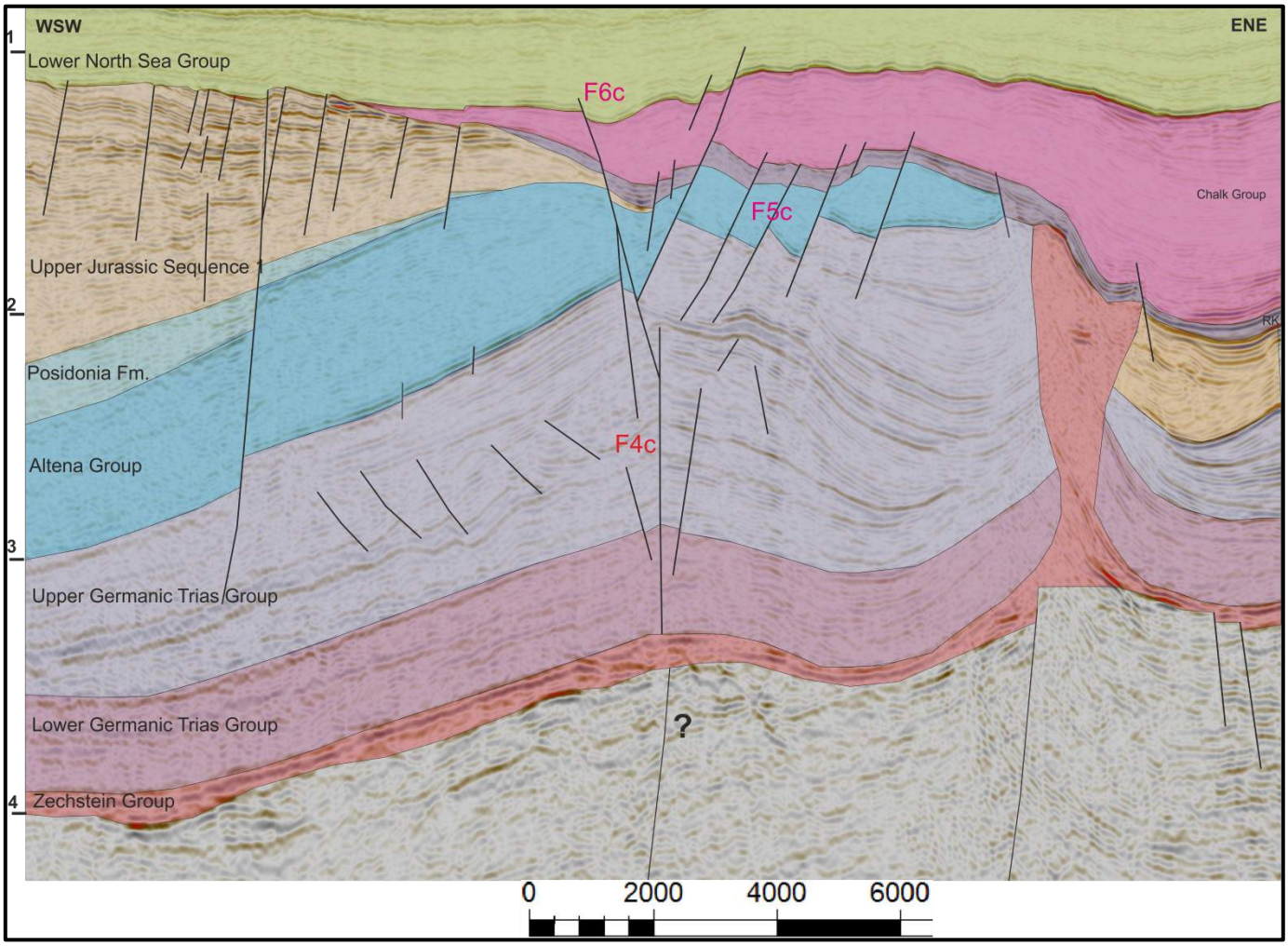

Fig. 38. ENE-WSW seismic cross-section showing the faults F4c, F5c and F6c. The location of the seismic line is indicated by the straight bright green line in Figure 36b.

Interpretations

Why is Fault F1c a strike-slip fault?

The nearly vertical fault plane of Fault F1c, as well as the concave upward bending of strata on either side of the fault, the upward widening of the fault pattern and the unresolved stratigraphic thickness differences on either side of the fault, leads to the interpretation that Fault F1c has accommodated strike-slip motions. This strike-slip motion would have brought a deeper part of the basin where more sediments had accumulated during the Lower Jurassic next to a more proximal part of the basin, where the Lower Jurassic formations are thinner. The option that a normal fault (with growth strata in the hanging wall) would be responsible for the observed stratigraphic thickness differences is ruled out because such a fault would have had a westward dipping fault plane. Additionally, the thinning of Jurassic strata towards the basin margin in the east can't explain the sharp contrast in stratigraphic thickness that is observed across the fault plain.

What is the sense of motion of Fault F1c and how much lateral displacement did occur along the fault plane of F1c?

The thickness differences in the Jurassic on either side of the fault can be used to obtain the shear sense of the strike-slip fault. They can also be used to make a rough estimate about the amount of displacement that was accommodated by Fault F1. This was done by making use of the thickness map of the Altena Group in Fig.36. From this map can be inferred that the regional depositional pattern is characterised by a general thickening of Lower Jurassic strata towards the south. The fact that the Lower Jurassic interval towards the west of Fault F1c is thicker than the Lower Jurassic interval towards the east of Fault F1c indicates that the block towards the west of the fault has moved in northern direction with respect to the eastern block, thereby opposing a relatively thick lower Jurassic interval at the west of the fault against a relatively thin Lower Jurassic interval at the eastern side of the fault. When regarding the 500ms contour line of the Lower Jurassic Thickness map (indicated by the dashed blue line in Fig. 36), an estimate about the amount of displacement on Fault F1c can be made by assuming that it was displaced as described above and that it originally correlates with the 500ms contour line on the other side of the fault. When this is done, the amount of displacement turns out to be in the order of 2km. It is imported to notice that the dashed blue line in Fig. 36 along which the distance was measured doesn't follow the outline of the light green area because this area contains some mapping uncertainty as it is close to Diapir B. Hence it was chosen to follow the normal distance between the 500 and 600ms contour line as is indicated by the regional depositional pattern, which leads to a curved dashed line.

Additionally a rough estimate on the amount of displacement that occurred along Fault F1c can be obtained by the drag that can be seen in Lower Jurassic crestal faults (encircled by the dashed blue line in Figure. 34b) the fact that these crestal faults curve into the salt diapir confirms the dextral sense of motion that was obtained from the interpretation of the thickness map of the Altena Group. When the distances between the tip of the crestal fault right next to the diapir, and the assumed normal location of the crestal fault is measured. A minimum of 700m of horizontal motion should have occurred along this part of the fault-diapir system.

When was Fault F1c active?

The fact that the fault is offsetting the Jurassic strata up to and including the Puzzle Hole formation indicates that the fault was active either during deposition of the Puzzle Hole formation but most likely after deposition of the Puzzle Hole formation. In the F11 block, the Lower North Sea Group is overlying the Puzzle Hole formation in the centre of the Dutch Central Graben. This means that there is a hiatus present where the Jurassic Sequences 2 and 3, as well as the entire Cretaceous is missing. It is likely that Fault F1 was active somewhere during this time interval. The minor offset which is present in the Lower North Sea Group is likely to be caused by a later episode of normal faulting along or above Fault F1c.

What is the relation between Fault F1c and the salt Diapirs A and B?

The fact that the strata of the Lower Jurassic Altena Group and the strata of the Upper Jurassic Sequence 1 thicken into salt Diapir A indicates that salt Diapir A was in the active piercing stage during this time period, thereby creating a rim syncline directly around the diapir which caused the strata of the Altena Group and the Jurassic Sequence 1 to thicken into the diapir. Salt B reached the piercing stage slightly later, as no thickening in the Altena Group can be observed towards the diapir. However, during the deposition of the Upper Jurassic Sequence 1, salt Diapir B must have been in the active piercing stage as well.
As mentioned, the exact timing of strike slip Fault F1c remains a bit elusive. However, activity on Fault F1c for sure postdates the puzzle hole formation and hence Jurassic Sequence 1. This means that the Diapirs A and B likely predate Fault F1c. Because the salt diapirs are mechanically weak, they have probably accommodated strike-slip motions in this area as well, which is supported by the drag that is observed at the crestal faults (Fig. 34b). It is suggested that because of the absence of salt in the area around F1c, strike-slip motion had to be accommodated in a brittle way by creating Fault F1c. Fault F1c hence links Diapirs A and B that likely have both accommodated strike-slip motions as well.

It is likely that strike-slip motion did not cease at Diapir B, but that it continued along Fault F4c. Surely Fault F4c shows characteristics of a strike-slip fault including a nearly vertical fault plane, upward widening of the fault pattern and a tip-shape of strata on either side of the fault. Therefore it is suggested that the strike-slip motion accommodated by Fault F1c continued via Diapir B into Fault F4c. The different strike of Fault F4c compared to Fault F1c could be explained by the presence of Diapir B, which could have refracted the strike-slip motion to some extent. However, this interpretation regarding strike-slip motions on Fault F4c needs to be hedged as the Upper Jurassic around F4c is missing due to erosion.

Case Study D; Strike-Slip faulting in the Terschelling Basin and on the Schill Grund High

Structural Observations

NW-SE to WNW-ESE striking faults.

Terschelling Basin

The Terschelling Basin is bounded in the North and South from the Schill Grund Platform and Central Offshore Platform by the Rifgronden fault zone (RFZ) and the Hantum Fault Zone (HFZ) respectively (Fig.39). The HFZ is charachterised by a generally straight ESE-WNW strike and dips towards the NE. When the HFZ approaches the Dutch Central Graben, it splits into multiple branches of which the most northern branch shows a curved geometry and eventually merges with the N-S trend of the Dutch Central Graben. The RFZ is composed of more shorter fault segments than the generally straight and continues HFZ. These fault segments display an overall en echelon type of geometry. The majority of the faults that form the RFZ dip towards the Southwest, but some antithetic faults are also present, forming a pop-up geometry on faults of the RFZ. Strata of the Upper Jurassic and the Lower Creataceous Rijnland Group thicken into the hanging wall of both the HFZ and the RFZ (Peeters, 2015). Strata of the Chalk Group and the Lower Paleogene North Sea Group are sometimes thicker in the footwall than in the hanging wall of the faults that form the HFZ and the RFZ. Besides the large RFZ and HFZ, also smaller NW-SE to WNW-ESE striking faults occur in the Terschelling Basin (Fig. 39). These faults generally detach on the Zechstein salt and also display thicker Upper Jurassic and Lower Cretaceous strata in their hanging wall (Fig. 39).

Schill Grund Platform.

On the Schill Grund Platform, the NW-SE, WNW-ESE fault trend is generally not well developed (Fig.40 and Fig. 41). However, there are some areas were thin-skinned extension occurred along WNW-ESE trending supra salt grabens (Figs. 41 and 43). These grabens show an increase in thickness of the Upper Cretaceous Rijnland Group. Some grabens additionally display a slighlty thinner Upper Cretaceous Chalk Group above their core. The Grabens detached on a thin layer of Zechstein salt. This thin layer of Zechstein salt has been pushed-up by another evaporite layer that has its origin in the Upper Rotliegend interval. This Upper Rotliegend evaporite seems to be present only in the southern part of the Schill Grund Platform. In the Teschelling Basin, no evidence of these Upper Rotliegend evaporites has been found.

N-S to NNE-SSW striking low Angle Detachment faults.

The Lower and Upper Triassic interval in the Terschelling Basin, and the adjacent Schill Grund Platform and southern part of the Central Offshore Platform, has been affected by a zone of low angle detachement faults. In the Terschelling Basin and on the Central Offshore Platform, there is one dominant low angle detachment fault (indicated as DF1 in Fig. 39). The low angle detachment faults strike roughly N-S on the Schill Grund High and on the Central Offshore platform (Figs. 39, 40 and 41). In the Terschelling Basin, the main low angle detachment fault trends more NNE-SSW. Additionally, also the salt walls in the Terschelling Basin, as well as the outline of the Lower Triassic Röt compartments that are bounded by the salt walls display this NNE-SSW trend.

The low angle detachment faults are not charachterised by true fault planes. In fact, movements are accomodated by the salt as extension continues. These kind of structures have been described by Hudec and Jackson (2007) as salt rollers. The Lower and Upper Triassic interval both downlap on the Zechstein salt that acts as a decollement for the salt rollers (Fig. 42). This downlapping is accompanied with a dramatic increase in thickness of the Upper Triassic interval (Fig. 42). Thickness maps of the Upper Triassic formations (Peeters, 2015) indicate that some low angle detachment fault segments caused a dramatic increase in the thickness of the Röt Formation,

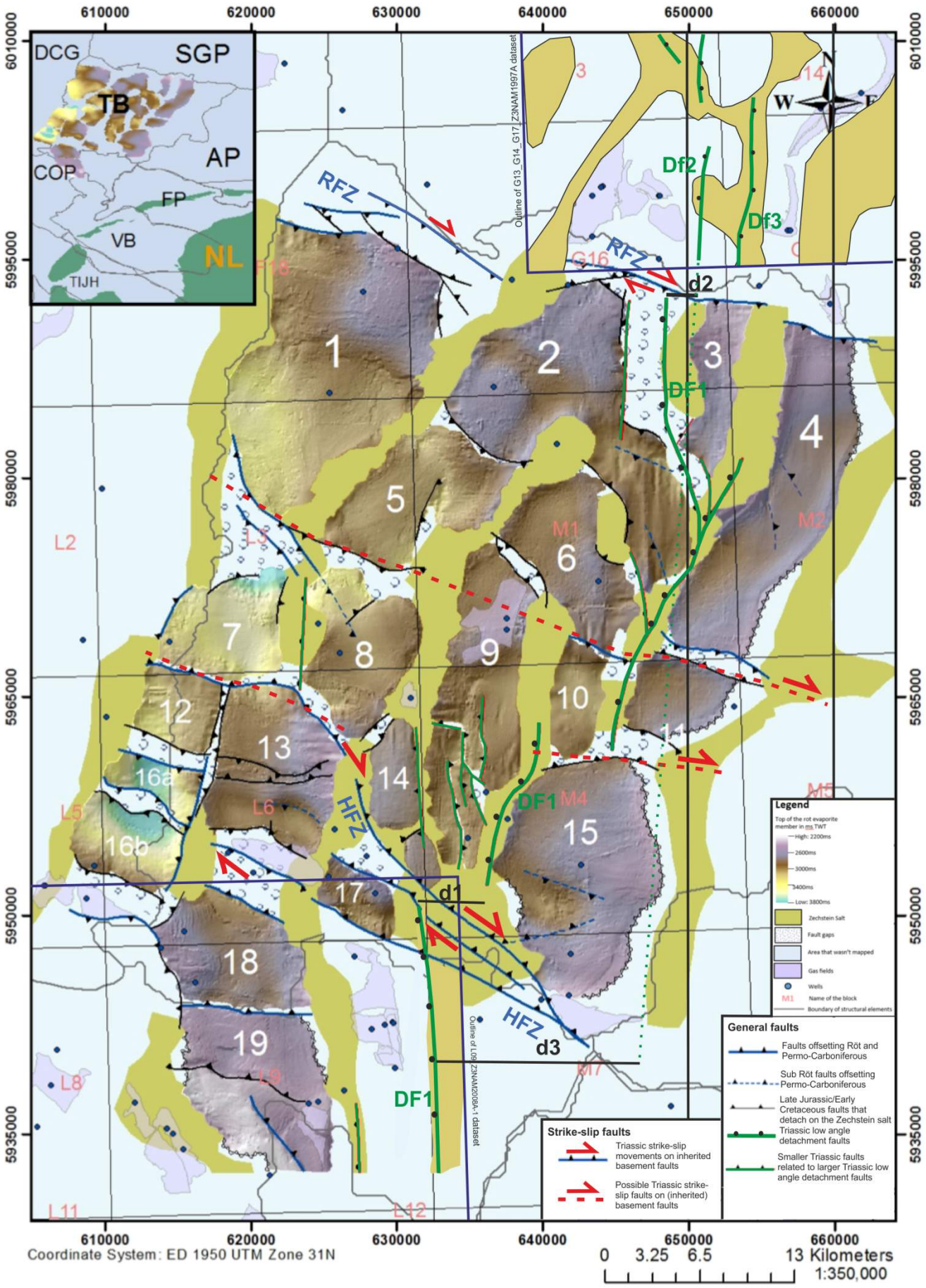

Fig. 39. Map showing the base of the Upper Triassic Röt evaporate in ms TWT. As well as the regional fault trends. Abbreviations; HFZ=Hantum Fault Zone, RFZ=Rifgrunden Fault Zone, DCG= Dutch Central Graben, SGP=Schill Grund Platform, TB= Terschelling Basin, AP=Ameland Platform, COP= Central Offshore platform, VB= Vlieland Basin, FP=Friesland Platform, TIJH=Texel IJsselmeer High. Picture modified from an EBN Project (Peeters, 2015)

while others show thicknening of the Muschelkalk Formation and/or the Keuper Formation. Locally also the the Latest Upper Triassic interval dramatically thickens due to movements along the detachment faults as is the case in the norhtern part of the Central offshore platform and in compartment 17 in the Terschelling Basin (Fig. 39)(De Jager, 2012; Peeters 2015). In these areas, Late Lower Triassic movements caused the deposition of a thick sandstone interval known as the Solling Fat Sandstone Member, which holds significant amounts of gas in the G14 fields (Fig. 39) (De Jager, 2012).

In the Terschelling Basin, the low angle detachment faults dip solely towards the WNW. In the Adjacent northern part of the Central Offshore Platform, the main low angle detachment fault dips towards the West. On the Schill Grund High, the low angle detachment faults form shorter segments and dip both towards the west, as well as towards the east. Thereby forming opposing pods of thickned Upper Triassic Strata (Fig. 40). On the Schill Grund Platform, some fault segments show a left stepping pattern (indicated with the letter A in Figure 40). This left stepping pattern can also be found in the basement faults underlying the Zechstein salt in this area (Fig. 41). Notewhorthy is also that the sub Zechstein basement faults display an overall NNW-SSE trend, which slightly contradicts with the N-S trending low angle Triassic detachment faults. The stepping geometry of the low angle detachment faults can also be observed in the Terschelling basin. Both left and right stepping of the main low angle detachment fault can be observed here, altough the right stepping pattern seems dominant (Fig. 39). Notewhorty is also the right stepping of fault DF1 across the Hantum fault zone and across the Rifgrunden Fault Zone. The right stepping of DF1 across the HFZ and RFZ, as well as within the Terschelling Basin causes that, altough DF1 on the Central Offshore Platfrom has the same strike as the low angle detachment faults on the Schill Grund High (named DF2 and DF3 in Fig 36), their present location is not inline with each other. Instead a distance d3 is present with respect to their imaginary continuation (Fig. 39).

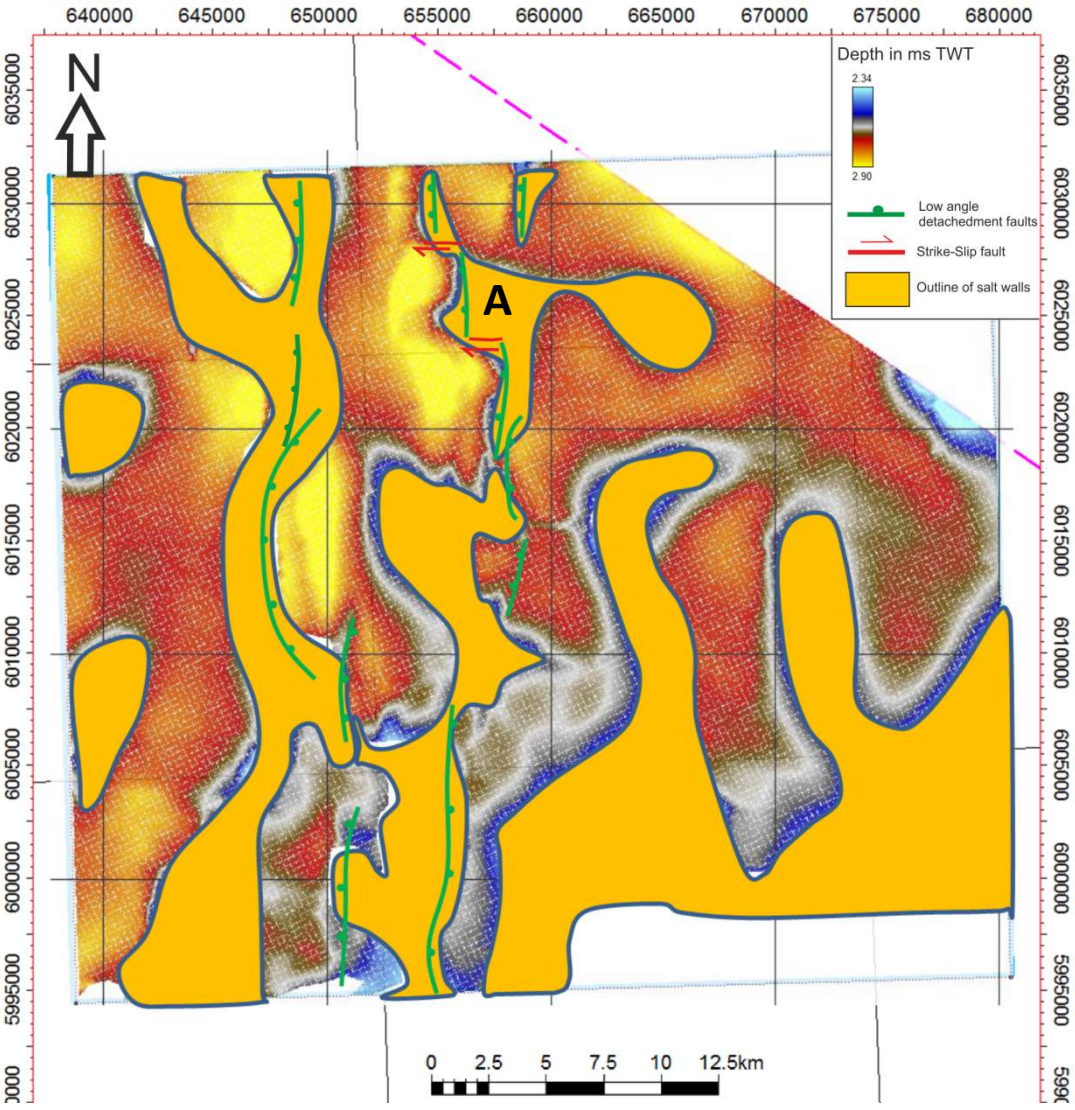

Fig.40. Map showing the base of the Zechstein Group at the Schill Grund High. The southeastern part of this map corresponds to the northeastern part indicated by the blue square in figure 39.

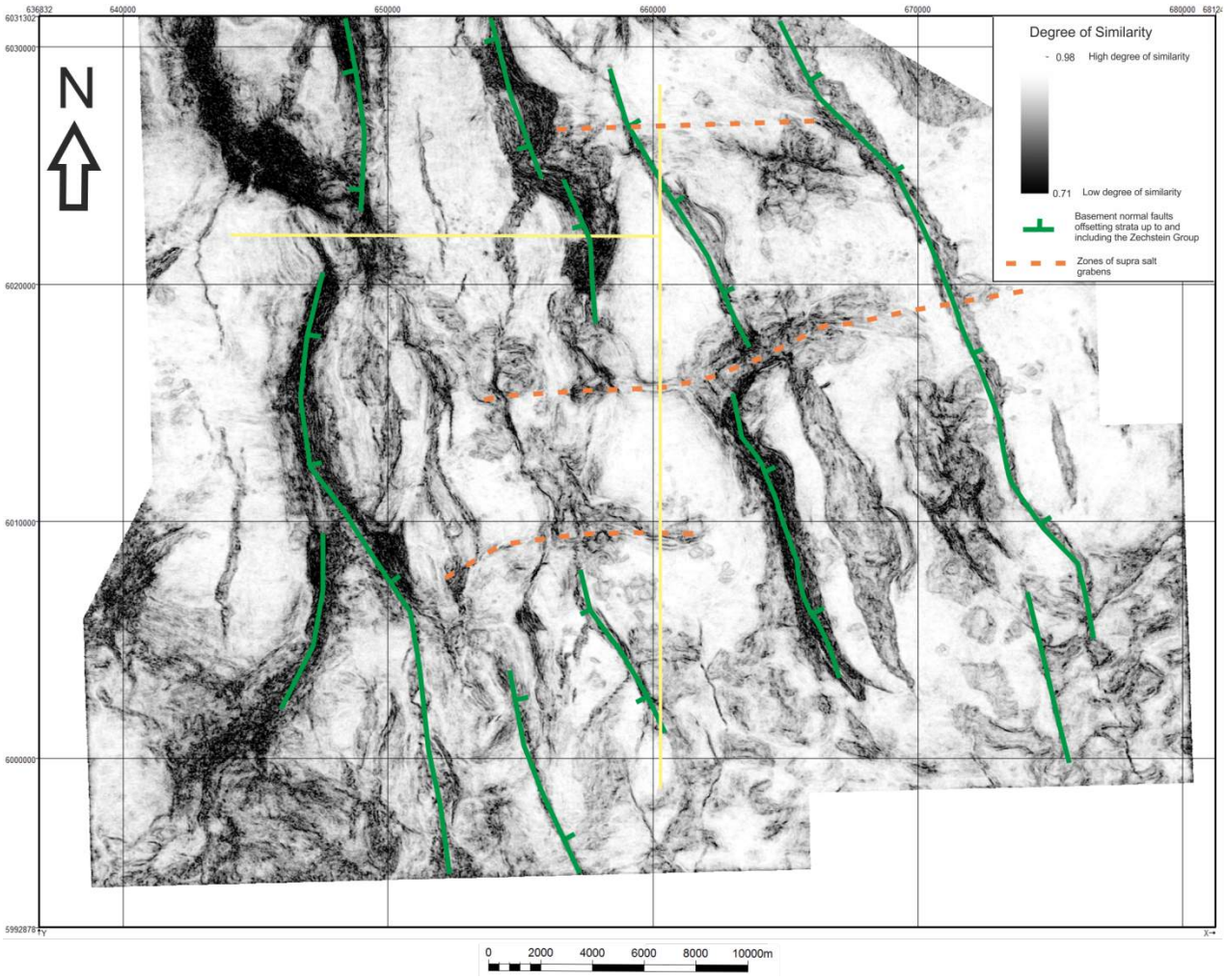

Fig.41. Map showing a similarity attribute of the base of the Zechstein Group at the Schill Grund high. The location of the cross-sections in fig. 39 and fig. 40 is indicated by the yellow lines.

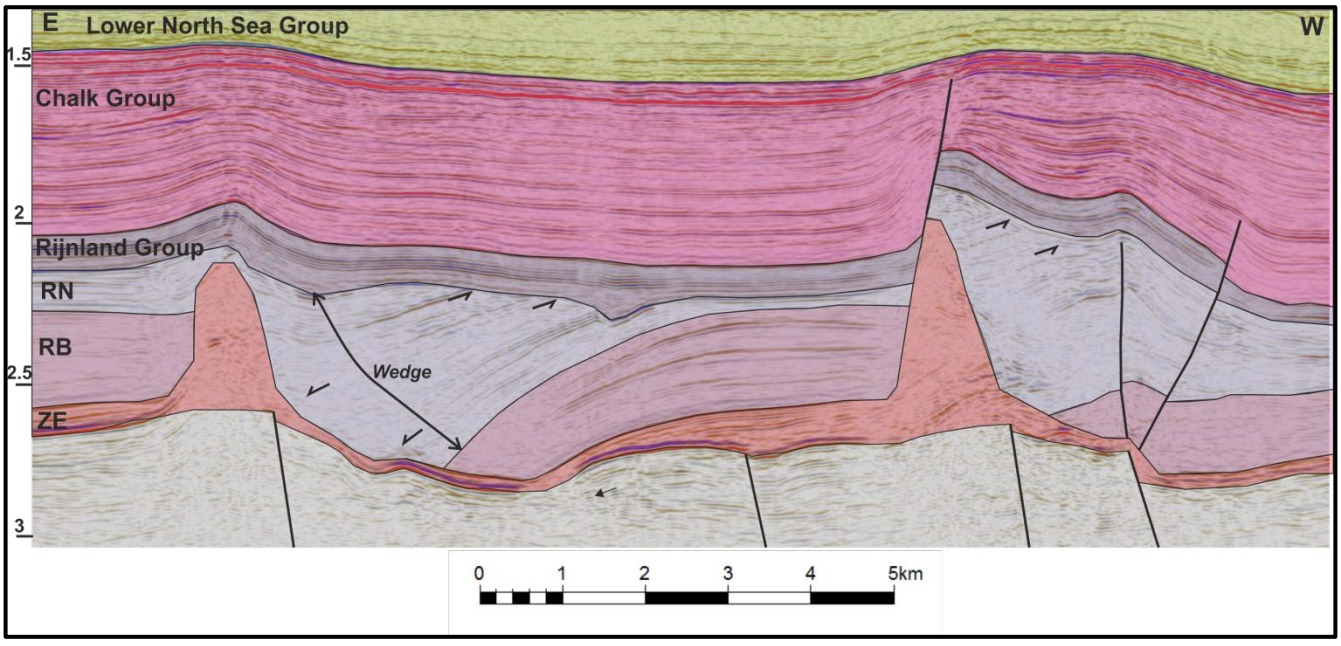

Fig.42. E-W cross-section through the northern part of the Schill Grund High, showing two westward dipping Upper Triassic low angle detachment faults. The most western low angle detachment fault has been inverted during the Upper Cretaceous.

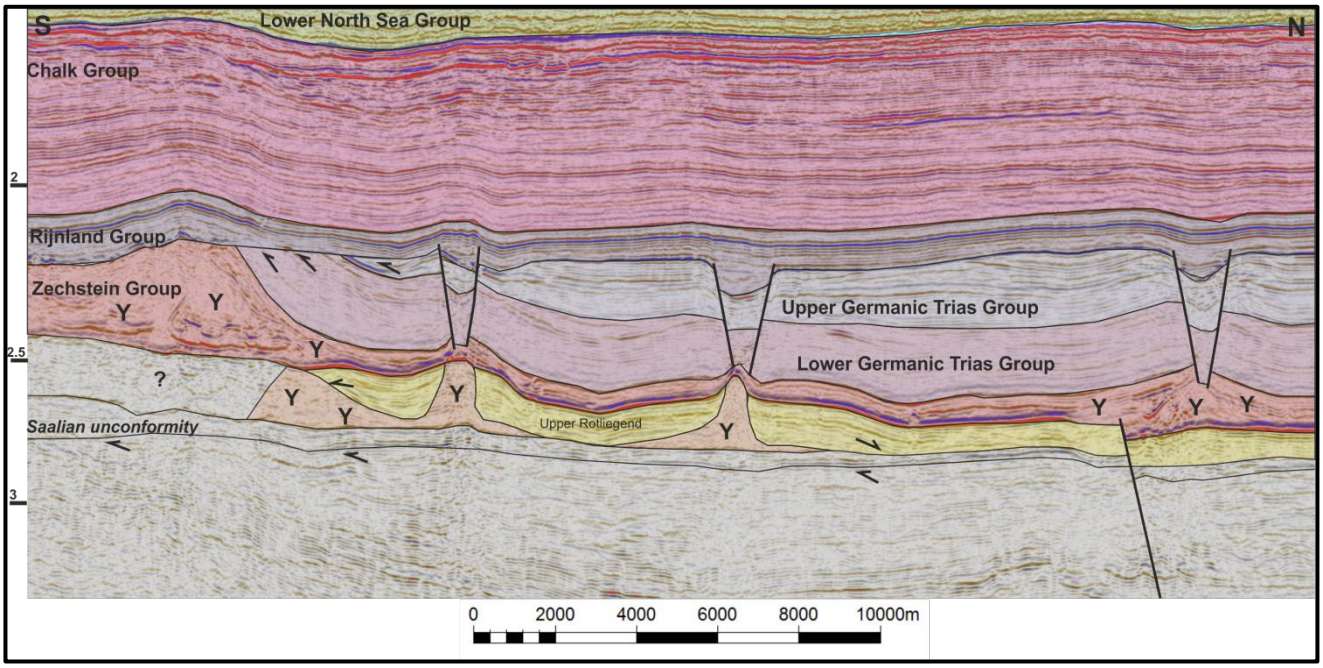

Fig.43. N-S cross-section through the Schill Grund High showing ESE-WNW trending supra salt grabens that formed during the Early Cretaceous as a result of thin-skinned extension. The southern graben was later inverted. Note also that the grabens caused the ascent of Upper Rotliegend Salt, which pushed the remaining Zechstein salt upwards. The location of the seismic line is indicated in figure 41.

Interpretations

Altough direct evidence for strike-slip movements in the Terschelling Basin and the adjacent platform areas is not straightforward, regional observations on fault and salt trends described above suggest that strike-slip movements occurred in the Terschelling Basin and to some extent on the adjacent platforms.

Thin skinned strike-slip-motions

The irregular thickness distribution of the Solling, Röt, Muschelkalk and Keuper formations indicates that activity along the low angle Upper Triassic detachment faults did not occur simultaneously. Additionally, the amount of extension on fault segments varies throughout the area. It is likely that these differences in timing and amount of extension led to strike-slip movements during the Middle and Upper Triassic and possibly the Lower Jurassic (altough no strata have been preserved of this interval in this area). Surely, differential motions over such a short area have to be compensated. This is indicated for example by the left stepping of the N-S trending low angle detachment fault in the northern part of the Schill Grund Platform (indicated by the letter A in Fig. 40) and the subsequent shift in depocenter towards the northwest (indicated by the arrow in Fig. 40). To form such a structure, the individual fault segments have to be linked by a transform fault that compensates for these differential motions. The strike-slip motions are likely accomodated by the Zechstein salt salt walls that developed in the area in response to regional extension. The motions along these faults is generally small and no evidence has been found that the displacements of these motions exceeds the width of the step between two individual low angle detachement faults. Hence, these displacements are generally in the order of 1 to 2km on the Schill Grund Platform. The displacement are likely larger in the Terschelling Basin, where the steps of the low angle detachment faults are larger than on the Schill Grund High.

These extensional and strike-slip motions are thin skinned as the low angle detachment faults used the Zechstein evaporite as a decollement. The N-S orientation of these low angle detachment faults on the Schill Grund and Central Offshore Platform indicates that the regional stress regime, causing these motions, was E-W extension. This corresponds with the (further) opening of the N-S oriented Dutch Central Graben in the Middle and Upper Triassic. However, these thin skinned motions had to be caused by motions along basement faults, as is indicated by analogue modelling (Vendeville ad

Jackson, 1992) . Indeed small offsets of the Zechstein Group are observed on the Schill Grund High (Fig. 42). The NNW-SSE trend that was recognised on the Schill Grund platform from the basement faults that offset the Zechstein Group might indicate that the NNW-SSE trend was already established and that the faults following this trend were (obliquely) reactivated during Middle-Upper Triassic E-W extension. In contrast to the Terschelling Basin, the Base of the Zechstein doesn't display a significant deepening towards the west on the Schill Grund Platform (Fig.42). This deepening of the Base of the Zechstein Group in the Terschelling Basin indicates that it is likely that gravitational gliding towards the west (in the direction of the Dutch Central Graben) enhanced thin skinned extension. This would explain why the low angle detachment faults in the Terschelling Basin solely dip towards the west, while on the Schill Grund Platform, they also dip towards the east.

Thick Skinned (basement) Strike-Slip motions in the Terschelling Basin.

The only direct evidence for strike-slip faults on basement faults are the en echelon geometry of the fault segments of the Rifgrunden Fault Zone (RFZ), which suggests that dextral motions occurred along this fault zone. Additionally, also the pop-up geometry of the RFZ may indicate that the fault has accomodated strike-slip motions, altough this pop-up geometry might also have been caused by Late Cretaceous inversion. No direct evidence was found for strike-slip motions on the Hantum Fault Zone. However, the fact that the main low angle detachment fault shows a significant rightstepping across the fault zone indicates that dextral strike-slip motions occurred on the Hantum Fault Zone (line d1 in Fig. 39). When the distance of the step across the HFZ is measured along the line d1, a dextral displacement of 5km à 6km is obtained. This displacement estimate might not be very reliable though, as both Late Jurassic/Early Cretaceous extension, as well as Late Cretaceous/Early Paleogene inversion may have modified the original displacement caused by the HFZ. Additionally, it can't be stated with certainty that the fault segments of Fault DF1 were originally attached in the first place. However, the fact that this stepping occurs exactly at the HFZ makes it very likely that the HFZ caused the majority of this displacement as indicated at place d1 in Fig.39. Hence, a dextral motion of 5 à 6km km might be a fairly good first order approximation of the strike-slip motion that occurred after the establishment of the low angle detachment fault. Surely, because the HFZ offsets the low angle detachment fault DF1, dextral motions on the HFZ must have postdated the latest Early Triassic, as this is the time that activity along this fault segment initiatd. However, it does not mean that dextral motions along the Hantum Fault zone must have postdated the Upper Triassic, when the low angle detachment faults became inactive. Surely, the low angle detachment faults and the dextral activity along the HFZ could have occurred simultaneously.

The main low angle detacement Fault DF1 also appears to be offseted by the RFZ in the north of the Terschelling Basin in a similar way as by the HFZ. On the Schill Grund Platform though, mulitple low angle detachment faults formed, hence it is a bit unambiguous if FD1 relates to FD2 or FD3 (. 39). However, because DF1 dips towards the west, it is likely related to DF2, which would indicate a dextral displacement of around 2.5km on the RFZ (indicated by line d2 in Fig. 39).

Overall, the NNE-SSW strike of the low angle detachment faults in the Terschelling Basin deviates from the low angle detachment faults on the Schill Grund Platform and the Central Offshore Platform. Additionally also the distribution of the salt walls and the intra-salt Triassic compartments shows this deviating NNE-SSW strike. It is suggested that this deviating trend can be explained by an overall dextral shearing of the Terschelling Basin along its northern (RFZ) and southern (HFZ) boundary faults. Additionally, strike-slip motions inside the graben might have occurred to accommodate for the differential motions between RFZ and HFZ (indicated by the dashed red lines in Fig. 39). To estimate the total amount of dextral displacement that occurred across the Terschelling Basin, an imaginary line from DF2 is drawn south following its strike. Subsequently, the distance between FD1 and this imaginary line is measured. This distance (d3 in Fig. 39) is approximately 13km. Again this distance only provides a rough first order approximattion of the total amount of dextral displacement across the Terschelling Basin, as later reactivation of faults might have changed the post-Triassic configuration.

5. Analogue Modelling Results

5.1 Experiment 1; Dextral Strike-Slip followed by Extension. Purely brittle experiment

Strike-Slip Phase

The strike-slip phase of this purely brittle model developed similar to classic Riedel experiments described i.a. by Tchalenko (1970) and Richard et al. (1995). Initially, Y shears and R shears developed during the strike-slip phase of model 1. The first Y and R shears developed after7% of bulk strike-slip (i.e. after 7% of the total amount of strike-slip movement, which was 3cm in this experiment). The R shears display an en echelon geometry and generally have an angle between 18° and 24° with the trace of the basement fault (i.e. the vertical in figures 44-46). The Y shears develop more or less parallel to the trace of the basement fault. After 25% of bulk strike-slip, the first P shears develop that link the R and Y shears (fig. 44). These P shears develop at a small angle of max 10° to the trace of the basement fault. As the R, Y and P shears become more and more connected, an anastomosing fault pattern develops, here referred to as main displacement zone; or F1. After 40% of bulk strike-slip, the displacement is almost solely accommodated by F1. The interference of P faults with R faults leads to a left stepping of fault F1 in the center of the experiment, where a pop-up is formed and to right stepping of the fault F1 at the lower and upper end of the experiment, where pull-aparts are formed (figures 45). The formation of these pull-aparts is enhanced due to the fact this area is close to the end of the experiment. Consequently, the F1 fault moves out of the experiment with a curve and enhances the subsidence in the pull-aparts. After 55 percent of bulk strike-slip, the main displacement fault zone F1 cuts the anastomosing fault pattern and the pop-up in the center is no longer active. From this moment displacement is solely accommodated by the main displacement fault zone F1 (fig. 46).

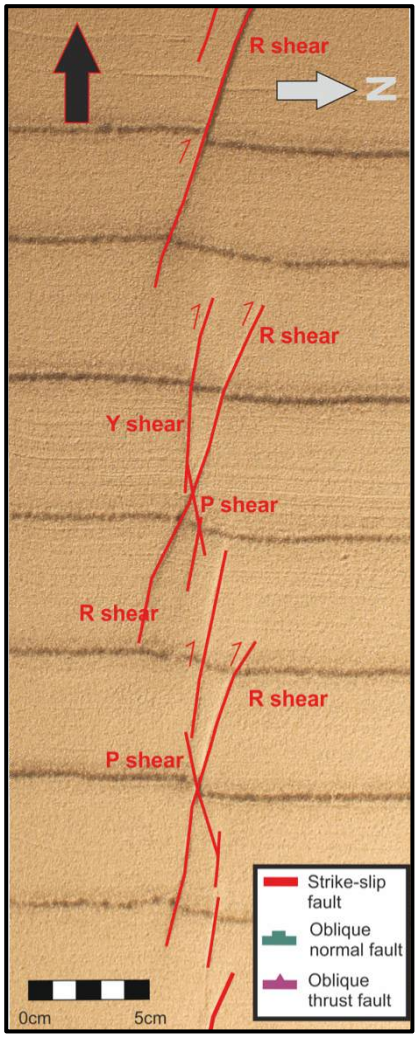

Fig. 44. Top view of model 1 after 28% of bulk strike-slip. The black arrow indicates the side of the experiment where the underlying moving plastic sheet is located. The grey arrow indicates the artificial north

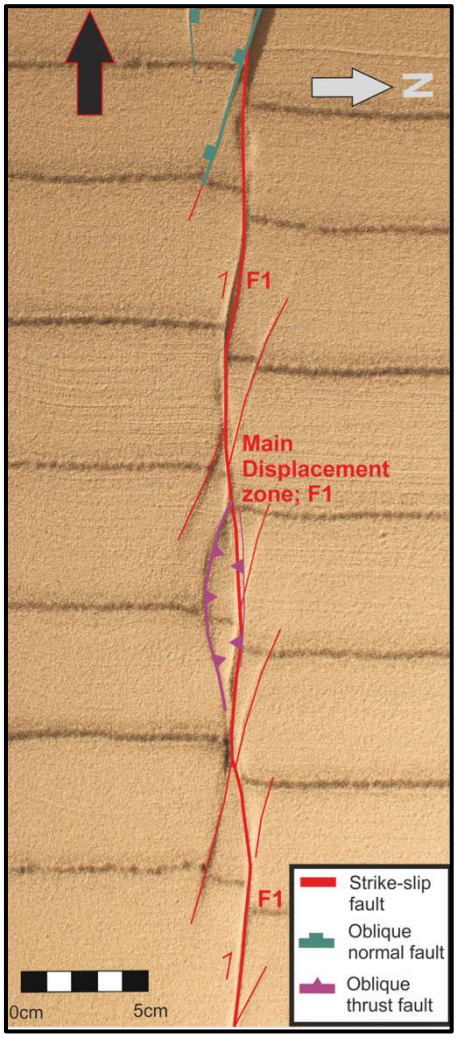

Fig. 45. Top view of model one after 40% of bulk strike-slip. Pop-ups and pull-aparts have formed due to interference between the linked P shears and Riedel shears. Nearly all displacement occurs along F1

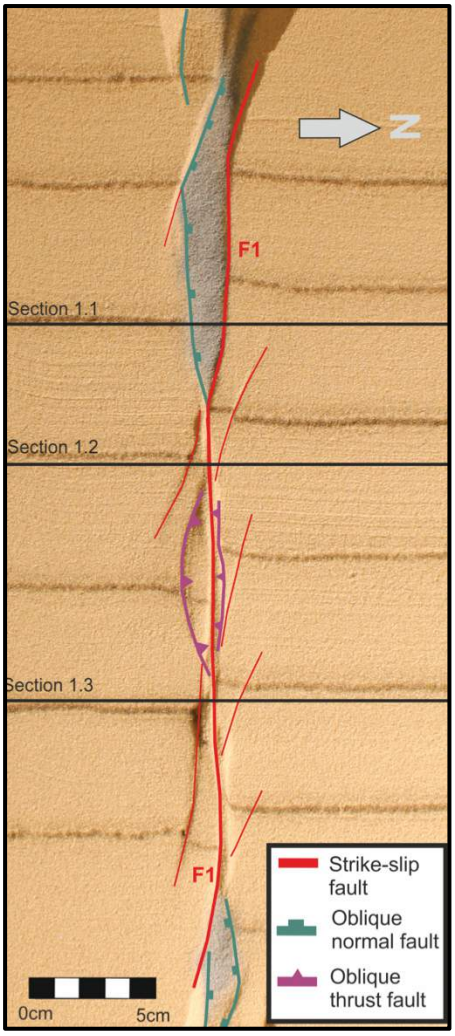

Fig. 46. Top view of model one at the end of the strike-slip phase. The locations of the cross-sections are indicated by the black lines.

Extension Phase

Initially, extension is accommodated along inherited R Riedel faults (fig.47 and figures 51-53). Subsidence on these faults is generally not very large and new normal faults develop after 20% of bulk extension(fig.49). The new normal faults first develop towards the artificial north of the strike-slip zone. Initially, these normal faults are relatively short and display a curved geometry. After 27% of bulk extension, these faults get interconnected and a long normal fault develops. This long normal fault first develops on the northern side of the graben. After 35% of bulk extension, a long normal fault has also developed on the southern side of the graben (fig.48). The new deformed normal faults accommodate less subsidence during this stage of the experiment at the western part of the experiment, in the area of the preformed pull-apart basin. After 50% of bulk extension, the long normal faults are fully developed over the entire length of the experiment and displacement solely takes place on these long normal faults (fig.49). The graben gradually subsides during the remaining time of the experiment and the basin floor stays pretty much horizontally. By the end of the extension phase, the former strike-slip zone is located in the center of the graben (cross sections 1.1, 1.2 and 1.3 in figures 51-53), Because it is burred by sediments, it can't be recognized anymore. The graben is at its widest in the western and in the eastern part of the experiment, where the pull-aparts structures had developed during the strike-slip phase.

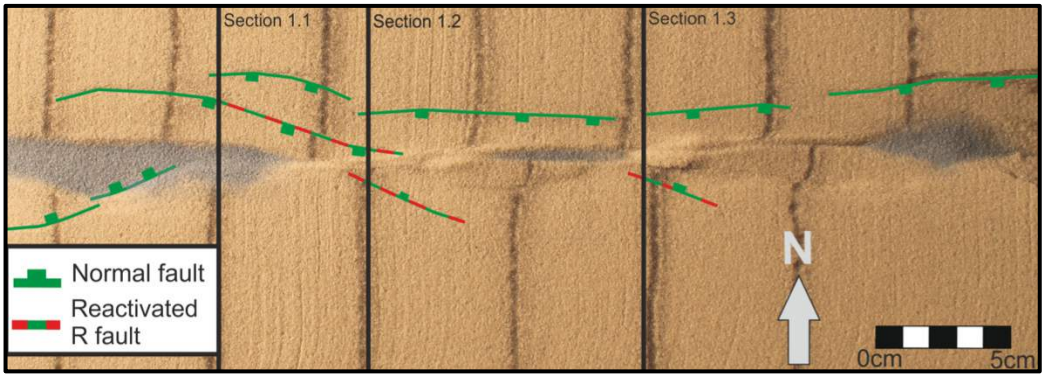

Fig. 47. Top View after 25% of bulk extension. Displacements are still partly accomodated by Riedel faults that developed during the strike-slip phase. Towards the north of the extinct strike-slip zone, a series of connected normal faults develop.The cros-section can be found in figures 51-53.

Fig. 48. Top View after 50% of bulk extension. The normal fault zone north of the extinct strike-slip zone is completely interconnected. Also in the south, a large normal fault is being formed. The large normal faults are not well developed yet in the area of the preformed pull-apart basin.

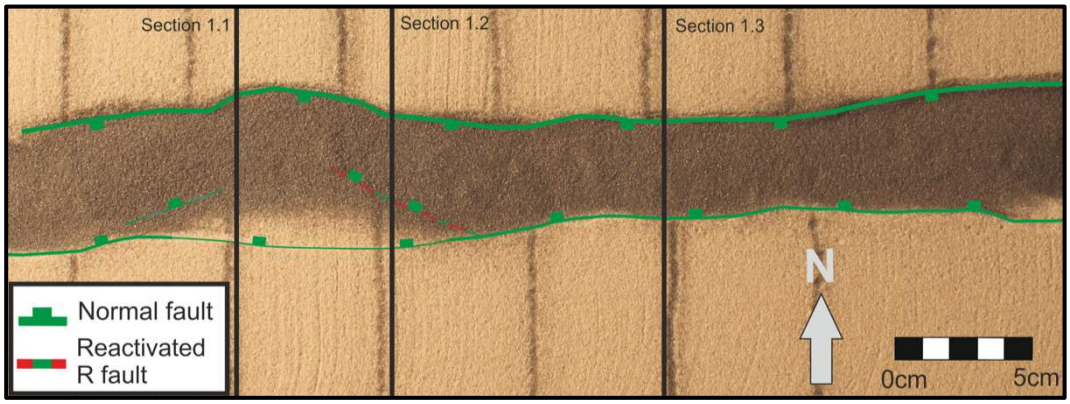

Fig. 49. Top View after 75% of bulk extension. During this stage of the experiment, the large normal faults that bound the graben accamodate all of the displacement.

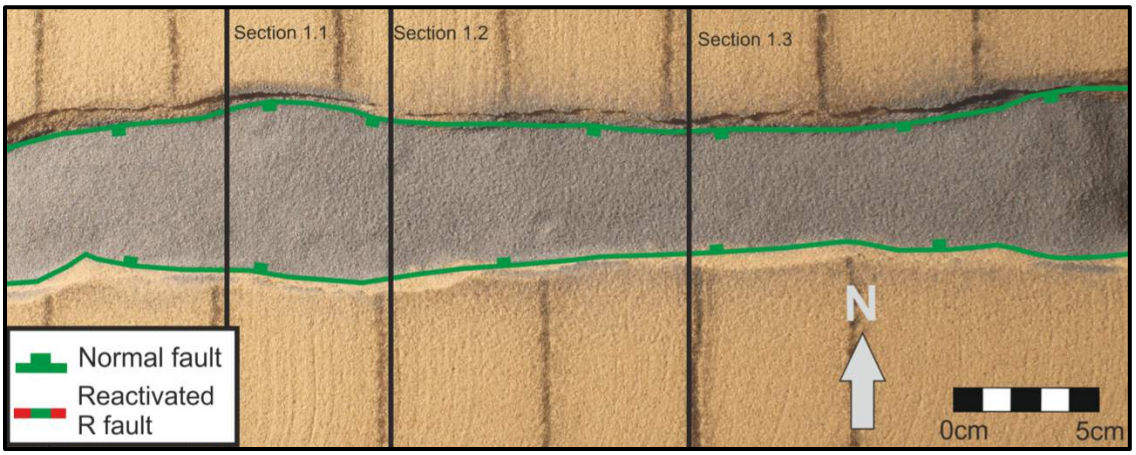

Fig. 50. Top View after the final stage of extension. The graben is at its widest where the pull aparts formed during the strike-slip stage. The strike-slip zone is located in the center of the graben but because it is covered by sediments, can't be recognized in plan view.

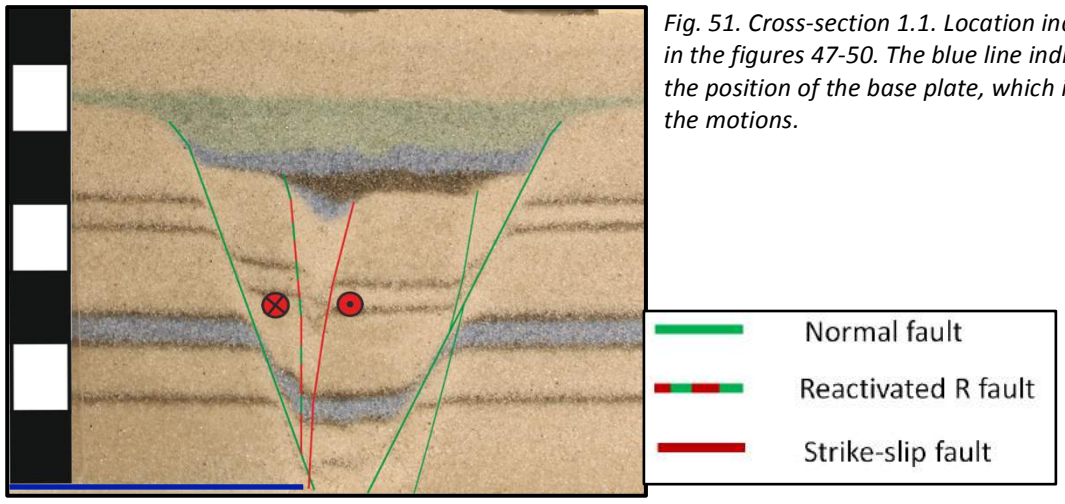

Fig. 51. Cross-section 1.1. Location indicated in the figures 47-50. The blue line indicates the position of the base plate, which induced the motions.

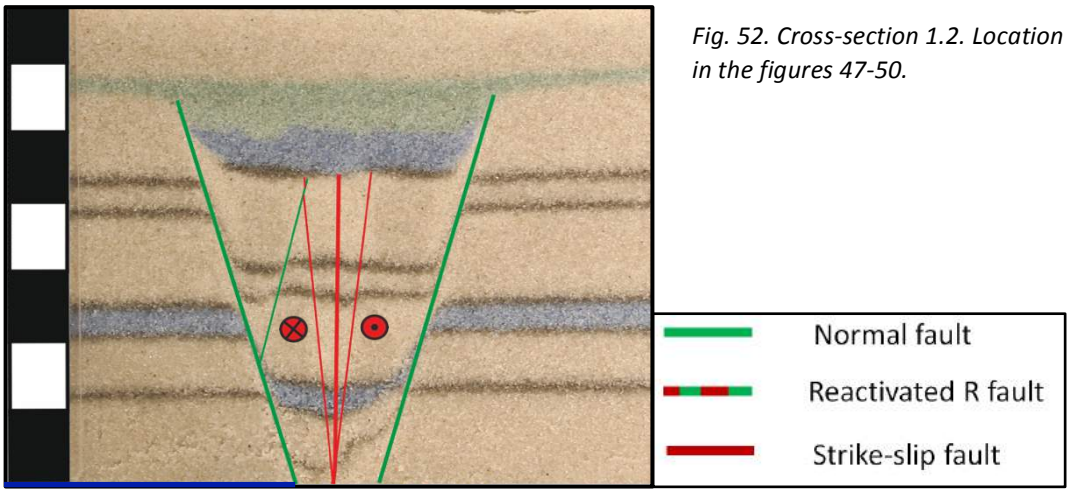

Fig. 52. Cross-section 1.2. Location indicated in the figures 47-50.

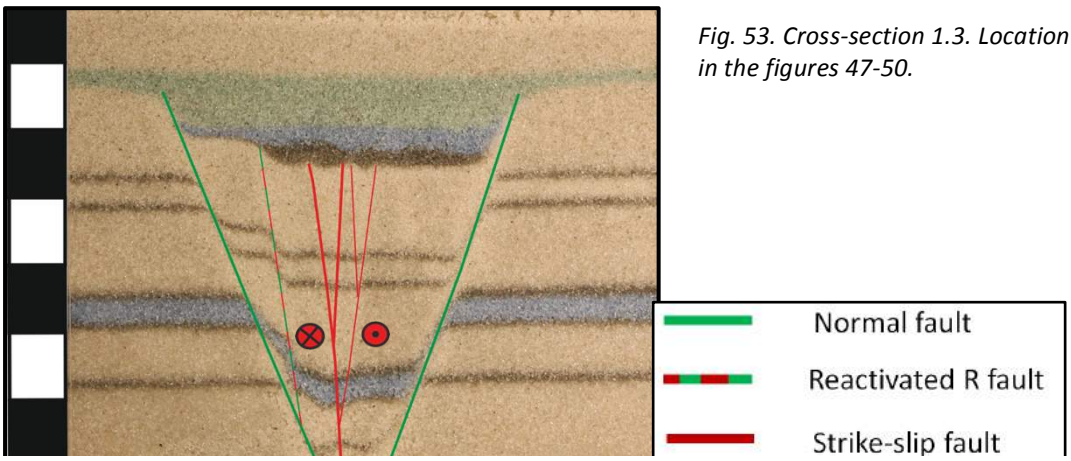

Fig. 53. Cross-section 1.3. Location indicated in the figures 47-50.

5.2 Experiment 2; Extension followed by Dextral Strike-Slip. Purely brittle experiment

Extension phase

After 15% of bulk extension, a series of normal faults with opposing fault dips formed. These faults initially had a slightly curved strike with a conchoidal fault plane. After 20% of bulk extension, these faults got interconnected and a graben formed in between the opposing faults; NF1 and NF2. When extension continued, subsidence in the graben was accommodated along these two faults. Both faults appeared to have accommodated similar amounts of displacement. After 55% of bulk extension, smaller normal faults started to formed inside the graben as well. Two antithetic faults that terminated on fault FN2 formed in the western part of the experiment (FN4 and FN5). FN5 was the latest to form and formed after 80% of bulk extension. In the eastern part of the experiment, a fairly large northward dipping fault formed (FN3) (fig.54).

Strike-Slip phase

During the first 20% of bulk strike-slip, strike slip movements were accommodated by Riedel R shears and eventually also Riedel P shears. The Riedel R shears were less well developed than during the strike-slip phase of model 1 and were also shorter. Only limited amounts of displacement, generally not more than 2mm developed along the R shears. The Riedel R shears as well as the P shears developed over the preformed FN1. However, a very minor amount of displacement was also accommodated by the preformed fault NF2 during the first 10% of bulk strike-slip (fig. 55). After this, no more movements occurred along NF2. After 20% of bulk strike-slip, strike-slip motion was solely accommodated on the main displacement Fault Zone F1, which formed due to reactivation of the pre-established fault NF1 (fig. 55 and fig. 56). After 25% of bulk strike-slip, a right stepping of fault F1 formed in the eastern part of the experiment (fig. 55). This right stepping continued to develop and after 27% of bulk strike-slip another oblique normal fault formed due to left stepping of fault F1 (fig. 55). This right stepping occurred due to the fact that base of fault FN3 is located close to the baseplate along which the motion takes place (fig. 54 and fig. 60). Hence in the eastern part, strike-slip motions are also accommodated by reactivation of fault FN3, which causes the right stepping of fault FN1 and the subsequent formation of a pull apart in the eastern part of the experiment. It is likely that this right stepping is enhanced by the fact that the experiment ends soon towards the east of the pull-apart basin. Hence the formation of this pull-apart is influenced by boundary effects. In the western part of the experiment, FN3 is absent and consequently nearly all of the displacement was accommodated by fault zone F1 that formed by reactivation of NF1.

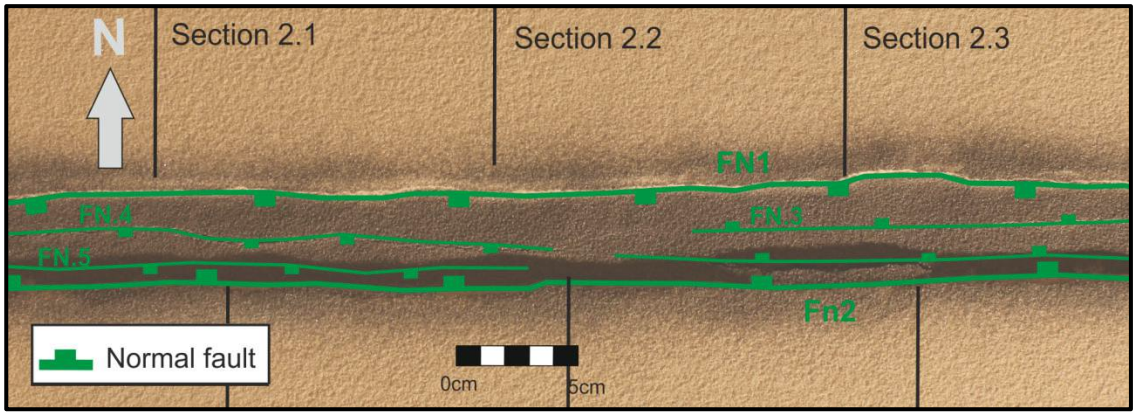

Fig. 54. Top View after the end of the extension phase of model 2. Most of the subsidence is accommodated by FN1 and FN2. However minor amounts of subsidence is also accommodated by faults FN2-FN5.

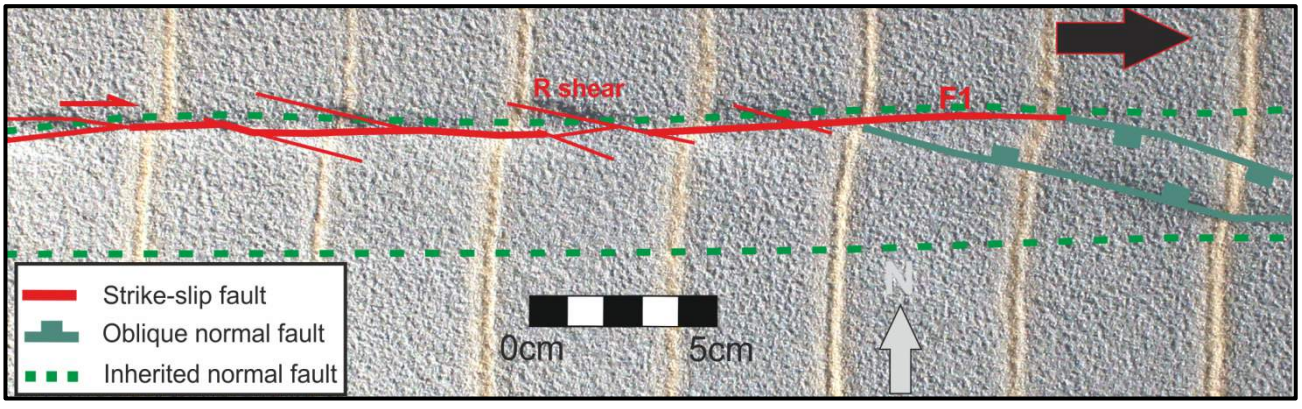

Fig. 55. Top View after 30% of bulk strike-slip. In the western part, motion is solely accommodated by fault F1. In the eastern part, the presence of FN3 causes right stepping of fault F1, enhanced by boundary effects due to the proximity of the edge of the model

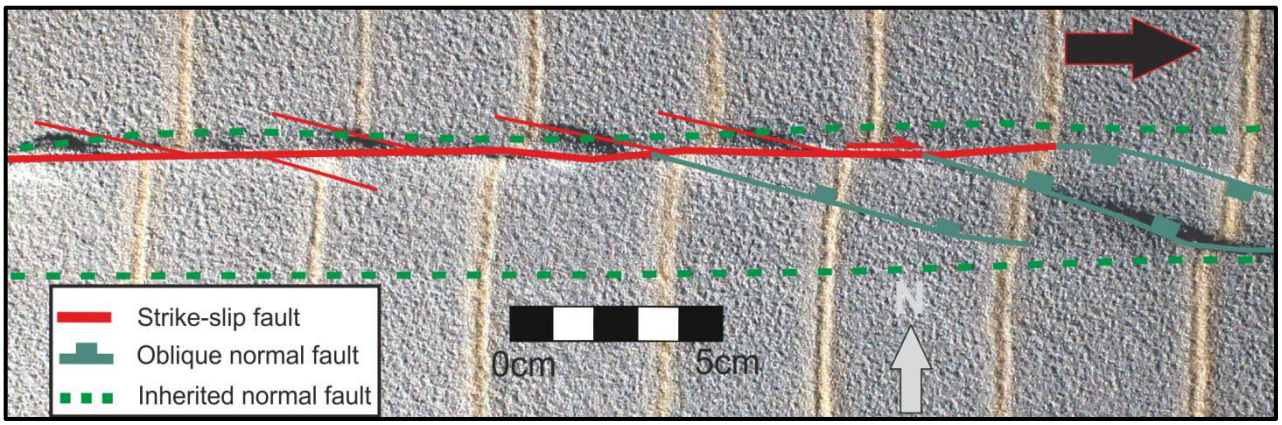

Fig. 56. Top View after 40% of bulk strike-slip. In the western part, motion is solely accommodated by fault F1. In the eastern part another oblique normal fault forms due to right stepping of fault F1

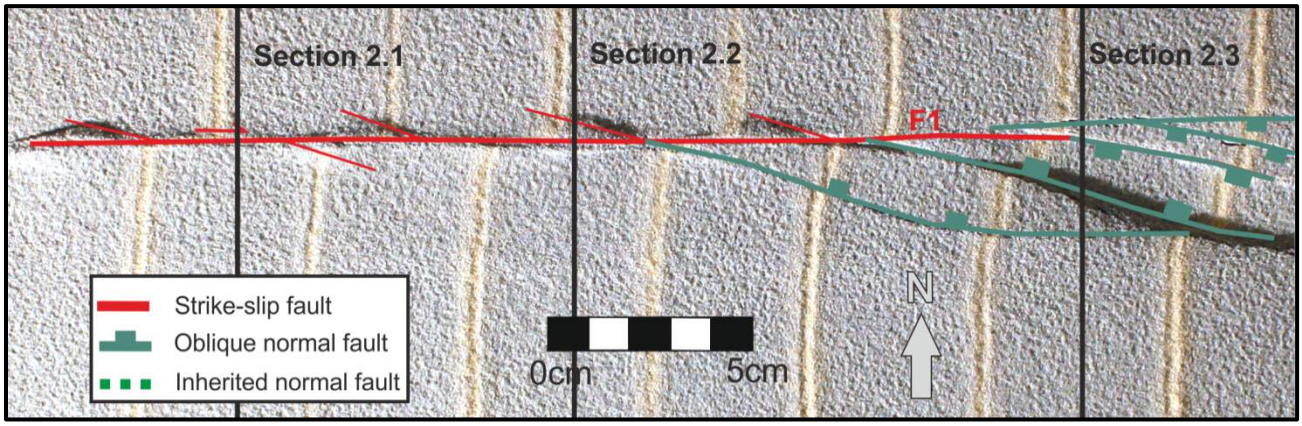

Fig. 57. Top view of model 2 after the end of the strike-slip phase. The locations of the cross-sections are indicated by the black lines.

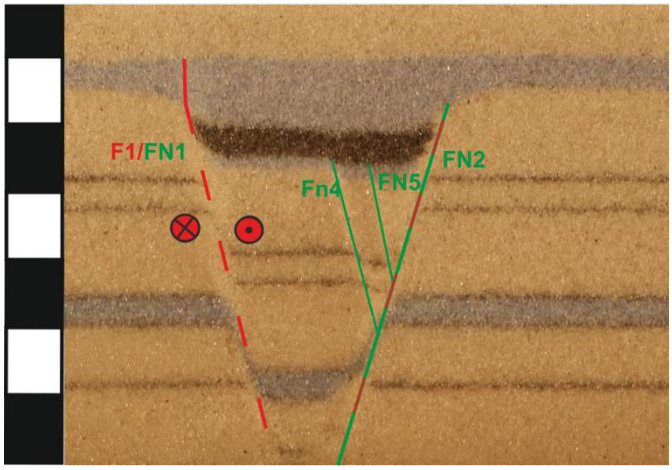

Fig. 58. Cross-section 2.1. Location indicated in figures 54 and 57

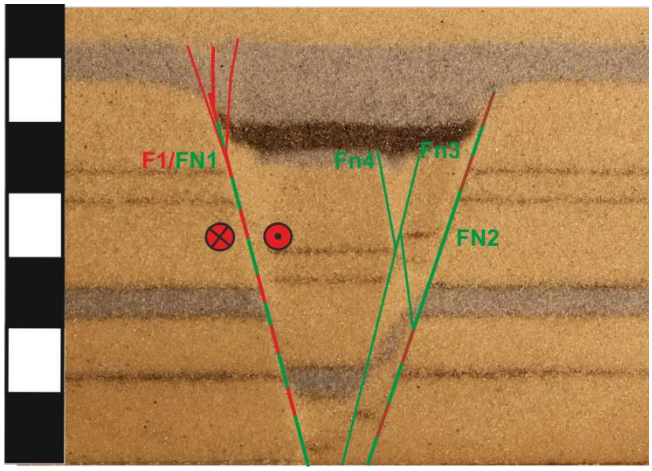

Fig. 59. Cross-section 2.2. Location indicated in figures 54 and 57

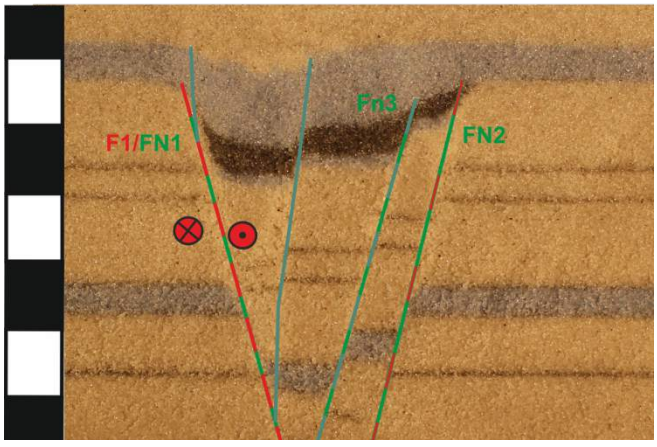

Fig. 60. Cross-section 2.2. Location indicated in figures 54 and 57

5.3 Experiment 3; Extension followed by dextral strike-slip; with vertical salt walls

Extension phase

During the extension phase, a symmetrical graben formed in the experiment. In contrast to experiment 2, no major boundary faults on either side of the graben can be observed at the surface of experiment 3 during the extension phase (Fig. 62). Instead, the graben subsides with a gradually curved geometry, showing the strongest subsidence in the center of the graben and the lowest towards the platforms (Fig. 61). With ongoing deformation, extension was also transmitted onto the platforms via the putti. This led to thin skinned extension on the platforms; both close to the graben, as well as further away from the graben. This thin skinned extension on the platforms lead to the formation of small Grabens in the brittle overburden above the putti (Fig. 62). Where extension localized and the supra salt grabens became deep enough, the putti was able to pierce through the overburden once the piercement threshold was overcome (as described by Vendeville and Jackson, 1992). This piercing stage is described by Vendeville and Jackson (1992) as the active stage of diapirism. Piercement of the silicon putti walls only occurred in this experiment on the graben shoulders bounding the basin and took place for the first time after 72 percent of bulk extension (Fig. 62). The piercement threshold was not overcome further on the platforms, as some sedimentation was also applied on the platforms, thereby balancing the loss in overburden in areas of localized thin skinned extension and prohibiting active piercement of the silicon putti walls further on the platforms. Consequently the largest silicon putti walls in this model are located on top of the footwall of the basement boundary faults. From Fig. 62 can be inferred that the northern salt wall runs approximately parallel to the graben. The southern salt wall makes a gently turn towards the south, as the salt wall towards the southeast of the graben is located further away from the basin. This can also be inferred when the cross-sections 3.1-3.3 are compared (fig. 65-67).

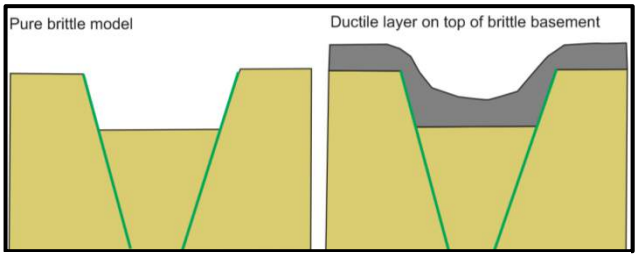

Fig. 61 Sketch indicating the difference in graben formation during pure extension for a purely brittle model (left) and a multilayer model (right).

Resting Phase

The salt walls that reached the active piercement stage during the extension phase, continued to grow passively and vertically upward during the resting phase, as sedimentation was applied every two hours. The silicon putti walls in the eastern and especially the southeastern part of the experiment didn't grew as high as the silicon putti walls in the western part of the experiment (fig. 62).

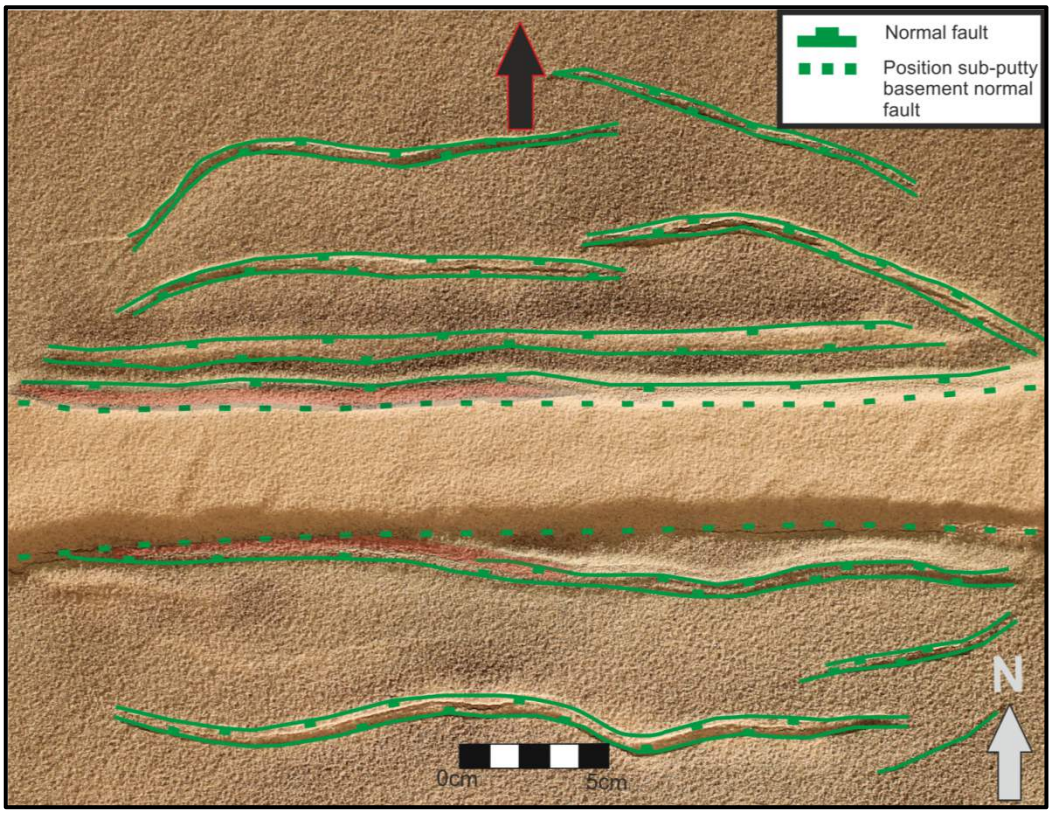

Fig. 62. Top View of model 3 after 75% of the extension phase. The transparent red areas indicate were the silicon putti walls reached the active piercing stage during this stage of the experiment. Both areas will expand slightly futher towards the east during the rest of the experiment. Towards the east, the putti walls will not reach the active piercing stage.

Strike-Slip phase

Strain Distribution

R Riedel shears are the first faults that form after 15% of bulk strike-slip. They first form above a zone which coincides with the northern silicon putti wall. Displacement along these faults is small; generally less than 1mm. After 20% percent of bulk strike-slip, the majority of the displacement in the overburden takes places at two faults which follow the outline of the silicon putti walls that have formed during the extension and resting phase (fig.63). Initially, some local pop-up structures and a pull-apart structure form due to interference of the main displacement zone F1 with the Riedel R-shears. After 25% of bulk strike-slip, the main displacement zone F1 cuts through these small zones of transpression and transtension. Although the majority of the strike-slip displacement is accommodated by F1 and F2, a significant amount of displacement is also accommodated by a network of small faults of which the far majority is located inside the graben (fig. 63). The amount of displacement on these individual faults is small, but all together they accommodate a significant amount of displacement which is higher than the displacement accommodated by fault F2 (fig. 68). The amount of displacement that is accommodated by F1 and F2, seems to be related to the height of the salt wall that is located at the base of these faults, as is indicated in figure 69 (see figure for more explanation). Another parameter that seems to control the amount of displacement along F1 and F2 is the horizontal between these faults and the trace of the basement fault, which is indicated in fig. 70.

Shape of the silicon putti walls

From the cross sections in figures 65-67 can be inferred that the shape of the northern silicon putti wall, along which the majority of the displacement occurs, deviates from the shape of the southern silicon putti wall. This difference becomes also clear when the shape of the northern putti wall is compared with the shape of a diapir that has developed after a similar amount of extension and resting were applied to an experiment (Scheffer, 2016 Appendix D). The difference lies in the shape of the northern putti wall, which is more triangular when compared to the silicon putti walls that have accommodated no or less strike-slip. Furthermore, the northern salt wall also appears to be thinner towards the top. Another difference is the small appendix that has formed during strike-slip on the top of the northern silicon putti wall at some places (Fig. 66). This appendix is absent at the silicon putti walls that accommodated no or less strike-slip.

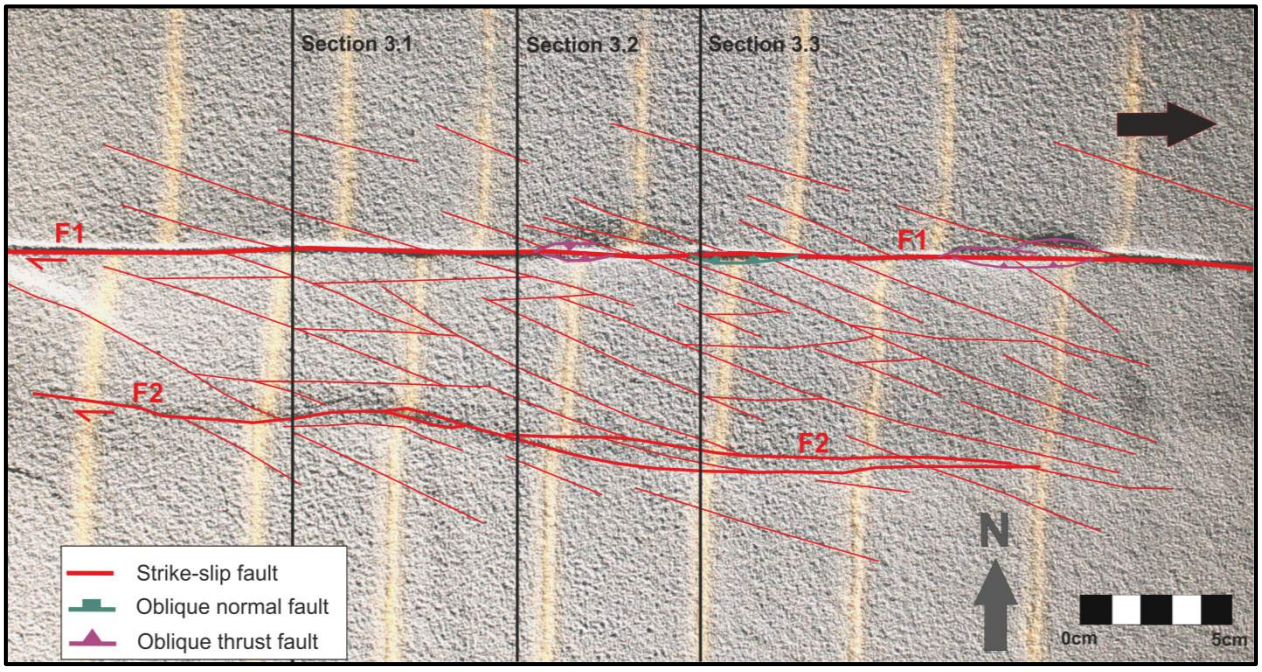

Fig. 63. Top view of the final stage of strike-slip deformation of model 3. It can be seen that most of the displacement on individal faults is accomodated by the faults F1 and F2. However, a fairly large amount of displacement is also accomodated by smaller faults of which the majority is located inside the graben.

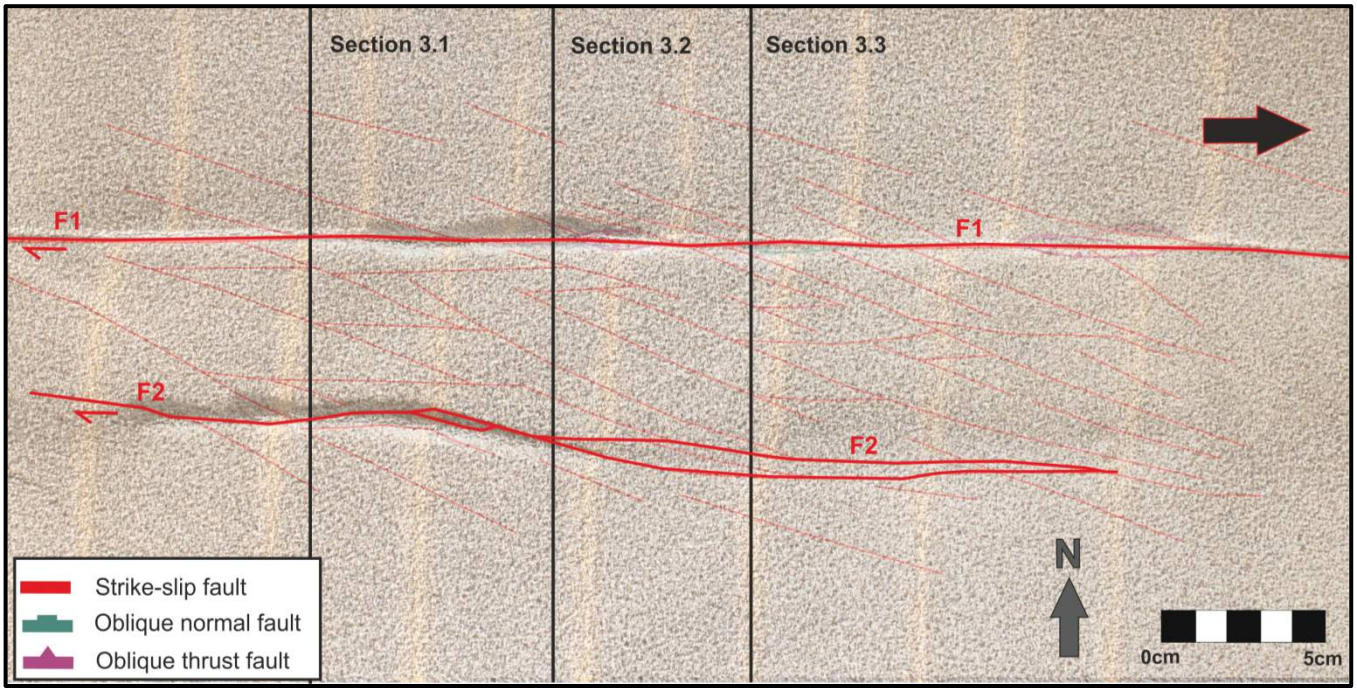

Fig. 64. Top View of the model after the end of the strike-slip phase. A transparant view of fig. .. is laid over the end of the strike-slip phase. Showing that the main strike-slip faults are located above the silicon putii walls.

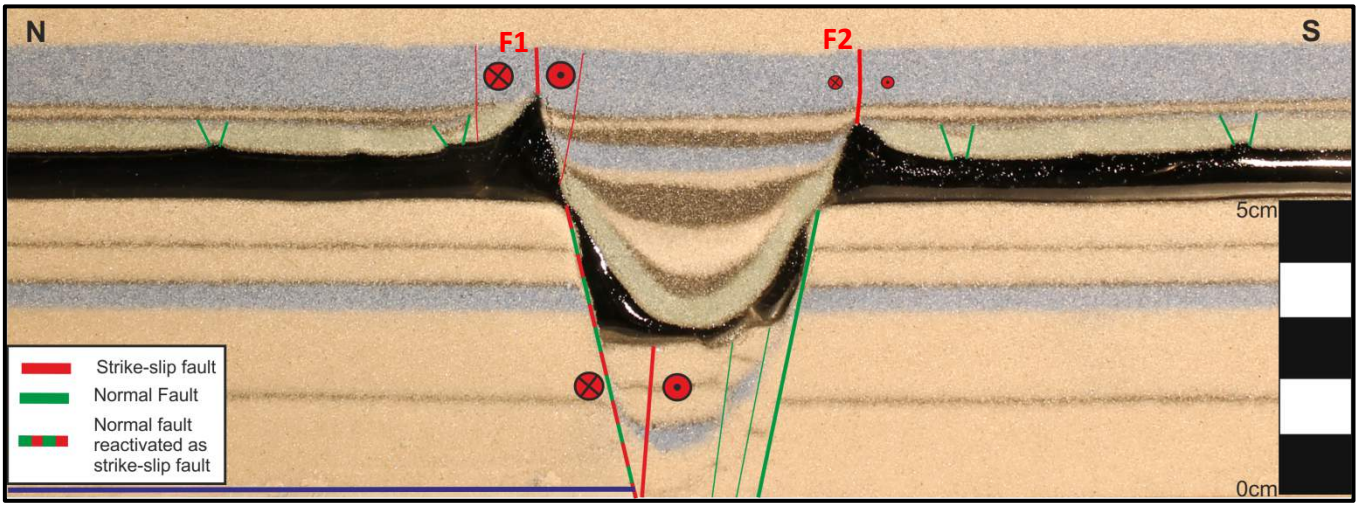

Fig. 65. Cross section 3.1. of model 3. The location of the cross-section is indicated in the figures 24 and 25. Clear in this cross-section is the small appendix that has formed on top of the northern (here left) silicon putti wall.

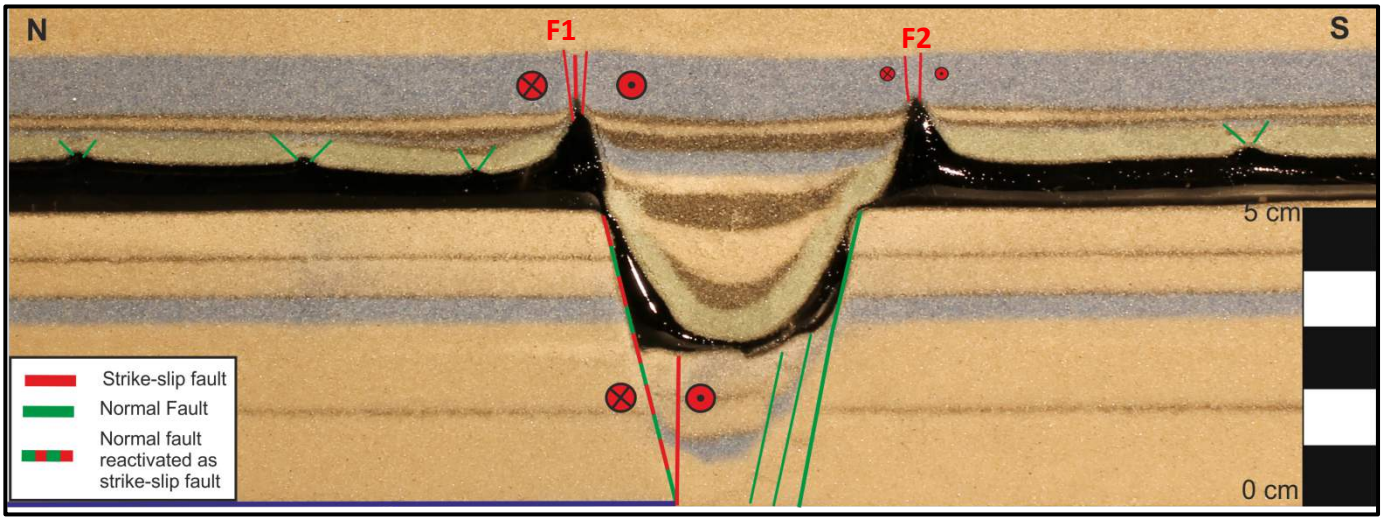

Fig. 66. Cross-section 3.2 of model 3. The location of the cross-section is indicated in the figures 24 and 25. Clear in this cross-section is the ore triangular and narrow shape of the northern (here left) silicon putti wall.

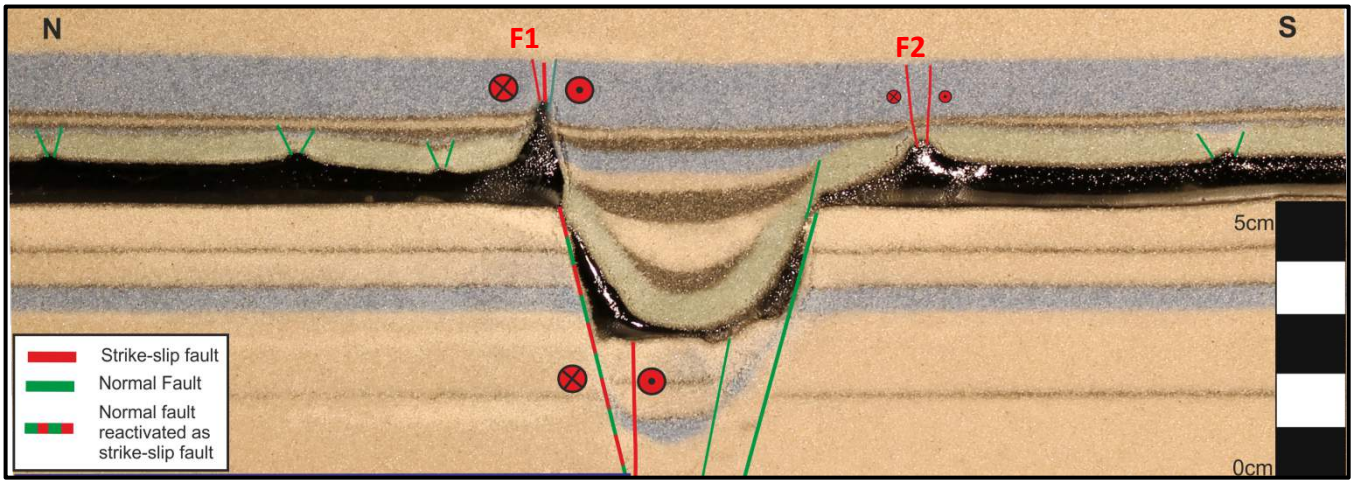

Fig. 67. Cross-section 3.3 of model 3. The location of the cross-section is indicated in the figures 24 and 25. Note the increased distance of the southern (here right) salt wall from the graben

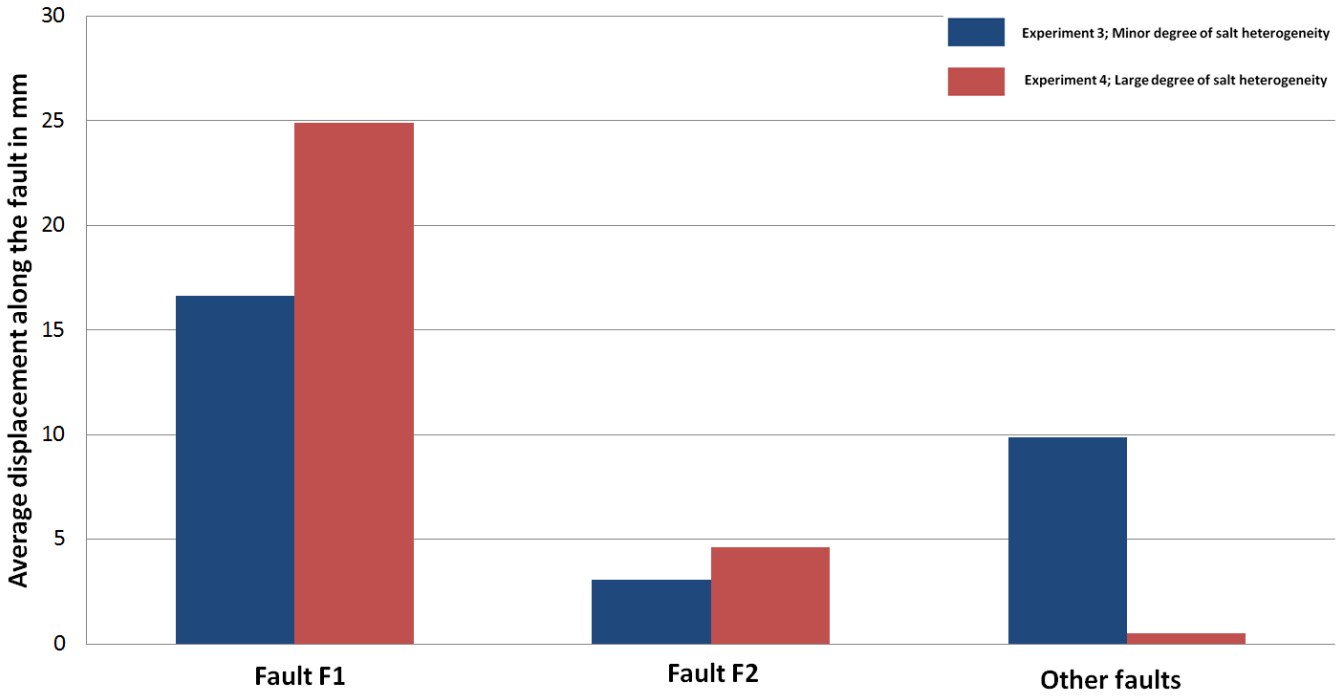

Fig. 68. Diagram indicating the average displacement along the faults F1, F2 and other faults for experiment 3 and 4. Noteworthy is the relatively large amount of displacement that is accommodated by other faults in experiment 3 with respect to experiment 4. The majority of these faults is located inside the graben, bounded by the two salt walls. The average was obtained by 7 measurements in each experiment; all measurements were taken along the white lines of figure 61

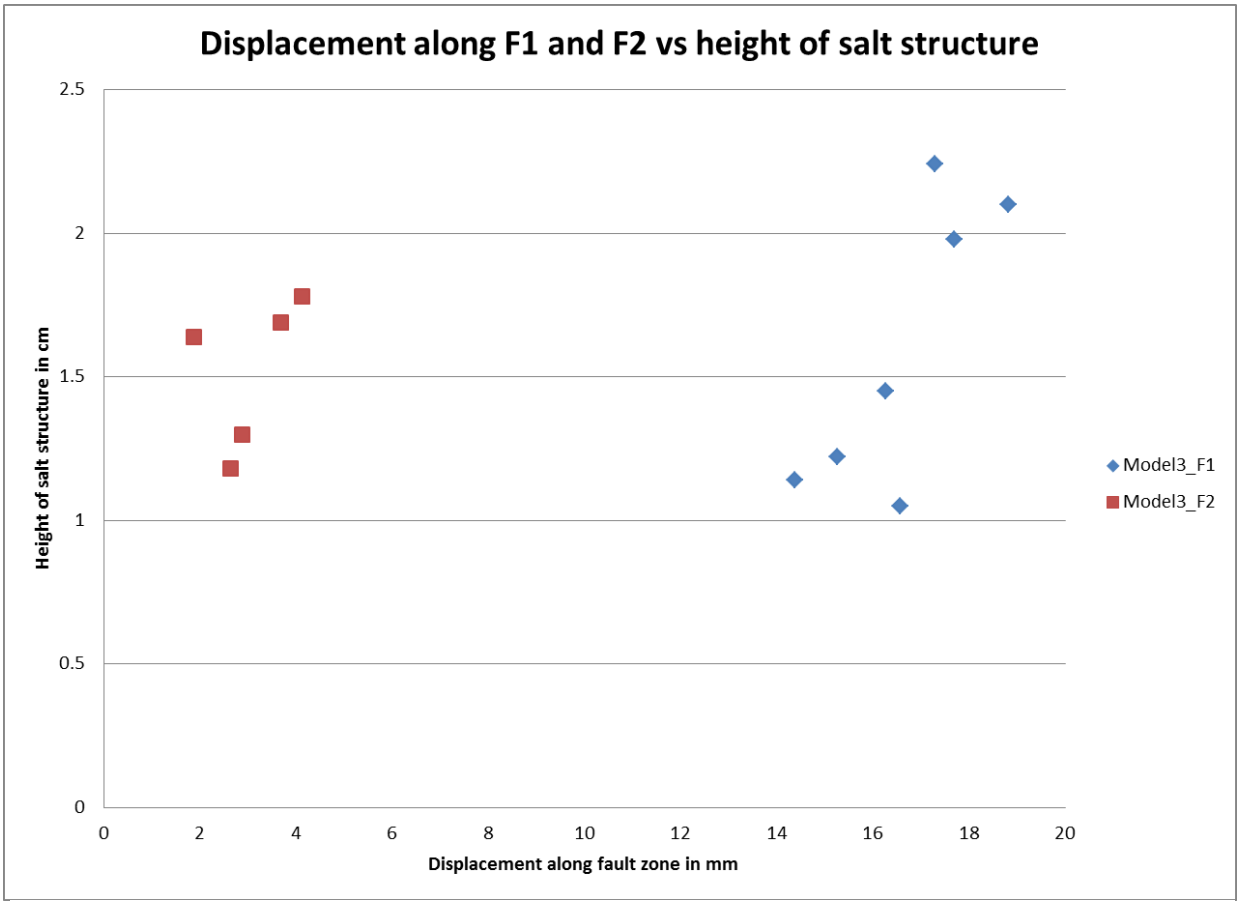

Fig. 69. Graph where the height of the salt structure is plotted against the amount of displacement that is accommodated by the faults F1 and F2 above it. The displacements were measured along 7 fault segments of fault F1 and 5 fault segments of fault F2, along the white lines in figure 24. The distance along F2 in the eastern part of the fault were to small to measure properly. Striking is that the higher the salt wall, the more displacement is accommodated by the fault above it and hence likely also by the salt wall itself.

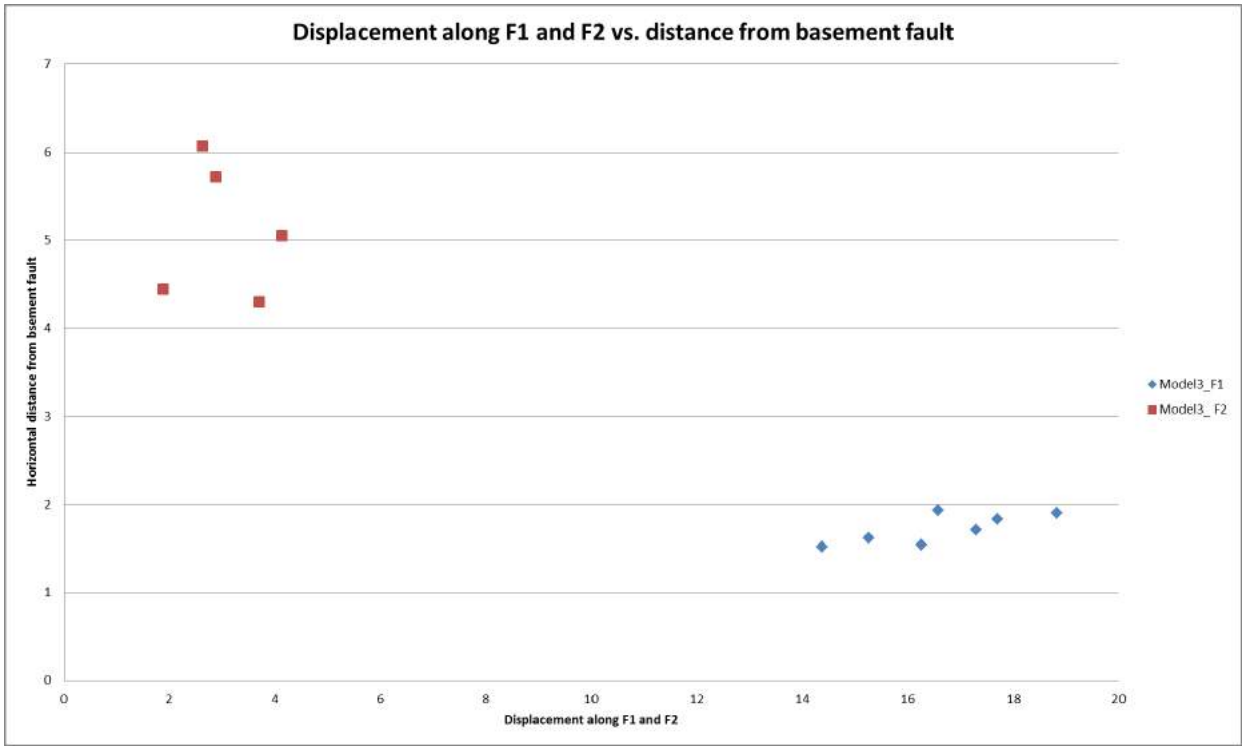

Fig. 70. Graph where the displacement along the faults F1 and F2 is plotted against the distance from the basement fault. Because it is not exactly sure where the faults in the basement are located, the distance between F1 (or F2) and the trace of the basement fault as defined by the location of the base plate was measured. The measurements along fault F1 suggest that there is a strong correlation between the distance of the basement fault and the displacement along F1.

5.4 Experiment 4. Extension followed by dextral strike-slip; large differences in salt wall orientation

Extension phase

During the extension phase, a graben formed in the experiment above the place where the base plate was pulled away. In contrast to experiment 2, no major faults can be observed at the surface of experiment 4. Instead, the graben subsides with a gradually curved geometry, showing the strongest subsidence in the center of the graben and the lowest towards the graben margin. With ongoing deformation, extension was also transmitted onto the overburden via the silicon putty, leading to thin skinned extension on the platforms; both close to the graben, as further away on the platforms. This thin skinned extension on the platforms resulted in the formation of small Grabens in the brittle overburden above the putty. Where extension localized and the supra salt grabens became deep enough, the putty was able to pierce through the overburden once the piercment threshold was overcome. This stage of diapirism was described by Vendeville and Jackson (1992) as the active stage of diapirism. The first places were piercing of the silicon putty occurred were the graben shoulders, located directly outside of the graben. The first piercing of the silicon putty occurred therefore on top of the footwall formed by the basement normal faults bounding the graben. Piercing of the silicon putty occurred in these places at 70 percent of bulk extension. After the initial piercment of the silicon putty, the silicon putty walls grew vertically upward, as can be inferred from fig. 71 and 72, which shows the end of the extension phase of model4. By the end of the extension phase, the silicon putty walls located on the platform shoulders, closest to the graben, had reached the active diapir stage on the full length of the model (fig. 71, 72). Two salt walls further away from the graben had also pierced the overburden in the southern part of the experiment. Anomalies to this general pattern of pierced salt walls occur in the areas A and B in figure 71. In these areas, the salt walls that pierced the overburden are not located directly on top of the hanging wall, but are located slightly further towards the platform.

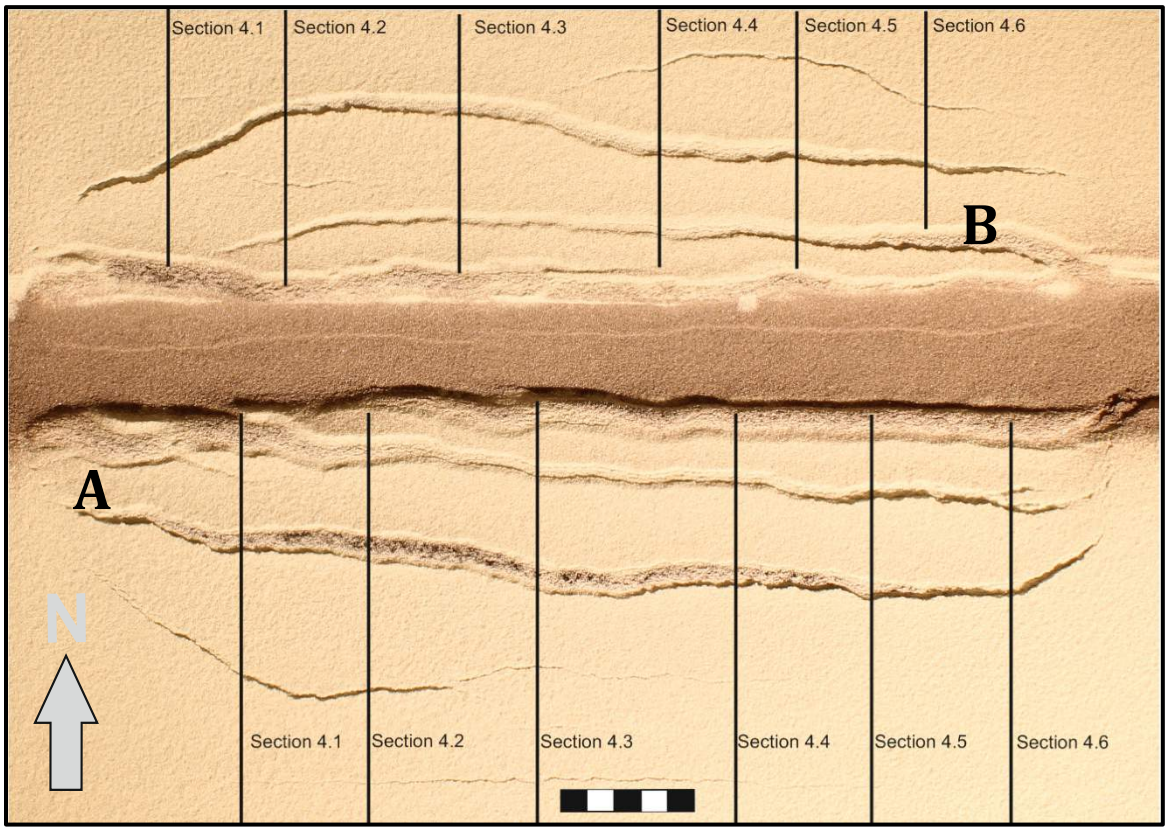

Fig. 71. Top view of model 4 at the end of the extension phase. This figure shows that the salt walls have reached the active stage over the full length of the experiment and grow vertically upward. Salt walls are located on the footwall close near the graben. Except for the locations A and D where the salt walls are located slightly further on top of the platforms.

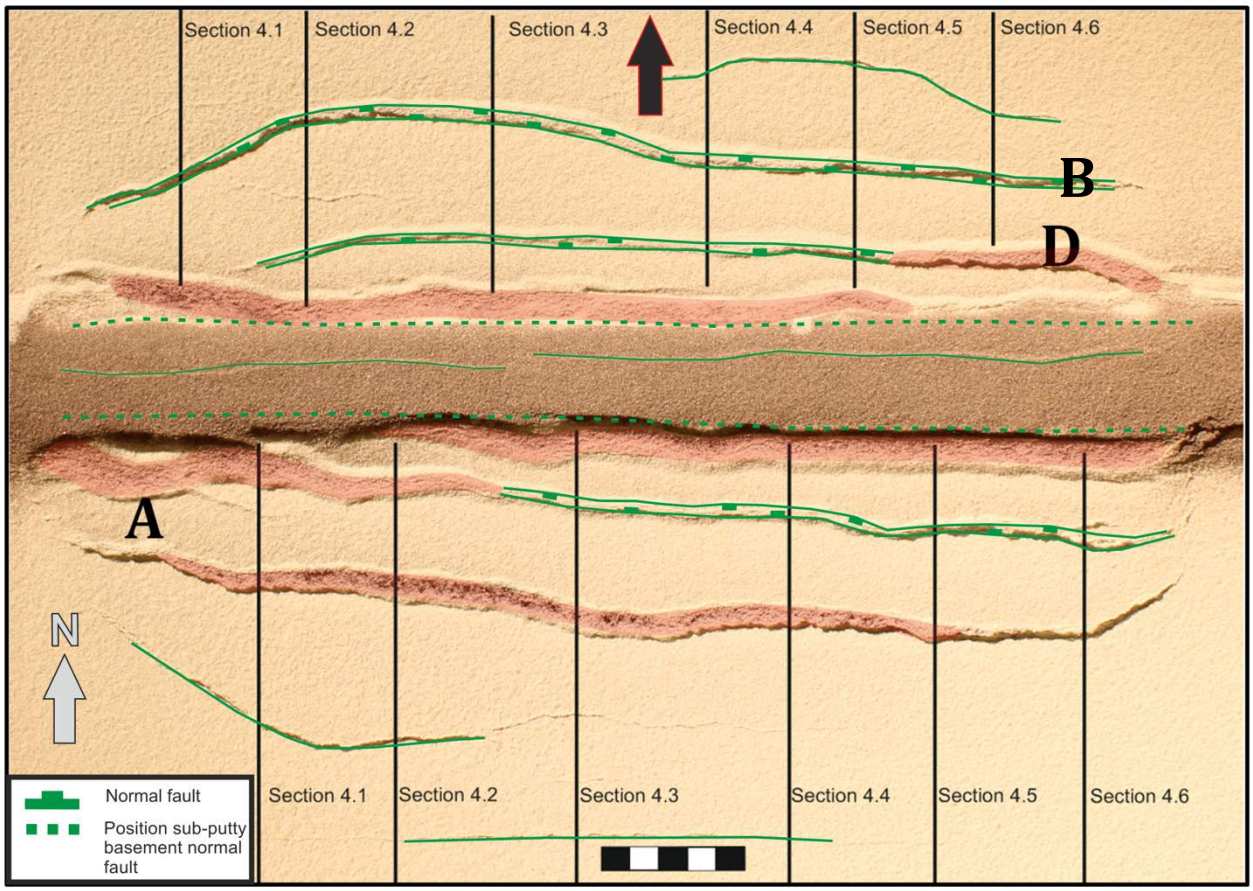

Fig. 72. Interpreted top view of model 4 at the end of the extension phase. The salt walls that have reached active piercing stage are indicated by the transparent red areas. For the uninterpreted top view see fig. 73.

Resting Phase

During the first two hours of the resting phase, the salt walls in the normally filled part of the basin grew vertically upward by passive diapirsm, as sedimentation kept on track with the vertical rise of the diapirs. This can be seen in fig. 73, where the blue part of the graben represents the normally filled part of the basin (part C) and the white part represents the underfilled part of the basin (part D) after the first two hours of the resting phase. In the underfilled part of the basin, gravity caused the salt walls to grow towards the graben and subsequently to spread onto the graben infill. This can be seen when the final stage of extension (fig. 71, 72) is compared with the first two stages of the resting phase (figures 73 and 74). This gravitational spreading of putty is visualized in fig. 74, where the distance D between two opposing salt structures is plotted against the resting time. This distance D was measured at 6 places of the experiment, indicated by the dashed yellow lines in fig. 73. From the graph in fig. 83 becomes clear that the distance between two opposing salt walls on either side of the graben remains largely the same in the normally filled part of the basin. In the underfilled part of the basin, which is represented by measurements along the lines of sections 4.1-4.4, it becomes clear that the salt structures have grown towards each other during the first four hours of the resting phase, which represents the time that the basin was extremely underfilled. This can also be inferred from the corresponding sections of the underfilled part of the basin (figures 77, 78, 79), where it can be seen that the silicon putty has spread on top of the thin white layer (figures 77 and 79) or on top of the black layer in a slightly later stage of the resting phase (fig. 78). During the last four hours of the resting phase, when the basin was less underfilled, the diapirs grew again almost vertically upward. Indicated by the waist shape figure of the diapirs (especially observed in the northern putty wall of figure 78, but also in the putty walls of the figures 77, 79), which indicates new active piercing after putty extrusion. Hence, after four hours of resting, the distance between the two opposing diapirs on either side of the graben doesn't decrease anymore (fig. 83).

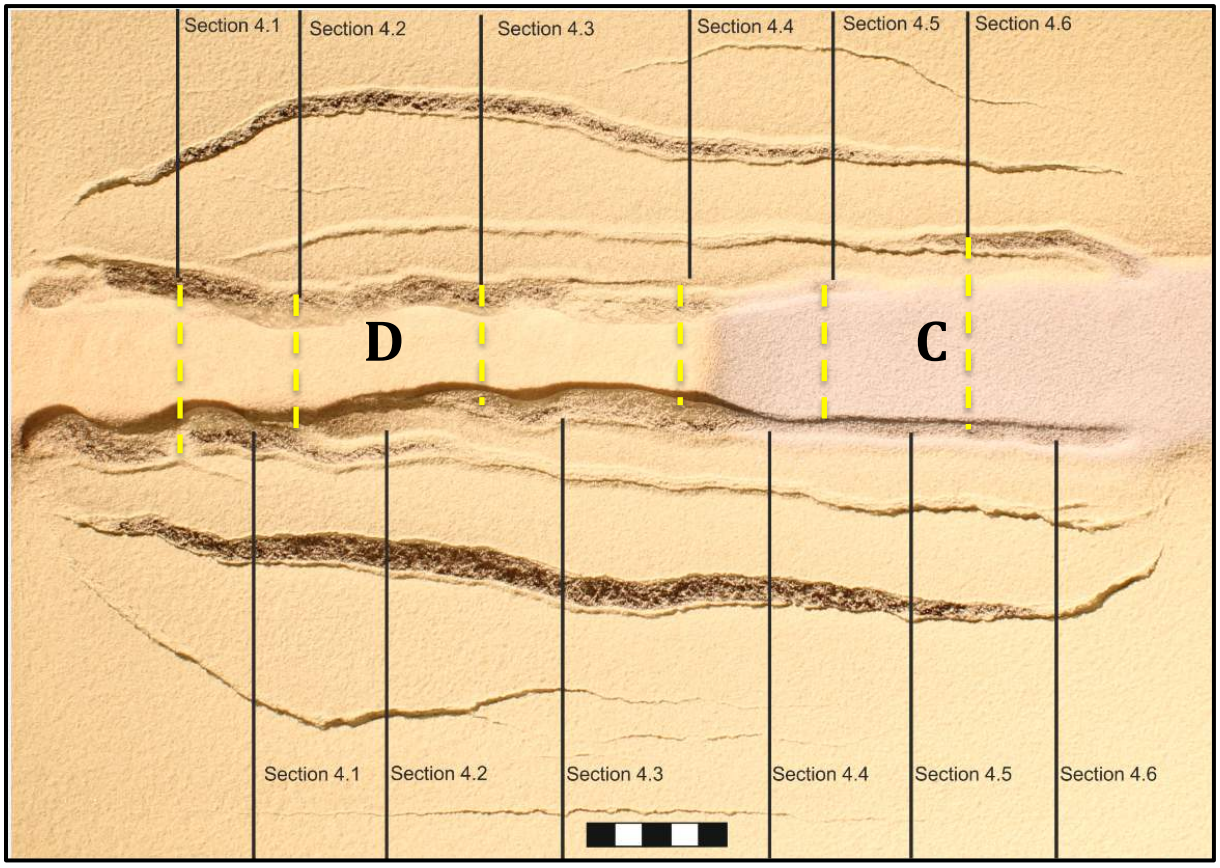

Fig. 73. Top view of model 4 after two hours of resting. The Blue part of the basin (part C)is normally filled, the white part of the basin (Part D)n is underfilled with a topography difference of 5mm between the basin floor and the surrounding platforms. During this phase of the experiment, the silicon putty in the underfilled part of the basin slowly spreads towards the center of the basin by gravitational spreading.

Fig. 76. Top View of the model after four hours of resting. During this part of the model, the left part of the basin was still underfilled, though slightly less than during the first two hours of the resting phase.

Fig. 75. Top View of the model after six hours of resting. During this part of the model, the left part of the basin was only slightly underfilled.

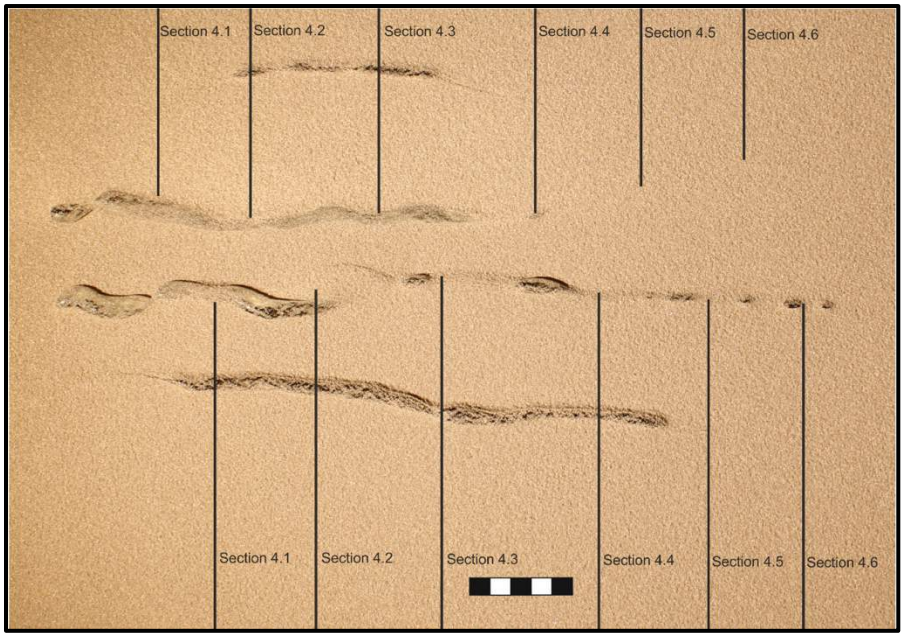

Fig. 76. Top View of the model after eight hours of resting. During this part of the model, the entire part of the basin was normally filled as is indicated by the absence of shadows north of the diapirs.

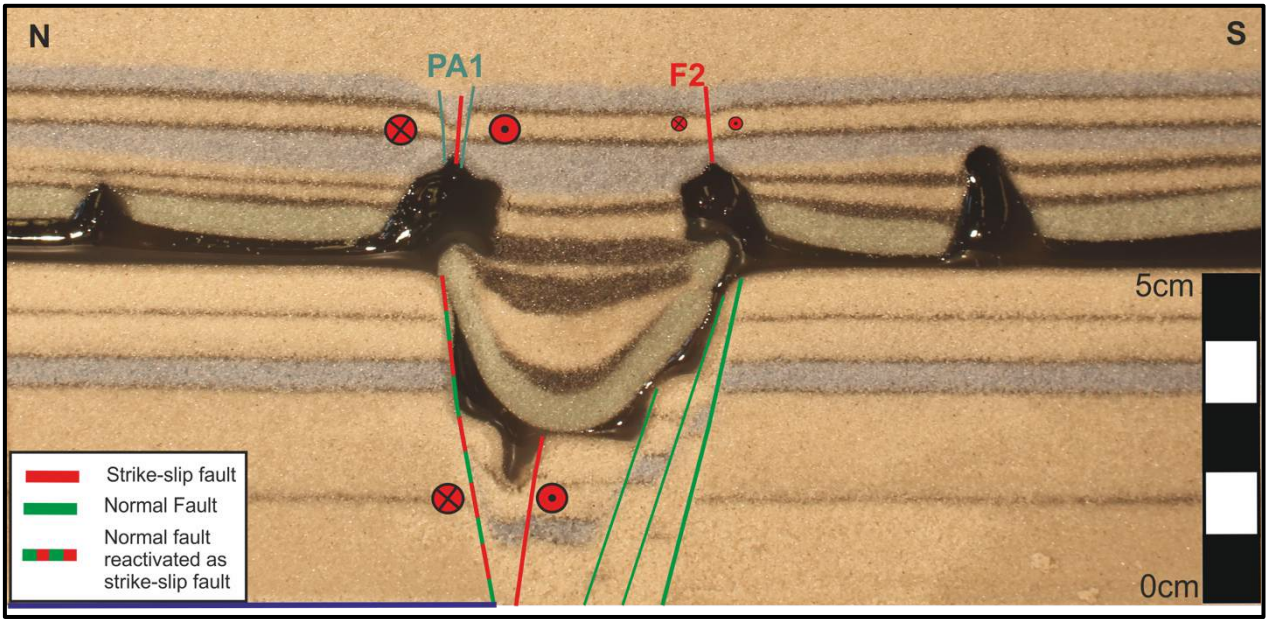

Fig. 77. Cross section 4.1. the location of the cross-section is indicated at the top views of the experiment.

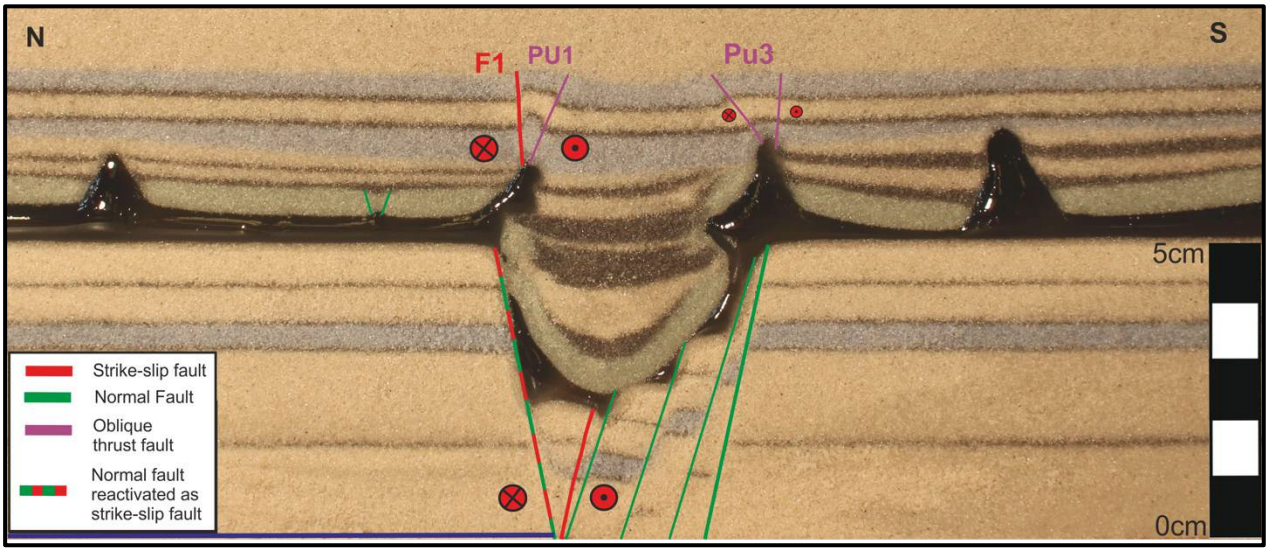

Fig. 78. Cross section 4.2. The location of the cross-section is indicated at the top views of the experiment.

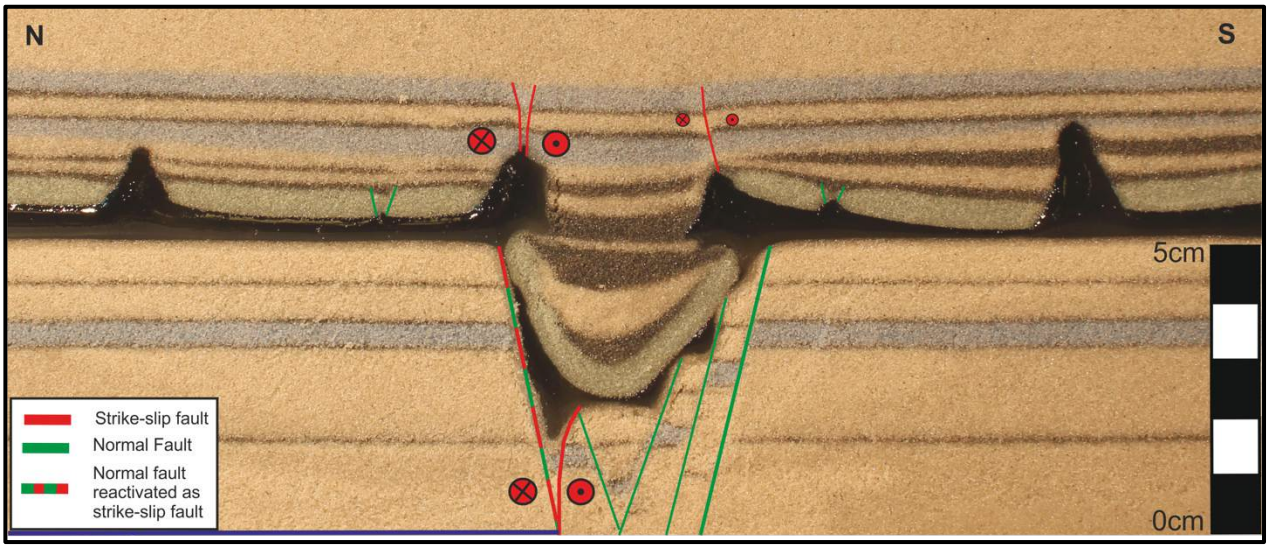

Fig. 79. Cross section 4.3. The location of the cross-section is indicated at the top views of the experiment.

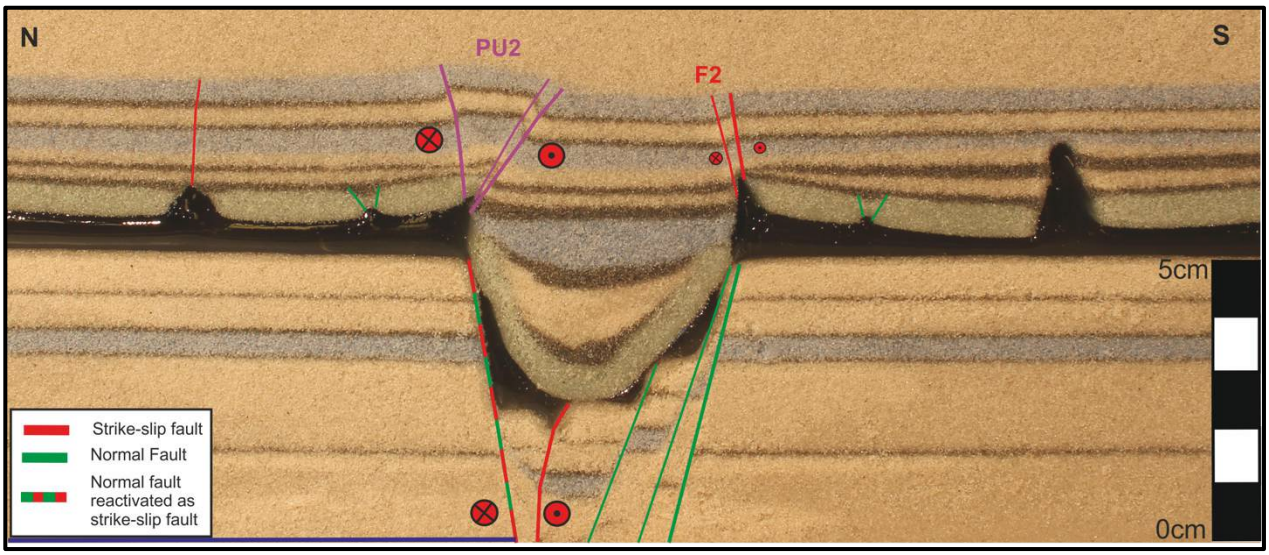

Fig. 80. Cross section 4.4. The location of the cross-section is indicated at the top views of the experiment.

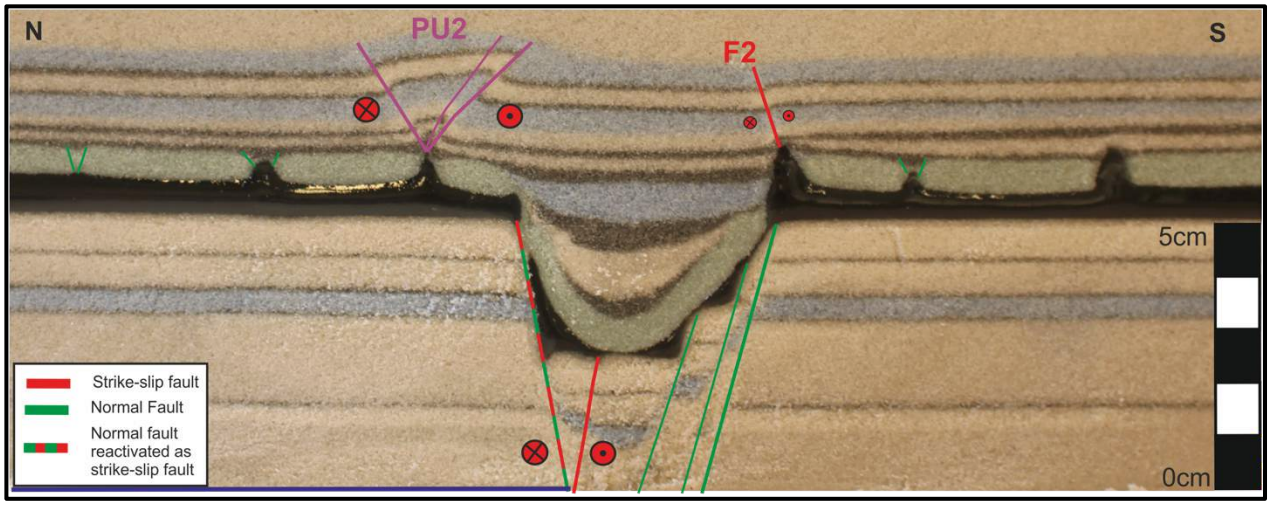

Fig. 81. Cross section 4.5. The location of the cross-section is indicated at the top views of the experiment.

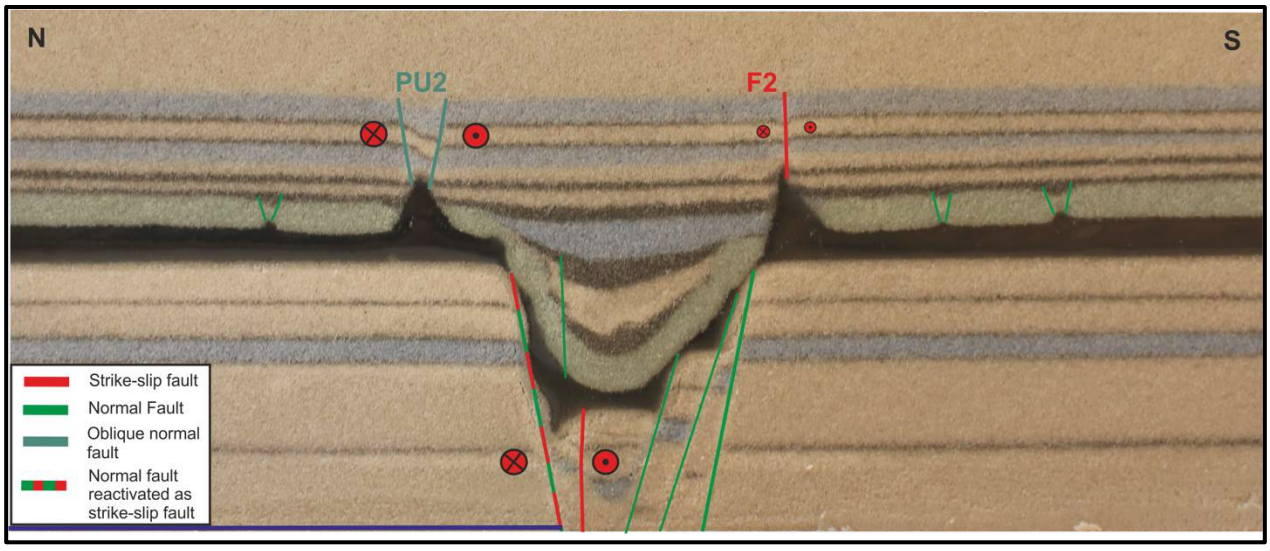

Fig. 82. Cross section 4.6. the location of the cross-section is indicated at the top views of the experiment.

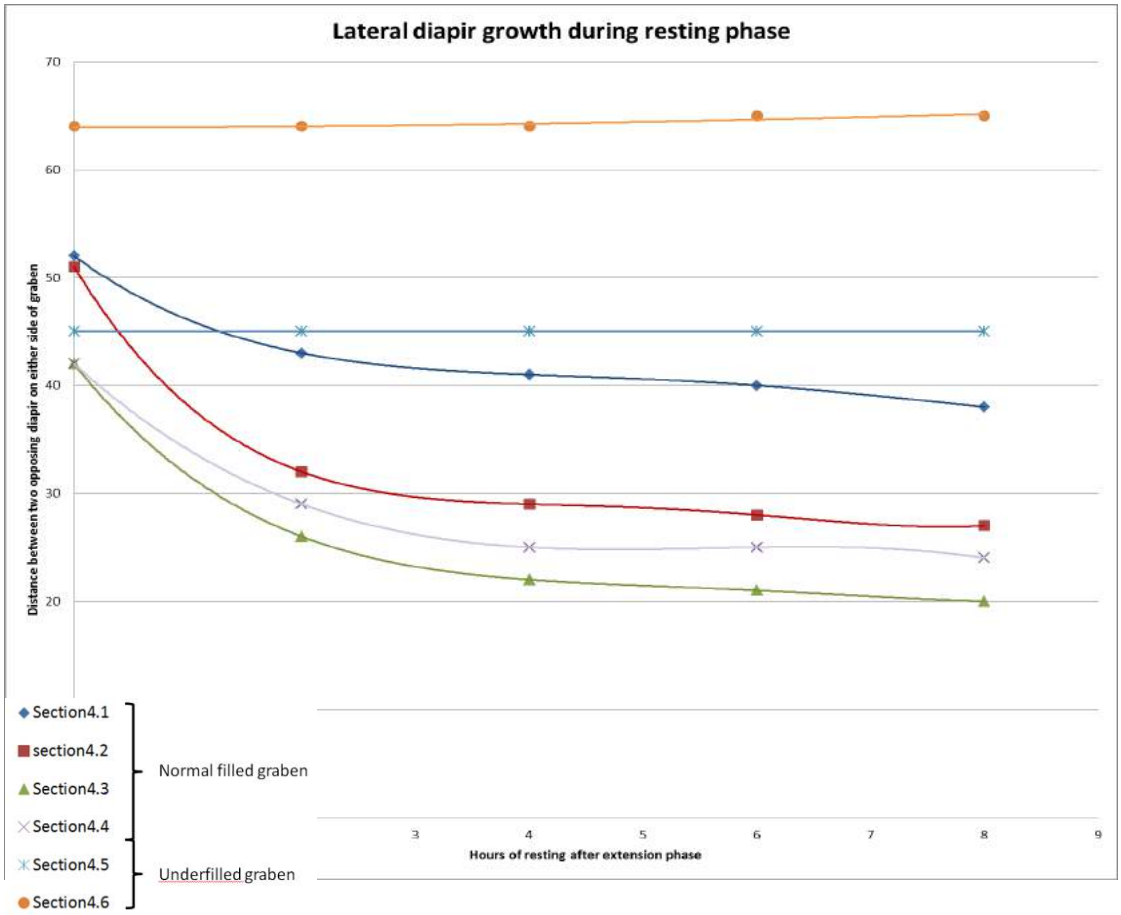

Fig. 83. Graph showing the distance between two opposing salt structures varying through time during the resting phase, indicating the differences in lateral salt movement when the underfilled part of the basin is compared to the normally filled part of the basin.

Strike-Slip phase

Strain distribution

The first structures that form during the strike-slip phase are R Riedel faults. These faults form after 5 percent of bulk strike-slip. Generally less than 1mm of displacement occurs on these faults and with a distance of around 5cm to 7cm in between two Riedel faults, they are quite widely spaced. After 15 percent of bulk strike-slip, these Riedel faults become inactive and most of the displacement takes place on two faults which are shown in figures 84, 85 and 86 as F1 and F2. Minor displacements (less than 1mm) occur at faults within the graben, which generally have display a R Riedel orientation (fig. 84-86). Additionally some minor displacements take place on slightly curved faults located on the platforms. In accordance with model 3, the major fault F1 and F2, as well as the slightly curved faults on the platforms, follow the outline of the salt walls (fig. 87). At the end of the experiment (fig. 86), most of the displacement has occurred on fault F1 as is indicated in figure 64.

Zones of transpression and transtension

During this experiment, several zones of transpression and transtension developed due to either left or right stepping on the strike-slip faults. After 20% of bulk strike-slip, the contours of a small pull apart (PA1) structure, as well as a small pop-up structure become visible in the western part of the experiment (PU1) (fig. 84). However, this pop-up quickly becomes inactive when F1 cuts through the pop-up structure (fig. 85). A larger pop-up structure (PU2) forms in the eastern part of the experiment due to left stepping of fault F1 (fig. 84-86). This pop-up structure remains active for the entire duration of the experiment and displays significant topography of up to 5mm with respect to the surrounding area. Towards the far east of the experiment, F1 steps to the right and a large pull-apart structure formed, showing up to 5mm of subsidence. A third pop-up

structure (PU3) forms due to left stepping of fault F2 (fig. 85 and 86). This pop-up structure remains also active for the entire duration of the experiment but topography is lower than at PU2.

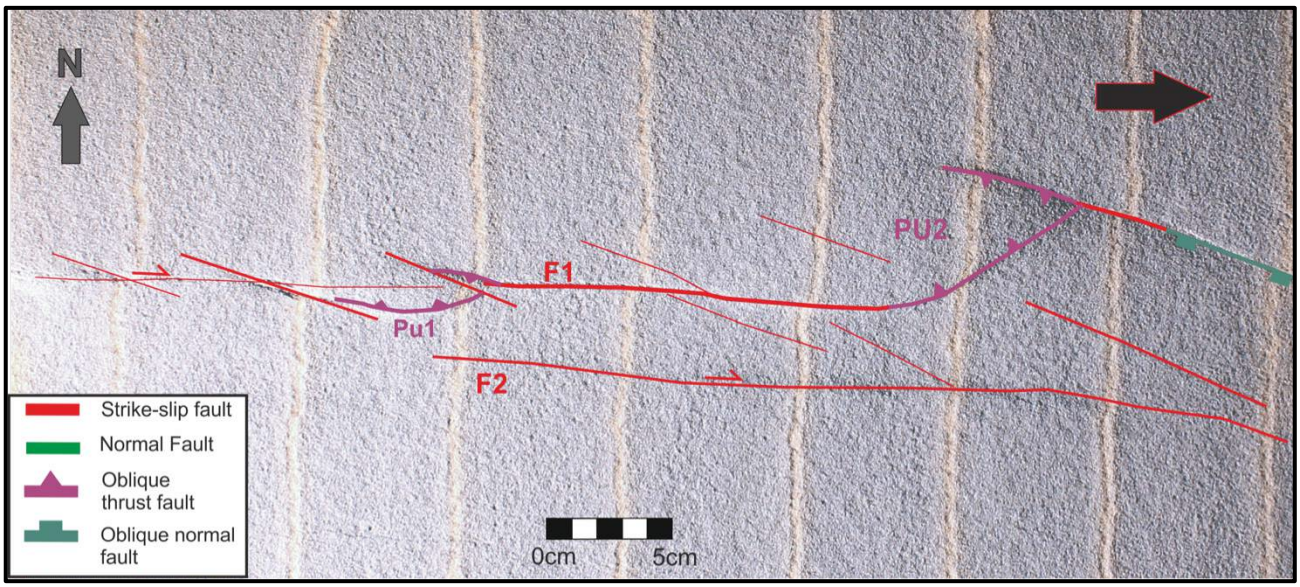

Fig. 84. Top View of the model after 33% of bulk Strike-slip. By this time, deformation already takes place along the main fault zones, which are located above the diapirs. Riedel faults have become largely inactive, except for the Riedel faults located insight the graben.

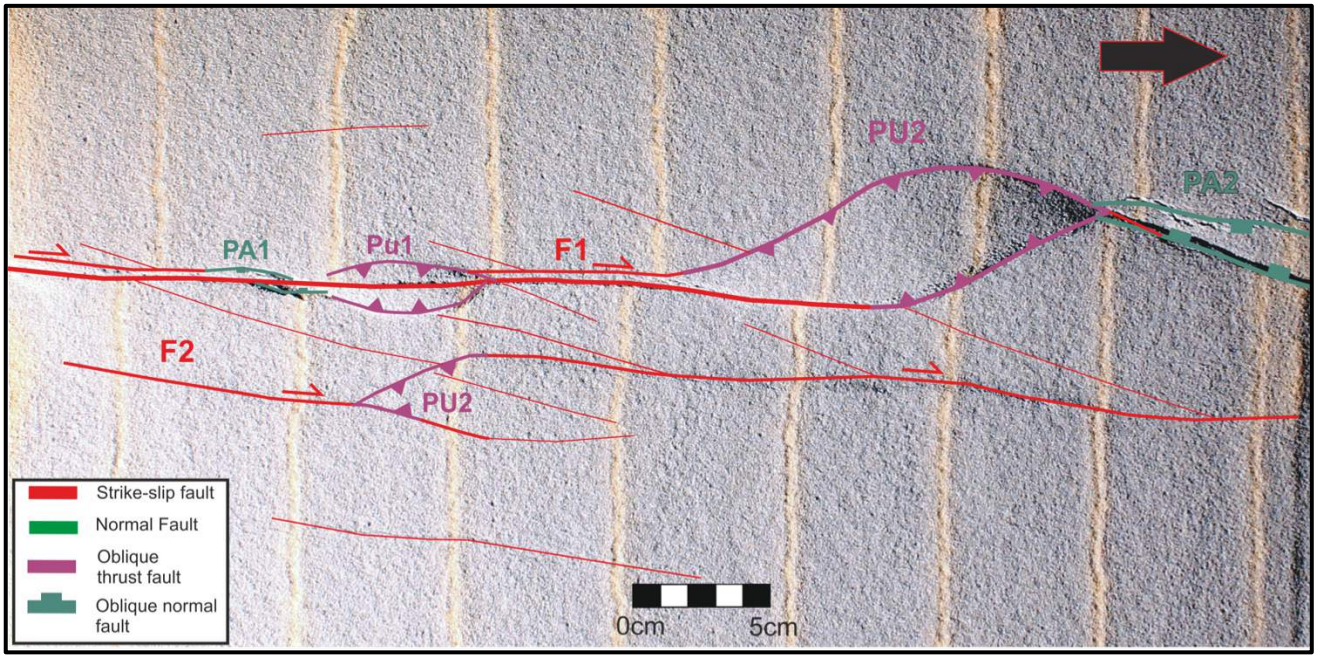

Fig. 85. Top View of the model after 66% of bulk Strike-slip. By this time, Pop up 1 has become inactive but pop-up 2, pull-apart 2 and pop-up 3 will remain active for the entire duration of the experiment.

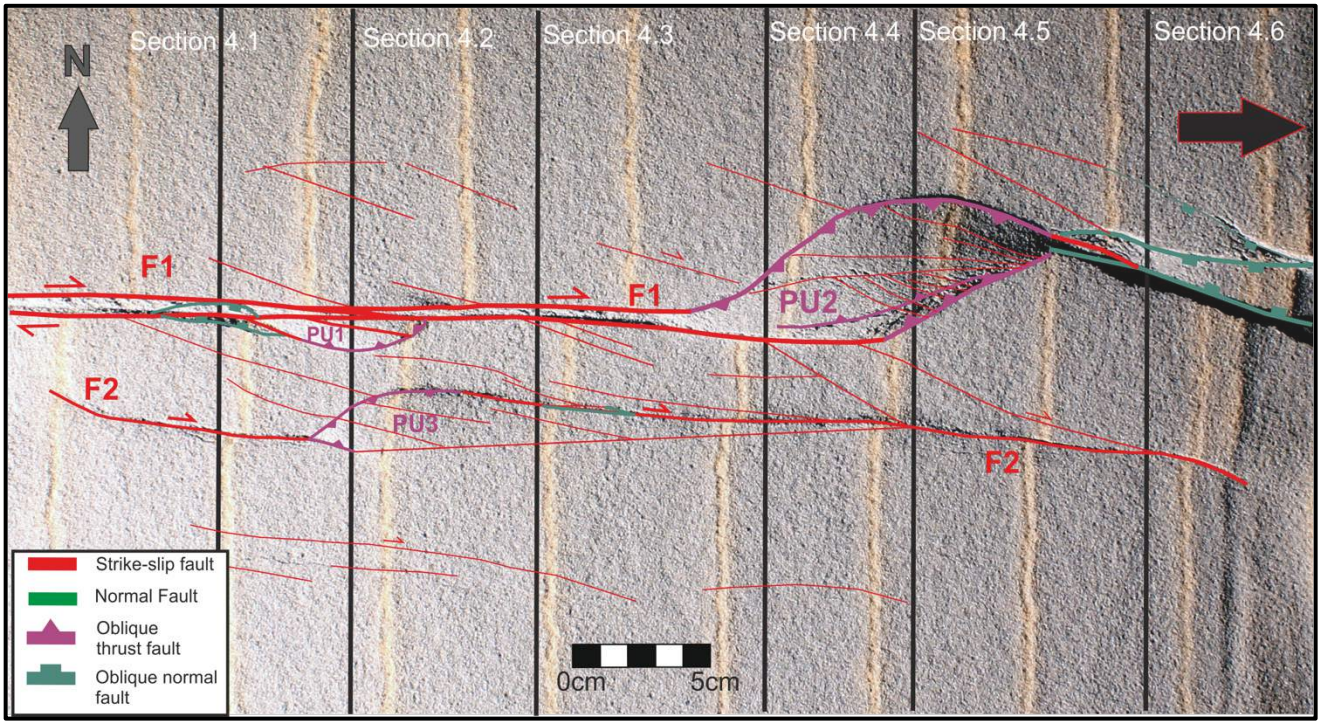

Fig. 86. Top View of the model end the end of the strike-slip phase.

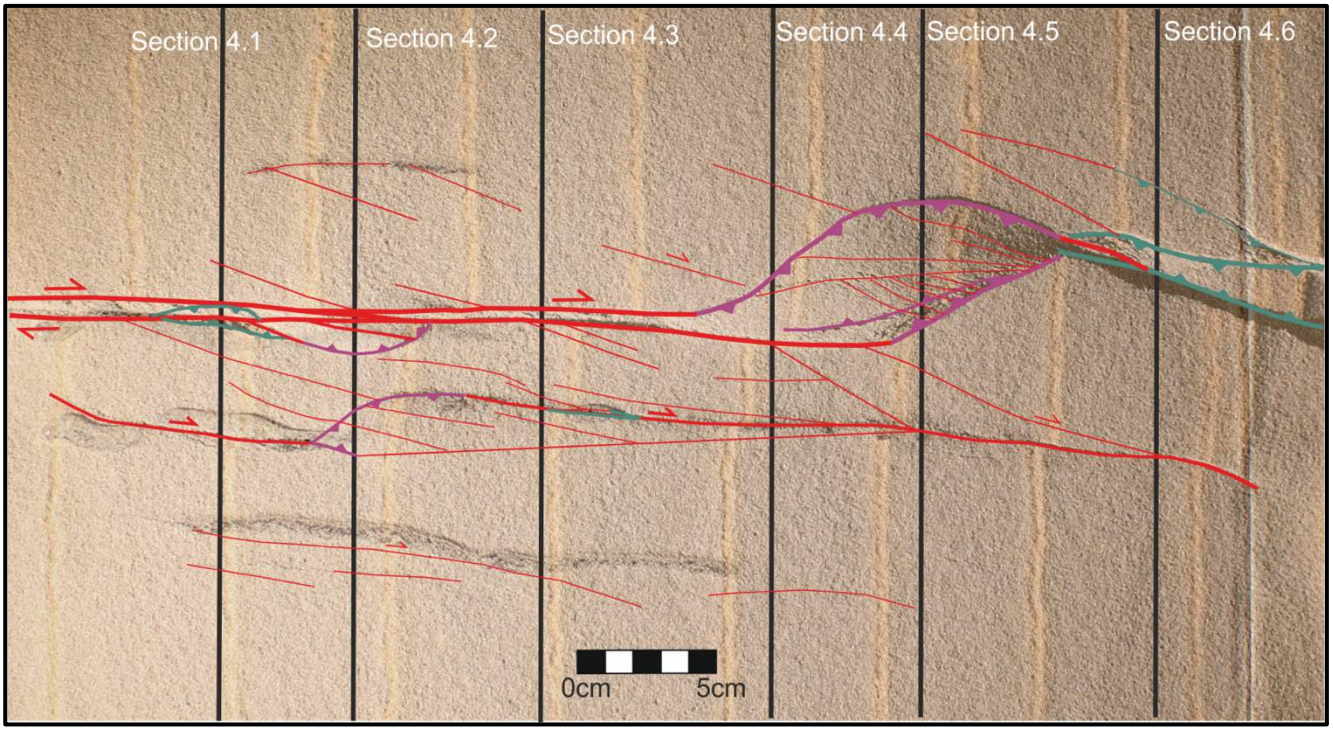

Fig. 87. Top View of the model after the end of the strike-slip phase. A transparent view of fig. 5 is laid over the end of the strike-slip phase. Showing that the main strike-slip faults are located above the silicon putty walls and that the pop-up and pull-apart structures are formed due to lateral variations in the distribution of the silicon putty walls.

5.5 Discussion of the models 2,3 and 4.

The models demonstrate that the presence of a weak layer in a preformed basin has a profound effect on the deformation pattern when the preformed basin is subjected to strike-slip deformation. In the western part of the purely brittle model 2, the strike-slip deformation is almost solely accommodated along the preformed normal fault, bounding the basin. Hence it is assumed that, in accordance with model 2, most of the deformation in the basement of models 3 and 4 is accommodated along the preformed, sub-salt basement fault as well as on some vertical strike-slip basement faults that can be recognized in cross section and terminate on the base of the silicon. The presence of the weak layer of silicon putty redistributes the strike-slip deformation and causes decoupling from the strike-slip deformation below the weak layer, with respect to strike-slip deformation above the weak layer. This decoupling results in different deformation patterns below and above the weak layer. The main strike-slip faults in the overburden follow the outline of the silicon putty walls, as can be inferred from figures 64 and 87. This can be explained from the mechanical strength of the supra-salt interval; which is lowest above the diapirs. The reason for this is twofold and can best be explained by fig. 88, which shows how the strength ($\sigma_1 - \sigma_3$) of a brittle and a ductile material depends on the thickness of the layer. From this figure can be inferred that the strength of the silicon putty decreases with increasing layer thickness. In contrary, the strength of the sand increases with decreasing layer thickness. Because of this material behavior, the models 3 and 4 are charachterised by lateral strength contrasts, as the basins are significantly stronger than the platform directly outside of the basins were the salt walls are located (fig. 89). The strength of the models also varies along strike, as diapirs don't reach the same height over the full length of the model. In model 3 for example, the southern diapir is significantly lower on the eastern side of the model than on the western side of the model. A higher diapir is mechanically weaker and fig. 69 indicates that the higher the diapir, the more displacement is accommodated along that diapir. This can be seen in in the southeastern part of model 3 were the diapir is lower. Above this diapir, strike-slip fault F2 is not well developed. Instead displacements are distributed over a larger area.

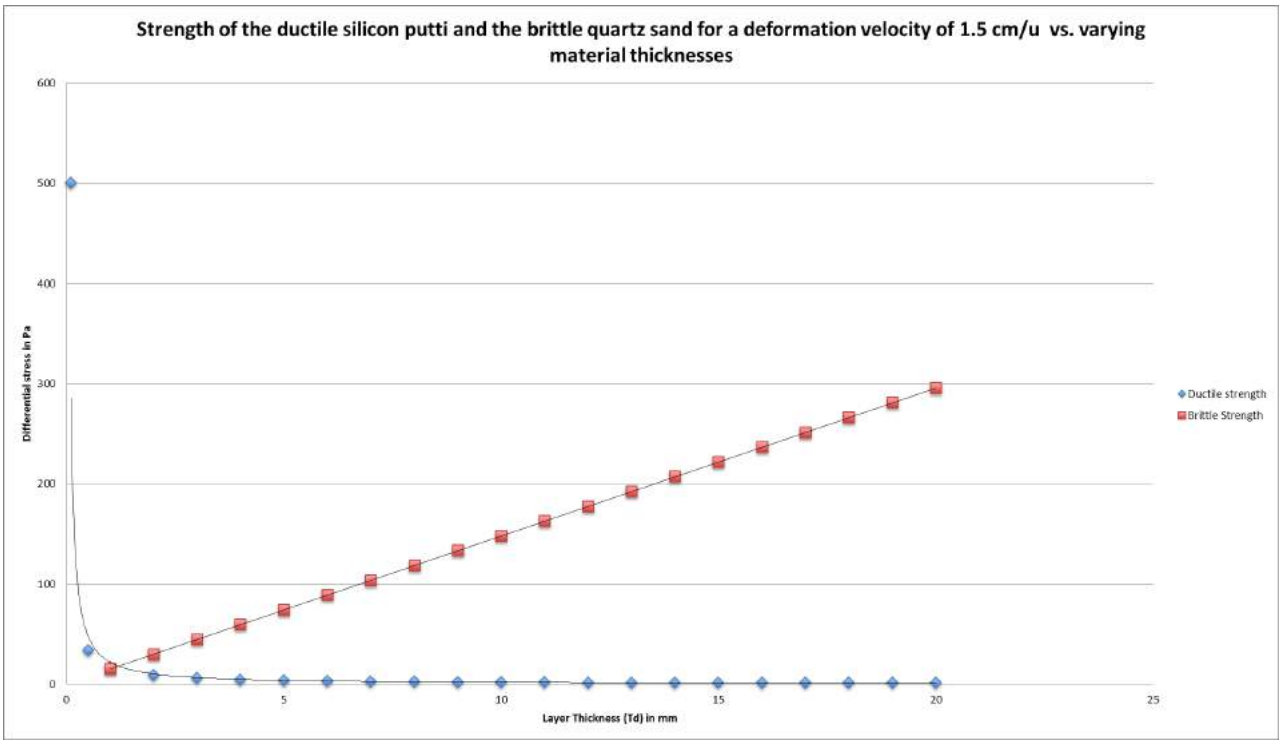

Fig. 88. Graph showing the variations of the mechanical strength of the silicon putti layer and the brittle quartz layers. It can be inferred from this figure that the silicon putti quickly becomes weaker for increasing thickness. The brittle quartz layers on the other hand linearly increase in strength with increasing thickness. The brittle strength was calculated by making use of equation 21. The ductile strength was calculated by making use of equation 22 (Smit, 2005).

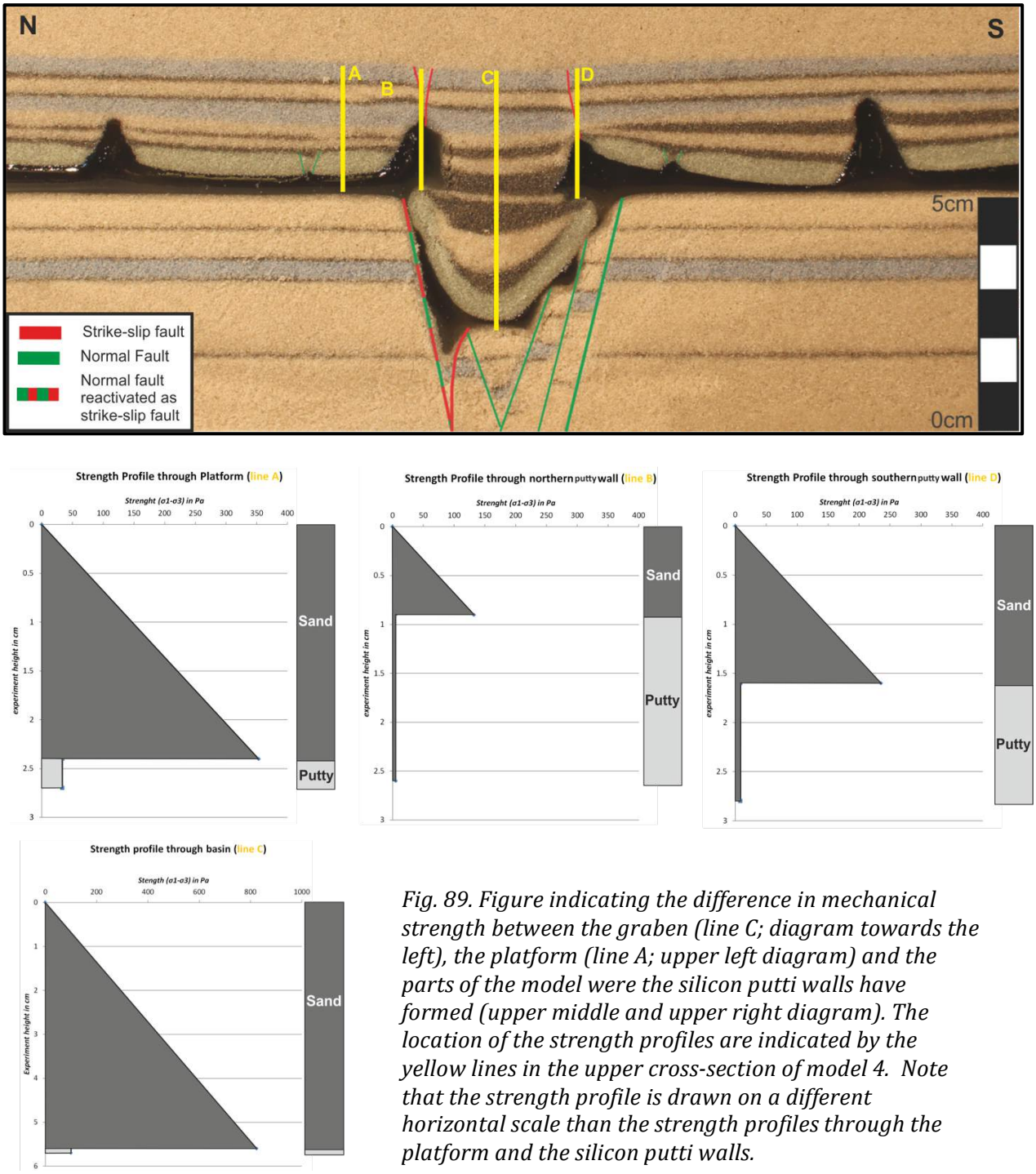

Fig. 89. Figure indicating the difference in mechanical strength between the graben (line C; diagram towards the left), the platform (line A; upper left diagram) and the parts of the model were the silicon putti walls have formed (upper middle and upper right diagram). The location of the strength profiles are indicated by the yellow lines in the upper cross-section of model 4. Note that the strength profile is drawn on a different horizontal scale than the strength profiles through the platform and the silicon putti walls.

When the models 3 and 4 are compared, it can be concluded that the models don't have the same lateral strength profile, as is indicated by Fig. 90. Surely, the silicon putty walls in model 3 are more evenly distributed than in model 4, as the silicon putty walls in model 3 run approximately parallel on either side of the graben (Fig. 90). Model 4 on the contrary shows a higher degree of variation in the distribution of putty, as silicon putty in this model extruded in the underfilled part of the basin. Because the main strike slip faults follow the outline of the silicon putty walls, sharp bends in the distribution of silicon putty walls causes right and left stepping of the main strike-slip faults in experiment 4 and the subsequent formation of profound pop-ups and pull-aparts. Because these sharp bends in silicon putty walls are absent in model 3, this model shows neither profound pop-up structures nor pull-apart structures.

Another difference between model 3 and 4 is the strain distribution inside the graben. Based on strength contrasts, one wouldn't expect to find much strike-slip displacement inside the graben, as

the brittle overburden here is relatively thick and the silicon putty relatively thin, making the center of the graben mechanically strong. However, as can be inferred from figure 68, a significant amount of the strike-slip displacement in model 3 is accommodated by small strike-slip faults in the graben. Although the amount of displacement on individual faults is very low (generally less than 1mm), together they accommodate a significant amount of displacement. The amount of strike-slip displacements in the graben is likely related to the distance between the two main strike-slip faults in the overburden. This distance is less in model 4 than in model 3, because the silicon putty walls in model 4 had extruded and hence had grown towards each other, thereby reducing the distance D (fig. 83). Because the main strike-slip-faults follow the outline of the silicon putty walls, also the main strike-slip faults are closer spaced with respect to each other in model 4 than in model 3. The majority of the displacement takes place on these two faults, which is also the case in model 3. However, most of the displacement occurs on the faults F1 and less on the faults F2. This means that the area between these faults has to partly accommodate this difference in displacement. The difference is thus accommodated by the graben in the form of small faults that together function as a zone of approximate simple shear. Because the distance between the two main strike-slip faults is smaller in model 4, the area of simple shear between the faults is less than in model 3. Hence less faults form and less displacement has to be accommodated on these faults. Additionally, the amount of displacement along a strike slip fault in the overburden depends on its distance with respect to the basement fault, as was inferred from fig. 70. Although this was only measured for strike-slip faults on top of the silicon putty walls, it is reasonable to assume that this is also valid for small strike-slip faults within the graben to some extent. Because the graben in model 4 is smaller, less difference in motion is present between the north and the south side of the graben. Hence less faults needed to develop in model 4.

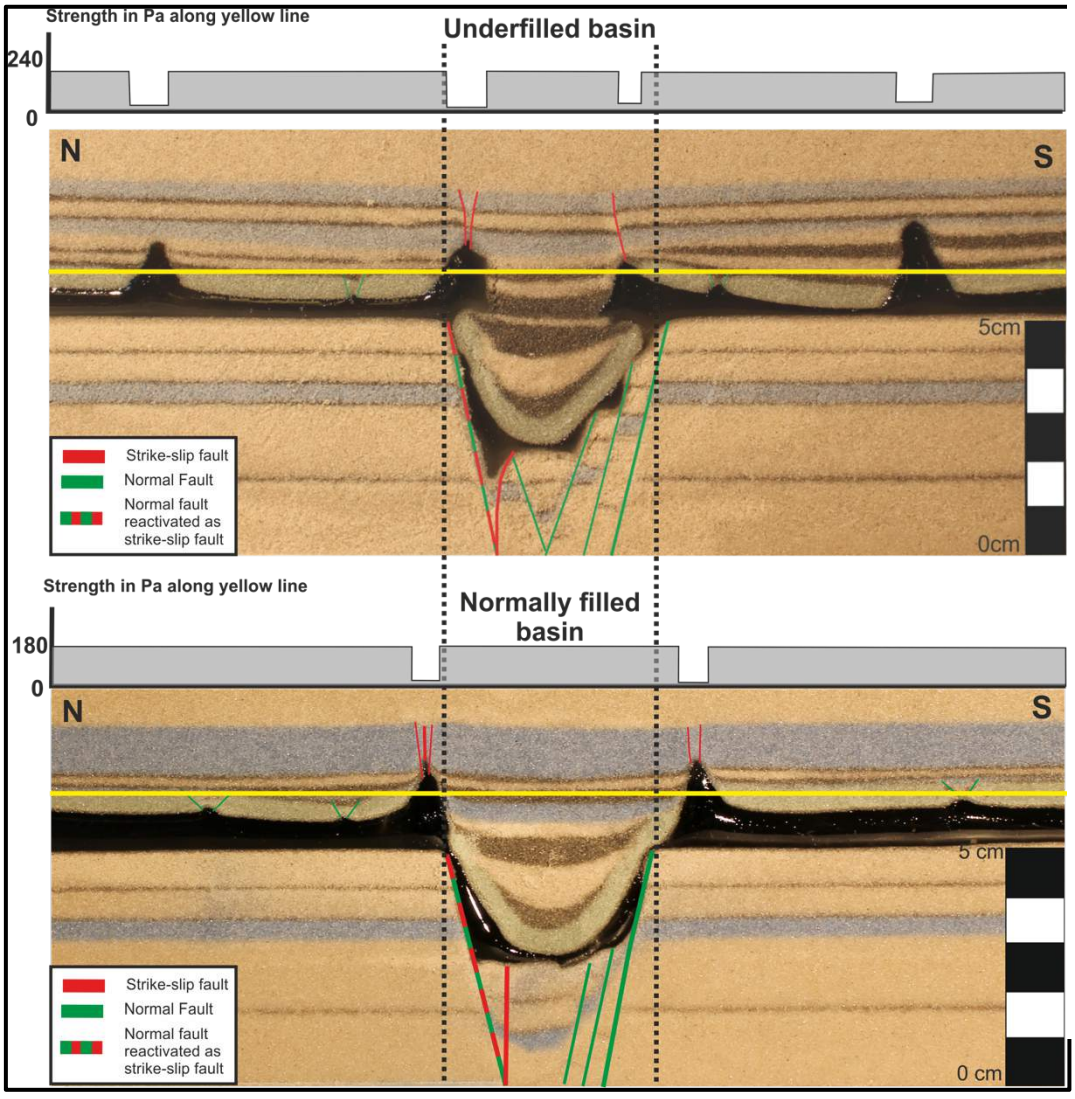

Fig. 90. Figure illustrating the lateral difference in strength between an underfilled graben with extruded putty (section 4.3) and a normally filled graben (section3.2). The vertical dased black lines intersect the top of the basement normal faults that bound that basement part of the graben. From these lines can be inferred that the brittle part of the sub putty graben is narrower for the underfilled basin than for the normally filled basin.

6. Integration and discussion

This study has provided better insights in several strike-slip movements that occurred in the Northern Dutch offshore in terms of timing, sense and amount of displacement and fault-salt interaction. In this section is discussed what could have caused the strike-slip motions that are observed in the Dutch Central Graben and Terschelling Basin (case study B-D) and to what extent the analogue models are a valid approximation for the observations regarding strike-slip movements in the northern Dutch Offshore.

6.1. Strike-slip motions in the Dutch offshore and analogue modelling

Strike-slip faulting has occurred during four time intervals in the northern Dutch offshore under regional extensional (Triassic, Jurassic and Lower Cretaceous) and compressional (Late Cretaceous) tectonics.

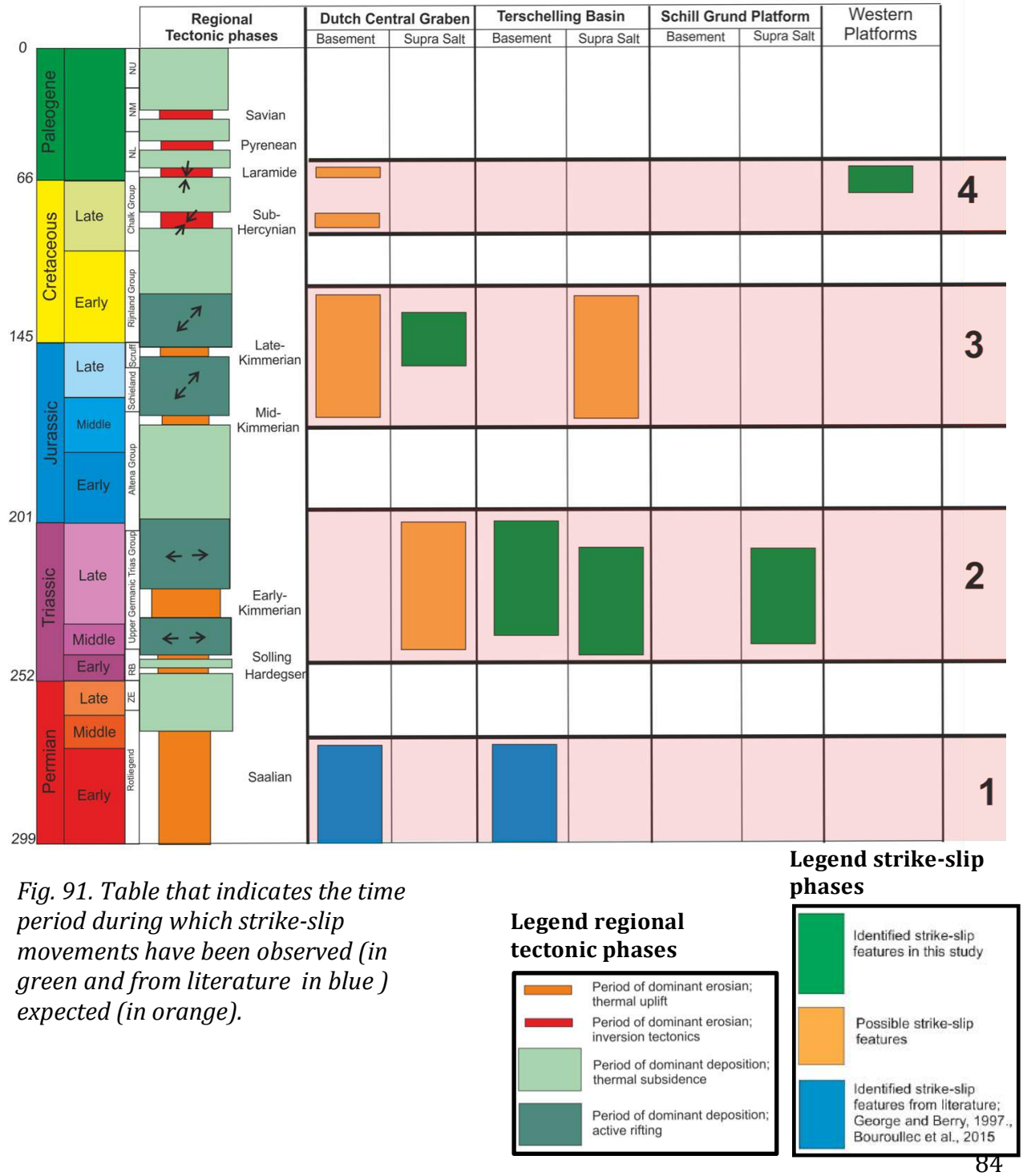

Fig. 91. Table that indicates the time period during which strike-slip movements have been observed (in green and from literature in blue) expected (in orange).

When the model of Kley et al., (2008b) (section2.4) is applied to the Dutch subsurface, one would expect that the Hantum Fault Zone and the Rifgronden Fault Zone accommodated dextral strike-slip motions during the Middle and Upper Triassic, thereby functioning as a transform fault zone to accommodate movements that resulted from active rifting in the Dutch Central Graben and the Lower Saxony Basin (Fig. 92). Evidence for these dextral movements were indeed found on the HFZ and RFZ in this study (Case Study D).

According to the model from Kley et al., (2008b), strike-slip motions could also have occurred during the Upper Jurassic and Early Cretaceous along preformed N-S trending basement faults that bound the Dutch Central Graben (Fig. 91 and Fig. 92). During this time, the N-S trending faults that bound the Dutch Central Graben could have functioned as an (oblique) transform fault zone that accommodated motions that resulted from active rifting in the Terschelling Basin and the Tail End Graben towards the north of the Dutch Central Graben (Fig. 93). According to the model from Kley et al., (2008b), these (oblique) strike-slip movements would have been sinistral. No evidence for these strike-slip faults was found in this study, although it has to be emphasized that the seismic resolution is insufficient underneath the Zechstein salt in the Dutch Central Graben to find direct evidence of these motions.

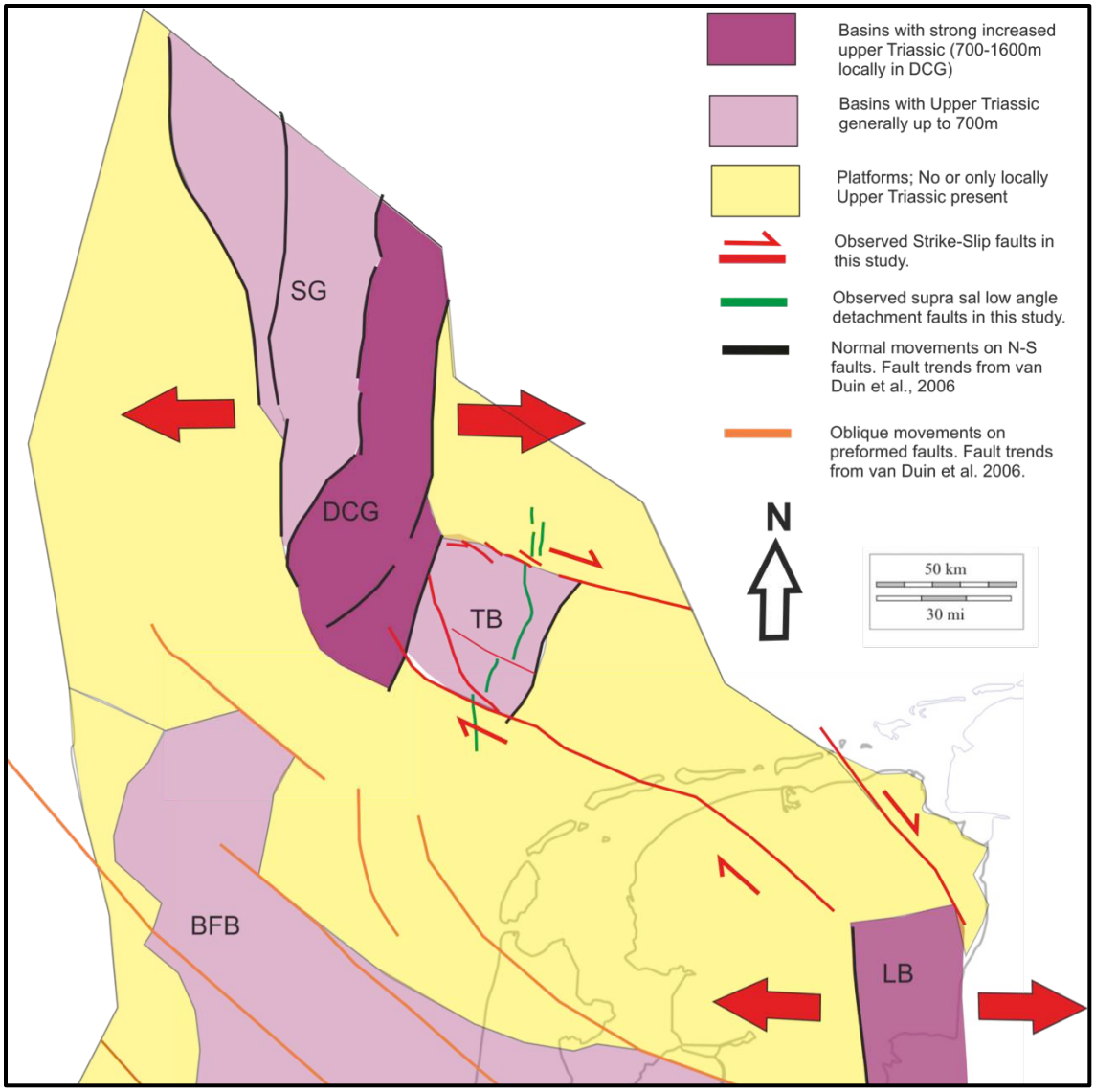

Fig. 92. Schematic map showing the geological setting of the Dutch subsurface during the Middle and Late Triassic. Abbreviations; BFB Broad Fourteens Basin, DCG Dutch Central Graben, LB Lower Saxony Basin, SG Step Graben, TB Terschelling Basin. Source for thickness distribution; Southern Permian Basin atlas.

Analogue models on the other hand have shown that strike-slip movements on (preformed) basement faults are redistributed by the overlying salt, thereby decoupling the supra-salt deformation pattern from the subsalt deformation pattern. Movements are preferentially transmitted and accommodated by salt diapirs as the supra salt interval is at its weakest here. The reason for this is twofold; 1) A package of salt becomes weaker with increasing salt thickness. 2) The overburden becomes weaker with decreasing sediment thickness. If sediments overlie salt diapirs or salt walls, strike-slip motions are transmitted via these salt structures into the overburden. Hence, basement induced strike-slip faults could preferentially be observed above diapirs. The reason that these faults are not observed above diapirs in the Dutch Central Graben and Terschelling Basin could be due to Mid-Kimmerian uplift and Late Cretaceous – Early Paleogene inversion and subsequent erosion. Surely, Mid-Kimmerian erosion has removed the entire Lower Jurassic as well as significant parts of the Upper Triassic in the Terschelling Basin, while Late Cretaceous – Early Paleogene inversion has removed large parts of the Upper Jurassic and Lower Cretaceous sediments in the Dutch Central Graben. Additionally, where the Upper Jurassic and Lower Cretaceous strata have been preserved in the Dutch Central Graben, renewed activity along salt walls and diapirs during Late Cretaceous – Early Paleogene inversion could have erased the evidence of strike-slip motions on preformed basement faults.

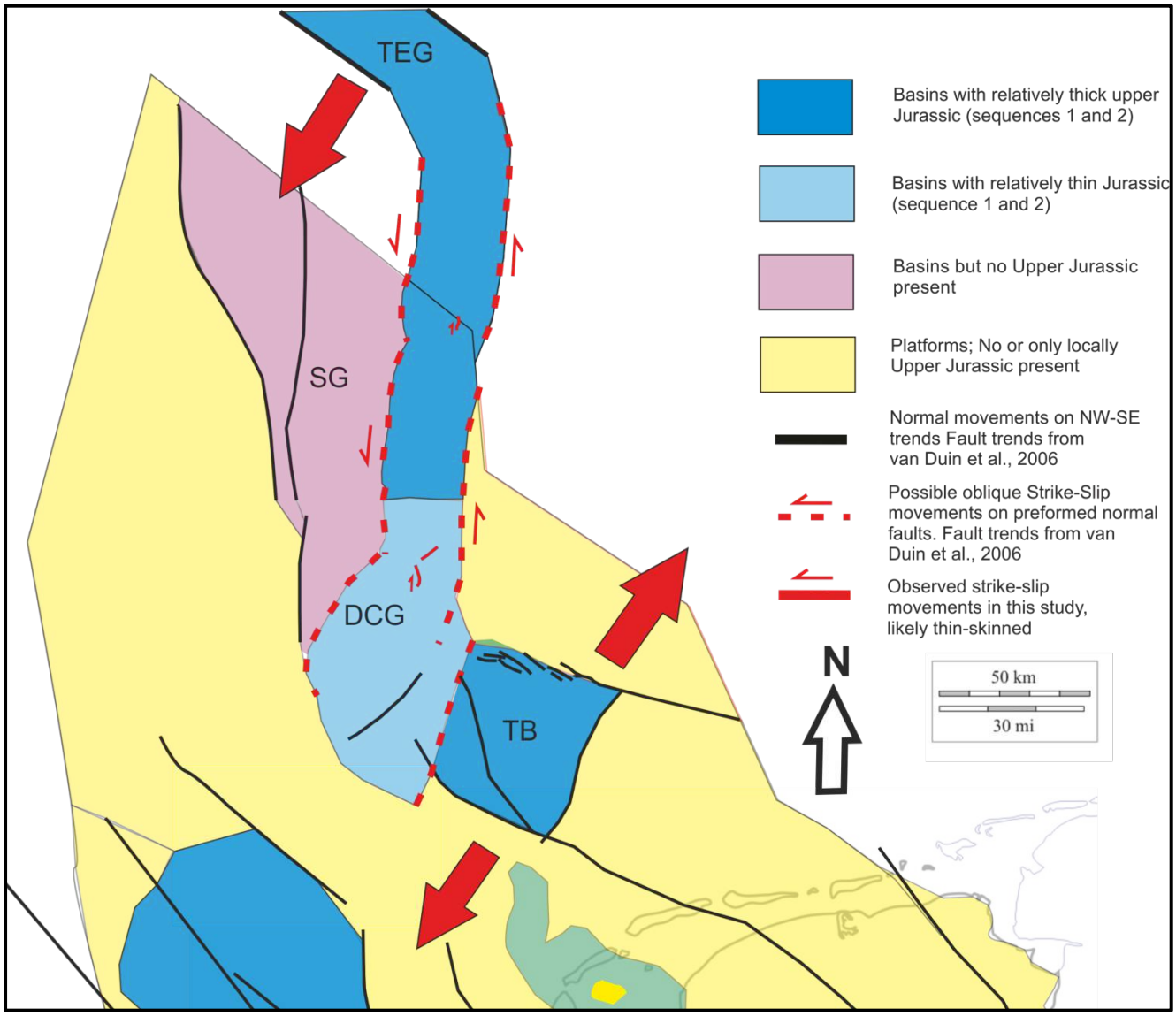

Fig. 93. Schematic map showing the geological setting of the Dutch subsurface during the Upper Jurasssic (Sequence 2 and 3). Abbreviations; DCG Dutch Central Graben, SG Step Graben, TB Terschelling Basin, TEG Tail End Graben. Source for thickness distribution; Southern Permian Basin atlas.

6.2. The origin of the observed strike-slip movements in the Dutch Central Graben

Thin-skinned vs. thick skinned

The observed strike-slip motions that are present in the Dutch Central Graben are located in the central parts of the basin. These motions are rather subtle; in the order of 700 to 2500m. The Late-Jurassic to Early Cretaceous timing of Faults F1b and F1c corresponds to a change in regional extension direction from approximately E-W towards NE-SW. As suggested by Kley et al., 2008b, this might have led to an (oblique) reactivation of preformed N-S trending faults. However, whether or not the observed supra salt strike-slip faults are induced by strike-slip movements on basement faults is difficult to say with certainty due to the resolution of the seismic data at this depth. The Zechstein salt surely seems thick enough in the entire part of the Dutch Central Graben to cause decoupling of the supra-salt with respect to the sub-salt interval. The analogue models described in this report have shown that when strike-slip motions occurred along basement faults, a small part of this motion is accommodated in the central part of the basin by several small faults, despite the increased mechanical strength of this part of the model. The amount of strike-slip that is accommodated in the central part of the basin seems to be controlled by the width of the basin as defined by the outline of the silicon putty walls. Hence, the strike-slip motions observed in the B18 and F11 blocks might have been caused by underlying basement strike-slip features.

Alternatively the strike-slip motions are purely thin skinned and accommodate differential motions during the Late Jurassic to Early Cretaceous on basement normal faults. In this scenario, the decoupling of the salt causes the local stress field above the salt to deviate from the stress field below the salt, which might have been purely extensional (fig. 94). Additionally, a component of gravitational gliding probably enhanced the strike slip-movements, as is indicated by the general northward deepening of the Dutch Central graben. The slightly curved geometry of faults F1b and F1c, favours the latter scenario, as basement strike-slip faults usually tend to be straighter, as is for example the case for the faults of FG1 on the western platform areas, described in case study A. Additionally, according to the model described by Kley et al., 2008, strike-slip motions on preformed basement faults would have been sinistral instead of dextral. Hence, it is suggested that F1b and F1c don't provide evidence for strike-slip movements on preformed N-S basement faults.

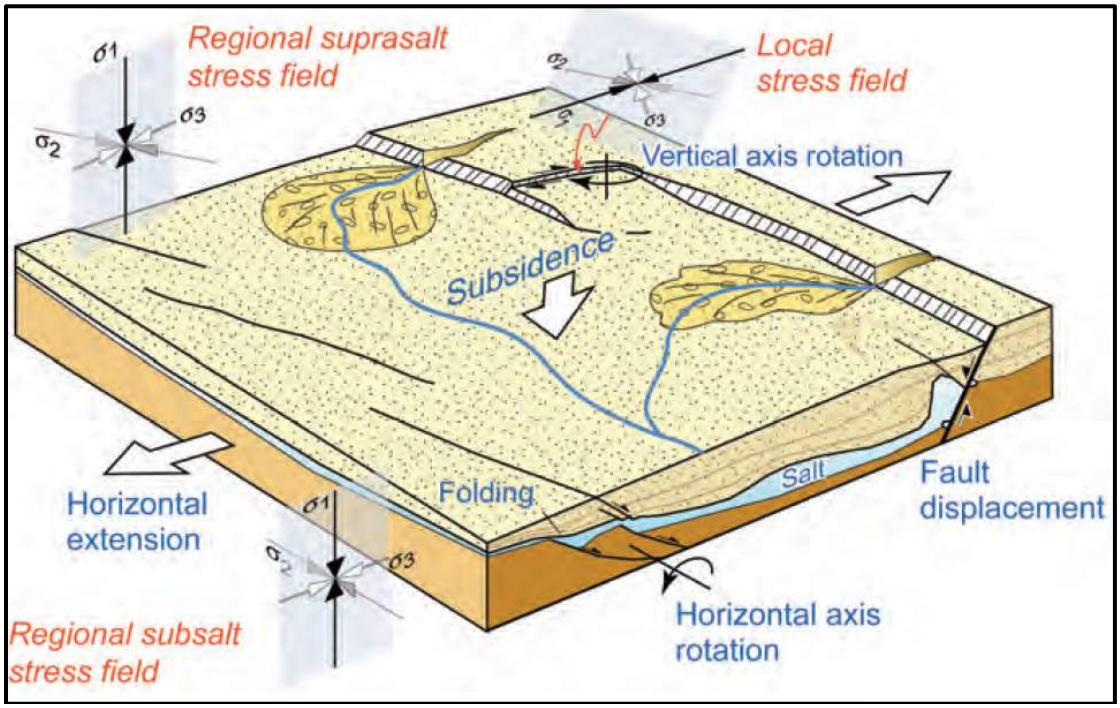

Fig. 94. Sketch that indicates how the local supra salt stress field can deviated from the regional stress field due to the presence of a salt layer. Figure from Kley et al., 2008

Regional structural evolution of the Central part of the Dutch Central Graben

An interpretation of the structural evolution of the area around fault F1c for the thin-skinned scenario is indicated in figures 95 and 96. According to this scenario, which is believed to be the most likely one, the first salt activity started during the Middle Triassic in response to normal movements along N-S oriented basement faults. Salt in this area reached the active piercing stage and evolved into the passive stage during the Late Triassic to Early Jurassic. When the regional stress regime changed towards NE-SW, new normal faults developed above the Zechstein salt (indicated in blue in fig. 96). It is likely that these thin skinned normal movements on ENE-WSW oriented faults are caused by normal movements on basement faults. However, it is hard to recognise these sub-salt faults in the seismic data. For sure, if new NW-SE basement faults developed, displacements were more subtle and not as large as during the Triassic along N-S trending basement faults. Additionally, also a component of gravitational spreading is likely to be involved, which is supported by the observation that NW-SE supra salt strike-slip faults all dip towards the N/NNE. Movements along these supra salt faults were not uniform throughout the basin, likely due to differential movements on basement faults, but certainly also due to the presence of salt walls and diapirs which had divided the brittle Mesozoic supra salt interval into several compartments, as they are laterally enclosed by salt walls in multiple areas. The differential motions between these compartments are primarily accommodated by the weak salt structures, as is shown by the analogue models. However, because salt walls don't fully enclose the different compartments, movements are transferred in the brittle interval in those places were the salt structures are absent (fig. 96). This scenario would explain both the curved geometry of fault F1c, as well as the different strike of fault F4c because fault F4c would transfer the motion between diapir B and the salt wall towards the northeast of diapir B in this scenario. Additionally, the interaction of the strike-slip faults F1c and F4c with salt diapir B, caused rotation of this diapir and likely also a component of compression on this diapir due to left stepping of the strike-slip fault.

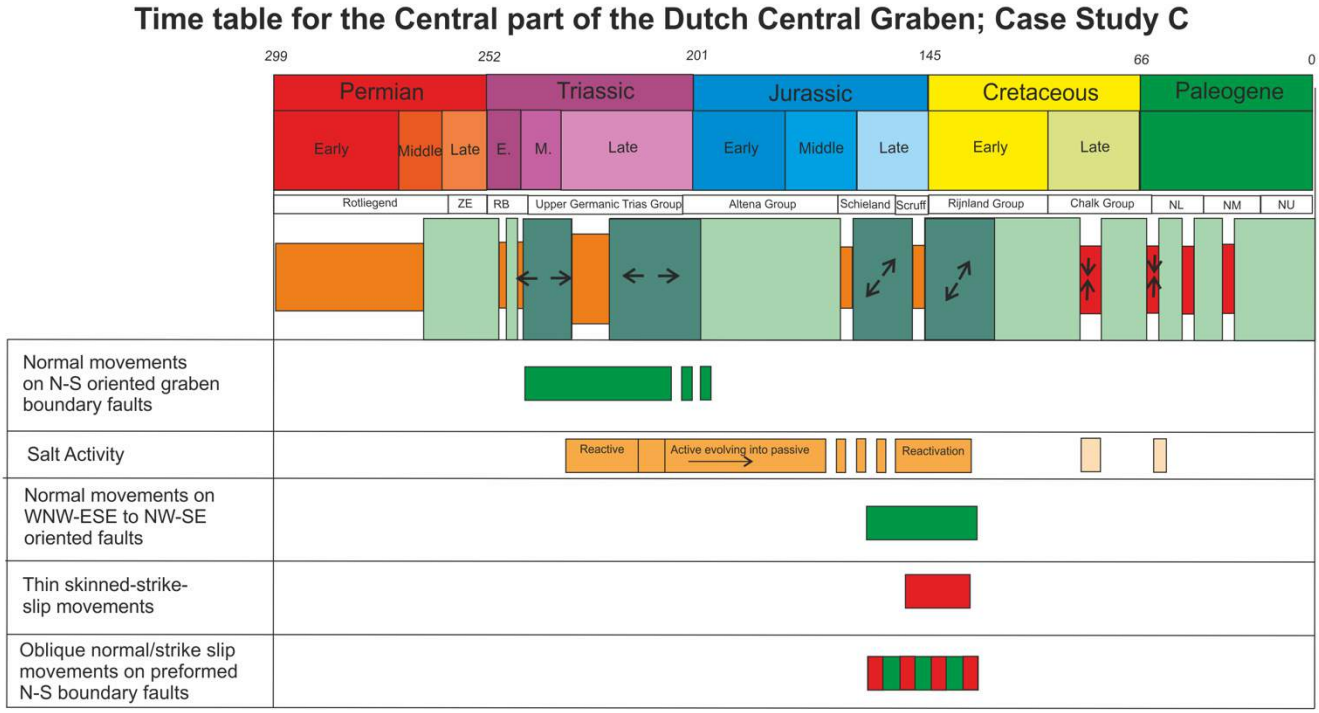

Fig. 95. Diagram indicating the time of activity for the main structural elements in the Central part of the Dutch Central Graben, as described in case study C.

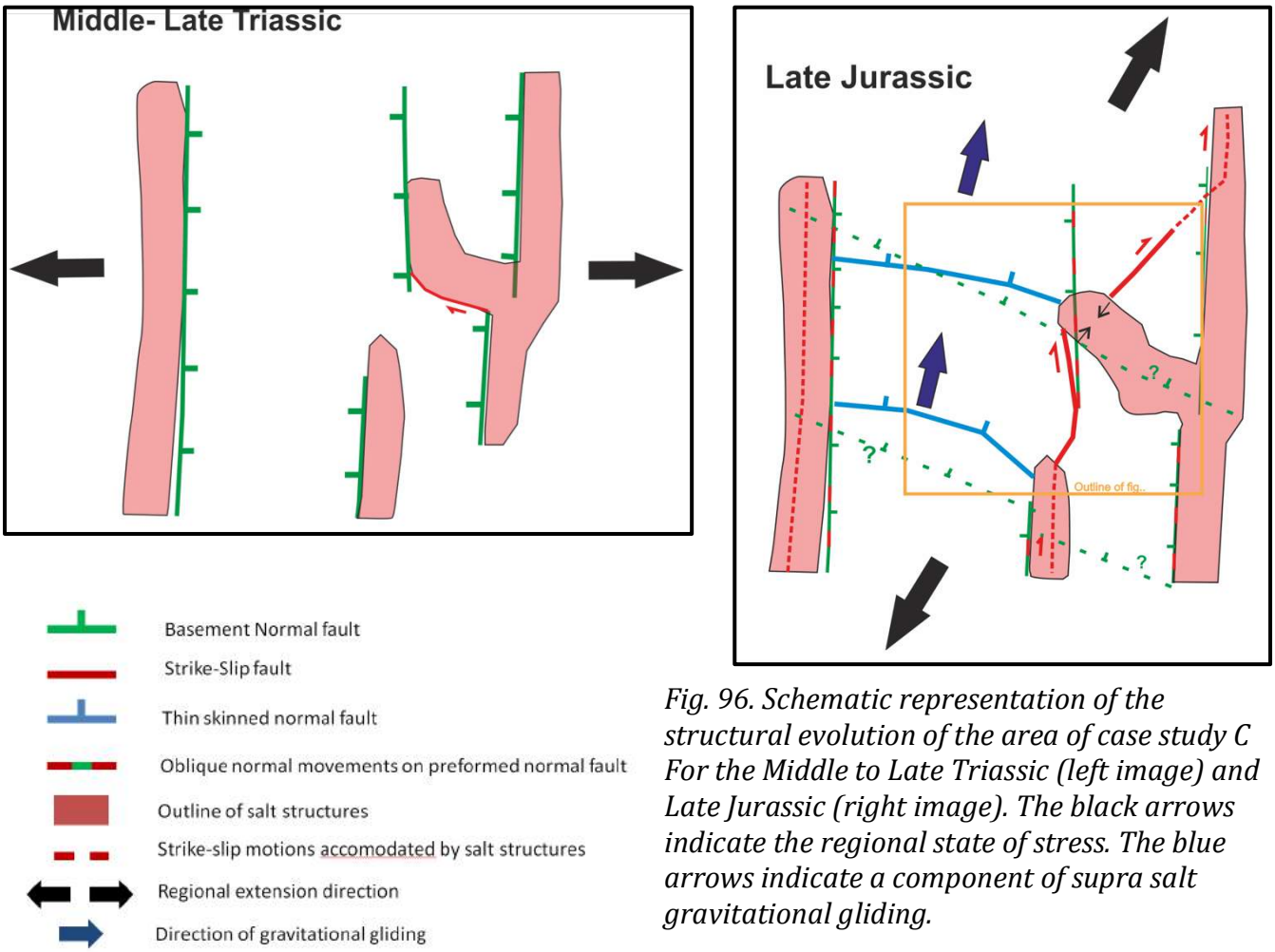

Fig. 96. Schematic representation of the structural evolution of the area of case study C For the Middle to Late Triassic (left image) and Late Jurassic (right image). The black arrows indicate the regional state of stress. The blue arrows indicate a component of supra salt gravitational gliding.

6.3 Strike-Slip motions in the Terschelling Basin and at the Schill Grund High

Thin-skinned motions

The thin skinned strike-slip motions that are present in the Triassic interval of the Terschelling Basin and at the Schill Grund High are likely caused by differential motions on sub-salt basement faults (fig. 94), to some extent similar to the strike-slip motions in the Upper Jurassic in the Dutch central Graben. However, there are some differences as the supra salt interval in the Terschelling basin was much thinner during the Upper Triassic, than the supra salt interval in the Dutch Central Graben during the Upper Jurassic. Additionally, salt structures were in an early stage of development in the Terschelling Basin during the Middle and Upper Triassic, as E-W extension during the Triassic triggered the first motions of Zechstein salt in the Terschelling Basin. Most salt structures in this area reached the piercing stage during deposition of the Late Triassic Keuper formation. This means that during the time of E-W extension and accompanied strike-slip motions, Zechstein salt was abundantly present to act as weak zones to accommodate for the differential motions (Fg. 97 In the Dutch Central graben, during the Upper Jurassic, salt structures were much more mature and salt walls and diapirs were generally already established. Hence differential motions on basement faults also had to be accommodated by the brittle supra-salt overburden in the absence of salt (Fig. 97), as is described in case study C.

Thick skinned motions

The stepping geometry of the N-S trending Middle to Late Triassic Low angle detachment fault zone over the WNW-ESE trending Hantum and Rifgrunden fault zone has been interpreted as evidence for post Early Triassic dextral strike-slip faulting along these fault zones. The fact that strike-slip motions occurred along the RFZ fault zone is furthermore supported by its en echelon geometry of fault segments. This is the first time that dextral displacements along these fault zones

have been estimated and that evidence is adduced that significant dextral faulting occurred along these fault zones during the Mesozoic. Dextral motions along the HFZ and RFZ correspond with the regional model for the Permian Basin area as proposed by Kley et al., 2008. Hence, it is suggested that the HFZ and to some extent the RFZ functioned as dextral transform fault zones to compensate for movements related to the opening of the Dutch Central Graben and to some extent the Lower Saxony Basin. As part of these dextral movements, the Terschelling Basin as a whole seems to have been dextrally sheared, explaining the deviating NNE-SSW trend that is displayed by the low angle detachment fault zone, the salt walls and the shape of the Lower Triassic compartments.

Regional Structural evolution of the Terschelling Basin

A time table for the Terschelling basin, indicating the activity of the main groups of structural features, is shown in Fig. 98 . Three stages of the interpreted structural evolution can be found in Fig. 99. First, during the Late Early Triassic (Fig. 99), activity started on N-S oriented basement faults bounding the Dutch Central Graben and probably on smaller N-S oriented basement faults underlying the Terschelling Basin. Extension accommodated by these faults was transmitted via the Zechstein salt into the Lower Triassic overburden, leading to the formation of initially N-S trending low angle detachment faults. In the Terschelling Basin, this E-W extension was enhanced by a westward component of gravity gliding, indicated by the overall westward deepening of the Terschelling Basin. Thin skinned extension triggered also the ascent of salt during the Middle-Triassic in the Terschelling Basin, where most salt structures reached the active piercing stage during the Upper Triassic. Differential motions along basement faults and due to differences in gravitational gliding, causde strike-slip motions, linking the motions between two segments of low angle detachment faults. These motions were accommodated by the salt which was abundantly present. After the initiation of activity on the low angle detachment faults, thick skinned dextral displacements commenced on the HFZ and RFZ, linking regional extension between the Dutch Central Graben and the Lower Saxony Basin. The dextral motions along the HFZ and RFZ dextrally offsetted the low angle detachment faults (fig. 99). Additionally, they caused overall shearing of the Terschelling Basin. The low angle detachment faults and dextral motions along the RFZ and HFZ most likely occurred simultaneously during the further period of E-W extension. Towards the Late Jurassic, when the direction of regional extension had changed, strike-slip motions no longer took place on the RFZ and HFZ. In contrast, they were activated in a normal way, thereby opening the Terschelling Basin (fig. 99). Finally, during the Late Cretaceous and Paleogene inversion pulses, the RFZ and HFZ underwent minor inversion.

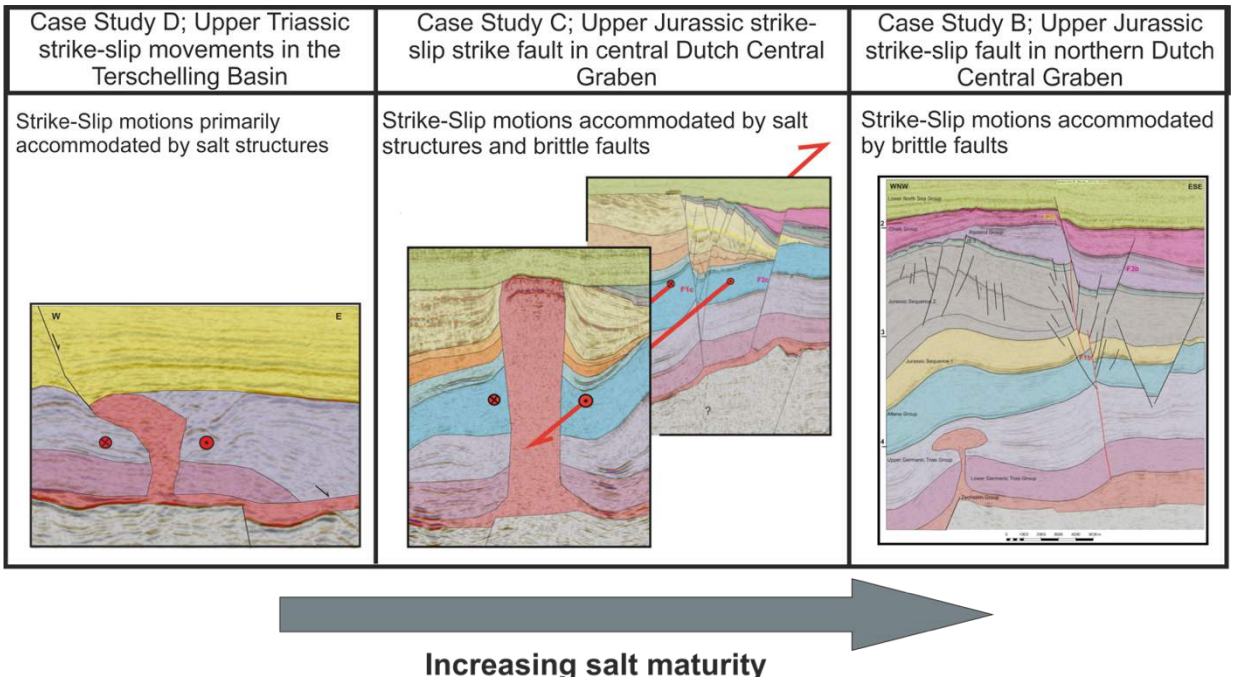

Fig. 97. Figure illustrating how the structural style of deformation of supra salt strike-slip movements depends on the presence of salt structures, which tend to be less abundant with increasing salt maturity.

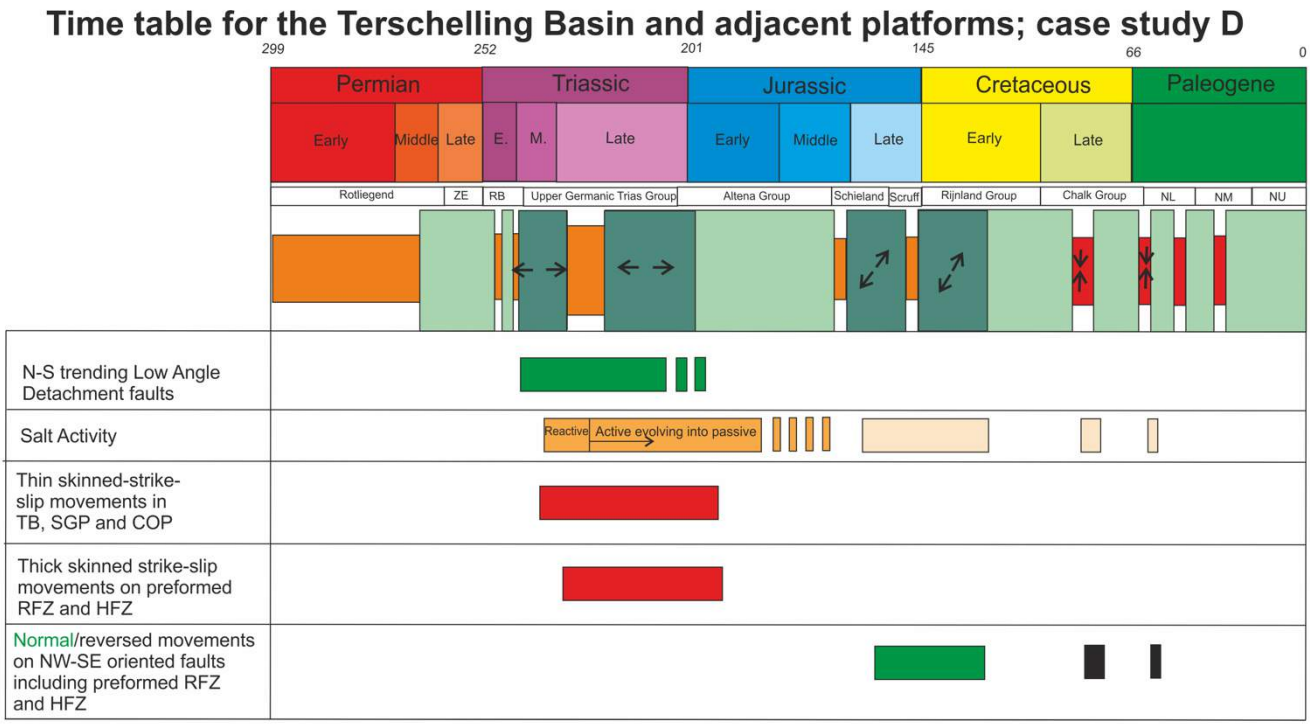

Fig. 98. Diagram indicating the time of activity for the main structural elements the Terschelling Basin and adjacent platforms, as described in case study D.

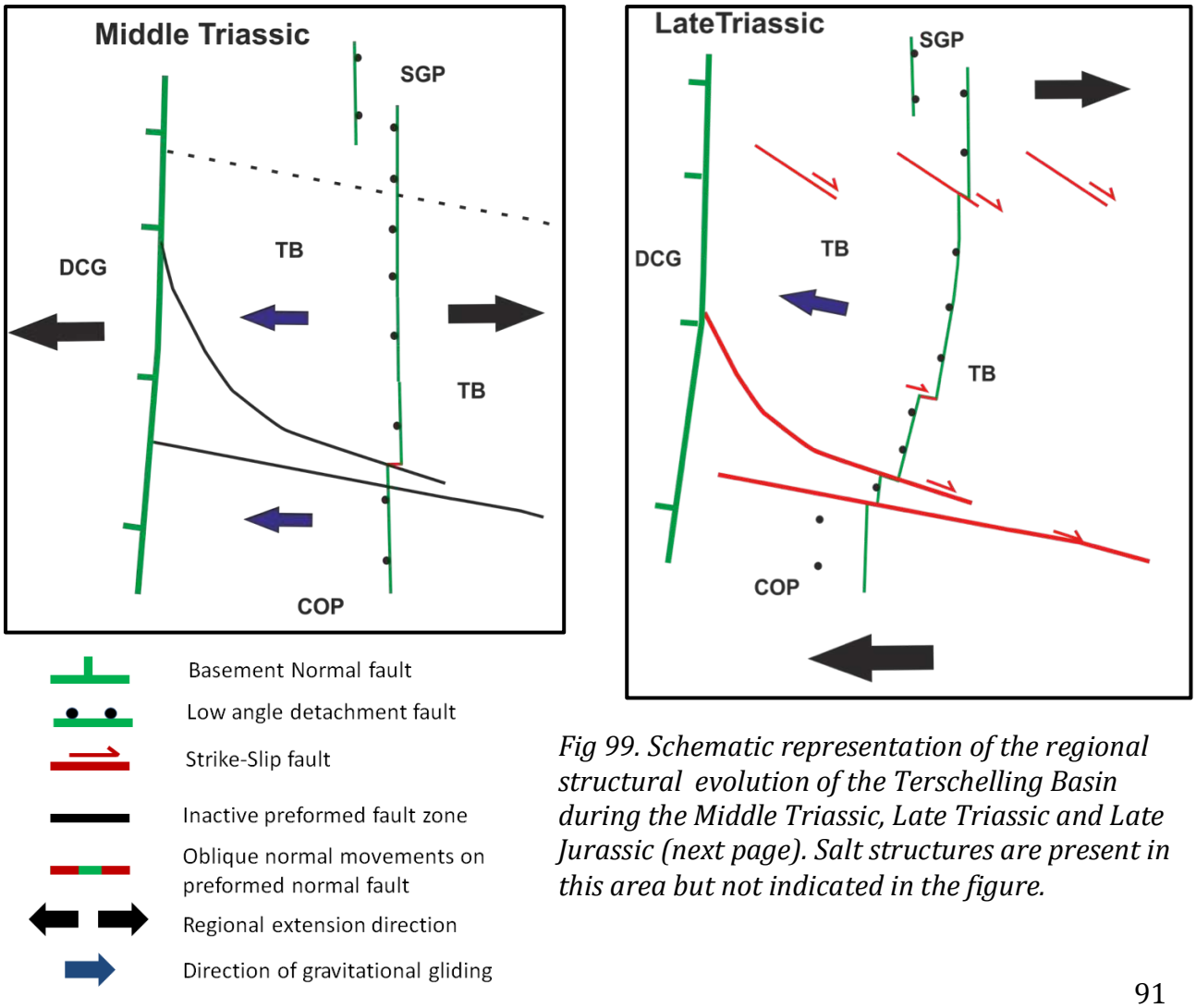

Fig 99. Schematic representation of the regional structural evolution of the Terschelling Basin during the Middle Triassic, Late Triassic and Late Jurassic (next page). Salt structures are present in this area but not indicated in the figure.

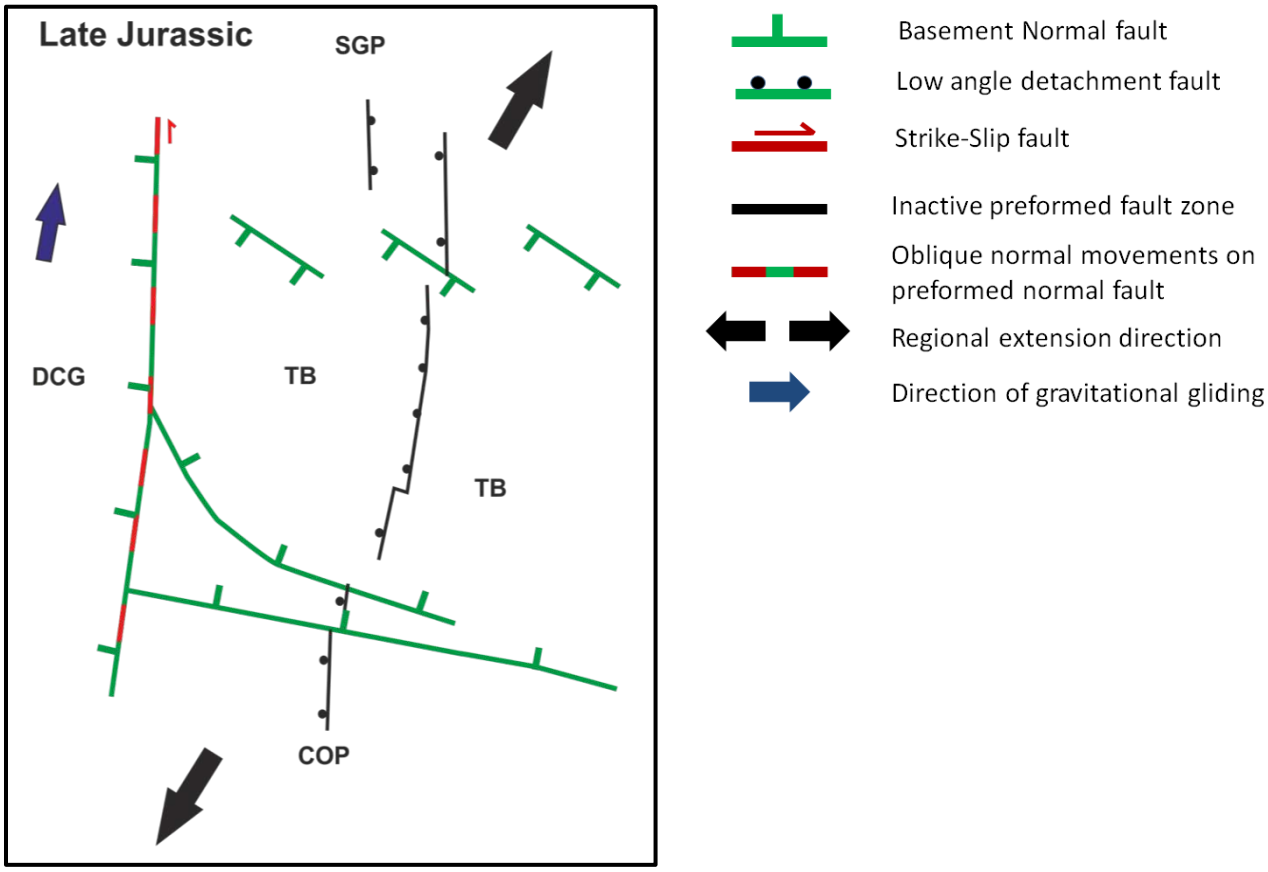

6.4. Natural analogies and comparison with other studies

Because of its rotation, the shape of salt diapir B (case study C) looks a bit like a rotated sigma clast in a sheared metamorphic rock (Fig. 100). Additionally, a striking-resemblance between diapir B and a diapir in the Great Kavir in northern Iran is present (Fig. 101) The diapir in northern Iran also shows the curved geometry of strike-slip faults upon the approach of the diapir. This rotation is also observed in analogue models performed by Dooley et al., (2012) (Fig. 11). Overall, the development of the area around case study C shows some analogy to the areas in the West African Passive margin (fig. 102). In this area, gravitational gliding towards the Atlantic has caused normal faulting in the higher part of the margin towards the continent and thrust faulting in the lower Atlantic part due to the presence of a salt layer, which acts as a decollement. Rates of gravitational gliding of the supra salt overburden were not the same everywhere so differential motions occurred between different blocks. These differential motions between the different blocks then led to strike-slip motions, which in analogy to the Dutch offshore and analogue modelling, are preferentially accommodated by salt structures. Additionally, the brittle interval in-between salt structures also has to accommodate these strike-slip motions, thereby linking the salt structures. However, the stronger component of gravitational gliding in the west African margin, has presumable caused larger supra-salt strike-slip motions, than in the Dutch Central Graben.

The Triassic compartments in the Terschelling Basin, which are surrounded on multiple sides by salt walls show an analogy with Cenozoic minibasins in the Gulf of Mexico. In this area, salt or salt welds that surround the minibasins primarily accommodate differential motions between adjacent minibasins (Fig. 103).

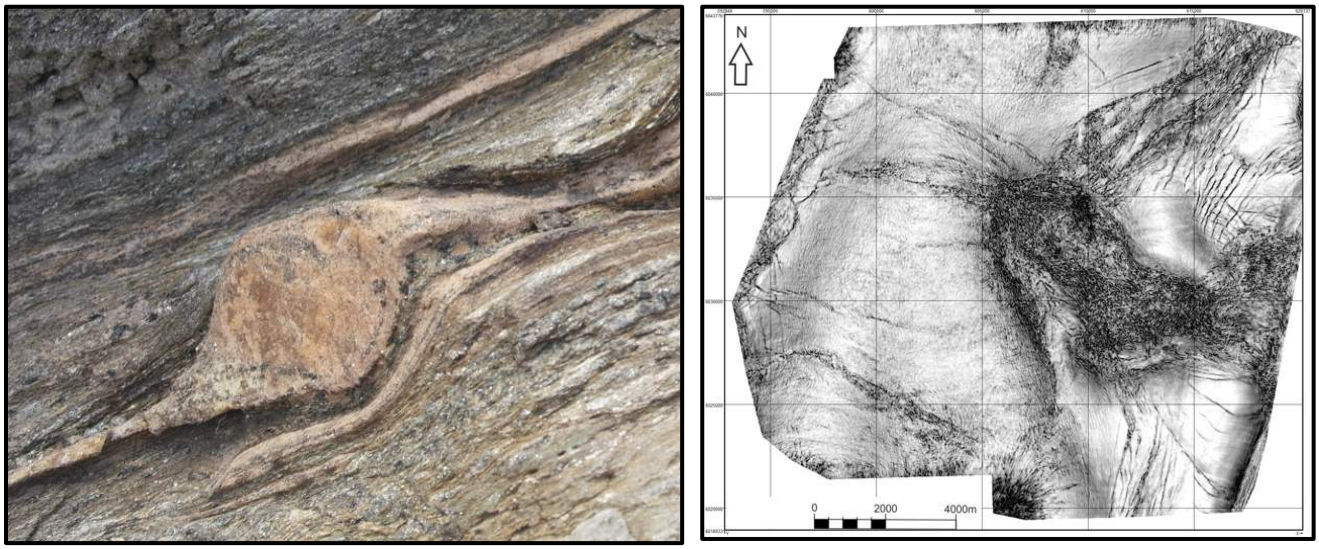

Fig. 100. The shape of salt diapir B discussed in case study C (right figure) shows geometrical similarities to a dextrally sheared sigma clast metamorphic shear zone (left figure). Left figure from Johanna Sommer; the art in science.

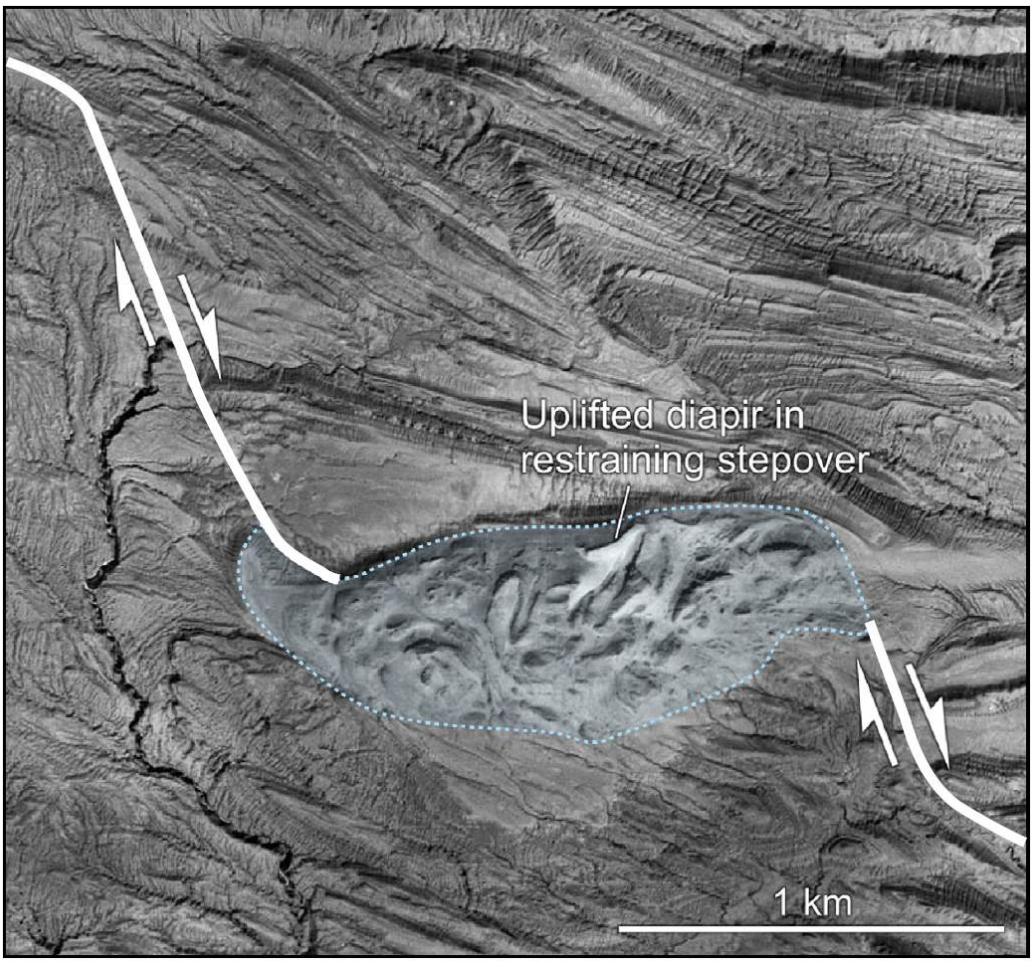

Fig. 101. Dextral strike-slip interaction with a salt diapir in the Great Kavir in northern Iran. The left stepping of the dextral strike-slip fault causes a restraining bend to develop over the diapir and causes localised compression, uplift as well as rotation of the salt dipair. Note the similarity between this diapir and diapir B in case study C (Fig. 100). Figure from Dooley and Schreurs, 2012.

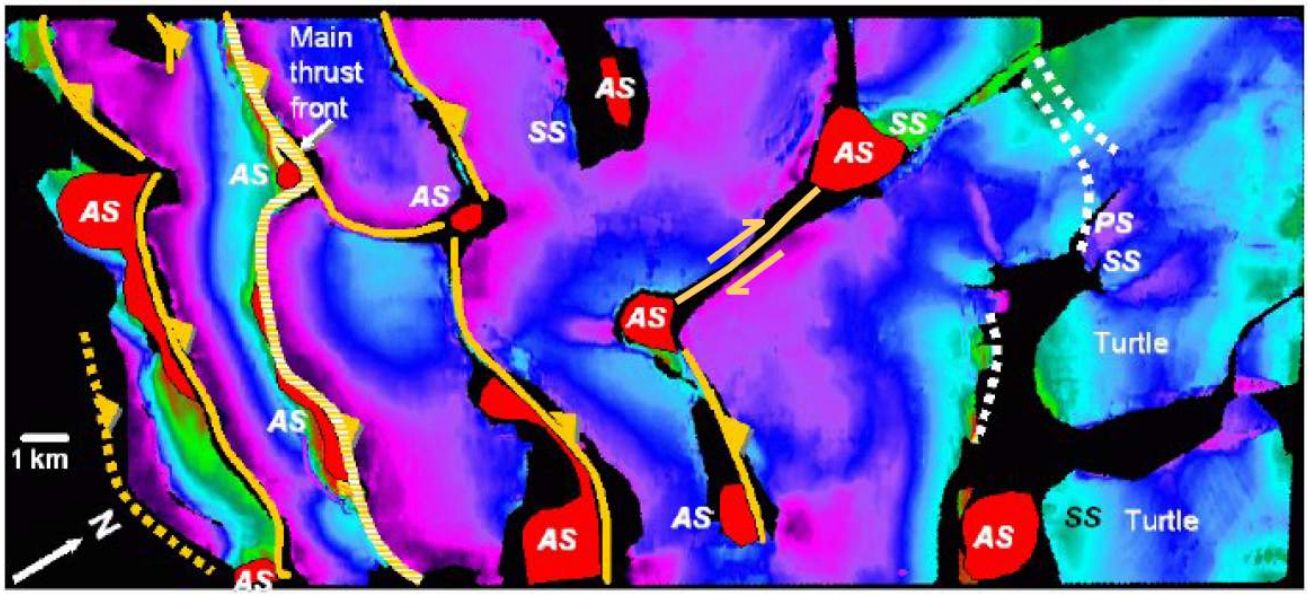

Fig. 102. Part of the west African margin before the country of Gabon, note that differential motions between different blocks are accommodated by salt structures (indicated in red) and brittle strike-slip faults that link these salt structures. Figure from Hudec and Jackson, 2004

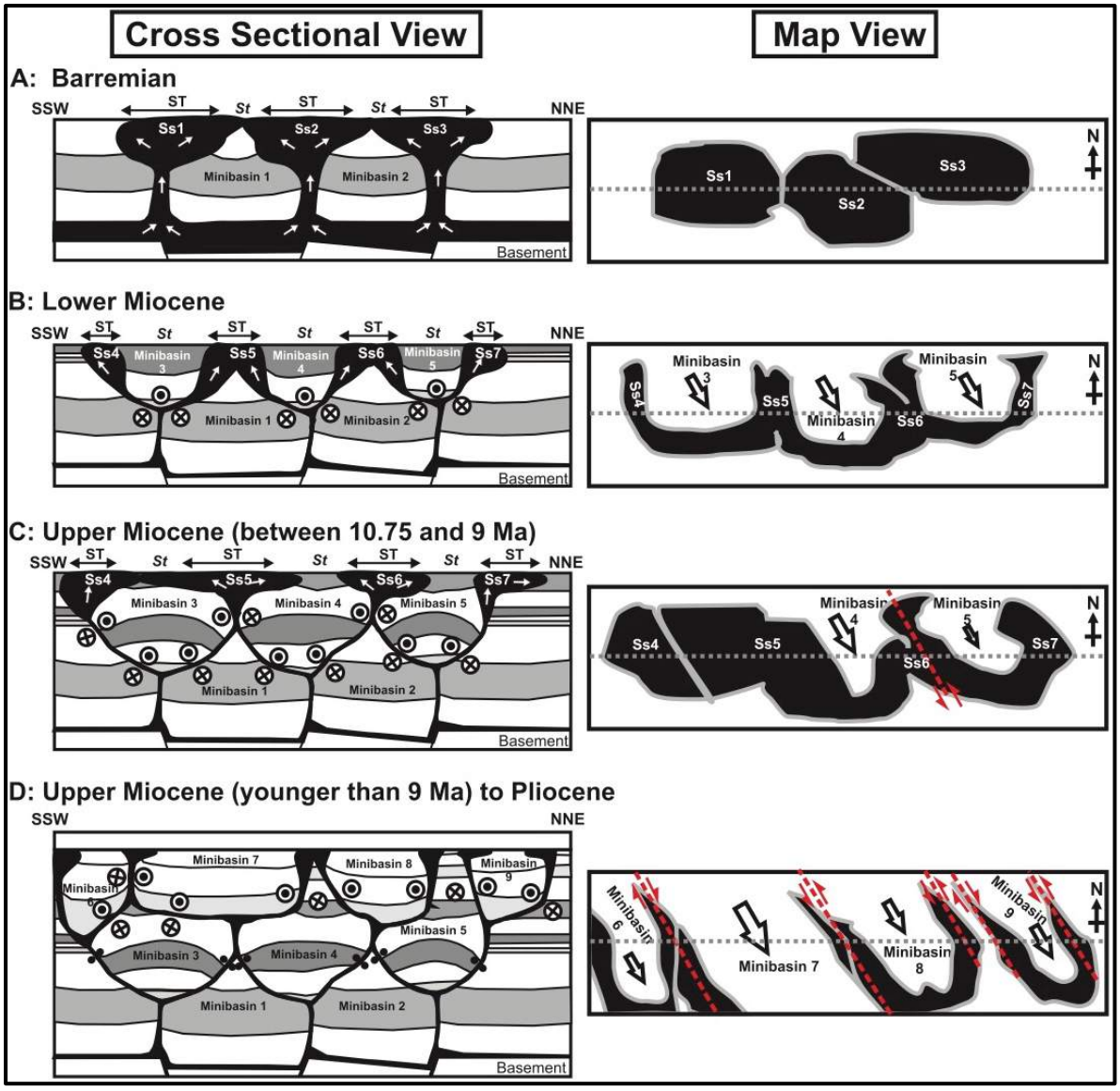

Fig. 103. Schematic figure showing the structural development of a complex of stacking minibasins. Differential motions between adjacent minibasins are accommodated via lateral motions along salt walls and salt welds. Fig. from bouroullec et al., 2016 in press.

7. Implications of strike-slip movements for hydrocarbon exploration

A proper understanding of strike-slip movements is of vital importance to assess all the components of a possible working hydrocarbon system. These components are; the presence of a structural trap, the presence of a seal and the occurrence of charge from deeper source rocks. A good structural trap related to strike-slip faulting can form due to the upward widening of the fault pattern, in combination with the tilting of fault blocks inside a strike-slip fault zone. An example of a working structural trap related to strike-slip faulting in the Dutch subsurface is the Pijnacker oil field, where oil is trapped in a positive flower structure (Racero-Baena and Drake, 1996). Additionally, strike-slip movements influence the reservoir quality on both side of the faults zone as strike-slip movements cause different blocks to move laterally with respect to each other. This means that in a rapidly changing depositional environment, such as during the Upper Jurassic in the Dutch Central Graben, reservoir qualities can differ significantly on one side of the strike-slip fault with respect to the other side of the strike-slip fault in the same stratigraphic interval. This is the case for instance, when material of a deeper part of the basin is brought laterally next to a more proximal part of the basin due to post-depositional strike-slip faulting. The influence of syn-depositional strike-slip faulting is poorly understood. But also here, it has to be taking into account that different rock types and different rock properties might be encountered on both sides of the fault, in the same stratigraphic interval. A good example of this, is the lateral stacking of alluvial fans along NW-SE striking Permian strike-slip faults as was observed by George and Berry (1997). Concerning the possibility of charge from sub salt source rocks, it is important that windows in the salt provide fluid conduits along which hydrocarbons can migrate. Hence, the question whether supra-salt strike-slip faults are triggered by sub salt basement strike-slip faults is of importance as a linked fault system could provide a fluid conduit along which hydrocarbons can migrate. However, this doesn't seem the case in the Dutch Central Graben, as supra salt strike-slip faults are likely purely thin skinned. However, charge could also originate from the supra salt Posidonia shale source rock in the Dutch Central graben.

8. Conclusions

The most important conclusions of this study are summarized below by answering the key questions that were addressed in this study.

Where are Mesozoic strike-slip faults located in the northern Dutch offshore and what is the timing, sense of displacement and amount of displacement?

Several Mesozoic strike-slip faults are present in the Northern Dutch offshore, both on the platform areas as well as in the basins (Fig. 20). The main conclusions in terms of amount- and sense of displacement, timing and fault salt relations are listed below per structural element and can also be found in Table 3 for individual faults and fault families.

- **Strike-slip faults on the western Platform areas**

A Group of SW-NE to WSW-ENE trending Late Cretaceous to Early Paleogene dextral strike-slip faults offsets and partly reactivates older fault trends, thereby forming pop-up and pull-apart structures. Offsets on individual strike-slip faults are in the order of 500-900m. The exact cause of these faults is uncertain but it is suggested that an approximate E-W directed ridge push force has played an imported role in the formation of these strike-slip faults.

- **Strike-slip faults in the Dutch Central Graben**

Several Late Jurassic/Early Cretaceous isolated strike-slip faults are present in the Dutch Central Graben. These faults are characterised by a curved strike that changes between approximately NW-SE to NE-SW. Estimated offsets on individual strike-slip faults range between 900 and 2500m.

- **Strike-slip faults in the Terschelling Basin and on the adjacent Schill Grund- and Central Offshore platforms**

Post Early Triassic and Pre- Late Jurassic dextral strike-slip movements have occurred on the preformed Hantum fault zone and Rifgronden fault zone. Dextral strike-slip movements on the Hantum Fault zone are estimated to be in the order of 5 à 6km. Dextral strike-slip movements on the Rifgronden Fault zone are estimated to be in the order of 2 à 3km. Strike-slip movements on basement faults also occur within the Terschelling Basin itself, accommodating differential movements for the overall dextral shearing of the basin. Thin skinned supra salt strike-slip motions occur both in the Terschelling Basin as well as on the adjacent platforms. These motions are primarily accommodated by salt walls and displacements are in the order of 1 à 2km.

Are the identified strike-slip faults in the salt controlled basins linked to deeper rooted basement faults and how are strike-slip motions on subsalt preformed basement faults distributed into the supra salt interval?

Analogue models show that subsalt strike-slip motions on inherited basement faults are transmitted into the supra salt overburden via the areas were the salt walls are highest, as this is the mechanically weakest part of the rock column.

Dutch Central Graben

- In accordance with the analogue models, the observed strike-slip movements in the Dutch Central Graben seem to be primarily accommodated by salt walls. Brittle strike-slip motions only occur in places were salt walls are absent to transfer motions between two salt structures. However, no evidence was found for strike-slip motions on

preformed N-S trending basement faults that bound the Dutch Central Graben. Instead, the strike-slip movements that were observed in the Dutch Central Graben are likely caused by differential motions on sub-salt normal faults, possibly enhanced by gravitational gliding.

Terschelling Basin

- Dextral basement strike-slip movements were accommodated in the Middle and Upper Triassic by the Hantum and Rifgronden Fault zones. Additionally the different Triassic compartments in the Terschelling Basin have moved laterally with respect to each other, where motions were primarily accommodated by the salt walls. To what extent these complex motions are caused by deeper rooted strike-slip faults is unclear. It is suggested that smaller strike-slip movements in the Terschelling Basin are purely thin skinned and originate from differential movements on sub salt normal faults, likely enhanced by a component of gravitational gliding. Larger strike slip movements are likely caused by deeper strike-slip basement faults.

Personal note

Unravelling the characteristics of a strike-slip fault in structurally complex basins such as the Dutch Central Graben and the Terschelling Basin is not straightforward. Analogue modelling has been helpful in unravelling some of the basic mechanisms regarding the distribution of strike-slip faults in a salt dominated basin. However analogue modelling is only a first order approximation for the complexity of nature and can't be used to model specific structures that have been affected by multiple deformation phases. Instead, a detailed structural analysis by making use of various thickness maps and attribute maps is a good way to gain more insight into the characteristics of specific faults. However, it has to be emphasized that estimated displacements from lateral offsets of older structures and thickness maps don't necessarily provide the original amount of displacement caused by strike-slip motions, as younger deformation phases may have reactivated the structure.

9. Recommendations for future work

- The analogue models described in this study consisted of an extensional phase, followed by a resting phase and finally a strike-slip phase. Hence, the models were used to study the distribution of strike-slip movements on inherited basement faults into the overburden of a mature salt basin. In the Terschelling basin on the other hand, strike-slip motions predate the main opening of the basin in the Upper Jurassic and Lower Cretaceous. Hence, during the time that the strike-slip motions took place (Middle and Upper Triassic), the salt structures were less mature. This means that the salt structures were less developed and that the basal salt layer was much thicker. Analogue models could be used to test the influence of a basement strike-slip fault on a thick but rather homogeneous upper crustal weak layer and a thin overburden.

- The analogue models described in this study show that strike-slip movements on a preformed sub-salt basement fault are primarily transmitted via the silicon putty walls. This led to the formation of strike-slip faults above the silicon putti walls in the brittle cover. Such supra salt wall strike-slip faults have not been observed in the seismic interpretation part of this study. It might very well be possible that evidence of these strike-slip faults is removed by later uplift and erosion or due to later reactivation of salt structures. However, it might be possible that there are some salt structures in the Dutch Central Graben that are overlain by Upper Jurassic and/or Cretaceous rocks and that have been relatively stable during Late Cretaceous inversion. If these strata are preserved above salt structures in the Dutch Central Graben, it would be interesting to see if they were affected by supra salt wall strike-slip faults. Additionally, such supra salt wall flower structures could provide structural traps for hydrocarbon accumulations.

- The analogue models 3 and 4 indicate that the amount of supra salt strike-slip movements in the graben depends on the distance between the salt walls on either side of the graben when sub-salt strike-slip movements occur on a preformed basement fault. It would be interesting to test this in a more quantitative way by performing multiple experiments with varying distance between the two opposing salt walls and better understand the relation between the width of the basin as defined by the salt walls, and the amount of strike-slip deformation that is accommodated by strike-slip faults in the graben.

- The seismic sections that are shown in this study are in seconds two way travel time (TWTT). Additionally, the isopach maps created in this study are also in second TWTT. Because seismic velocities differ with depth and with rock type, some intervals may appear thicker on a seismic line than others. Hence, a good velocity model, allowing the conversion from time to depth would considerably increase the reliability of the interpretations.

- Several strike-slip faults in the northern Dutch offshore have been identified in this study and a detailed structural analysis of some of these faults has led to a better understanding in terms of timing, fault salt interaction and sense- and amount of displacement. However, it is highly likely that there remain more unidentified structures that have accommodated strike-slip movements. Similar to this study, future studies could be devoted to gain more insight in the structural development of additional strike-slip features in the Netherlands. These studies could provide valuable information about the geological history of the Dutch offshore and for future hydrocarbon exploration. Additionally, when more strike-slip features are identified, larger trends could become visible, which could lead to an overall better understanding of the geological evolution of the Northern Dutch offshore.

10. Acknowledgements

First of all, I would like to thank TNO for providing me with the opportunity to perform my MSc. Research at their research institute and allowing me to work on an interesting and challenging topic for six months. I enjoyed working in the international, informal and yet very informative atmosphere of TNO and for this I would like to thank all the people that work at TNO.

A special word of thanks to my supervisors; Jeroen Smit and Renaud Bouroullec for their help throughout the project. To you I say: "Thank you for giving me this opportunity and thank you for sharing your expertise and ideas with me. I hope you can forgive me my occasional stubbornness. I've really appreciated your involvement in the project; which was manifested by many discussions, but also by eating a pizza after a long day in the lab, or *fruit des mer* after a day in the field". Special thanks also to Dimitrios for providing me with the opportunity to work in the teclab at the UU. Additionally, I would like to thank all the people who were working at the Teclab of the UU, especially Bram Scheffer and Dagmar Smit. Their models provide valuable contributions to the understanding of salt behaviour under extensional and strike-slip conditions. At TNO, I would also like to thank Mart Zijp for his help with the seismic data and Geert de Bruin for sharing his expertise on the OpendTect Software. At EBN, special thanks to Marten ter Borgh for pointing out the presence of the SW-NE striking strike-slip faults on the western platforms, which were described in case study A of this study.

11. References

- Arthaud, F. and P. Matte 1977. Late Paleozoic strike-slip faulting in southern Europe and northern Africa: result of a right-lateral shear zone between the Appalachian and the Urals. Geological Society of America Bulletin, v. 88, p. 1305-1320.
- Bouroullec, R., G. de Bruin., Geel, Munsterman, D., K. Verreusel, R.M.C.H., 2015 TNO Focus Project
- Brun, J.P., 2009; Mauduit, T.P. O., 2009., Salt Roller: Structure and kinematics from analogue modeling., Journal of marine and petroleum geology, 26, 249-258
- Brun, J.P., 2002., Deformation of the continental lithosphere: insights from brittle-ductile models., Geological Society Special Publication., V.200., p. 355-370
- Byerlee, J., 1978., Friction of rocks., Pure and Applied Geophysics, V.116., p.615-626
- Clausen, J.A., Gabrielsen, F.H., Reksnes, P.A., Nysaether, E., 1999., Development of intraformational (Oligocene-Miocene) faults in the northern North Sea: influence of remote stresses and doming of Fennoscandia., Journal of Structural Geology 21, 1457-1475
- Davy, P., Cobbold, P.R., 1991., Experiments on shortening of a 4-layer model of the continental lithosphere. Tectonophysics, V. 188, p.1-25
- De Jager, J., 2003., Inverted basins in the Netherlands, similarities and differences., Netherlands Journal of Geosciences/Geologie en Minbouw 82: 339-349
- De Jager, J., Geluk, M.C., 2007, Geological development. In; Wong, T.E., Batjes, D.A.J. and de jager, J. (eds): Geology of the Netherlands. Royal Netherlands Academy of Arts and Sciences (KNAW), Amserdam: 5-26
- De Jager, J., 2012., the discovery of the Fat Sand Play 9Solling Formation, Triassic), Northern Dtuch offshore – a case of serendipity. Netherlands Journal of Geosciences., Vol. 91-4. P. 609-619
- Donato, J.A., Martindale, W. & Tully, M.C., 1983. Buried granites within the Mid North Sea High. Journal of the geological Society 140: 825-837
- Dooley, T.P., Jackson, M.P.A., Hudec, M.R., 2009., Inflation and deflation of deeply buried salt stocks during lateral shortening., Journal of Structural Geology. V. 31., p. 582-600
- Gast, R. & Gundlach, T. (2006): Permian strike slip and extensional tectonics in Lower Saxony, Germany. [Permi- sche Blattverschiebungs- und Dehnungstektonik in Niedersachsen, Deutschland.] – Z. dt. Ges. Geowiss., 157: 41–56, Stuttgart
- Geluk, M.C., 2005. Stratigraphy and tectonics of Permo-Triassic basins in the Netherlands and surrounding areas. PhD thesis, University of Utrecht: 171 pp.
- Geluk, M.C., Paar, W.A., Fokker, P.A., 2007., Salt., Geology of the Netherlands, royal Netherlands academy of Arts and Sciences., pp.283-294
- George, G.T., Berry, J.K., 1997., Permian (Upper Rotliegend) synsedimentary tectonics, basin development and paleogeography of the southern North Sea., Geological Society, London, Special Publications 1997; v. 123; p. 31-61
- Goetze, C., Evan, B., 1979., Stress and temperature in the bending lithosphere as constrained by experimental rock mechanics., geophysical journal of the royal astronomical society., V. 59., p. 463-478
- Harding, R., Huuse, M., 2015., Salt on the move: Multi stage evolution of salt diapirs in the Netherlands North Sea., Marine and Petroleum Geology, V.61, p.39-55
- Heybroek, P., 1974., Explanation to tectonic maps of the Netherlands., Geologie en Mijnbouw, V.53, p.43-50
- Hudec, M.R., Jackson, M.P.A., 2007., Terra infirma: Understanding salt tectonics., Earth Sciences Reviews, V. 82., p. 1-28
- Hubbert, M.K., 1937., Theory of scale models as applied to the study of geologic structures., Geological Society of America Bulletin, V.48., p.1459-1519
- Jackson, M.P.A. and Hudec, M.R. and, 2009., Interplay of basement tetctonics, salt tectonics, and sedimentation in the Kwanza Basin, Angola., aapg

- Kley, J., Franzke, H.J., Jähne, C., Krawczyk, C., Lohr, T., Reicherter, K., Scheck-Wenderoth., Sippel, J., tanner, D., van Gent, H., On strain and stress regarding the Central European Basin System.
- Kombrink, H., 2008. The Carboniferous of the Netherlands and surrounding areas; a basin Analysis. Proefschrift.
- Kombrink, H., doornenbal, J.C., duin, E.J.T., Den Dulk, M., Van Gessel, S.F., Ten Veen, J.H. & Witmans, n., 2012. New insights into the geological structure of the Netherlands; results of a detailed mapping project. Netherlands Journal of Geosciences 91-4:419-446
- Kiersnowski, H., Buniak, A., 2006., Evolution of the Rotliegend Basin of northwestern Poland., Geological Quarterly, 2006, V50.p.119-138
- Mann, P., 2007., global catalogue, classification and tectonic origins of restraining- and releasing bends on active and ancient strike-slip fault systems., Geological Society, London, Specical Publications, V.290,p13-142.
- Mart, Y. and Ross, D. A., 1987., Post-Miocene rifting and diapirism in the northern Red Sea., Mar. Geol. 74, 173-190.
- Munsterman, D.K., Verreussel, R.M.C.H., Mijnlieff, H.F., Witmans, N., Kerstholt-Boegehold, S., 2012., Revision and update of the Callovian-Ryazanian Stratigraphic Nomenclature in the northern dutch Offshore, i.e. central Graben Subgroup and Scruff Group. Netherlands Journal of Geosciences-Geology en Mijnbouw, 91 (4): 555-590.
- Nalpas, T., Le Douaran, S., Brun, J.P., Unternehr, P., Richert, J.P., 1995., Inversion of the Broad Fourteens Basin (offshore Netherlands), a small-scale model investigation., Sedimentary Geology, V. 95, p.237-250
- Peeters, S.H.J., 2015., Towards better understanding of the highly overpressured Lower Triassic Bunter reservoir rocks in the Terschelling Basin., MSc. Intern project Utrecht University at EBN
- Pfiffner, O.A., Ramsay, J.G., 1982., Constraints on geological strain rates: Arguments from finite strain states of naturally deformed rocks., Journal of Geophysical Research., V. 87., p. 311-321
- Racero-Baena, A., and Drake, S.J., 1996, Structural style and reservoir development in the West Netherlands oil province in H.E. Rondeel, D.A.J. Batjes, and W.H. Nieuwenhuijs, eds., Geology of gas and oil under the Netherlands: Dordrecht, Kluwer Academic Publishers, p. 211-227.
- Remmelts, G., 1995 Fault-related salt tectonics in the Southern North Sea, the Netherlands., in: M.P.A. Jackson, D.G. Roberts, S. Snelson (Eds.), Salt tectonics: a global perspective, AAPG memoir. 65 (1995), pp. 261-272
- Scheffer, B., 2016., Analogue modeling of salt diapirism: Example of North-Sea Central Graben., BSc. Thesis Utrecht University
- Smit, D., 2016., Salt tectonics in strike-slip settings: application to the North Sea. BSc. Thesis Utrecht University.
- Smit, J.H.W., 2005., Brittle-Ductile coupling in thrust wedges and continental transforms. PhD thesis.
- Smit, J.H.W., Brun, J.P., Fort, X., Cloetingh, S., Ben-Avraham, Z., 2008a., Salt tectonics in pull-apart basins with application to the Dead Sea Basin., Tectonophysics. V. 449., P. 1-16
- Smit, J.H.W., Brun, J.P., Fort, X., Cloetingh, S., 2008b. Pull-apart basin formation and development in narrow transform zones., Tectonics., V 27 (6), TC6018
- Smit, J,H.W., J.D. van Wees and S. Cloetingh (in press), The Thor suture zone: From subduction to intraplate basin setting. Geology, DOI:10.1130/G37958.1
- Spiers, C.J., Schutjens, P.M.T.M., Brzesowsky, R.H., Liezenber, J.L., Zwart, H.J., 1990., Experimental determination of constitutive parameters governing creep of rocksalt by pressure solution., Geological Society Special Publication., V.54. p. 215-227
- Ten Veen, J.H., van Gessel, S.F., van Dulk, M., 2012., Thin- and thick-skinned salt tectonics in the Netherlands; a quantative approach., Netherlands Journal of Geosciences, 91, v.4.
- Tusheim, F., 1960., Mechanism of salt migration in northern Germany: Association of Petroleum geologists Bulletin, V. 44, p. 1519-1540.

- Vagnes, E., Gabrielsen, R.H., Haremo, P., 1998., Late Cretaceous-Cenozoic intraplate contractional deformation at the Norwegian continental shelf: timing, magnitude and regional implications.
- Van Adrichem Boogaert, H.A. & Kouwe, W.F.P., 1993-1997. [Stratigraphic unit]. In: Stratigrpahic Nomenclature of the Netherlands
- Van Duin, E.J.T., Doornenbal, J.C., Rijkers, R.H.B., Verbeek, J.W., Wong, Th.E., 2006., Subsurface structure of the Netherlands – Results of recent onshore and offshore mapping. Netherlands Journal of Geosciences Vol. 85-4. P. 245-276
- Van Keken, P.E., Spiers, C.J., van den Berg, A.P., Muyzert, E.J., 1993., The effective viscosity of rocksalt:implementation of steady-state creep laws in numerical models of salt diapirsm., Tectonophysics., V. 225. p. 457-476.
- Verweij, J.M., Souto Carneiro Echternach, M., Witmans, N., 2009 - Terschelling Basin and southern Dutch Central Graben Burial history, temperature, source rock maturity and hydrocarbon generation - Area 2A TNO report - TNO-034-UT-2009-02065
- Van der Zwan, C.J., Spaak, P., 1992., Lower to Middle Triassic sequence stratigraphy and climatology of the Netherlands, a model., Palaeogeogrpahy, Paleoclimatology, Paleoecology, V.91,p.2277-290
- Van Wees, J.D., Cloetingh, S., 1996., 3D flexure and intraplate compression in the North Sea Basin., Tectonophysics, V. 266, p.343-359
- Van Wees, J.D., Stephenson, R.A., Ziegler, P.A., Bayer, U., Mccann, T., Dadlez, R., Gaupp, R., Narkiewicz, M., Bitzer, F., Scheck, M., On the origin of the Souther Permian Basin, Central Europe., Journal for Marine and Petroleum Geology, V.17, p.43-59.
- Van Wijhe, D.H., 1987; Structural evolution of inverted basins in the Dutch offshore., Tectonophysics, V. 137, p.171-219
- Van Winden, M., 2015., Salt tectonics in the northern Dutch offshore., MSc. thesis Utrecht University conducted at EBN and TNO.
- Vendeville, B.C. and Jackson, M.P.A., 1992., The rise of diapirs during thin-skinned extension.
- Weijermans, R., Schmeling, H., 1986., Scaling of Newtonian and non-Newtonian fluid dynamics without inertia for quantitative modelling of rock flow due to gravity (including concept of rheological similarity)., Physics of the Earth and Planetary Interior., V. 43., p. 316-330
- Wessel, P., and Müller, R.D., 2007, Plate tectonics, *in* Schubert, G., and Watts, A.B., eds., Crust and Lithosphere Dynamics: Treatise on Geophysics, Volume 6: Elsevier, p. 49–98.
- Ziegler, P.A., 1990a. Geological Atlas of Western and Central Europe (2nd edition). Shell Internationale Petroleum Maatschappij B.V; Geological Society Publishing House (Bath): 239 pp.
- Ziegler, P.A., 1990b. Tectonic and paleogeographic development of the North Sea Rift system. In; Blundell, D.J. & Gibbs. (eds): Tectonic Evolution of the North Sea rifts. Oxford Science Publications (Oxford): 1-36

12. Appendix A

This appendix shows an impression of the work done by Dagmar Smit (BSc. Thesis 2016). Smit (2016) performed analogue models that investigated the role of strike-slip faulting on an initially uniform high weak layer of silicon putty. Smit (2016) i.a. found that the formation of sub salt pull-apart- and pop-up structures has a profound influence on the ascent of salt under strike-slip conditions. Additionally, the ascent of salt is enhanced when surface topography of the brittle overburden (created by the strike-slip deformation) is reduced by erosion. Additionally, sedimentation and a resting phase are of influence on the ascent of silicon putty.

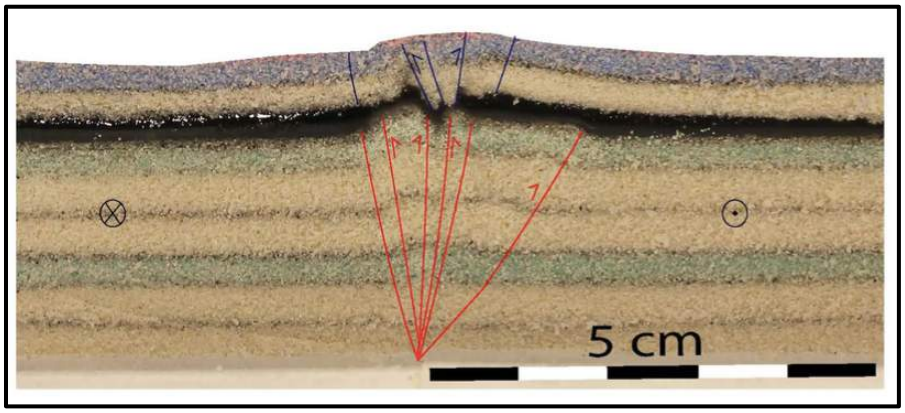

Left Figure; Cross-section through model 3 from Smit (2016), where the model underwent strike-slip faulting without erosion, resting and sedimentation. The ascent of silicon putty is limited, but some small appendix like structures form in the putty. *Figure from Smit (2016)*

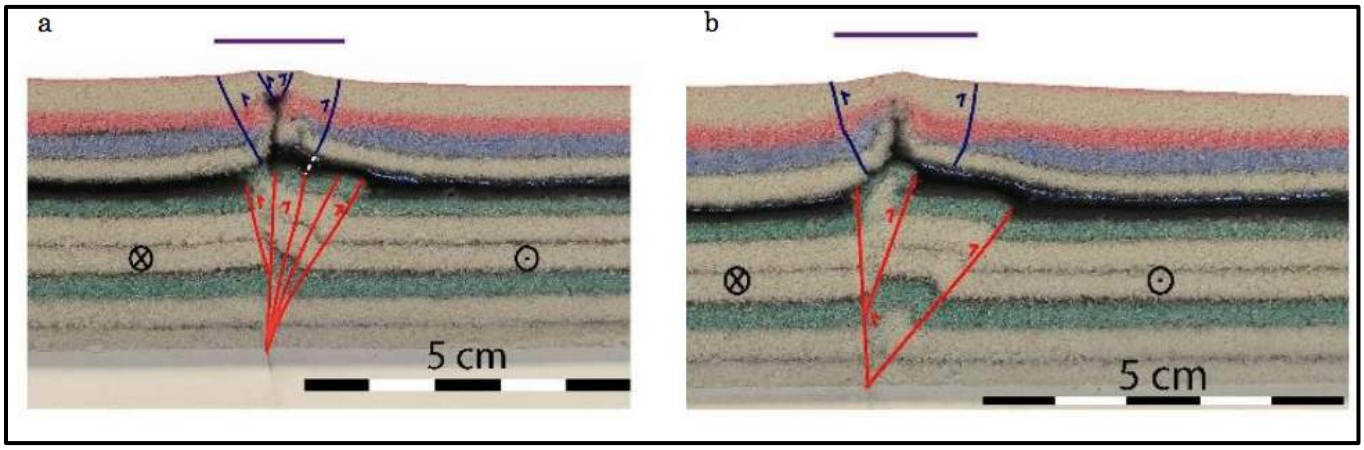

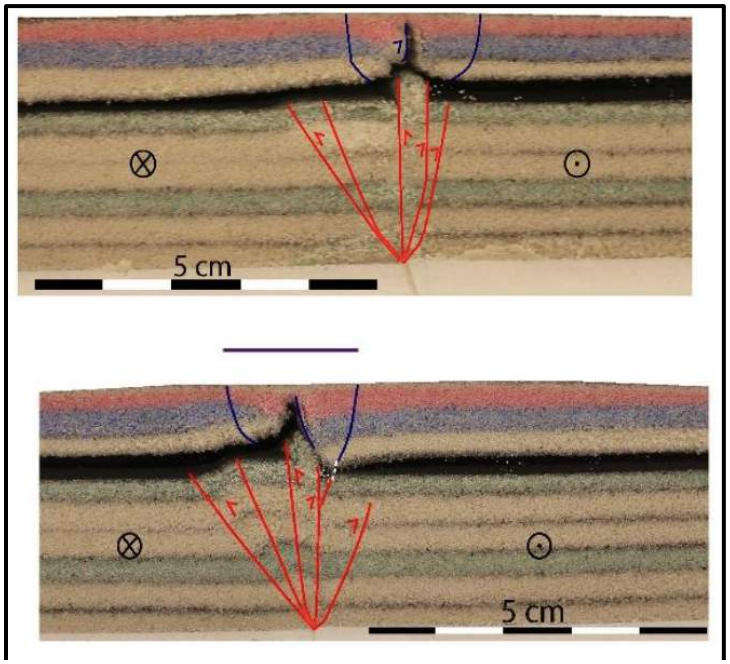

Upper two figures; Cross-section through model 6 from Smit (2016). *Left two figures;* Cross-sections through model 7 from Smit (2016). In both model 6 and 7, erosion and sedimentation were applied to the model. Additionally, a resting phase was applied to model 7. Note that the ascent of putty is stronger than in model 3. Also note that the salt structures are narrower and more angular than the salt structures that form under extension (Vendeville and Jackson, 1992; Scheffer, 2016). *Figures from Smit (2016)*

Appendix B

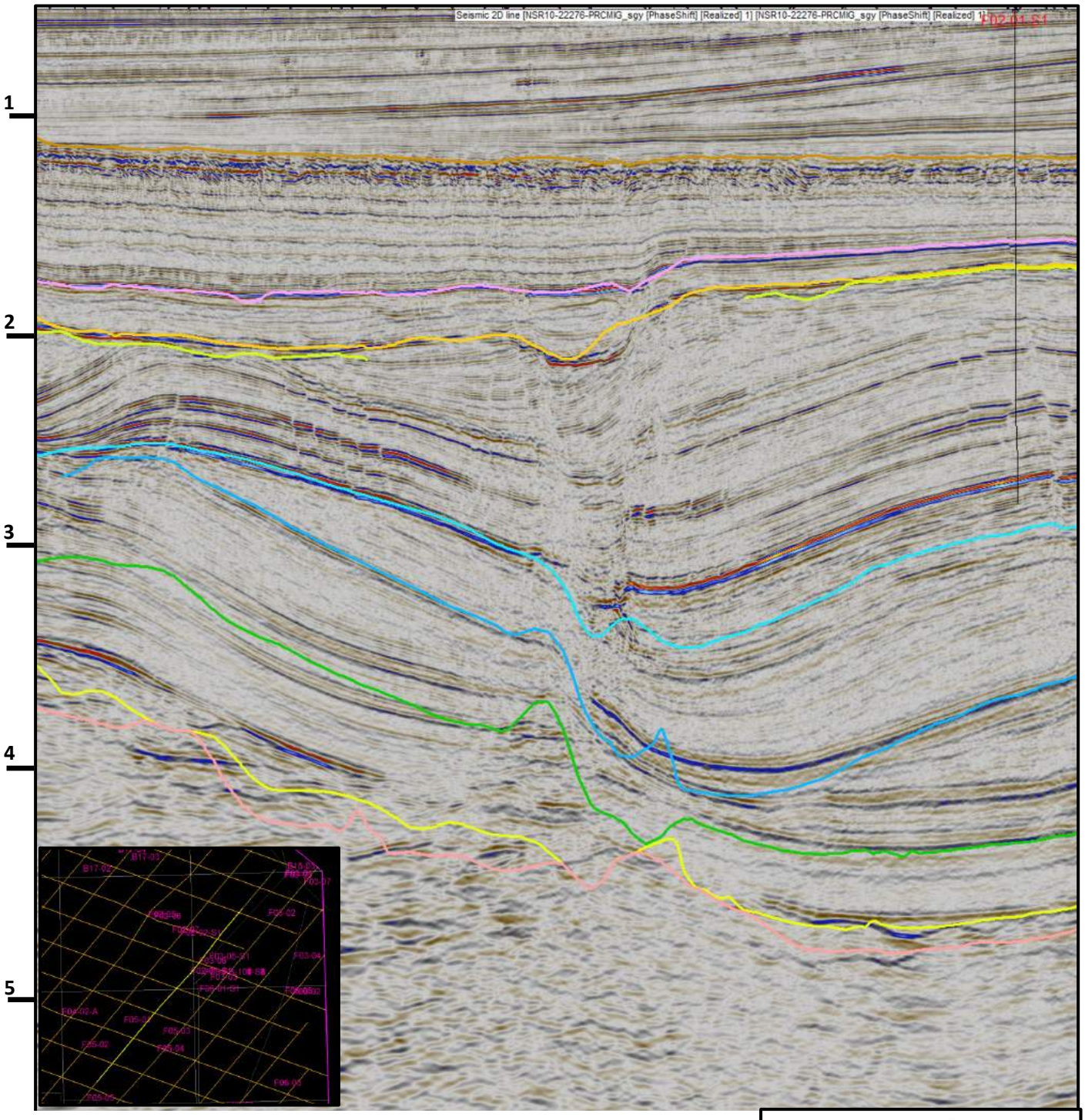

Seismic line (NSR10-22276-PRCMIG_SGY) showing a group of faults. Because of their steep fault plane, upward widening of the fault pattern and tipi shape of the Triassic and Lower Jurassic strata, it is likely that these faults accommodated strike-slip motions. Additionally, some salt is present in between the faults of this structure. This becomes better visible on a NSR line perpendicular to this line. The exact timing is poorly constrained, as well as the strike of the fault due to a lack of available seismic data in this part of the Dutch offshore. The main stratigraphic groups are indicated by a regional seismic mapping project, performed by TNO. As can be seen in this figure, the resolution of the interpretation is too low to properly track the horizons along the fault zone. Location of the seismic line with respect to other NSR lines is indicated in lower figure in yellow.

Appendix 2

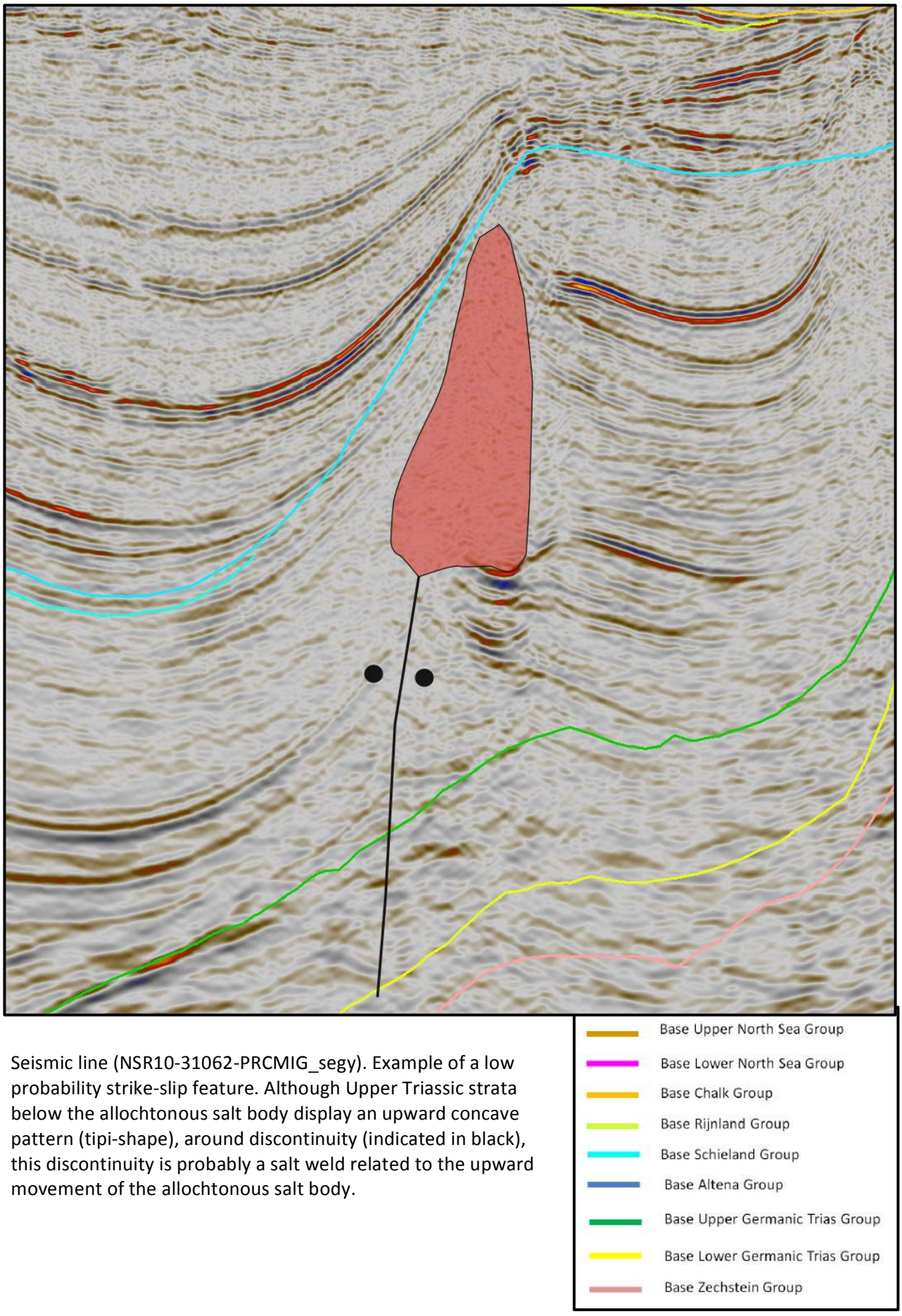

Seismic line (NSR10-31062-PRCMIG_segy). Example of a low probability strike-slip feature. Although Upper Triassic strata below the allochtonous salt body display an upward concave pattern (tipi-shape), around discontinuity (indicated in black), this discontinuity is probably a salt weld related to the upward movement of the allochtonous salt body.

Appendix D

This appendix shows an impression of the work done by Bram Scheffer (BSc. Thesis 2016). Scheffer (2016) performed analogue models that investigated the role of syn-kinematic sedimentation and different deformation rates on the ascent of silicon putty. Smit (2016) i.a. found that syn-kinematic sedimentation has a profound influence on the ascent of salt under extensional conditions. Additionally, a lower deformation rate tends to form more mature salt structures.

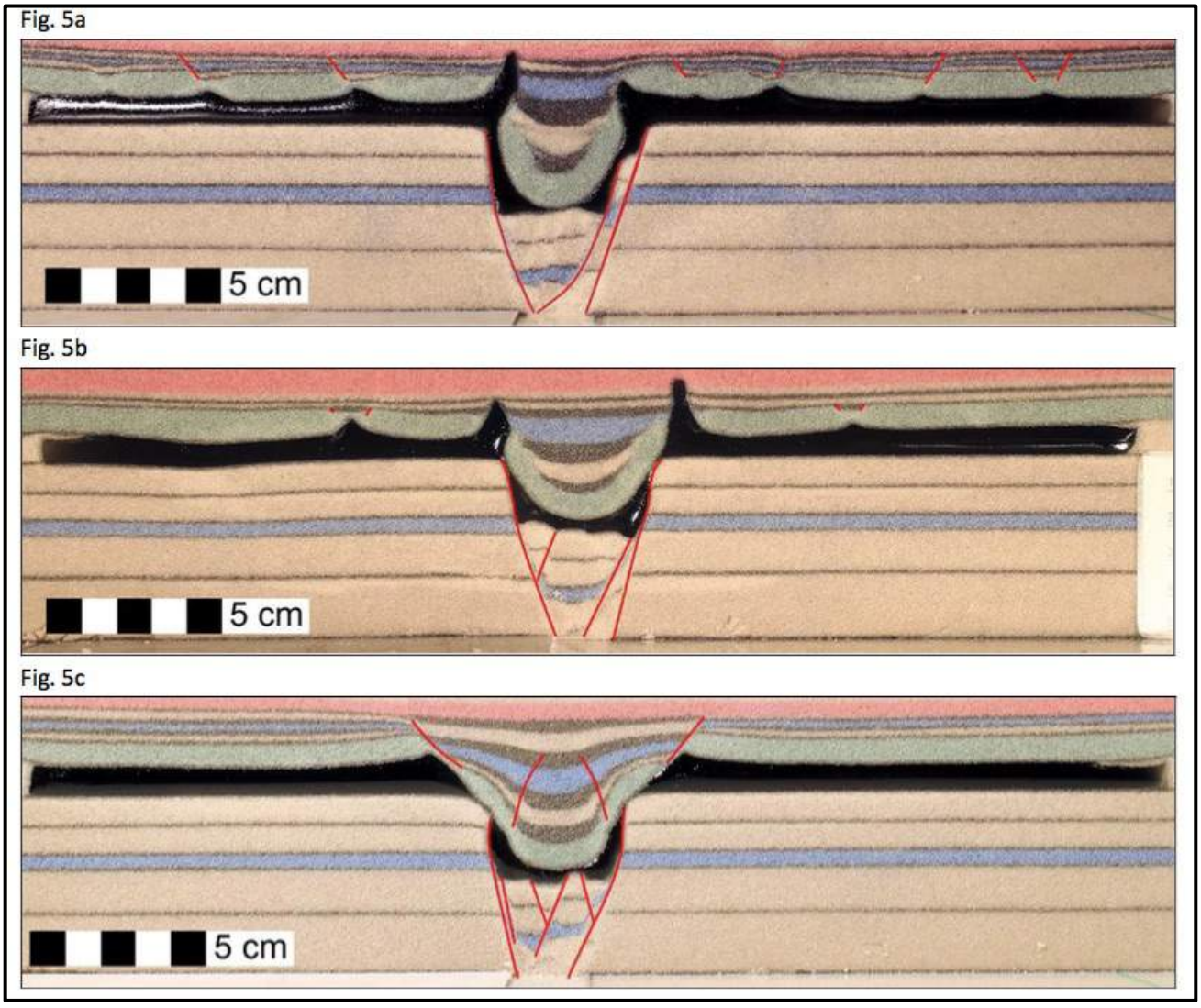

Figure showing the influence of syn-kinematic sedimentation on the ascent of silicon putty with varying amounts of sedimentation. In the top figure, sedimentation rates were less than the subsidence rate of the graben. In the middle figure, sedimentation rates were approximately equal to the subsidence rate of the graben. In the bottom figure, sedimentation rates were higher than subsidence rate of the graben. *Figure from Scheffer, 2016.*